INTERACTION OF HYDROGEN WITH TANTALUM METAL AND ITS ALLOYS

By

MANJU TAXAK

(CHEM01200804028)

Bhabha Atomic Research Centre, Mumbai

A thesis submitted to the

Board of Studies in Chemical Sciences

In partial fulfillment of requirements

For the Degree of

DOCTOR OF PHILOSOPHY

Of

HOMI BHABHA NATIONAL INSTITUTE

January, 2014

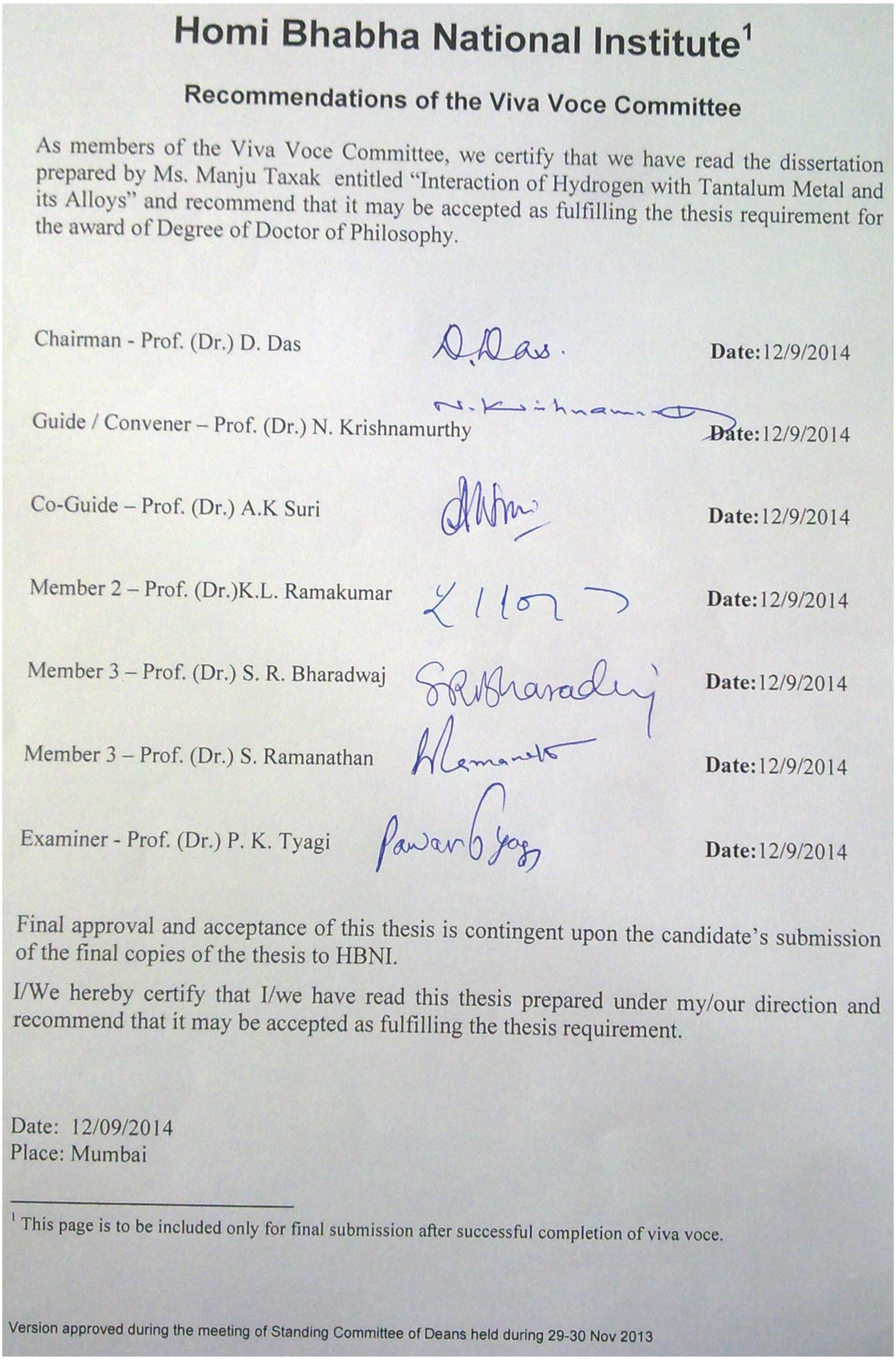

Homi Bhabha National Institute[1]

Recommendations of the Viva Voce Committee

As members of the Viva Voce Committee, we certify that we have read the dissertation prepared by Ms. Manju Taxak entitled "Interaction of Hydrogen with Tantalum Metal and its Alloys" and recommend that it may be accepted as fulfilling the thesis requirement for the award of Degree of Doctor of Philosophy.

Chairman - Prof. (Dr.) D. Das D.Das. **Date:** 12/9/2014

Guide / Convener – Prof. (Dr.) N. Krishnamurthy N. Krishnamurthy **Date:** 12/9/2014

Co-Guide – Prof. (Dr.) A.K Suri **Date:** 12/9/2014

Member 2 – Prof. (Dr.)K.L. Ramakumar **Date:** 12/9/2014

Member 3 – Prof. (Dr.) S. R. Bharadwaj SRBharadwaj **Date:** 12/9/2014

Member 3 – Prof. (Dr.) S. Ramanathan **Date:** 12/9/2014

Examiner - Prof. (Dr.) P. K. Tyagi Pawan Tyagi **Date:** 12/9/2014

Final approval and acceptance of this thesis is contingent upon the candidate's submission of the final copies of the thesis to HBNI.

I/We hereby certify that I/we have read this thesis prepared under my/our direction and recommend that it may be accepted as fulfilling the thesis requirement.

Date: 12/09/2014
Place: Mumbai

---

[1] This page is to be included only for final submission after successful completion of viva voce.

Version approved during the meeting of Standing Committee of Deans held during 29-30 Nov 2013

STATEMENT BY AUTHOR

This dissertation has been submitted in partial fulfillment of requirements for an advanced degree at Homi Bhabha National Institute (HBNI) and is deposited in the Library to be made available to borrowers under rules of the HBNI.

Brief quotations from this dissertation are allowable without special permission, provided that accurate acknowledgement of source is made. Requests for permission for extended quotation from or reproduction of this manuscript in whole or in part may be granted by the Competent Authority of HBNI when in his or her judgment the proposed use of the material is in the interests of scholarship. In all other instances, however, permission must be obtained from the author.

Manju Taxak

DECLARATION

I, hereby declare that the investigation presented in the thesis has been carried out by me. The work is original and has not been submitted earlier as a whole or in part for a degree/ diploma at this or any other Institution / University.

Manju Taxak

Dedicated to……..

My Parents

ACKNOWLEGEMENT

Firstly, I would like to pay my prime gratefulness to **Almighty God** whose blessings powered me to complete my work. I feel immense pleasure to express my intense gratitude to my esteemed supervisor, **Professor N. Krishnamurthy**, and Co-guide, **Professor A.K. Suri** for their valuable guidance, constant encouragement and active support during my research work. Their inspiration for intuitive analysis and more than all their readiness to comply for extensive discussions at every stage of this work needs special admiration. I am equally thankful to **Dr. G.P. Tiwari** for his constant suggestions from the stage of planning and execution of the work.

I am highly thankful to **Dr. Alok Awasthi, Dr. R.N. Singh, Dr. R. Tewary, Dr. Sanjay Kumar** for their grateful help by providing necessary facilities and helpful discussion during my research work. My sincere thanks are due to **Mr. D. K. Sahoo, Dr. T.S.R.Ch. Murthy, Mr. Jitendra Sonber** and **Dr. Abhishek Mukherjee** for their valuable suggestions and support. Huge thanks to **Mr. Yatin Thakur** for his valuable help in redrawing the figures for thesis.

Special thanks go to **Dr. R. Kameswaran, Mr. B. Kalekar, Mrs. S. Smita**, ACD, BARC, and to **Dr. M. Arunachalam**, Head, NCCCM, Hyderabad for helping in chemical analysis. Thanks go to **Dr. Sanjay Rai,** RRCAT, Indore for XRD analysis and **Mr. Bhaskar Paul** and **Mr. Jitendra Kumar** for SEM and EDX analysis.

It gives me immense pleasure to thanks the members of the doctoral committee **Prof. D. Das** (Chairman), **Prof. K.L. Ramakumar** (Member), **Prof. S. R. Bharadwaj** (Member) and **Dr. S. Ramanathan** for their critical review and suggestions during the progress review and pre-synopsis viva-voce. I would like to thank to all those members of materials group, who helped me directly or indirectly during my research work.

I am greatly indebted to my school teachers, **Science Master Dhyansingh** and **Master Rohtas Singh** for their precious direction during my school days. I owe my deepest gratitude to **Prof. S.P. Khatkar** and **Prof. K.K. Verma** from M.D.U. Rohtak and **Mrs Anupama Gupta** (Chemistry lecturer) from JVMGRR College, Ch. Dadri for their valuable guidance and encouragement during M.Sc. and B.Sc.

I would like to express my enormous feeling of thanks to my maternal uncle, **Ex-Headmaster Dharamveer Singh**, and **Omveer Singh** for their continuous inspiration and affection since my childhood.

My thanks are also due to my dear friends **Sonu Taxak, Janesh, Swait, Anil, Neelam, Niharika, Vikas, Jigyasha, Poulami, Deepak** and all those friends who helped me in difficult stages during the work.

Finally, I am heartily thankful to **My Parents** who are the **authentic God** for me, for giving me this opportunity and their faith, love, inspiration and continuous moral supports. My great thanks go to my charming sisters **Dimpal, Dr. Sunita, Anju** and lovely brother **Kulvir Taxak** for their continuous co-operation, care, understanding and encouragement. Without their support, it would have been extremely difficult to complete this project. I am thankful to my **Booaa Ji** and my all relatives for their moral supports during my study and to achieve this stage of my life. A special thank goes to my **Parents in-law** and **Grandmother In-law** for motivating me during my research work. Last but most importantly, I am tremendously thankful to my loving husband, **Ashok Bhakar** for helping me in various issues relating with the manuscript preparation to the thesis writing including scientific discussion, papers communication, and data analysis. His mental support, encouragement, care, Patience and unwavering love were definitely the bedrock for me upon which I have completed my thesis project work.

Manju Taxak

CONTENTS

TITLE **Page No.**

Abstract i

Synopsis iii

List of Publications xvii

List of Figures xix

List of Tables xxv

Acronyms xxvii

1 Introduction 1 – 28

1.1 Background 1

1.2 The Refractory Metals 10

1.3 Tantalum 10

1.3.1 Physical and Mechanical Properties of Pure Tantalum 11

1.3.2 Chemical Properties of Pure Tantalum 13

1.3.3 Applications of Tantalum 14

1.4 Tantalum-Hydrogen System 15

1.5 The Nature and Location of Hydrogen in Metals 16

1.6 Metals-Hydrogen Interaction 18

1.7 The Mechanism of Hydrogen Absorption in Metals 22

1.8 Research Objectives and Methodology 27

1.9 Overview of the Thesis 27

2 Literature Review 29 – 59

2.1 Introduction 29

2.2 Solubility of Hydrogen in Metals 29

2.2.1 Dependence of Hydrogen Solubility on Pressure 34

2.2.2 Dependence of Hydrogen Solubility on Temperature 35

2.3 Diffusion of Hydrogen in Metals 37

2.4 Permeability of Hydrogen in Metals 40

2.5 Tantalum as hydrogen permeation membrane 43

2.6 Thermodynamics of Hydrogen in Metals 47

2.7 Mechanism and Kinetics of Hydrogen Entry into Metallic Systems 54

2.8 Summary 59

3 Experimental Techniques 61 – 87

3.1 Introduction 61

3.2 Materials Preparation 61

3.2.1 Preparation of Alloys by Arc Melting Technique 61

3.2.2 Analysis of the Samples 63

3.2.3 Samples Cutting and Preparation for Hydrogen Charging 64

3.3 Equipment Used for Hydrogen Charging 64

3.3.1 Sievert’s Apparatus 64

3.3.2 Hydrogen Generator 67

3.4 Procedure for Hydrogen Charging 69

3.4.1 Procedure for P-C-T Equilibrium Hydrogen Measurement 69

3.4.2 Procedure for Hydrogen Absorption Kinetics Study 70

3.5 Analytical Techniques 71

3.5.1 Glow Discharge-Quadrupole Mass Spectrometry (GD-QMS) 71

3.5.2 Inert Gas Fusion (IGF) Technique 72

3.5.3 X-Ray Diffraction (XRD) 75

3.5.4 Scanning Electron Microscopy (SEM) 76

3.5.5 Energy-Dispersive X-ray Spectroscopy (EDS/EDX) 77

3.5.6 Vickers Hardness 78

3.6 Methods Used for the Solubility, Thermodynamics and Kinetics Studies 80

3.6.1 Hydrogen Solubility Calculation 80

3.6.1.1 Using Pressure Drop Method 80

3.6.1.2 Using Gas Law 80

3.6.1.3 Using Gravimetric Techniques 81

3.6.2 Estimation of Enthalpy of Solution for Hydrogen in Ta and Ta-Alloys from P-C-T Data 82

3.6.2.1 Application of Vant's Hoff Equation 82

3.6.2.2 Use of Sievert's Law 84

3.6.3 Kinetics Equation 85

3.6.3.1 The Rate Equation for the Kinetics of Solid-Gas Reaction 85

3.6.3.2 Arrhenius Equation 87

3.7 Summary 87

4 Results and Discussion 89 – 144

4.1 Introduction 89

4.2 Materials Characterization 90

4.3 Hydrogen Solubility in Tantalum 100

  4.3.1 Change in Lattice Parameter of Tantalum due to Dissolved Hydrogen 100

    4.3.1.1 Ta-H System - Increase in the Lattice Parameter 104

  4.3.2 The Equilibrium P-C-T Data for Ta-H System 105

4.4 Solid Solubility of Hydrogen in Ta–X Alloys (X = Ni, Cr, Fe, and Al) 106

  4.4.1 Thermodynamics Parameters for the Ta-X-H System (X = Ni, Cr, Fe and Al) 124

  4.4.2 Discussion on Hydrogen Solubility in Ta-X Alloys (X = Ni, Cr, Fe and Al) 131

    4.4.2.1 Thermodynamics Consideration 131

    4.4.2.2 Electronic Contribution 132

    4.4.2.3 Atomic Size Consideration 135

    4.4.2.4 Chemical Behavior of Alloying Elements 137

4.5 Summary 143

5 Hydrogen Absorption Kinetics of Ta-Al Alloys 145 – 169

5.1 Introduction 145

5.2 Theory of Gas-Solid Reaction Kinetics 145

5.3 Reaction Models for Hydrogen Absorption 151

5.4 Kinetic Equations 157

5.5 Hydrogen Absorption Curves 158

5.6 Reaction Mechanism 162

5.7 Activation Energy 165

5.8 Summary 169

6 Conclusions and Recommendations 171-173

6.1 Conclusions 171

6.2 Suggestions for Further R&D Work 172

7 References 175 – 186

ABSTRACT

Tantalum is a potential candidate material for the hydrogen separation membrane due to its large hydrogen solubility and good hydrogen diffusivity. The permeability is a product of solubility and diffusivity. The hydrogen solubility in tantalum and its alloys is one of the parameters responsible to estimate the permeability. The hydrogen embrittlement associated with tantalum at low temperature is the main limitation of its use in membrane applications. Alloying with the elements which are having less hydrogen solubility or destabilize the hydrides can be a way to overcome this limitation. In the present work, the effect of nickel, chromium, iron and aluminium on the solubility of hydrogen in tantalum has been investigated. Ta-alloys with Ni, Cr, Fe and Al within solid solubility limit were prepared using arc melting in an inert atmosphere. Pressure-composition-isotherms (*P-C-T*) equilibrium measurements have been investigated in the temperature range (673-873) K for Ta-H and Ta-M-H systems [M = Ni, Cr, Fe and Al] using a Sievert's apparatus. The dissolved hydrogen was within the solid solubility range corresponding to the temperature and followed the Sievert's law. From the equilibrium *P-C-T* data, the thermodynamic parameters: the relative partial molar enthalpy, entropy and Gibb's free energy for the solution of hydrogen in these alloys are evaluated using Sievert's relationship. The hydrogen solubility in tantalum-alloys decreases with increase in the alloying elements composition. This decrease in solubility is attributed to increase in lattice strain energy of the alloys or due to very less solubility of hydrogen in these elements or the chemical inertness of these alloying elements towards the hydrogen. The relative partial molar enthalpy becomes less negative with increase in alloying elements composition whereas entropy values are almost constant.

In addition, the isothermal hydrogen absorption kinetics of unalloyed tantalum and tantalum-aluminium alloys has been investigated in the temperature range of (673-973) K. The reacted fraction of hydrogen, α, was calculated from the experimental data of hydrogen absorption in different tantalum-aluminium alloys as a function of time using pressure drop method. The function $g(\alpha)$, giving the best linearity with time is indicative of the mechanism of hydrogen absorption. The rate function of hydrogen absorption and the kinetic parameters are obtained from the linear regression fitting of $g(\alpha)$ versus time plots. The mechanism of three-dimensional diffusion is the intrinsic rate-limiting step of hydrogen absorption processes in the studied temperature range. The apparent activation energy for the absorption of hydrogen in these alloys also calculated using Arrhenius equation that increases linearly with increase in the aluminium content in the alloys.

The thermodynamic and kinetics data for the solution of hydrogen in tantalum and its alloys can be used to process the design for Ta-based materials for various hydrogen atmosphere applications and can also be utilized in various modeling studies for hydrogen solubility and permeability.

Keywords: Tantalum; Alloying elements (Ni, Cr, Fe and Al); Hydrogen solubility, Sievert’s constant, Thermodynamics parameters, Hydrogen absorption kinetics, Activation energy.

SYNOPSIS

Introduction

The development of hydrogen based energy utilization is attractive in view of attendant benefits such as reduction in the global warming and minimization of investment in infrastructure and energy cost [1]. In this situation, the advances in the technology for production, purification, storage and supply of hydrogen will become increasingly important [2-3]. Hydrogen separation techniques also find applications in chemical, petrochemical, microelectronic industries, fuel cells and “Vision 21” program of DOE [4-5]. This is creating a persistent interest in developing economically feasible methods for the hydrogen purification/separation. However, the development of hydrogen separation membrane is an important technical issue. The rapid development of membrane reactors and fuel cells has witnessed increasing interest in dense composite membranes for hydrogen separation and purification [6-7]. The ideal hydrogen separation/purification membrane should have high hydrogen permeability and good mechanical properties [8] and should be capable of functioning in a flowing gas at high temperature and high pressure. Tantalum is a promising material as a component in hydrogen separation membranes operating at a range of temperatures and pressures [4, 7, 9]. It has high hydrogen permeability [4]. Compared to palladium, it is cheaper and possesses order of magnitude larger hydrogen permeability [4].

Literature Review

Two main limitations of tantalum metal to be commercially usable as a permeable membranes material are its tendency for surface oxidation and for hydrogen embrittlement [4, 7-8]. Surface oxidation of tantalum can be minimized by coating with

Pd [10]. Hydrogen embrittlement problem arises from the change of lattice parameter or formation of hydrides [10]. Therefore, for a given temperature and pressure, reducing the hydrogen solubility could be considered as an approach to preserve mechanical properties of the membrane [11]. Alloying can be an effective way to control the hydrogen solubility without varying other parameters like temperature or hydrogen pressure. The effect of Fe, Al, Ni, Cr, Mo, Cu, Pd, and Sn on the solubility and permeability of group V elements, vanadium and niobium have been earlier investigated and reported in the literature. In all of these cases, the experiential solubility and permeability is inferior to that of pure metal. Importantly, however, the embrittlement resistance and durability of these alloys are much better than the pure metal, while the permeability is still greater than the leading palladium alloy [11-16]. As permeability is a product of solubility and diffusivity, therefore, measuring the solubility of hydrogen in Ta and its alloys highlights one of the parameters that determines the permeability. Moreover, the solubility measurement also helps to obtain thermodynamic parameters for the solid solution of hydrogen in tantalum and its alloys.

Thermodynamic quantities for Ta-H system have been reported by many investigators using experimentally determined P-C-T curves and it was found that the relative partial molar enthalpies, $\overline{\Delta H_H}$ and entropies, $\overline{\Delta S_H}$, of hydrogen are virtually constant with respect to temperature for a given concentration in the considered temperature range [17-24].

The present work aims to evaluate the effect of Ni, Cr, Fe and Al (within solid solubility limit in Ta matrix) as alloying element on the solubility of hydrogen in bcc tantalum and on the thermodynamic parameters of Ta-H system. This information has not been previously reported in the literature. Solid solution alloys avoid the hydrogen embrittlement which occurs in a two-phase alloy. Isothermal as well as isobaric P-C-T equilibrium measurements have been investigated in the temperature range of 673 – 873 K and the hydrogen pressure range of 0.6-1.2 atmospheres for tantalum and its solid solution alloys mentioned above at different compositions. The thermodynamic parameters - relative partial molar enthalpy, entropy and Gibb's free energy for solutions of hydrogen in tantalum alloys were also calculated.

Experimental Techniques

Sample Preparation

Various alloys of tantalum (Ta-Al, Ta-Cr, Ta-Fe and Ta-Ni) within solid solubility range were prepared using arc melting in an inert atmosphere. To prepare these alloys, high purity (>99.8%), Aldrich make tantalum foil and Al, Cr, Ni and Fe thin sheets were used. The melting was repeated 6-10 times to make the alloys homogeneous. The alloy was obtained in a button form. It was cold rolled to 0.3 mm thickness and cleaned with acetone. After rolling, the sheets were cut into small specimens using an EDM cutting machine. Before hydrogen charging, all the samples were cleaned chemically using an acid solution ($HF:HNO_3:H_2SO_4::2:2:5$) and mechanically polished on emery paper followed by cleaning with acetone. The homogeneity of the alloys was checked by measuring their Vickers Hardness and by line scans SEM-EDS analysis. The elemental compositions of all samples were analyzed by Glow Discharge - Quadrupole mass Spectrometry (GD-QMS). Phase characterizations of the alloys were performed using X-ray diffraction (XRD).

Hydrogen Charging

A Sievert's apparatus was used for both hydrogen solubility and kinetic studies. The sample was placed into a quartz sample holder which was then kept inside the reaction chamber. A high vacuum, of the order of 10^{-6} torr, was created inside the system using rotary and diffusion pumps. The sample was heated at 1183 K under this high dynamic vacuum condition to activate the sample surface. The system was backfilled with hydrogen and then cooled down to room temperature. The temperature was further raised to 1183 K and then system was re-evacuated to 10^{-6} torr to release the entire hydrogen from the sample. This process was repeated several times. The process is commonly employed to activate the sample before hydrogen charging by introducing micro cracks. The sample was then cooled up to the required temperature. To obtain isothermal PCT curves, hydrogen was introduced into the system from the hydrogen generator at the constant temperature and to a predetermined pressure level (initial pressure reading). The sample started absorption of hydrogen at a fixed temperature and drop in the system pressure was observed. After some time, pressure inside the system became constant. When constant pressure was observed continuously for 24 hrs, then it was assumed that equilibrium has been achieved in the system (final pressure reading). Equilibrium values were confirmed by repeating the cycles. At the end of the run, the furnace was switched off and removed away from the reaction chamber and the valve connecting the sample holder to the remaining system was disconnected. The reaction chamber was rapidly cooled by quenching so that hydrogen absorption during cooling could be minimized. Sample was taken out from the tube. The amounts of hydrogen dissolved in the samples were determined by inert gas fusion technique, and the results were checked against the value obtained by pressure drop method.

To investigate the kinetics of hydrogen absorption in the Ta-Al alloys, the changes in pressure values with time at a constant temperature were noted and the fraction reacted / fraction absorbed (α) of hydrogen was calculated.

Results and Discussion

Effect of Ni, Cr, Fe and Al as alloying elements on the solubility behavior of hydrogen in tantalum

XRD pattern of Ta-alloys indicated that all the alloys are single phase bcc solid solution. Addition of the alloying elements to tantalum shifted the pure Ta peaks toward the higher 2θ values which indicate that lattice parameter of Ta has decreased on the addition of these elements. Scanning Electron Microscopy (SEM) and EDS analysis of alloys indicate that alloys are homogeneous and there is no other phase formation. Ta-H phase diagram [17], shows that at temperature higher than 334 K, a single homogeneous α-phase exists in which metal atoms occupy a bcc lattice. In our study, all the experiments are carried out at temperature above 334 K and the dissolved hydrogen is observed within the solid solubility limit and following the Sievert's law which states that

$c \alpha \sqrt{p}$

or

$c = K_s \sqrt{p}$

or

$K_s = c / \sqrt{p}$

Where, c is the amount of dissolved hydrogen, p is the hydrogen gas pressure, and K_s is the Sievert's constant.

The square root dependence follows from the fact that hydrogen dissolves in atomic form in the host matrix [12]. The effects of alloying elements are observed in isobaric as well as in isothermal P-C-T measurements which indicate that solubility of hydrogen in Ta decrease with increasing content of alloying elements. That the dissolution follows Sievert's law is confirmed from the linear behavior of isothermal P-C-T curves.

The decrease in hydrogen solubility may be due to change in strain energy of dissolved hydrogen due to presence of different size interstitial sites around a substitutional atom. It may be attributed to repulsive interaction between H and alloying atoms [15]. According to Pauling, the atomic radii of Ta, Ni, Cr, Fe and Al are 146, 124, 128, 126 and 143 pm respectively. The lattice parameter of Ta decreases with the addition of these atoms. Therefore, the lattice size and interstitial sites size decrease and hence solubility decrease. The decrease of hydrogen solubility in Ta-alloys could be explained due to increase in lattice strain energy as proposed by Brodowsky [25]. The change in electronic structure may also be responsible for change in the hydrogen solubility. The electronic effects appear to be more important in controlling the overall solubility in the matrix. Several investigators have discussed the possibility of a correlation between the effective free electron concentration of an alloying addition and its effect on the solubility of hydrogen in base metal. Hence, for given hydrogen pressure, if partial molar enthalpy of electrons is increased on the addition of alloying elements, the concentration of dissolved hydrogen will decrease. In the present study, electron factor does not seem to be more important, the electronegativity of Ta being smaller than all of these alloying elements (Ni, Cr, Fe and Al).

Thermodynamic parameters for the solubility of hydrogen in Ta and Ta-alloys

The K_s values were calculated using Sievert's law for the solution of hydrogen in Ta and Ta-alloys at three different temperatures and at one atmosphere hydrogen pressure. The Sievert's constant (K_S) is related with change in enthalpy, $\overline{\Delta H_H}$ and change in entropy, $\overline{\Delta S_H}$ of the solution for hydrogen [26] by the following relations,

$$K_s = {c}/{\sqrt{p}} = \exp\left(-\frac{\overline{\Delta H_H}}{RT}\right)\exp\left(\frac{\overline{\Delta S_H}}{R}\right)$$

or

$$\log K_s = \log\frac{c}{\sqrt{p}} = -\frac{\overline{\Delta H_H}}{4.575T} + \frac{\overline{\Delta S_H}}{4.575}$$

From the slope and intercepts of log K_S vs 1/T (K) plots, the values of relative partial molar enthalpy and entropy of solution of hydrogen can be calculated. The relative partial molar Gibb's free energy is related with the relative partial molar enthalpy, $\overline{\Delta H_H}$ and the relative partial molar entropy, $\overline{\Delta S_H}$ by the following relation:

$$\overline{\Delta G_H} = \overline{\Delta H_H} - T\overline{\Delta S_H}$$

Thus, using the $\overline{\Delta H_H}$ and $\overline{\Delta S_H}$ values, the relative partial molar Gibb's free energy could also be calculated at different temperatures. The enthalpy of solution for hydrogen in tantalum is increasing with increase in the content of alloying element in tantalum matrix while entropy values are nearly constant.

Hydrogen absorption kinetics of Ta-Al alloys

The reaction mechanism for the absorption of hydrogen in the metals and alloys involves the following steps: gas-phase mass transport of hydrogen on the alloy surface, physisorption of hydrogen gas molecules, dissociation of hydrogen molecules into atomic form and chemisorption on the surface, surface penetration of hydrogen atoms, hydrogen atoms diffusion through the hydride layers and hydride formation.

The slowest among these steps is the rate determining step. Generally the method used to study the kinetics is to fit the time dependent reacted fraction (α) to various analytical rate expressions, through which reaction mechanism and intrinsic rate limiting steps are determined [27].

The rate equation for the kinetics of solid-gas reaction is expressed as follows:

$$\frac{d\alpha}{dt} = kf(\alpha)$$

Where, α is the reacted fraction at time t, k is rate constant, f(α) is a function determining the mechanism of the reaction and g(α) is the integral form of f(α), i.e.

$$g(\alpha) = \int \frac{d\alpha}{f(\alpha)} = kt$$

Based on experimental data of hydrogen absorption curve, the reacted fraction, α can be calculated as follow:

$$\alpha = \frac{p_0 - p_t}{p_0 - p_{eq}}$$

Where, p_0 is the initial pressure, p_t is the pressure at time t and p_{eq} is the final equilibrium pressure.

The function g(α) giving the best linearity with time is considered as the mechanism for hydrogen absorption in Ta-Al alloys. The rate function of hydrogen absorption and the kinetic parameters k are obtained from the linear regression fitting. The apparent activation energy for hydrogen absorption in these alloys is calculated using Arrhenius equation

$$k = Ae^{-E_a/RT}$$

or

$$\ln k = \ln A - \frac{E_a}{RT}$$

Where, A is the pre-exponential factor, R is the molar gas constant (J/mol K), T is the process temperature (K) and E_a is the apparent activation energy of the process (kJ/mol).

When rate constants at different temperatures are extracted from hydrogen absorption curves for Ta-alloys, the E_a for hydrogen absorption can be obtained from the slope of lnk vs 1/T plots. The apparent activation energy for the absorption of hydrogen by tantalum is increasing with increase in the alloying content in tantalum.

Direction for Future Work, Summary and Conclusions

Direction for Future Work

Tantalum is considered as a potential candidate material for hydrogen separation membrane functioning in a flowing gas at high temperature and high pressure for the separation of hydrogen from a mixture of gases. In the present thesis, the investigation is carried out on the solubility of hydrogen in various tantalum alloys with nickel, chromium, iron and aluminium at different compositions.

To evaluate the use of tantalum alloys for membranes for hydrogen permeation, further investigations are also required. These are on direct experimental determination of permeability, evaluation of mechanical properties of tantalum alloys before and after hydrogen loading, as a function of temperature. Finally, the use of tantalum and tantalum alloys membranes in actual devices for hydrogen separation.

Summary & Conclusions

- ☐ Vacuum arc melting is a suitable technique for the preparation of homogeneous tantalum alloys with nickel, chromium, iron and aluminium.
- ☐ The solubility of hydrogen in tantalum and its alloys is obeying the Sievert’s law in the considered temperature range (673 K-873 K) and it is decreasing on the addition of nickel, chromium, iron and aluminium as alloying elements.
- ☐ The decrease in solubility may be attributed to increase in lattice strain energy and due to increase in e/a ratio. The decrease in lattice parameter of tantalum on the addition of alloying elements decreases the size of interstitial sites and hence, hydrogen solubility.
- ☐ The solubility of hydrogen in tantalum and tantalum-alloys increases with increase of hydrogen pressure but the solubility decreases with increase in temperature. This is also reflected by exothermic solution of hydrogen in all these samples.
- ☐ The relative change in enthalpy for the solution of hydrogen in tantalum increases with increase in concentration of these alloying elements whereas entropies values are nearly constant.
- ☐ The $\overline{\Delta H_H}$ and $\overline{\Delta S_H}$ values are constant in the considered temperature range (673 K - 873 K) and virtually independent of dissolved hydrogen concentration (0.367 wt % - 0.068 wt %).

- ☐ The apparent activation energy for the solution of hydrogen in tantalum is increasing on the addition of aluminium as alloying elements in tantalum.

References

[1] Michael Hirscher, Handbook of Hydrogen Storage, WILEY-VCH Verlag Gmbh & Co. KGaA, Weinheim, 2010.

[2] T. M. Adams, J. Mickalonis, Hydrogen permeability of multiphase V–Ti–Ni metallic membranes, Materials Letters 61 (2007) 817–820.

[3] B. Ernst, S. Haag, M. Burgard, Permselectivity of a nickel/ceramic composite membrane at elevated temperatures: A new prospect in hydrogen separation? Journal of Membrane Science 288 (2007) 208–217.

[4] K.S. Rothenberger, B.H. Howard, R.P. Killmeyer, A.V. Cugini, R.M. Enick, F. Bustamante, M.V. Ciacoo, B.D. Morreale, R.E. Buxbaum, Evaluation of tantalum-based materials for hydrogen separation at elevated temperatures and pressures. Membrane Sci 218 (2003) 19–37.

[5] S.-Y. Jeon, D.-K. Lim, M.-B. Choi, E.D. Wachsman, S.-J. Song, Hydrogen separation by Pd–$CaZr_{0.9}Y_{0.1}O_{3-\delta}$ cermet composite membranes, Separation and Purification Technology 79 (2011) 337– 341.

[6] Y. Zhang, R. Maeda, M. Komaki, C. Nishimura, Hydrogen permeation and diffusion of metallic composite membranes, Journal of Membrane Science 269 (2006) 60–65.

[7] S. M. Kim, D. Chandra, N. K. Pal, M. D. Dolan,W. M. Chien, A. Talekar, J. Lamb, S.N. Paglieri, T. B. Flanagan, Hydrogen permeability and crystallization kinetics in amorphous Ni-Nb-Zr alloys, International Journal of Hydrogen Energy, 37 (2012) 3904-3913.

[8] S. Hara, N. Hatakeyama, N. Itoh, H.M. Kimura, A. Inoue, Hydrogen permeation through amorphous -Zr36−xHfxNi64- alloy membranes, Journal of Membrane Science 211 (2003) 149–156.

[9] R. Grena, M. Celino, P. Tarquini, “DFT study of interstitial hydrogen in tantalum lattice”, Int. J. Hydrogen Energy, 36 (2011) 13858–13865.

[10] N. M. Peachey, R. C. Snow, R. C. Dye, Composite Pd/Ta metal membranes for hydrogen separation, Journal of Membrane Science, 111 (1996) 123-133.

[11] K. H. Kim, J. H. Shim, B. J. Lee, Effect of alloying elements (Al, Co, Fe, Ni) on the solubility of hydrogen in vanadium: A thermodynamic calculation, International Journal of Hydrogen Energy, 37 (2012) 7836 – 7847.

[12] M. Amano, M. Komaki and C. Nishimura, Hydrogen permeation characteristics of Pd-coated V-Ni alloy membrane, Journal of the Less-Common Metals, 172-174 (1991) 727-731.

[13] Y. Zhang, T. Ozaki, M. Komaki, C. Nishimura, "Hydrogen permeation characteristics of vanadium-aluminum alloys", Scripta Mater., 47 (2002) 601–606.

[14] R. Burch and N. B. Francis, Pressure-Composition-Temperature relationships in niobium alloy-hydrogen systems. J Less-Common Metals 49 (1976) 371-384.

[15] A. Inoue, M. Katsura and T. Sano, The solubility of hydrogen in Nb-Mo alloy. J Less-Common Metals 55 (1977) 9-23.

[16] J. F. Lynch, J. J. Reilly and F. Millot, The absorption of hydrogen by binary vanadium-chromium alloys. J Phys. Chem. Solids 39 (1978) 883-890.

[17] A San-Martin and F D Manchester, The H-Ta (Hydrogen-Tantalum) System. J Phase Equilibria 12 (3) (1991) 332-343.

[18] M.W. Mallett and B.G. Koehl, J. Electrochem. Thermodynamic Functions for the Tantalum-Hydrogen System. Soc. 109 (1962) 611-616.

[19] E. Veleckis and R.K. Edwards, Thermodynamic Properties in the Systems Vanadium-Hydrogen, Niobium-Hydrogen, and Tantalum-Hydrogen. J. Phys. Chem. 73(3) (1969) 683-692.

[20] P. Kofstad, W.E. Wallace, and L. J. Hyvonen, Thermodynamics of Formation of Tantalum-Hydrogen Solid Solutions from Vapor Pressure Data. J. Am. Chem. Soc. 81(19) (1959) 5015-5019.

[21] J.A. Pryde and I.S.T. Tsong, Thermodynamic Functions and Phase Diagrams of Tantalum-Hydrogen and Tantalum + Deuterium Systems. Trans. Faraday Soc. 67 (1971) 297-304.

[22] Philippe Lecocq and Charles Wert, Equilibrium in Hydride formation in

Tantalum. Thin solid Films, 25 (1975) 77-84.

[23] O. J. Kleppa, P. Dantzer, and M. E. Melnichak, High-temperature thermodynamics of solid solutions of hydrogen in bcc vanadium, niobium, and tantalum. J. Chem. Phys. 61 (10) (1974) 4048-4058.

[24] P.G. Dantzer and O.J. Kleppa, High-Temperature Thermodynamics of Dilute Solutions of Hydrogen and Deuterium in Tantalum and in Dilute Tantalum-Oxygen Solid Solutions. J. Solid State Chem. 24 (1978) 1-9.

[25] H Brodowsky, Non-ideal solution behaviour of hydrogen in metals. Ber. Bunsenges. Phys. Chem. 76 (1972) 740-746.

[26] J.D.Fast, Interaction of metals and Gases, vol.1, Thermodynamics and Phase Relations, Macmilllan Press Ltd., London and Basingstoke, Philips, 1965.

[27] K.C. Chou, Q. Li, Q. Lin, L.J. Jiang, K.D. Xu, Kinetics of absorption and desorption of hydrogen in alloy powder. Int. J. Hyd. Energy, 30 (2005) 301-309.

List of Publications

Journals Papers

[1] **Manju Taxak**, S. Kumar, S. Sheelvantra, N. Krishnamurthy, Effect of iron on the solubility of hydrogen in tantalum, **Journal of Materials Science**, Accepted. DOI: 10.1007/s10853-014-8557-9

[2] **Manju Taxak,** Sanjay Kumar, N. Krishnamurthy, Thermodynamic Parameters for the Ta-Cr-H Solid Solution from Equilibrium P-C-T Data, **J. Chem. Thermodynamics**, 67 (2013) 48-54.

[3] **Manju Taxak**, S. Kumar, B. Kalekar, N. Krishnamurthy, Effect of nickel addition on the solubility of hydrogen in tantalum, **Int. J. Hydrogen Energy**, 38 (2013) 7561-7568.

[4] **Manju Taxak,** Sanjay Kumar, N. Krishnamurthy, A.K Suri, G.P.Tiwari, Change in lattice parameter of tantalum due to dissolves hydrogen, **Int. J of Processing and Application of Ceramics**, 6(2) (2012) 73-76.

[5] **Manju Taxak**, N. Krishnamurthy, Effect of Aluminum on Hydrogen Absorption Kinetics of Tantalum, **Journal of alloys and compounds**. Revision required.

[6] **Manju Taxak**, S. Kumar, N. Krishnamurthy, Thermodynamic Parameters for the Solubility of Hydrogen in Tantalum-Aluminium Alloys, To be communicated.

Conference Papers

[1] **Manju Taxak**, S. Kumar, B. Kalekar, S. Smita, N. Krishnamurthy, “Effect of Aluminium on Hydrogen Solubility in Tantalum” **Hydrogen and Fuel Cells Conference-2013**. Accepted. Held in Napa Valley, California. July 12-15, 2013.

[2] **Manju Taxak**, S. Kumar, S. Smita, B. Kalekar, N. Krishnamurthy, “The Effect of Iron on the Solubility Behavior of Hydrogen in Tantalum” **Proceedings of 5th International Conference on Hydrogen Safety**, Brussels, Belgium, September 9-11, 2013. ID: 100, P. 112.

[3] **Manju Taxak**, S. Kumar, S. Smita and B. Kalekar, “Solid Solubility of Hydrogen in Ta-Cr Alloys” **Proceedings of DAE-BRNS 4th Interdisciplinary Symposium on Materials Chemistry**, Editors: D. Tyagi, A.M. Banerjee, K. Bhattacharyya, S. Nigam, S. Verma, A.K. Tripathi, D. Das, Mumbai, India 2012. P. 157-158.

[4] **Manju Taxak**, S. Kumar, B. Kalekar, S. Smita, N. Krishnamurthy, A K Suri and G.P Tiwari, Solid Solubility of Hydrogen in Ta-Ni alloys, **Proceedings of National Symposium on Materials and Processing**, Editors: A. Ghosh, A.K. Sahu, C.S. Vishwanadhan, S. Ramnathan, R.C. Hubli, G.P. Kothiyal, Mumbai, India 2012. P. 311-313.

[5] **Manju Taxak,** S. Kumar, A. Mukherjee, N. Krishnamurthy and A. K. Suri “Lattice expansion of tantalum due to dissolved hydrogen” **Proceeding of the 18th International Symposium on Thermal Analysis,** Editors: R. Agrawal, L Varshney, Y.K Bhardwaj, R.A Jat, S.K Rakshit, K.L Ramkumar, Mumbai, India 2012. P. 333-335.

List of Figures

S. No.	**CAPTIONS**	**Page No.**
Fig. 1.1	Hydrogen energy system	6
Fig. 1.2	Ta-H phase diagram	16
Fig. 1.3	Octahedral sites and tetrahedral sites in FCC, HCP and BCC lattice	17
Fig. 1.4	Schematic of one-dimensional Lennard-Jones potential energy diagram of hydrogen approaching a metallic surface	19
Fig. 1.5	One dimensional potential energy diagram for (I) a hydrogen atom and(II) for a hydrogen molecule approaching a metal surface	19
Fig 1.6	Schematic representation of hydrogen absorption mechanism	23
Fig. 2.1	Hydrogen solubility in several transition elements at gaseous hydrogen pressure of 1 atm.	31
Fig. 2.2	Pressure-composition isotherm for Ta-H system	33
Fig. 2.3	Diffusion coefficient of hydrogen in several transition metals	38
Fig. 2.4	Diffusion coefficients of H and D in the V, Nb, Ta and Pd	39
Fig. 2.5	Hydrogen permeability in several transition elements	42
Fig. 2.6	Schematic pressure - composition isotherm	47
Fig. 2.7	Schematic P-C-T diagram at different temperature $(T_1<T_2<T_3<T_c)$, and the van’t Hoff plot.	49

Fig. 2.8 Pressure-composition-isotherms for the Ta-H system 53
Fig. 2.9 Thermodynamic data for Ta-H system [69Vel] 54
Fig. 2.10 Hydrogen absorption isotherms of tantalum at various temperatures 55
Fig. 2.11 $log(a/(a-x))$ vs. time plot for tantalum hydriding at different temperatures 56
Fig. 2.12 Temperature dependence of the hydrogen absorption rate of three typically prepared tantalum specimens 57
Fig. 2.13 Typical variation of $1/\sqrt{p}$ as a function of time for the rate of evolution of hydrogen from tantalum wire at different temperatures 58
Fig. 2.14 Logarithms of the slopes of the curves in Fig. 2.13 plotted as a function of reciprocal temperature 58
Fig. 3.1 Arc melting furnace connected with vacuum pump 63
Fig. 3.2 Sievert's apparatus 65
Fig. 3.3 A block diagram of Sievert's apparatus 66
Fig. 3.4 Schematic of capacitance manometer 66
Fig. 3.5 Schematic GDMS Probe Tip 71
Fig. 3.6 A flow chart for hydrogen analysis 73
Fig. 3.7 A flow chart for oxygen and nitrogen analysis 74
Fig. 3.8 (a) A Vickers hardness tester (b) Schematic diagram of Vickers hardness test 78
Fig. 4.1 (a) & (b) As prepared alloy buttons and (c) & (d) Pieces of alloys after EDM machining 90

Fig. 4.2 SEM micrograph and EDS analysis of the Ta – 1.7 Ni alloy 92

Fig. 4.3 SEM micrograph and EDS analysis of the Ta – 2 Cr alloy 93

Fig. 4.4 SEM micrograph and EDS analysis of the Ta – 3.2 Fe alloy 93

Fig. 4.5 SEM micrograph and EDS analysis of the Ta – 2.4 Al alloy 93

Fig. 4.6 Ta-Ni phase diagram 95

Fig. 4.7 Ta-Cr phase diagram 96

Fig. 4.8 Ta-Fe phase diagram 96

Fig. 4.9 Ta-Al phase diagram 97

Fig. 4.10 (a) XRD pattern of Ta and Ta-Ni alloys (b) Shifting of 211 peak position with Ni content 98

Fig. 4.11 (a) XRD pattern of Ta and Ta-Cr alloys (b) Shifting of 211 peak position with Cr content 98

Fig. 4.12 (a) XRD pattern of Ta and Ta-Fe alloy (b) Shifting of 211 peak position with Fe content 99

Fig. 4.13 (a) XRD pattern of Ta and Ta-Al alloys (b) Shifting of 211 peak position with Al content 99

Fig. 4.14 XRD pattern of pure and hydrogen charged Ta specimens 101

Fig. 4.15 Lattice parameter of tantalum as a function of the dissolved hydrogen concentration 103

Fig. 4.16 The relative change in lattice parameter of Ta-H alloys as a function of hydrogen concentration 104

Fig. 4.17 Schematic representation of H in metals 105

Fig. 4.18 Experimental data for solubility of hydrogen in tantalum is shown on Ta-H phase diagram 106

Fig. 4.19 Amount of hydrogen dissolved in tantalum with respect to nickel concentration in tantalum 109

Fig. 4.20 Amount of hydrogen dissolved in tantalum with respect to chromium concentration in tantalum 110

Fig. 4.21 Amount of hydrogen dissolved in tantalum with respect to iron concentration in tantalum 111

Fig. 4.22 Amount of hydrogen dissolved in tantalum with respect to aluminium concentration in tantalum 112

Fig. 4.23 Variation in amount of dissolved hydrogen with respect to the concentration of alloying elements in different tantalum alloys at (a) 673 K (b) 773 K and (c) 873 K. 113

Fig. 4.24 Isobaric *P*-*C*-*T* equilibrium curves for the solubility of hydrogen in Ta and Ta-Ni alloys at (a) 0.64 Atm, (b) 0.72 Atm, (c) 0.8 Atm and (d) 0.88 Atm 114

Fig. 4.25 Isobaric P-C-T equilibrium curves for the solubility of hydrogen in Ta and Ta-Cr alloys at (a) 0.64 Atm, (b) 0.72 Atm, (c) 0.8 Atm and (d) 0.88 Atm 115

Fig. 4.26 Isobaric *P*-*C*-*T* equilibrium curves for the solubility of hydrogen in Ta and Ta-Fe alloys at (a) 0.64 Atm, (b) 0.72 Atm, (c) 0.8 Atm and (d) 0.88 Atm 116

Fig. 4.27 Isobaric *P*-*C*-*T* equilibrium curves for the solubility of hydrogen in Ta and Ta-Al alloys at (a) 0.64 Atm, (b) 0.72 Atm, (c) 0.8 Atm and (d) 0.88 Atm 117

Fig. 4.28 Isothermal *P*-*C*-*T* equilibrium curves for the solubility of 118 hydrogen in Ta and Ta-Ni alloys at (a) 673 K, (b) 773 K and (c) 873 K

Fig. 4.29 Isothermal *P-C-T* equilibrium curves for the solubility of hydrogen in Ta and Ta-Cr alloys at (a) 673 K, (b) 773 K and (c) 873 K 119

Fig. 4.30 Isothermal *P-C-T* equilibrium curves for the solubility of hydrogen in Ta and Ta-Fe alloys at (a) 673 K, (b) 773 K and (c) 873 K 120

Fig. 4.31 Isothermal *P-C-T* equilibrium curves for the solubility of hydrogen in Ta and Ta-Al alloys at (a) 673 K, (b) 773 K and (c) 873 K 121

Fig. 4.32 Isothermal P-C-T equilibrium curves showing the comparison behavior of alloying elements on the solubility of hydrogen in tantalum at (a) 673 K, (b) 773 K and (c) 873 K 122

Fig. 4.33 Isobaric P-C-T equilibrium curves showing the comparison behavior of alloying elements on the solubility of hydrogen in tantalum at (a) 0.64 Atm, (b) 0.72 Atm, (c) 0.8 Atm and (d) 0.88 Atm 123

Fig. 4.34 Variations in K_s values with temperature for Ta-H and Ta-M-H systems (M = alloying elements) 127

Fig. 4.35 Ni-H phase diagram 138

Fig. 4.36 Cr-H phase diagram 139

Fig. 4.37 Fe-H phase diagram 139

Fig. 4.38 Al-H phase diagram 140

Fig. 5.1 Generalized α – time plot, summarizing kinetic behavior observed for isothermal decompositions of solids 146

Fig. 5.2 Schematic representation of hydrogen absorption mechanism 151

Fig. 5.3 Results of model calculations for the absorption of hydrogen 156

Fig. 5.4 Isothermal hydrogen absorption kinetics curves for (a) pure Ta, (b) Ta-1Al, (c) Ta-1.6 Al and (d) Ta-2.4 Al alloys at different temperatures 159

Fig. 5.5 Reacted fraction *(α)* vs Time (min) curves for hydrogen absorption at different temperatures in (a) pure Ta, (b) Ta-1Al, (c) Ta-1.6 Al and (d) Ta-2.4 Al alloys 161

Fig.5.6 The best fitting mechanism functions for hydrogen absorption at different temperatures in (a) pure Ta, (b) Ta-1Al, (c) Ta-1.6 Al and (d) Ta-2.4 Al alloys. 163

Fig. 5.7 Arrhenius plots, lnk vs $1/T$ (10^{-3} K^{-1}) for the hydrogen absorption kinetics in Ta and Ta-Al alloys 167

Fig. 5.8 Variation in activation energy for hydrogen absorption in Ta-Al alloys as a function of aluminium composition 167

List of Tables

S. No.	CAPTIONS	Page No.
Table 1.1	Properties of hydrogen separation membranes	8
Table 1.2	Physical and mechanical properties of pure tantalum	12
Table 2.1	Hydrogen solubility values for different metals	30
Table 2.2	The equations for hydrogen in tantalum	44
Table 2.3	Published literature data for apparent hydrogen permeability of tantalum disks	46
Table 2.4	Enthalpy of solution of hydrogen in elements of periodic system	51
Table 4.1	Vickers hardness of Ta and Ta-alloys at room temperature	91
Table 4.2	Chemical compositions (atom percent) of tantalum and its alloys	94
Table 4.3	Variation in dissolved hydrogen concentration in tantalum as a function of charging time	101
Table 4.4	Change in the lattice parameters of tantalum as a function of dissolved hydrogen concentration	102
Table 4.5	The amount of hydrogen in wt %, dissolved in tantalum and its – alloys at three temperatures 673, 773 and 873 K and different hydrogen pressures	108
Table 4.6	Sievert's constant, K_S for hydrogen in Ta and its alloys	125
Table 4.7	The values for the relative partial molar enthalpy and entropy	127

for the solution of hydrogen in the tantalum metal and its alloys

Table 4.8 Relative partial molar Gibb’s free energy for the solution of hydrogen in the tantalum metal and its alloys 130

Table 4.9 Electronegativites of the elements (Pauling scale) 134

Table 4.10 Variation in H-solubility with respect to change in *e /a* ratio 135

Table 4.11 Variation in hydrogen-solubility in different tantalum alloys with respect to change in lattice parameter 136

Table 4.12 Amount of hydrogen dissolved in pure Ta, Ni, Cr, Fe and Al at three different temperatures at one atmosphere hydrogen pressure 137

Table 4.13 The temperature dependent hydrogen solubility equations in metal-hydrogen systems at one atmosphere hydrogen pressure 141

Table 5.1 Rate equations which have found application in kinetic studies of solid phase reaction 149

Table 5.2 Mechanism function of the kinetics 150

Table 5.3 Kinetic parameters, equations and activation energies for hydrogen absorption reaction in Ta and Ta-Al alloys 165

Acronyms

MW	Megawatt
%	Percent
^oC	Degree centigrade
mol	Mole
m	Meter
s/sec	Second
at	Atom
wt	Weight
atm	Atmosphere
ppm	Parts per million
g	Gram
cc	Cubic centimeter
p	Pressure
K	Kelvin or reaction equilibrium constant
Pa	Pascal
T	Temperature
k	Kilo or Boltzmann constant or rate constant
m	Meter
M	Mega or magnification or metal
W	Watt
J	Joule
Ω	Ohm

bcc/BCC	Body centered cubic
fcc/FCC	Face centered cubic
hcp/HCP	Hexagonal close packed
O	Octahedral
T	Tetrahedral
R	Universal gas constant or radius or resistance
E_D	Dissociation energy
Å	Angstrom
α	Solid solution phase or reacted fraction
β	Hydride phase
G	Gibbs energy
H	Enthalpy or heat
S	Entropy or solubility
Δ	Change
*	Transition state
ads	Adsorption
kJ/mol	Kilo Joule per mole
c	Concentration or constant
p	Proton
e or e^-	Electron
a	Activity or initial mole fraction
K_S	Sievert's constant
$\overline{G_H}$	Partial molar Gibb's free energy of hydrogen in metal
G_{H_2}	Molar Gibb's free energy of gaseous hydrogen at a given pressure

$G^0_{H_2}$	Molar Gibb's free energy of gaseous hydrogen at 1 atm pressure
$\overline{\Delta G_H}$	Relative partial molar Gibb's free energy
$\overline{\Delta H_H}$	Relative partial molar enthalpy
$\overline{\Delta S_H}$	Relative partial molar entropy
D	Diffusivity
n	Number of moles or integer
d or t	Thickness
E_d	Activation energy for diffusion
mm	Millimeter
cm	Centimeter
ϕ	Permeability or number of empty sites on the surface of metals
D_o	Diffusion coefficient
exp or e	Exponential
P-C-T	Pressure-composition-temperature
x	Concentration or Mole fraction
T_c	Critical temperature
cal	Calorie
deg	Degree
t	Time
mg	Milligram
min	Minute
ν_H	Hydrogen absorption rate
P	Power

KWH	Kilowatt hour
V	Voltage or volume
I	Current
A	Ampere
hr	Hours
DC	Direct current
μ	Micro or chemical potential
λ	Wavelength
d_{hkl}	Inter planer spacing between the crystal planes
θ	Angle
eV	Electron volt
nm	Nanometer
M	Mega or Magnification
W or w	Width or weight
Z	Atomic number
H_V	Vickers hardness
σ_μ	Tensile strength
α	Reacted fraction
$f(\alpha)$	Function determining the mechanism of the reaction
$g(\alpha)$	Integral form of $f(\alpha)$
eq	Equilibrium
E_a	Activation energy
A	Pre-exponential factor or Arrhenius factor or frequency factor
HV	Vickers hardness number

a.u.	Arbitrary units
a	Lattice parameter
hkl	Miller indices
Å	Angstrom
M^+	Metal ion
H^+	Hydrogen ion
Me	Metal
e/a	Electron to atom ratio
$G_{H_2}^{(gas)}$	Molar free energy of hydrogen gas at a given pressure
$G_{H_2}^{0}$	Molar free energy of hydrogen gas at 1 atmosphere pressure
$\overline{G_{H^+}}$	Partial molar free energy of proton
$\overline{G_{e^-}}$	Partial molar free energy of electron
$\overline{G_{H^+}^{*}}$	Partial molar free energy of protons extrapolated to unity concentration
pm	Picometer
a'or B'	Constant
X_H	Hydrogen concentration
H/M	Hydrogen to metal atomic ratio
ph	Physisorption
θ_{ph}	Concentrations of physisorbed hydrogen
ΔH_{ph}^{0}	Enthalpy for physisorption of hydrogen
ch	Chemisorptions
θ_{ch}	Concentration of chemisorbed hydrogen

k_f	Rate constants in the forward directions
k_b	Rate constants in the backward directions
E_f	Activation energies for the forward directions
E_b	Activation energies for the backward directions
$\phi_\beta(r_0)$	Vacancy in the sublattice just below the surface
$c_{\phi\beta}(r_0)$	Hydrogen concentration in the vacancies in subsurface layer just below the surface
j	Diffusion current density
b	Mobility
$\phi_\beta(r_\alpha)$	Vacancy in α phase
$c_{\phi\beta}(r_\alpha)$	Hydrogen concentration in the vacancies in α phase
p_0	Initial pressure
p_t	Pressure at time t
p_{eq}	Final equilibrium pressure
r	Correlation coefficient
SD	Standard deviation

Chapter 1

Introduction

1.1 Introduction

The limited availability of fossil fuels, exponentially increasing global energy demand and the global warming caused by the use of fossil fuels has led to a search for alternate sources of clean and renewable energy and energy carriers [1, 2]. An energy carrier is a substance or system that enables movement of energy in usable form from one place to another. Alternative energy refers to energy sources which are alternative to the fossil fuel. These sources are generally renewable in nature and have low carbon emission [3]. They include solar, wind, hydroelectric, geothermal, biomass and hydrogen energy sources [3, 4]. A brief note on them follows:

Solar Energy:

Solar energy is all about using sunlight as the source of energy. The Sun can be considered as a huge fusion reactor that has been operating over last several billion years. It provides enough energy in one minute to supply the world’s energy needs for one year [5] and in this way, the earth receives an incredible supply of solar energy all the time. In fact, the amount of solar radiation striking the Earth in three-days is equivalent to the energy stored in all fossil energy sources in the earth [6]. The light from the Sun is widely and freely available to most of the habitated regions of the earth. Energy from the Sun is captured through ages in a variety of devices and contraptions using myriad ideas and concepts. One of the most tangible concepts is the solar panel. The solar panels function through the photovoltaic effect whereby certain materials collect solar radiation from the sun and actively convert it in to electricity. Solar panels are made of several individual solar cells. When the solar cells are exposed to sunlight, the p-n junction diodes convert the energy from sunlight into usable electrical energy. The energy generated from photons striking the surface of the solar panel allows electrons to be knocked out of their orbits and released. The electric fields in the solar cells pull these free electrons in a directional current, from which electricity can generate. The more total electricity can be produced by increasing the number and the quality of the solar cells in a solar panel [7, 8]. Solar energy is cost effective and renewable but not constant. It can only be obtained during daytime. The other concern is only fifty percent of energy received by a solar panel can be converted into electricity [6].

Wind Energy:

The wind energy is clean and renewable. Wind is all that is needed to reap the benefits. A windmill emits nothing harmful, which means no greenhouse gas contribution to the atmosphere. The first known use of wind energy was in 5000 BC when people used sail to navigate the Nile River [9]. Windmills have been used for pumping water and grinding grains [5]. A typical windmill is a huge fan-like standing structure that converts wind energy into rotational energy by means of vanes called blades. Wind is of use due to its kinetic energy and when the wind blows and the blades of the mill spin, which in turn power an electricity generator. These energy harvesters work easily and they can, in principle, be set up anywhere [9].

The wind energy was being exploited at a relatively slow speed in the past and the extent and speed of its exploitation has increased tremendously in the more recent past all over the world. The reasons being high investment cost and materials and technology input need for increasing efficiency. However wind energy has various long-term benefits to offer. It’s best to have wind farms at countryside locations like farms and ranches. This will also improve the rural economies.

The modern wind power industry began in 1979 with the serial production of wind turbines [10]. A wind turbine is a windmill-like structure specifically developed to generate electricity. Worldwide, many thousands of wind turbines are now operating, with a total capacity of 194,400 MW [10]. Europe accounted for 48% of the total in 2009.

Hydroelectric Energy:

Water energy or hydroelectric energy or hydropower is the power generated by moving water [5]. Generally, the dams on the rivers are used in order to transform the motive power (kinetic energy) of water into electricity. When water falls down from a high dam, it rotates the blades of turbine, which in its turn results in electricity production in a generator. In fact, about 20% of all electricity, consumed in the world is generated by water. In certain countries, like Norway, virtually all the electricity is produced at the hydroelectric power plants [11, 12]. It is interesting to note that the Niagara Falls, easily the most famous of all a natural waterfalls, powered the first hydroelectric plant in 1879 [13]. A typical hydro plant is a system with three parts: an electric plant where the electricity is produced; a dam that can be opened or closed to control water flow; and a reservoir where water can be stored [5]. The water behind the dam flows through an intake and pushes against blades in a turbine, causing them to rotate. The turbine spins a generator to produce electricity. The amount of electricity that can be generated depends on how far the water drops and how much water moves through the system [13]. The conversion efficiency of a hydroelectric power plant depends mainly on the type of water turbine employed and can be as high as 95% for large installations [11]. The electricity can be transported over long-distance electric lines to homes, factories, and businesses

Geo-thermal Energy:

'Geo' means Earth and 'thermal' means heat. Geo-thermal means energy from the heat of the Earth [5]. The temperature of the Earth's core is about 4000 ^{o}C at the center. It is believed that if we drill just three miles down the crust, we can reach the temperature of around 100 ^{o}C (boiling temperature of water) [14]. This heat is used to generate steam which in turn can run a turbine and a generator. Geothermal energy can also be gathered from landforms like volcano and volcanic structure which vent out Earth's heat [14].

The technology for converting geothermal energy into useful heat and electricity can be categorised as geothermal heat pump, direct-use applications (uses heat from a geothermal source directly in an application) and geothermal power plant [5]. Geothermal heat pump systems consist of basically three parts: the ground heat exchanger, the heat pump unit, and the air delivery system (ductwork). The heat exchanger is basically a system of pipes called a loop, which is buried in the shallow ground near the building. A fluid (usually water or a mixture of water and antifreeze) circulates through the pipes to absorb or relinquish heat within the ground [15]. Geothermal heat pump uses energy near the surface of the earth to heat and cool the buildings [5]. Geothermal power plant uses steam or hot water from geothermal reservoirs to turn turbines and generate electricity [5].

Biomass Energy:

The term “biomass” refers to organic matter that has stored energy through the process of photosynthesis [5]. It exists in one form as plants and may be transferred to the animal’s bodies and their wastes through the food chain. This energy can be converted to human use through the combustion process [5], which also release carbon dioxide along with the energy stored in the plant materials. Biomass has become one of the most commonly used renewable sources of energy in the last two decades, second only to hydropower in the generation of electricity. Biomass energy is such a widely utilized source of energy, due to its low cost and local availability (15 % of the total world energy supply and about 35% in developing countries for heating and cooking) [16].

Hydrogen Energy:

Hydrogen is not an energy source, but an energy carrier because it takes a great deal of energy to extract it from water [17]. “Hydrogen energy” is among the most viable solutions to the energy problem. In the hydrogen energy system, molecular hydrogen is utilized as the energy carrier from the point of production to the point of use. Hydrogen is attractive as an energy carrier for both mobile and stationary applications [17-27].

Water is converted into hydrogen and oxygen using various energy sources including renewables and nonrenewables [28]. For example, solar power can be used to split water into hydrogen and oxygen. The hydrogen can then be used as a portable energy for transportation or other uses. The uses may take the route of chemical reactions to extract/realize the energy carried by hydrogen by the classical boiler type system wherein hydrogen undergoes combustion or through devices called fuel cells hydrogen can output electricity on combination with oxygen to form water. A general hydrogen energy system is shown in Fig. 1.1 [28].

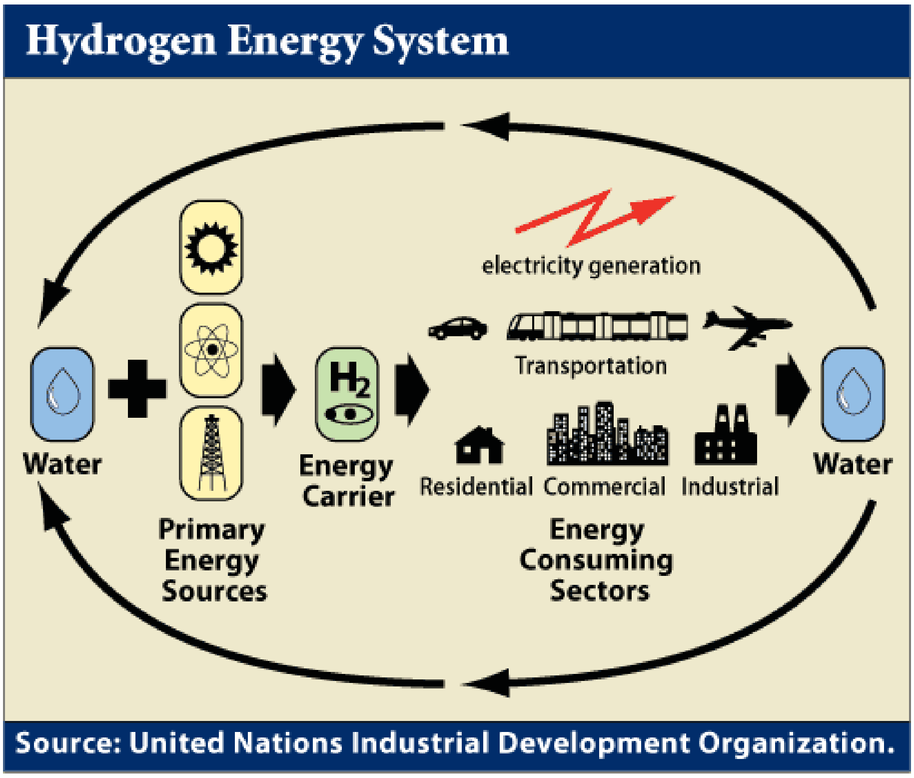

Source: United Nations Industrial Development Organization.

Fig.1.1 Hydrogen energy system [28]

Hydrogen produces water on burning - zero carbon emission at the point of use. Its transportation and storage are more efficient than of electricity. However, there are a number of challenges associated with use of hydrogen. Although hydrogen is naturally abundant element [29] in the universe, is practically unavailable in its pure form on Earth. That is why it cannot be used as a direct energy source, like oil, gas, or coal. All this hydrogen is bound to oxygen in the form of water or to carbon in the form of hydrocarbons. That is why, in order to use hydrogen as energy source, It should first be separated from the original association. Once hydrogen is released from one of these sources it must then be purified and either utilized immediately or stored and transported for later use. The production, purification/separation, storage and recovery of hydrogen each represent a significant technological barrier to be conquered before the realization of hydrogen energy [30-32]. Apart from the role as direct energy carrier articulated in an exemplary manner by the Vision 21 program of U.S. DOE for developing the technology necessary for ultra-clean, near-zero emission, fossil fuel-based energy plants that will be needed in the coming decades of the 21st century. There exists already a large demand for hydrogen in the metallurgical, chemical, petrochemical, microelectronic, pharmaceutical and textile industries [33-34]. “The goal of Vision 21 is to effectively address the environmental concerns associated with the use of fossil fuels for producing electricity and transportation [33, 35]. Around 2 % of the worldwide primary energy (a form of energy found in nature that has not been subjected to any conversion or transformation process) is utilized for the hydrogen production with annual yield of ~ 850 billion cubic meters [36]. Therefore, it is clear that a cost-effective and efficient means to hydrogen purification will always be a necessity, irrespective of the extent to which the world switches to hydrogen energy. Hydrogen gas is purified mainly by passing through a hydrogen permeation membrane [37]. Hydrogen permeation membranes can be broadly classified into polymer (organic), ceramic, carbon, and metallic [38-40]. This classification allows a direct assessment of membrane permeability, selectivity, operating conditions and cost. The relevant information about each membrane type is given in Table 1.1.

Table 1.1 Properties of hydrogen separation membranes [39-40]

	MembraneType				
	Dense Polymer	**Micro porous Ceramic**	**Dense ceramic**	**Porous Carbon**	**Metallic**
Temperature	< 100°C	200-600 °C	600-900 °C	500-900 °C	200-600 °C
H_2 Selectivity	5-500	5-139	>1000	10-1000	>1000
H_2 Flux*	0.1-1	60-300	6-80	10-200	100-1000
Stability Issues	Swelling, compaction	Stabilty in Water vapor	Stabilty in CO_2	Brittle, oxidizing environments	Embrittlement
Poisoning Issues	HCl, SOx	None	H_2S	Strongly adsorbing vapors	H_2S, HCl, CO
Materials	Polymers	Silica, Alumina, Zirconia, Titania, Zeolites	Proton conducting ceramics	Carbon	Pd alloys
Transport Mechanism	Solution-diffusion	Molecular sieving	Solution-diffusion	Surface-diffusion and Molecular sieving	Solution-diffusion

** units are 10^{-3} mol/m^2/s at a pressure difference of 1atm.[1atm.= 101325Pa]*

Although almost all industrial gas separation processes use polymeric membranes, but interest in metal membranes continues, mostly for the high-temperature membrane reactor applications and for the preparation of pure hydrogen for fuel cells [41-43]. The interest in the interaction of hydrogen with transition metals began in the early 1860's with the work of Deville and Troost [44] who measured the permeability of hydrogen through heated iron and platinum. On the basis of their work, in 1866, Thomas Graham [45] measured the permeability of hydrogen through palladium first time and indicated it to be usable for devices for hydrogen permeation. Palladium and Pd-based alloys have been developed for use as hydrogen permeation membrane [37]. Pure palladium absorbs 600 times its volume of hydrogen at room temperature and is measurably permeable to the gas [41], but their high cost and limited availability are limitations for their widespread industrial use [37]. Hydrogen permeates a number of other metals including tantalum, niobium, vanadium, nickel, iron, copper, cobalt and platinum [46]. In most cases, the metal membrane must be operated at high temperatures (>300 ^{o}C) to obtain useful permeation rates and to prevent embrittlement and cracking of the metal by sorbed hydrogen.

Various researchers have tried to develop low cost and high performance non-Pd based alloys for hydrogen separation membrane [37]. Graham described the solution diffusion process, where he postulated that the permeation process involved the dissolution of hydrogen, followed by the transmission of the dissolved species through the membrane [47]. Since, permeability of any gas is a product of diffusivity and solubility. Group V, metals, vanadium, niobium and tantalum are considered to be the candidate materials for hydrogen permeation membrane because they have usable values for these two parameters [48]. The hydrogen permeability in group V metals have been reported in the literature [46] that indicates that these metals based alloys candidate for non-Pd hydrogen permeation membrane [49-54]. The present thesis focuses on tantalum and this chapter is a brief introduction to the relevant background information on tantalum and certain aspects of hydrogen interaction with metals

1.2 The Refractory Metals

The elements in the periodic table having high melting point, strong chemical reactivity to interstitial elements but generally a remarkable stability with respect to corrosion by acids bases, even liquid metals and many other fluids are referred to as refractory metals. Examples are the metals titanium, zirconium, hafnium, vanadium, niobium, tantalum, molybdenum and tungsten occurring in the group IV to VI of the periodic table [55-58]. The refractory metals and their alloys are having the above combination of physical, chemical and certain other special properties which confer on them advantages for use in various applications in certain areas of modern technology such as the nuclear, aerospace, electronics, biomedical industries besides the conventional chemical industries [59]. Tantalum, for example, is considered as a typical refractory metal for use in many of these industries. It is also considered as suitable for hydrogen energy technology, for example, as a material for hydrogen separation membrane. It has large hydrogen solubility and considerable hydrogen diffusivity apart from a host of good technological properties.

1.3 Tantalum

It occurs naturally in the mineral tantalite [(Fe, Mn) Ta_2O_6], always together with the chemically similar element niobium [60-62]. The process history of tantalum is closely related to that of niobium. Until the middle of the 19th century it was still unclear whether they were actually individual elements. They have a characteristic body-centered-cubic structure. The average content of tantalum in the Earth's crust is about 2 ppm [63-64] and that of niobium is 24 ppm **[**65].

1.3.1 Physical and Mechanical Properties of Pure Tantalum

Tantalum is a blue-gray, lustrous transition metal and highly corrosion resistant to a variety of liquid media at a range of temperatures. It has a very high melting point, low vapor pressure and good mechanical properties even at elevated temperatures. The physical and mechanical properties of elemental tantalum are summarized in Table 1.2 **[55, 59-60, 66-68**].

Table 1.2 Physical and mechanical properties of pure tantalum

Property		**Tantalum**
Atomic number		73
Atomic weight		180.95 [g/mol]
Atomic Volume		10.90 [cc/g-atom]
Melting point		3293 [K]
Boiling point		6373 [K]
Vapor pressure	at 1800 °C (2073 K)	5×10^{-8} [Pa]
	at 2500 °C (2773 K)	5×10^{-3} [Pa]
	at melting point	0.89 [Pa]
Density at 20 °C		16.60×10^{3} [kg/m^{3}]
Lattice structure		Body centered cubic
Lattice constant		330.3×10^{-12} [m]
Coordination number		8
Hardness at 20 °C	cold-worked	180 - 300 [HV10]
	recrystallized	80 - 100 [HV10]
Ultimate tensile strength		241 MPa
Yield strength		180 MPa
Elongation		45 %
Thermal conductivity at 20 °C		54 [W/(m.K)]
Specific heat at 20 °C		0.14 [J/(g.K)]
Electrical conductivity at 20 °C		8×10^{-6} [1/(Ω.m)]
Specific electrical resistance at 20 °C		0.13 [(Ω.mm^{2})/m]
Thermal neutron capture cross section		2.13×10^{-27} [m^{2}/atom]
Recrystallization temperature	(1 hour at temp)	1173 - 1723 [K]
Superconductivity (transition temperature)		< 4.5 [K]

1.3.2 Chemical Properties of Pure Tantalum

Tantalum is one of the most inert metals as regards reactions with chemicals at temperature below 150 °C [55]. The presence of a thin, impervious, self curing oxide film, Ta_2O_5, on the surface of tantalum makes it remarkably resistant to corrosion in acids and to several other chemicals common in industrial applications. Tantalum is attacked slowly by strong alkalis, rapidly by fluorine and hydrofluoric acid, more rapidly by fuming sulphuric acid, and vigorously by a mixture of hydrofluoric and nitric acids. At temperatures below 150 °C, tantalum is almost completely immune to attack by aqua regia and by sulphuric acid and also inert to hydrochloric acid at all concentrations and at temperature up to about 95 °C. Tantalum is not attacked by nitric acid upto 70 % concentration at temperatures upto 190 °C. In general, tantalum is completely resistant to organic compounds and liquid alkali metals like lithium and sodium [61].

Tantalum is rather reactive at high temperatures [63-64, 69**]**. On reaction with oxygen or air, it converts to the pentoxide Ta_2O_5 [63-64, **70]**. Tantalum reacts with molecular hydrogen at temperature above 250 °C but even at room temperature with atomic hydrogen generated for example by an electrolysis process [55]. It absorbs hydrogen above 300 °C. Hydrogen absorption results in an expansion of body-centered crystal lattice and results in an increase of molecular volume. All the halogens react with tantalum forming tantalum halides [71] in the oxidation states of +5, +4, and +3 [72**]**. Tantalum reacts with nitrogen directly to form the nitrides TaN and Ta_2N [55, 73]. Tantalum also reacts directly with carbon, boron, silicon and aluminium at elevated temperature to form carbides, borides, silicides and aluminides as Ta_2C, TaC, TaB, TaB_2, $TaSi_2$, $TaAl_3$ and Ta_3Al respectively [55, 63-64, 74**]**.

1.3.3 Applications of Tantalum

One of the main uses of tantalum is in the manufacturing of capacitors in the electronic industry **[55]**. The large dielectric constant of the thin oxide film on tantalum is the key property used here. Tantalum capacitors have the highest specific capacity and can be remarkably compact in size [60-61, 75]. The chemical inertness, excellent corrosion resistance, high temperature strength and good thermal conductivity of tantalum makes it a valuable substance for the chemical process equipments like heat exchangers, condensers, thermowells, and lined vessels and it is also a good substitute for platinum **[55, 60, 67, 76**]. Tantalum crucibles are used for high temperature reactions, thin film deposition, distillation and the melting of special glasses.

The inertness towards the body fluids, good tolerance by body tissues and excellent biocompatibility of tantalum has made it a very useful biomedical metal [77]. It is used in prosthetic devices, implants, sutures wires and surgical repairs **[55, 60**].

The low natural abundance, specialized technology needed to produce pure elemental metal leading to its limited availability and high cost, all limit the bulk use of tantalum to very special applications [66]. In oxygen environment, tantalum applications are limited upto 300 °C due to its susceptibility to embrittlement. For nitrogen and hydrocarbons the maximum application temperature is 700 °C [59].

In the context of the present work, both the solubility of hydrogen in tantalum and the transport of hydrogen in tantalum are important in the consideration of permeation of the gas through the metal. These two properties as well as the structural integrity of tantalum in the presence of hydrogen, and as influenced by the temperature and composition of tantalum based alloys also need to be considered in the evaluation of tantalum materials for possible use in hydrogen permeation devices.

1.4 Tantalum-Hydrogen System

Tantalum can absorb large amount of hydrogen and form the hydrides. It also becomes embrittled by relatively even a small amount of hydrogen at low temperatures [78]. The pressure-composition-temperature phase diagram for tantalum-hydrogen system, at one atmospheric hydrogen pressure [79] is shown in Fig. 1.2. The tantalum hydrides are stable only at low temperature. The hydrogen solubility in tantalum decreases with increasing temperature and approaches to very low solubility above approximately 870 ^{o}C. Hence, relatively large amount of hydrogen is required to cause embrittlement at higher temperature. Embrittlement of tantalum by hydrogen is associated with change in lattice parameter or hydride formation [78]. However, no investigations have been found in the open literature on the mechanism of embrittlement of metals at higher temperatures.

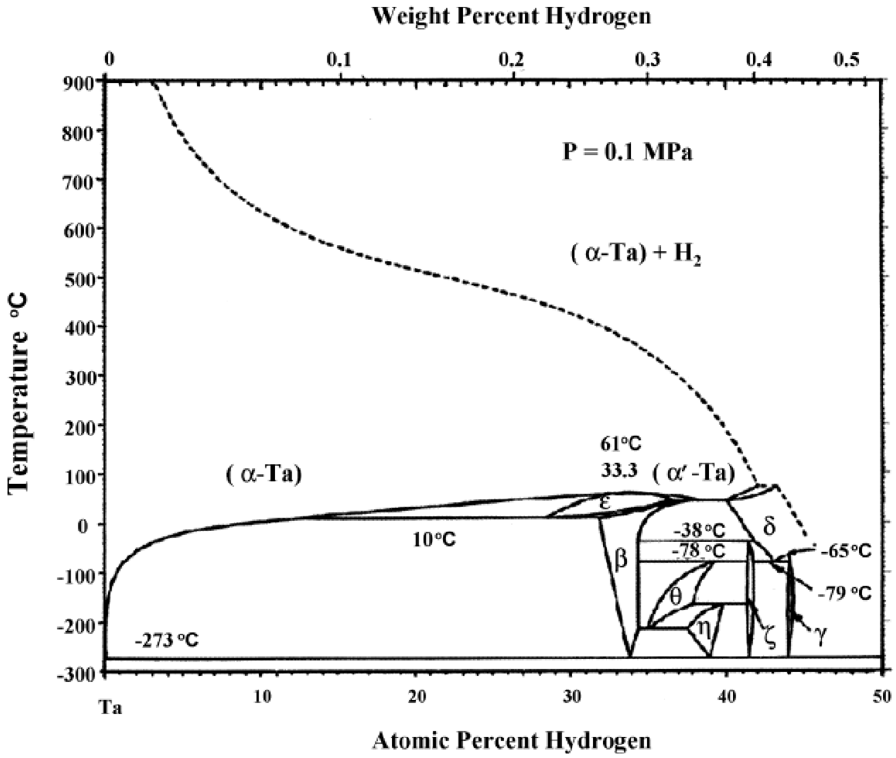

Fig. 1.2 **Ta-H phase diagram** *at 0.1MPa Hydrogen Pressure* [79]

The hydrogen goes into the interstitial sites up to the solid solubility limit (primary solid solution). It may distort or expand the original structure but does not bring any change in the crystal structure. When the dissolved hydrogen exceeds the solid solubility limit at a given temperature, a different phase is formed. Similar to Nb-H system, at high temperature, only single phase (solid solution) exists in Ta-H system (above 61^0C) [78] and a solid solution remain in equilibrium with the hydrogen gas at 1 atm pressure. Other *P-C-T* equilibrium data suggested that a two-phase region exists at some temperature below 100 ^{o}C [80].

1.5 The Nature and Location of Hydrogen in Metals

The observed expansion of the metal lattice upon hydrogen absorption gives the information about the state of the dissolved gas. The volume occupied by a hydrogen atom is substantially smaller than the volume occupied by the host metal atom. Therefore, the expansion of the metal indicates that the hydrogen occupies interstitial sites within the lattice. This conclusion has been confirmed by x-ray and neutron diffraction studies [81-82].

The location of hydrogen in metals has been explained from the geometry of face-centered cubic (FCC), hexagonal close packed (HCP) and body-centered cubic (BCC) structures as illuminated in Fig. 1.3 [83-84]. In the BCC structure there are three octahedral and six tetrahedral interstitial sites per host atom whereas in the FCC and HCP structures, one octahedral site and two tetrahedral interstitial sites per host atom are present [85-88].

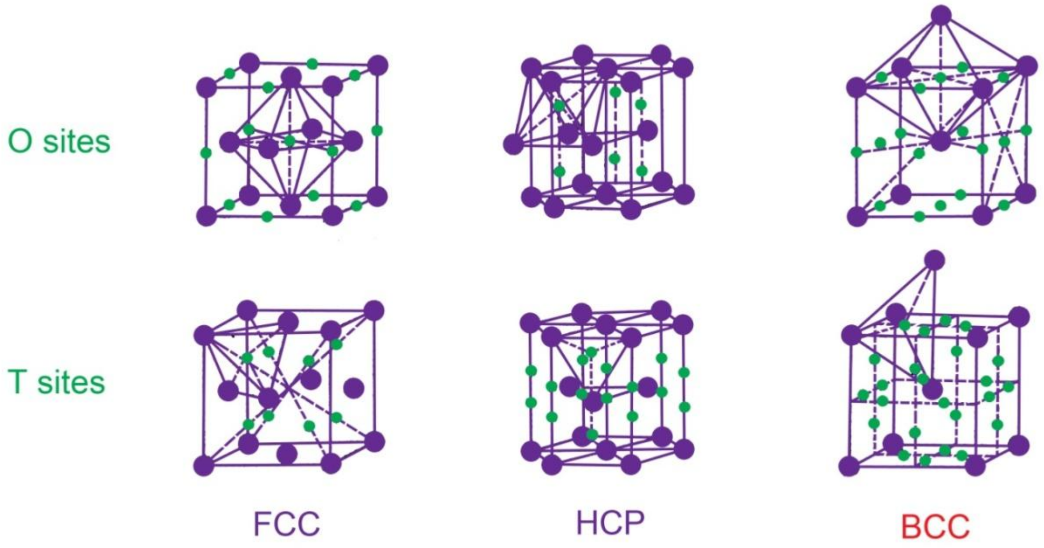

Fig. 1.3 Octahedral sites and tetrahedral sites in FCC, HCP and BCC lattice, *Purple circles are lattice locations, green circles are interstitial sites locations* [83-84]

Hydrogen will preferentially occupy the sites with a larger free volume as these are the positions of local minima of potential energy. BCC structure is an open structure and its packing efficiency is lower compared with FCC and HCP lattice. The octahedral and tetrahedral interstitial sites per host atom in BCC lattice are thrice as numerous than those in FCC and HCP lattices, which means that more number of interstitial sites are available for hydrogen occupancy in BCC structure alloys [85-86]. The size of the interstitial hole can be estimated by calculating the length of the vector from a nearest neighbour atom to the interstitial location [85]. The length of this vector minus the radius of the host atom (R) gives the approximate radius of the interstitial hole. In closed packed structure i.e. HCP and FCC, the size of octahedral site (r_6) is ~ $0.414R$ and of tetrahedral site (r_4) is ~ $0.225R$ while in BCC structure, r_6 is ~ $0.153R$ and r_4 is ~ $0.291R$. From these numbers, one can conclude that the absorbed hydrogen will occupy the octahedral sites in FCC and HCP metals while it will occupy the tetrahedral sites in BCC metals [89].

1.6 Metals-Hydrogen Interaction

Hydrogen atoms are very small, occupy interstitial sites and are extremely mobile in many metals even at relatively low temperatures. The reaction of hydrogen gas with a metal is described in terms of a simplified one-dimensional potential energy curve (one-dimensional Lennard-Jones potential model) way back in 1932, by Lennard-Jones as shown in Fig. 1.4 [90] and in Fig. 1.5 [91].

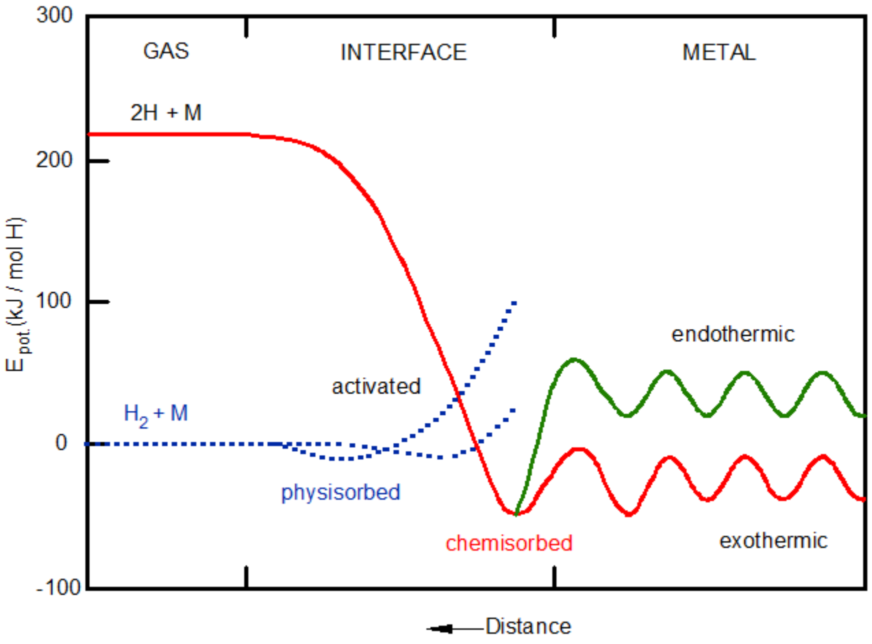

Fig. 1.4 **Schematic of one-dimensional Lennard-Jones potential energy diagram of hydrogen approaching a metallic surface** [90, 92]

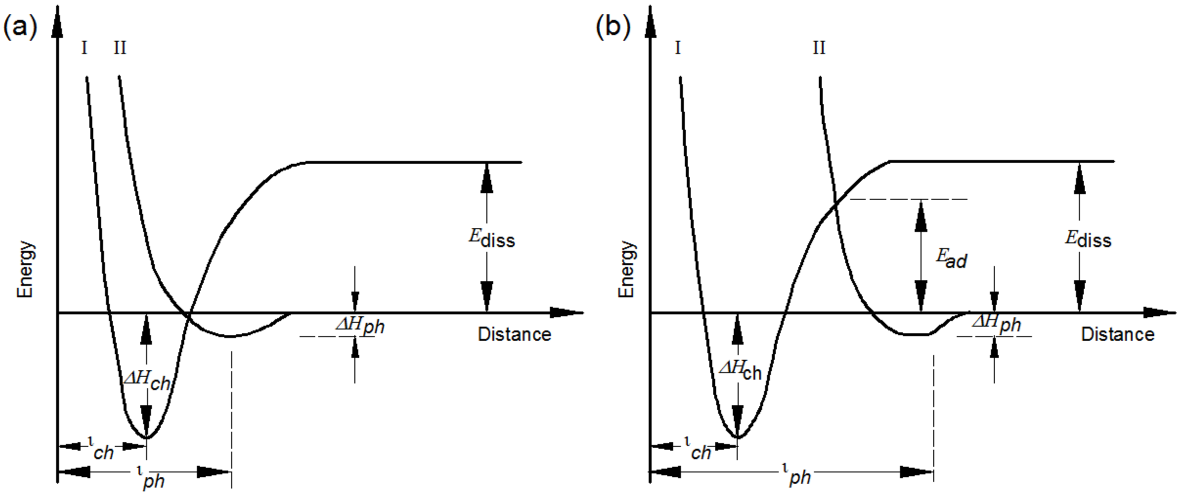

Fig. 1.5 **One dimensional potential energy diagram for (I) a hydrogen atom and (II) for a hydrogen molecule approaching a metal surface.** *In (a) close contact with the surface is attained while in (b) this contact is obstructed* [91]

Far from the metal surface, the potential of a hydrogen molecule and of two hydrogen atoms are separated by the dissociation energy (E_D = 435.99 $kJ\cdot mol^{-1}$). The first attractive interaction of the hydrogen molecule approaching the metal surface is the van der Waals force leading to the physisorbed state (E_{Phys} >>10 $kJ.mol^{-1}$). Closer to the surface the hydrogen has to overcome an activation barrier for dissociation of the hydrogen molecule and formation of metal-hydrogen bond. The height of the activation barrier depends on the surface elements involved. Hydrogen atoms sharing their electron with the metal atoms at the surface are then considered in the chemisorbed state (E_{Chem} >>50 $kJ.mol^{-1}H_2$). The chemisorbed hydrogen atoms may have a high surface mobility, interact with each other and form surface phases at sufficiently high coverage. In the next step the chemisorbed hydrogen atom can jump in the subsurface layer and finally diffuse on the interstitial sites through the host metal lattice. The hydrogen atoms contribute with their electron to the band structure of the metal [90].

In Fig. 1.5, the curve labelled **II** characterizes the potential energy of molecular hydrogen as a function of distance from the metal surface. The zero-energy reference point is taken as the energy of the molecule at infinite distance from the surface and therefore curve **II** falls directly on the x-axis at large distances. Following this curve toward the metal surface (decreasing x values) reveals that close to the surface there is a small potential well representing physical adsorption, or physisorption, of the molecule to the surface as indicated by the shallowness of the potential well. For molecular hydrogen, the equilibrium distance for this interaction (l_{ph}) is 2 to 3$\AA$ [93]. The curve labelled **I** represents chemical adsorption, or chemisorption, of atomic hydrogen onto the surface. The heat of chemisorption is much larger than physisorption and the distance of the hydrogen atom from the surface (l_{ch}) corresponds to that of a chemical bond – between 0.5 and 1.0 $Å$.

A molecule will move toward the surface along curve **II** and at first penetrate the physisorption well. If the molecule has enough energy it can climb the back of the potential well getting nearer to the metal surface and enter at the intersection of curves **I** and **II**. At this distance the valence electrons of the molecule can interact with the conduction electrons in the metal and allow dissociation of the hydrogen molecule by forming a more energetically favourable atom/metal bond rather than overcoming the energy stored within the H-H bond. The result as shown in Figure 1.5 (a) is nonactivated, dissociative adsorption which has been shown to be the condition for hydrogen adsorption on nearly all clean transition metal surfaces [94].

The effect of surface contamination on the adsorption process has been shown in Fig. 1.5 (b). Both curves **I** and **II** are the same as in Fig. 1.5 (a) with the slight change that curve **II**, physisorption, has been shifted to some extent to the right, representing the existence of some barrier between the hydrogen molecule and the metal surface. This barrier could be anything such as already adsorbed atom (O, N, C, H) to a stable chemical barrier such as a surface oxide. Although, the molecule can be physisorbed onto the surface of the contaminant, but the physisorption process does not bring the molecule sufficiently close to the metal surface to allow electronic interaction. Therefore, a substantial energy barrier (E_{ad}) must be overcome for the molecule to dissociate and chemisorb onto the surface. This process represents a major problem for Group V metals and iron due to their tendency to form a stable oxide layer [33, 95-96]. The use of these materials as hydrogen separation membrane has remained impractical due to their tendency to oxidize and necessity for high temperature operation to avoid hydride formation in these metals. Owing to the favourable permeability of these materials over

Pd-based materials, much effort has been directed to overcome this problem. Generally, the surface is coated with a thin layer of Pd to protect from oxidation and catalyze the surface hydrogen dissociation. Again, the high temperature necessary to avoid hydride formation [26, 33, 96-99]. Therefore, alloying could be considered as another option to overcome these issues.

1.7 The Mechanism of Hydrogen Absorption in Metals

Hydrogen has a unique capability to enter into many solid metals directly from its ordinary gaseous state [100], and its penetrative ability is much enhanced by ionization or when dissociated to atoms. A term “occlusion” is used for a diffusive process in which hydrogen is taken up directly from the gas or absorbed in the metal either by electrolytically or by chemical displacement [100]. When hydrogen is absorbed into the host metal, however, it is deposited on the metal, but the product is still wholly metallic in character, and this process is known as occlusion. Tantalum metal, in its normal state, is inert toward gaseous hydrogen, at ordinary temperature and pressure. On gradually heating in hydrogen, the metal starts absorption of hydrogen [100]. During gaseous hydrogen charging, the major reactions occurring on metal surface are the dissociation of hydrogen molecules into atoms, adsorption of these atoms on the metal surface, their absorption and diffusion into the bulk metallic phase [101]. The rate controlling step among these reactions depends on the hydrogen charging pressure, diffusion of hydrogen in metallic phase, and other factors [102-103]. A schematic diagram of the mechanism of hydrogen absorption in metals is shown in Fig. 1.6 [101]. The process occurs in a manner typical of any gas-metal interaction also depicted in the figure.

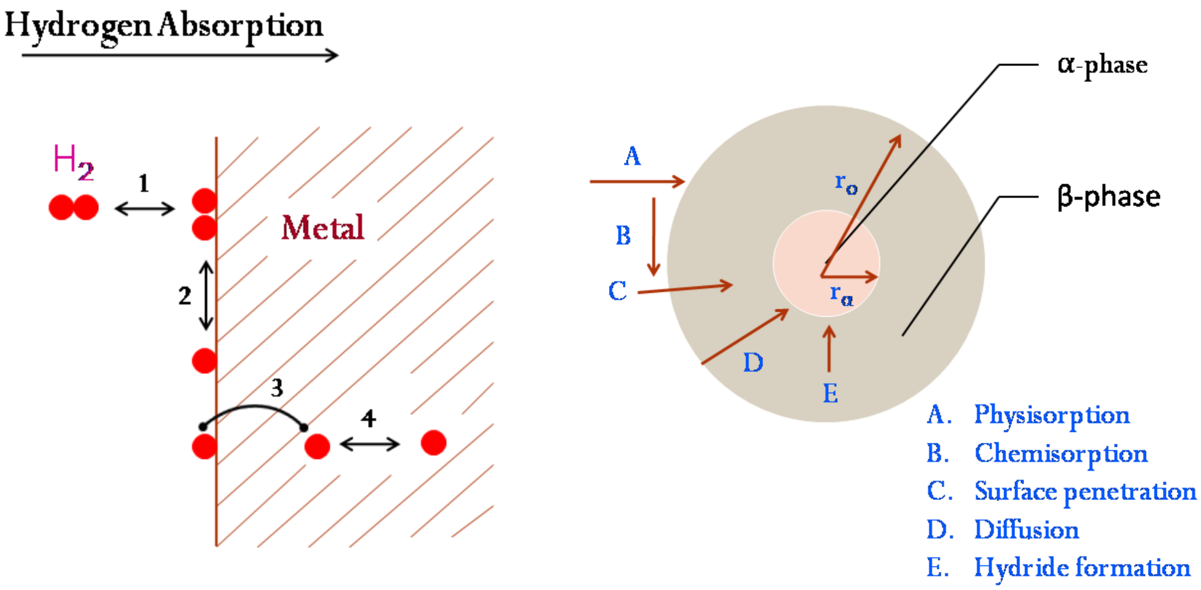

Fig 1.6 **Schematic representation of hydrogen absorption mechanism [101]**

1. Physical adsorption (Physisorption)
2. Chemical adsorption (Chemisorptions)
3. Solution formation (Surface penetration + Diffusion)
4. Bulk compound formation (Hydride formation)

Adsorption occurs at the surface of the metal while solution formation and bulk compound formation take place when the gas has entered the matrix.

1. Physical adsorption (Physisorption)

Adsorption is the process in which solute particles (gas, liquid, solid) are attached to the surface of a solid. Physical adsorption depends more on the surface of the metal and less on the properties of the gas [104]. The solute particles which are adsorbed / attached on the surface are known as adsorbate while the corresponding surface at which particles / adsorbates are attached is known as adsorbent. Physical adsorption occurs and is sustained by weak van der Waals forces **[105].** The adsorption is a spontaneous process resulting in decrease in free energy of the system. Prior to adsorption, gas molecules freely move in three dimensions, but when these are adsorbed on the surface their movement is restricted to two dimensions, at most, so that entropy of the system is reduced during adsorption process. According to thermodynamic relationship

$$\Delta G = \Delta H - T\Delta S \tag{1.1}$$

ΔH in this case is called the “enthalpy of adsorption”. As adsorption phenomenon is spontaneous and accompanied by decrease in entropy, so ΔH must be a large negative value. Hence all the adsorption processes are exothermic and magnitude of the heat of adsorption gives information about the type of interaction forces between the surface and the adsorbing species [104]. The weak bonding of physiosorption is due to induced dipole moment of a non polar adsorbate interacting with its own image charge in polarizable solid. If the attractive forces holding the adsorbate to the adsorbent are strong and comparable to those typically involved in chemical reactions the term chemisorptions or activated adsorption is applied. During chemisorption, gas molecules are dissociated into atoms and only one chemisorbed layer can form on the surface, while in van der Waals adsorption, gas molecules are adsorbed and several layers may be built up on the surface (multilayer adsorption).

2. Chemical absorption (Chemisorptions)

It was found that the dissociation of hydrogen molecule is a major step in hydrogen absorption process [106]. However, only a single surface site is involved in this step

$$H_2\text{ (ads)} = [H_a\text{ (ads)} \ldots H_b\text{ (in lattice)}]^* = 2H\text{ (dissolved)} \tag{1.2}$$

Where, H_a is the one H atom adsorbed on the external surface of the metal, H_b is the second H atom in a subsurface interstitial position and * is the transition state. In transition state (*), H_2 molecule is normal to the metal surface. The enthalpy difference between H_a and H_b, is to be about 8 kJ / mol. A weakly bound adsorbed hydrogen being in equilibrium with the hydrogen absorbed in the lattice was confirmed by allowing for the fact that a H atom in the first layer below the surface would be more stable than a H atom deep in the bulk [**106]**.

3. Solution formation (Surface penetration + Diffusion)

The gases dissociated into atoms are absorbed by the metals (resulting in the formation of gas-solid solution) more rapidly than those that are in molecular form initially. The degree of dissociation of a gas increases with temperature and rate of its absorption by the metal increases correspondingly **[107].** At a given temperature, the solubility of hydrogen in a metal increases with increasing pressure of hydrogen gas and at low hydrogen concentration (within solid solubility limit), the amount of hydrogen, *x* dissolved in a metal is directly proportional to the square root of gaseous hydrogen pressure, *p*.

$$x \alpha \sqrt{p} \tag{1.3}$$

The square root dependence on pressure comes from the fact that H_2 molecules are dissociated into atoms while getting dissolved in metals. This relation is known as Sievert's law. This law is obeyed by metal-hydrogen systems [102]. Since the temperature dependence of the solubility shows a thermal-activation type of behaviour, the overall expression for the solubility takes the form **[108]**

$$x = \sqrt{\frac{p}{p_0} e^{\Delta S_s / k} e^{-\Delta H_s / kT}} \tag{1.4}$$

Where, ΔH_s is called the enthalpy of solution and ΔS_s is the entropy of solution referred to the H_2 gas of pressure P_0 and temperature T. According to Fukai, ΔH_s is determined by the gross electronic structure of host metal **[108].** The exceptionally fast diffusion of hydrogen in metals can be explained by assuming that the hydrogen moves from one interstice to another as protons. It is possible that inside the metal, H dissociates into hydrogen ion (H^+) and electron (e) and the equilibrium exists of the simple form

$$H = H^+ + e \tag{1.5}$$

In the past, **[89]** this view is supported by the fact that electrolytic transport of hydrogen takes place in the direction of negative electrode when a direct current is passed through metals.

4. Bulk compound formation (Hydride formation)

The hydrogen atoms enter into the interstitial sites between metal atoms of the lattice and form the interstitial solid solution. The dissolved hydrogen atom does not replace the metal atoms from their positions in the lattice, although the original arrangement of metal atoms may be distorted or expanded. However, when the solubility of hydrogen atoms in a metal matrix is exceeded at a given temperature, a hydride phase is formed. The crystal structure of hydride phase is usually different from that of the solvent metal. However, because of limited number of interstitial sites, the composition of solid solution cannot go beyond a definite upper limit **[107].**

1.8 Research Objectives and Methodology

Tantalum is considered as a potential candidate material for the hydrogen separation membrane operating in a flowing gas at high temperature and high pressure for the separation/purification of hydrogen from a mixture of gases. The performance of the membrane depends on permeability of hydrogen through it. The permeability, in turn, depends on the solubility of hydrogen and the diffusion coefficient of hydrogen in the metal. Both solubility and diffusion coefficient are affected by the presence of other elements (substitutional impurities) in the metal. The influence of selected alloying elements on the solubility of hydrogen in tantalum is presently investigated. The various primary solid solution alloys of tantalum with nickel, chromium, iron and aluminium (Ta-Ni, Ta-Cr, Ta-Fe and Ta-Al) has been prepared using arc melting in an inert atmosphere. The effects of nickel, chromium, iron and aluminium on the solubility of hydrogen in tantalum have been investigated in a temperature range of (673 – 873) K and pressure range of (0.6 - 1.2) atmospheres using a Sievert’s apparatus. From the solubility data, obtained in the form of (equilibrium pressure-composition-temperature) graphs, the influence of the alloying elements on the hydrogen solubility is elucidated. Thermodynamic parameters of the solution process, namely, the Gibb’s free energy, enthalpy and entropy for each of the solutions are evaluated. In addition, the hydrogen absorption kinetics in the Ta-Al alloys and the possible reaction mechanisms are also analyzed.

1.9 Overview of the Thesis

The present thesis comprises of 6 chapters. Chapter 1 has presented a brief introduction about the various alternate sources of energy, tantalum, tantalum-hydrogen system and the process of hydrogen interaction with metallic system. The work carried out so far and the literature survey providing published information already available on the topic of the present work and sets the background for the presentation of the research work contained in the thesis is presented in the next chapter. Chapter 3 deals with the methodologies that are used for the preparation of tantalum-alloys, details of the various techniques that have been used for their physical and chemical characterization, the design of the Sievert’s apparatus and method used for equilibrium hydrogen charging. The results and discussions pertaining to the effect of nickel, chromium, iron and aluminium as alloying elements on the solubility of hydrogen in tantalum and on the thermodynamic parameters of tantalum-hydrogen system are presented in chapter 4. In Chapter 5 the studies carried out on isothermal hydrogen absorption kinetics and reaction mechanism of the tantalum-aluminium alloys are presented. Chapter 6 deals with the conclusions of the present study and possible directions of future work.

Chapter 2

Literature Review

2.1 Introduction

The work carried out so far and the literature surveys providing published information on the topic related with the present work are presented in this chapter. Much of the published information pertains to various basic aspects of the interaction of hydrogen with metals, viz., solubility, diffusivity, permeability of hydrogen in metals, and thermodynamics and kinetics aspects of metal-hydrogen systems.

2.2 Solubility of Hydrogen in Metals

The work on hydrogen solubility has all along been motivated by the benefits to be derived from an evaluation of both the applied and basic research points of view. Gases can get integrated into the metal dissolving in it and form the solid solution. As a result, the lattice dimensions and the density of the metal is change. The rate of dissolution depends on the degree to which the constituent processes are disposed to occur - the adsorption, the dissolution and the transport. Gases which cannot diffuse, e.g. inert gases, do not dissolve in metals. The dissolution of gases in metals occurs via energy changes - endothermic as well as exothermic processes. The experimental methods and theoretical treatments for solubility of hydrogen in metal are presented by many authors/researchers in both research papers and textbooks [1-2, 46, 81,100,102,107-113]. The literature values for the solubility of hydrogen in selected metals are presented in

Table 2.1 [81] in addition with the experimental techniques used for measurement of the solubility.

Table 2.1 Hydrogen solubility values for different metals [81]

Metal	Hydrogen concentration (H/M)	Temperature (K)	Experimental technique
V	9.1×10^{-3}	320-520	Steady-state resistance measurement
Nb	3.9×10^{-3}	320-520	Steady-state resistance measurement
Ta	1.3×10^{-2}	320-520	Steady-state resistance measurement
Fe	$\leq 6.0 \times 10^{-5}$	710-820	Hydrogen flux measurement
Ni	$\leq 3.0 \times 10^{-4}$	720-900	Hydrogen flux measurement
Pd	$\leq 1.6 \times 10^{-2}$	520-620	Hydrogen flux measurement
Ti	0.32	1070	Hydrogen flux measurement
Zr	4.6×10^{-3}	570	Steady-state resistance measurement

The hydrogen dissolved up to solid solubility limit in metals does not bring any changes in the crystal structure of metals; only single phase is present. Further uptake of hydrogen may lead to change the crystal structure of host metal and results in the formation of hydrides; e.g. M_2H, MH_2 or MH_3. The metal hydrides are formed generally by loading hydrogen into the metal either electrolytically or from a gas phase. The hydrogen atoms expand the crystal lattice of host metal during hydrogenation and causing changes in the physical properties of metal. The changes in physical properties on the hydrogen absorption may be in lattice parameters, thermal expansion coefficient, elastic constant and electrical resistivity [108, 113]. The change in the crystal structure of host metal may also induce changes in their electronic structure. Wallace et.al [114] have noted that magnetic properties of metal hydrides are also different from that of the pure metal. That hydrogen uptake sharply affects the mechanical properties of metals and results in the hydrogen embrittlement have long been known [108, 113].

The solubility of hydrogen in several transitions metals over a range of temperatures has been shown in Fig 2.1 [**100, 115-116**]. It may be observed from Fig. 2.1 that depending on the solubility range desired in a device, the metal and temperature regime may be chosen.

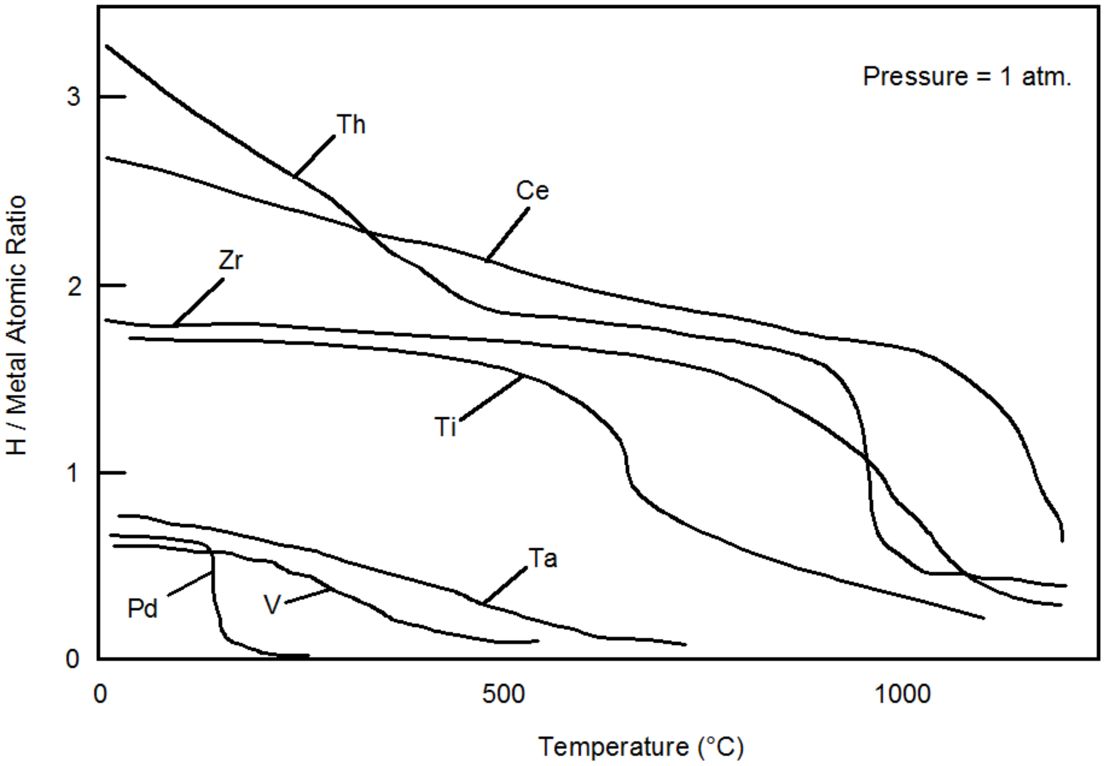

Fig. 2.1 Hydrogen solubility in several transition elements at gaseous hydrogen pressure of 1 atm. [100, 115-116]

In a device using a hydrogen separation/permeation membrane, hydrogen absorption may be cyclic and concentrations may have to fluctuate considerably across the thickness of the membrane. The large volumetric and structural variation associated with hydrogen dissolution and the hydride formation may lead to membrane failure. This method of failure is generally known as hydrogen embrittlement and applies to all form of metals. This problem can be avoided either by constructing the membrane with a material and using it in a regime which does not involve formation of a hydride or it may be inferred from Fig. 2.1 that a decrease in hydrogen concentration in the metal is observed with increasing temperature. A rapid decrease in hydrogen concentration indicates the presence and hence the decomposition of a hydride. The decomposition temperature is also strongly pressure dependent: the lower the ambient hydrogen pressure, the lower will be the decomposition temperature. Theoretically a membrane can function above the hydride decomposition temperature without suffering from hydrogen embrittlement. Fig. 2.1 shows that at a gaseous hydrogen pressure of 1 atmosphere, to avoid the hydride formation in Th, Ce, and Zr, an operation temperature in excess of 1000 °C is necessary whereas a temperature in excess of 700 °C is necessary for Ti. The high temperatures necessary to avoid hydride formation in these metals makes their use in hydrogen separation membranes difficult. The hydride decomposition temperature in Pd is below ~150 °C while in Ta and V, the gradual transitions occur between 200 °C and 600 °C. Therefore, these materials could be more preferable for use in and as hydrogen separation membranes.

In case of Ta, the operating temperature for a membrane can also be determined from Ta-H phase diagram which is shown in Fig. 1.2 in chapter 1 [79,117-118]. The Ta-H phase diagram indicates that at temperature higher than 334 K (61^{o}C), there is no stable hydride phase and only a homogeneous α-phase (Ta-H solid solution) exists in which metal atoms occupy a bcc lattice [119] and disordered hydrogen reside in tetrahedral holes of the bcc lattice [81,120-121]. The equilibrium pressure-composition isotherms for the solubility of hydrogen in tantalum [122] are shown in Fig. 2.2

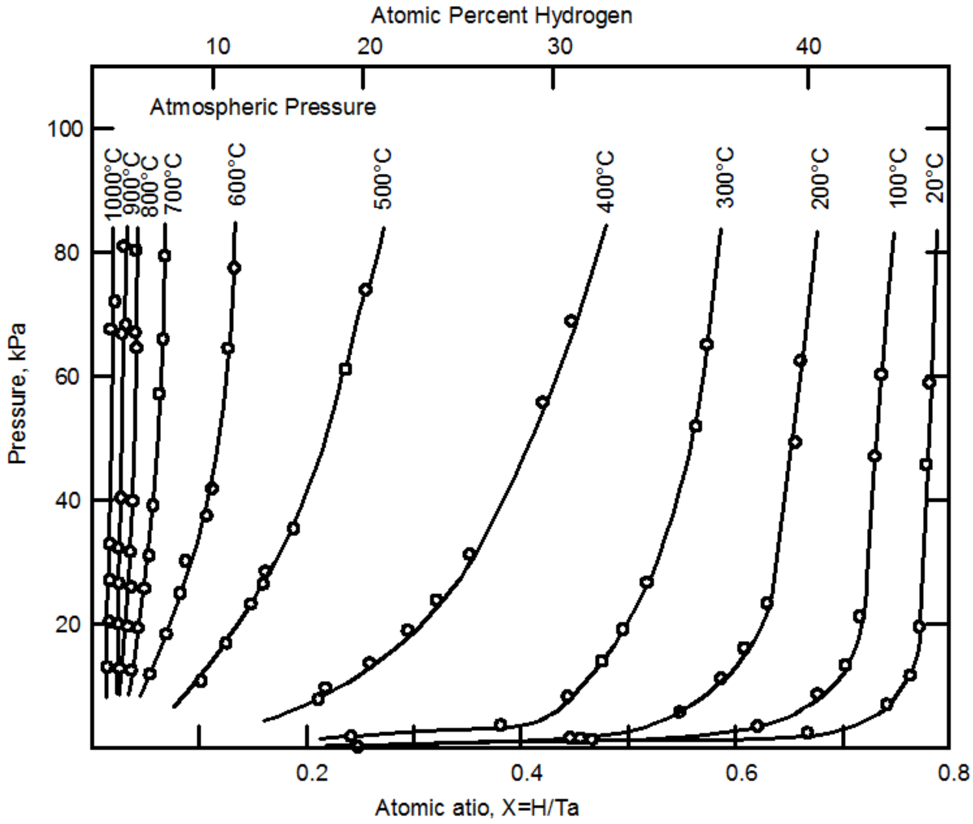

Fig. 2.2 Pressure-composition isotherm for Ta-H system [122]

The maximum solubility of hydrogen at one atmosphere pressure in tantalum is H/M = 0.79 (~7000 ppm) at 20 ^{o}C [122]. This may be noted that at temperature above 600^{o}C hydrogen solubility in tantalum is low and the metal can be exposed to hydrogen for extended periods [123]. The hydrogen absorption and embrittlement can occur during heating and cooling through the lower temperature ranges. Hydrogen can be easily removed from tantalum by heating in vacuum at temperature of 600 ^{o}C or higher.

X-ray diffraction study of Ta-H system has been carried out by various researchers [123-126]. Hagg [125] observed three phases at room temperature: a bcc phase from 0 to 12 at% hydrogen, a hcp phase at about 33 at% hydrogen and a face centered orthorhombic phase at about 50 at% hydrogen. Horn and Ziegler [126] has observed that up to 34 at% hydrogen in tantalum, only single phase (bcc) exists at room temperature whereas lattice expansion is observed with the increment of hydrogen concentration [127]. Brauer et al and Stalinski have reported two phases in Ta-H system at room temperature separately [78].

2.2.1 Dependence of Hydrogen Solubility on Pressure

When hydrogen dissolves in metals, the process involves its dissociation into atoms [128]:

$$H_2 = [H] + [H] \tag{2.1}$$

The equilibrium constant of this reaction is given by

$$K = \frac{a_H^2}{p_{H_2}} \tag{2.2}$$

For the small amount of dissolved hydrogen in metals, its activity is proportional to its concentration, and the equation becomes [128]

$$K = \frac{[\%H]^2}{p_{H_2}} \tag{2.3}$$

This equation reveals that the amount of hydrogen dissolved in a metal is proportional to the square root of the equilibrium hydrogen gas pressure.

$$[\%H] = K\sqrt{p_{H_2}} \tag{2.4}$$

In agreement with this equation, for the solid solubility of H_2 gas in metals, the concentration of dissolved hydrogen is always found experimentally to be proportional to the square root of hydrogen gas pressure [129] in the range where Eq. (2.1) holds. This

√P relation originally elucidated by Sievert and his coworkers is known as Sievert's law [116].

2.2.2 Dependence of Hydrogen Solubility on Temperature

Apart from the dependence on pressure, the solubility of gases in metals is also dependent on temperature. The dependency can be related as [128]:

$$K_s = c/\sqrt{p} = \exp\left(-\overline{\Delta H_H}/RT\right)\exp\left(\overline{\Delta S_H}/R\right) \tag{2.5}$$

Hydrogen dissolves in the metals in atomic form.

At equilibrium,

$$\overline{G_H} = 1/2\,G_{H_2} = 1/2\left(G^0_{H_2} + RT\ln p_{H_2}\right) \tag{2.6}$$

Where, $\overline{G_H}$ is the partial molar Gibb's free energy of hydrogen in metal, G_{H_2} is the molar Gibb's free energy of gaseous hydrogen at a given pressure, and $G^0_{H_2}$ is the molar Gibb's free energy of gaseous hydrogen at 1 atm pressure [128]. Eq. (2.6) is valid only for the pressures at which gas is behaving ideally.

Eq. (2.6) can be rewritten as

$$\overline{\Delta G_H} = \overline{G_H} - 1/2\,G^0_{H_2} = 1/2\,RT\ln p_{H_2} \tag{2.7}$$

Where, $\overline{\Delta G_H}$ is the partial molar Gibb's free energy of hydrogen in metal with respect to gaseous hydrogen at 1 atm or the relative partial molar Gibb's free energy. This relative change in Gibb's free energy is related with the relative change in enthalpy, $\overline{\Delta H_H}$

(relative partial molar enthalpy) and the relative change in entropy, $\overline{\Delta S_H}$ (relative partial molar entropy) by the following relation:

$$\overline{\Delta G_H} = \overline{\Delta H_H} - T\overline{\Delta S_H} \tag{2.8}$$

For dilute solution of gases in metals, within solid solubility limit, the equation below is valid:

$$\overline{\Delta H_H} - T\overline{\Delta S_H} = -RT \ln a \big/ \sqrt{p} \tag{2.9}$$

For very dilute solution of hydrogen in metals, the activity of hydrogen, *a* in metal may be replaced by weight percent hydrogen in the solution, *c* and equation (2.9) can be written in the form:

$$\ln K_s = \ln c \big/ \sqrt{p} = -\overline{\Delta H_H} \big/ RT + \overline{\Delta S_H} \big/ R \tag{2.10}$$

or

$$K_s = c \big/ \sqrt{p} = \exp\left(-\overline{\Delta H_H} \big/ RT\right) \exp\left(\overline{\Delta S_H} \big/ R\right) \tag{2.11}$$

From these equations, it is observed that solubility is not only dependent on temperature but also on pressure [128, 130]. One important conclusion derived from these equations is that the solubility of hydrogen in a metal at constant pressure will increase with the temperature if reaction is endothermic, i.e. $\overline{\Delta H_H}$ is positive (e.g. Cu, Ag, Cr, Mo, W, Fe, Co, Ni, Al, Pt), whereas the solubility will decrease with increasing temperature if the reaction is exothermic, i.e. $\overline{\Delta H_H}$ is negative (e.g. Ce, La, Ti, Zr, Hf, Th, V, Nb, Ta, Pd).

In the simplest case, $\overline{\Delta H_H}$ and $\overline{\Delta S_H}$ are nearly independent of temperature and from equation (2.10), one should get a straight line when *log c* is plotted against 1/*T* at constant pressure for the dilute solution of hydrogen in metal.

2.3 Diffusion of Hydrogen in Metals

Gases adsorbed on the surface of the metal diffuse inside the bulk of the metal in atomic form [104]. Diffusion is the process of leveling of the activity of hydrogen throughout the region under consideration there by attaining a condition of equilibrium between the gas in the metal and that in system surrounding. Only certain gases can diffuse through certain metals but hydrogen diffuses in many metals. The diffusion coefficient of hydrogen in selected metals is given in Fig. 2.3. The general trend is an exponentially increasing diffusion coefficient with increasing temperature, reflecting the activated nature of the diffusion process.

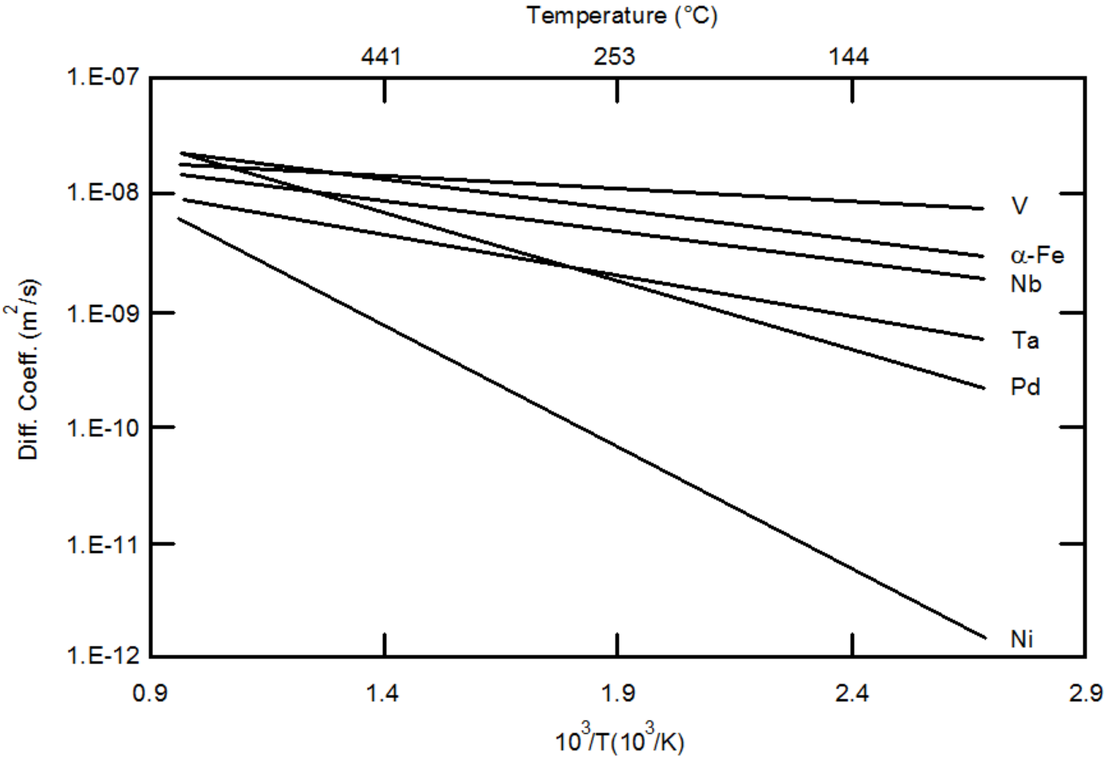

Fig. 2.3 Diffusion coefficient of hydrogen in several transition metals [46]

The rate of diffusion of diatomic gases through metals is expressed by the formula [131]

$$D = \frac{n}{d}\sqrt{p}.e^{-E_d/2RT} \tag{2.12}$$

where D is the amount of gas diffusing through unit area of a specimen of unit thickness per unit time at an absolute temperature T when the metal is exposed to gas at a partial pressure p, n and R are constants, E_d is the activation energy for diffusion, characteristics of a given system (gas/metal), and d is the thickness of the specimen. Generally the rate of diffusion is expressed as number of moles of gas passing per unit area per unit time or the volume of gas in cm^3 passing through 1 mm^2 of the surface in 1 *sec* at a given temperature [131].

From the Eq. (2.12), it is clear that rate of diffusion increases rapidly with increase of temperature while with increase of pressure; rate varies in proportion to the square root of pressure. The diffusion rate is inversely proportional to the thickness of metal through which gas is passing. The above relation is not valid for the metals whose surface is coated with some oxide or other films. In such cases, diffusion does not depend on gas pressure. The rate of diffusion is not influenced by the grain size as diffusion occurs principally through crystal lattice of the metal and not through the grain boundaries or cleavage planes [104]. The presence of impurities affects the rate of diffusion due to changes in crystal lattice of the metal. The atoms of hydrogen gas have small volume (size) and hence diffuse more rapidly in metals than other gases. The diffusion coefficients of hydrogen/deuterium in the V, Nb, Ta and Pd have been shown in an Arrhenius plot in Fig 2.4 [132].

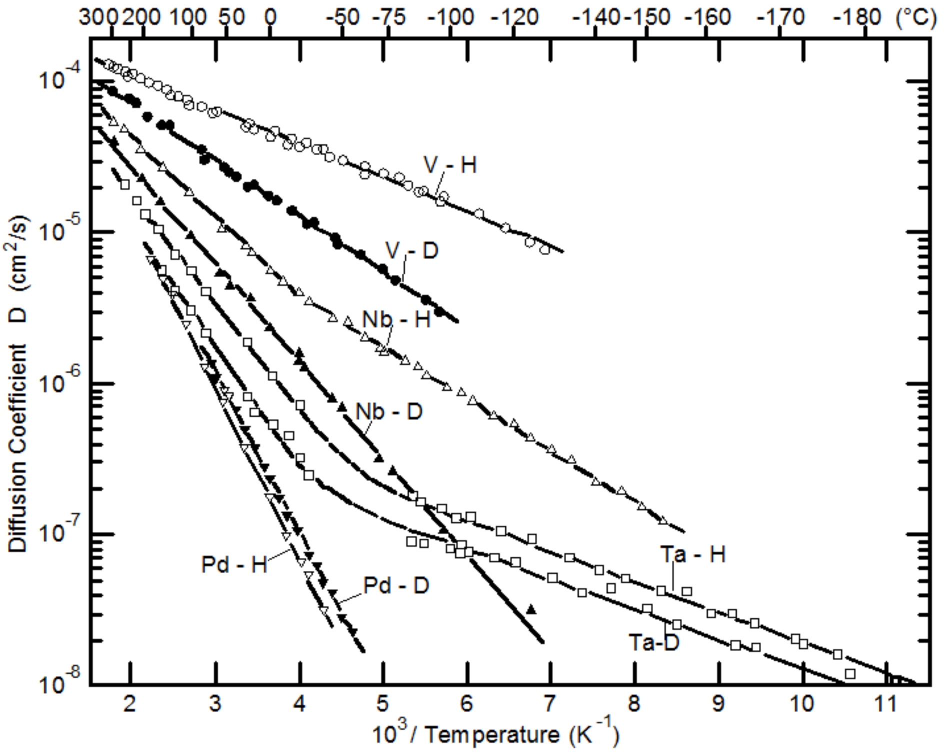

Fig. 2.4 **Diffusion coefficients of H and D in the V, Nb, Ta and Pd [132]**

Fig. 2.4 has indicated that diffusion coefficient of H in group V metals is larger than in Pd. At room temperature, their values are in the range of 10^{-5} cm^2/s in group V metals but only 10^{-7} cm^2/s in palladium.

The smaller activation energy (given by the slope of the corresponding curve in the figure) for diffusion in BCC metals is due to the smaller atomic packing factor of 0.68 in BCC materials versus 0.74 in FCC materials. The less tightly packed BCC structure has larger gaps for hydrogen to penetrate in the diffusion process resulting in lower activation energy [132].

2.4 Permeability of Hydrogen in Metals

Permeability is defined as a product of solubility and diffusivity that was discussed in earlier sections. The aim of the present section is to combine the results from those sections and present permeability information for a variety of pure metals. From this data estimation of the expected performance of several competing membrane materials can be made.

The diffusion and permeation of hydrogen through metals is occurring in the following stages [104]: dissociation of molecular hydrogen and development of activated adsorption on the surface, release of hydrogen from the adsorbed layer and its passage into solution, movement of dissolved hydrogen through the crystal lattice (diffusion proper), passage of hydrogen through the bulk of metal to the adsorbed state on the opposite side, recombination to form hydrogen molecules and desorption of hydrogen molecules.

The rate of passage of hydrogen through the metal is known as “coefficient of permeability” and this is measured in cm^2/sec. This coefficient defines the rate of liberation of gases from the metal. However, it encompasses the three consecutive stages of diffusion but not simply third stage that is diffusion proper, that's why it is not called "coefficient of diffusion" [104].

In most of the cases, the dissociation of molecular hydrogen and condition of the metal surface play a key role on the interaction of hydrogen with metal. However, metal, in its normal state is impermeable to gas of atmospheric pressure, but takes hydrogen readily inside the lattice when liberated upon it electrolytically or by chemical displacement. A rough metal surface provides a larger area for activated adsorption. Permeability can also be increased by plastic deformation. The increase of permeability is accompanied by increase of occlusive capacity **[100].** The permeability of several metals to hydrogen as a function of temperature is shown in Fig. 2.5 **[40, 133-134]**. These values are not measured across the entire temperature range but instead are extrapolated from the temperature dependence of the diffusion coefficient and solubility of each material from measurements made in a region where Sieverts' Law is obeyed (hydrogen behaves as an ideal solution in the metal) [33].

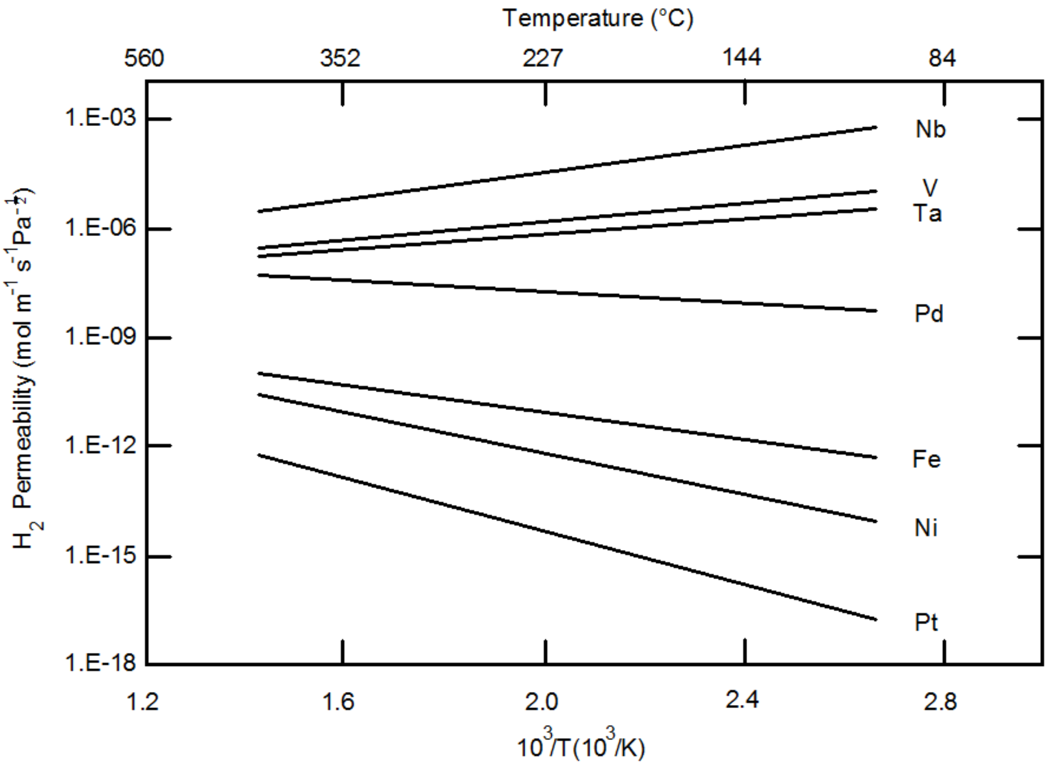

Fig. 2.5 Hydrogen permeability in several transition elements [40, 133-134]

It is indicated from Fig. 2.5 that there is a transition in activation energy from positive to negative on moving from the metal with the lowest permeability, Pt, to the metal with the highest permeability, Nb, with the change in slope of each curve from negative to positive values. Referring back to Fig. 2.3, the diffusion coefficient of each of these metals has a negative slope, which associates with the positive activation energy. Therefore, this shift in the temperature dependence of the permeability for some of these materials points out that the permeability behavior may be basically controlled by the hydrogen solubility [104].

The temperature dependence of Sievert's Law is given by Eq. (2.10) where $\overline{\Delta H_H}$ and $\overline{\Delta S_H}$ are the relative change in enthalpy and the entropy for solution of hydrogen in metals, respectively, both in the limit of infinite dilution.

Since the permeability is the product of diffusion coefficient and solubility and is expressed by the formula,

$$\Phi = D_0 \exp\left(\frac{\overline{\Delta S_H}}{R}\right) \cdot \exp\left(\frac{-\left(E_d + \overline{\Delta H_H}\right)}{RT}\right) \qquad (2.13)$$

The apparent activation energy for hydrogen permeability will be the sum of the heat of solution and activation energy of diffusion. For strong exothermic absorbers of hydrogen (Ta, V, Nb) the large negative heat of absorption compensates the activation energy for diffusion resulting in a negative activation energy for permeation (decreasing values with increasing temperature). For moderately exothermic and endothermic absorbers, the diffusion term dominates and the apparent activation energy for permeation remains positive. Comparing the overall magnitudes of permeability in Fig. 2.5, it is observed that the Group V metals, namely, vanadium, niobium and tantalum are considerably better than palladium over the entire temperature range. Moreover, the difference in cost and relative abundance between these materials and Pd make them potentially more attractive materials for hydrogen permeation.

2.5 Tantalum as Hydrogen Permeation Membrane

The ideal hydrogen permeation membrane should have high hydrogen permeability and good mechanical properties [135] to endure the required pressure difference between the upstream and downstream sides, high temperature, and to be resistant to hydrogen induced mechanical degradation. Tantalum is considered as a promising material as a component in hydrogen separation membranes operating at a range of temperatures and pressures [33, 43, 99,136]. Tantalum has large hydrogen solubility and considerable hydrogen diffusivity. The equations for hydrogen in tantalum are given in Table 2.2 [134]. Compared to Pd, Ta is relatively cheaper and possesses an order of magnitude larger hydrogen permeability [33, 48, 99-100, 134, 137-140].

Table 2.2 The equations for hydrogen in tantalum [134]

Solubility, S(H_2/Ta)	$= 0.132 \exp(4050/T)$ mol/m^3.Pa$^{1/2}$	(2.14)
Diffusivity, D(H_2/Ta)	$= 4.4 \times 10^{-8} \exp(-1620/T)$ m^2/s	(2.15)
Permeability, ϕ (H_2/Ta)	$= 5.8 \times 10^{-9} \exp(2430/T)$ mol/m. s .Pa$^{1/2}$	(2.16)

Tantalum is a mechanically sound material that can easily be integrated into a metal infrastructure for service over a wide temperature range. Incidentally, tantalum could be used as a crucible material readily permeable to hydrogen, for the hydrogenation of alkaline earth metals in the temperature range of 900-1213 K [139].

The hydrogen embrittlement and tendency to pulverization during hydrogenation are the main issues preventing use of tantalum metal commercially for hydrogen permeation membrane [33, 43,135,141]. The change of lattice parameter or formation of hydrides mainly at low temperatures leads to hydrogen embrittlement [26]. Therefore, reducing or moderating the hydrogen solubility in tantalum in a controlled manner could be thought of as an approach to make mechanical properties of the membrane more suitable [23]. The addition of alloying elements which are having less hydrogen solubility or that do not form the metal hydrides could be a useful way to control the hydrogen solubility, to destabilize the hydrides and hence, to preserve the mechanical properties of the membrane without altering parameters such as temperature or hydrogen pressure [23,137]. The effects of Fe, Al, Ni, Cr, Mo, Cu, Pd, and Sn as alloying additions on the solubility and permeability of group V elements have been reported in the literature [23, 50, 53, 142-149]. In all the alloys, the observed solubility and permeability is lower than pure metal. Significantly, though, the resistant to hydrogen embrittlement and strength of these alloys are much better than the pure metal, while the permeability is still greater than the leading palladium alloy [100]. The effects of Ni, Cr, Fe and Al on the solubility of hydrogen in tantalum studied in the present thesis have not previously been reported in the literature. The literature data available for the apparent hydrogen permeability of tantalum is shown in Table 2.3 in a range of temperature and pressure [33].

Table 2.3 Published literature data for apparent hydrogen permeability of tantalum disks [33]

	Investigator	X_{Ta} (mm)	X_{Pd} (μm)	T (K)	$P_{Tot.Feed}$ (kPa)	$P_{H2.Feed}$ (kPa)	$P_{tot.Per}$ (kPa)	$P_{H2.Per}$ (kPa)	K× 10^8 (mol/msPa$^{0.5}$)	R^2 (k×10^8)	K× 10^8 (mol/msPa^n)	n	R^2
	Ta7 (NETL)	1	0	973	130.6-2910.5	116.0-2585.7	126.4	0.27-3.45	1.73	0.985	0.185	0.65	0.996
2	Ta7 (NETL)	1	0	1073	130.6-2903.6	116.0-2579.5	126	0.25-3.43	1.25-3.71	0.903	0.024	0.77	0.976
3	Ta7 (NETL)	1	0	1173	130.6-2931.5	116.0-2604.4	125.7-126.4	0.54-3.31	1.75	0.976	6.710	0.59	0.966
4	Ta7 (NETL)	1	0	873	106.9-1611.4	94.9-1583.7	125.7-127.1	0.08-1.70	0.94	0.888	0.0054	0.86	0.997
5	Pd/Ta (Buxbaum,1996)	0.07-0.54	~1	693	101-303	101-303	0-150	0-150	14.50	NA	NA	NA	NA
6	Pd/Ta (Buxbaum,1996)	NA	~1	682	20-101	20-101	~0	~0	11.00	NA	NA	NA	NA
7	Pd/Ta (Buxbaum,1996)	NA	~1	697	20-101	20-101	~0	~0	13.00	NA	NA	NA	NA
8	Pd/Ta (Buxbaum,1993)	2	2	616	373	280	101	5	7.50	NA	NA	NA	NA
9	Pd/Ta (Buxbaum,1993)	2	2	630	373	280	101	5	7.90	NA	NA	NA	NA
10	Pd/Ta (Buxbaum,1993)	2	2	644	373	280	101	5	8.80	NA	NA	NA	NA
11	Pd/Ta (Buxbaum,1993)	2	2	658	373	280	101	5	9.80	NA	NA	NA	NA
12	Pd/Ta (Buxbaum,1993)	2	2	671	373	280	101	5	10.70	NA	NA	NA	NA
13	Pd/Ta (Buxbaum,1993)	2	2	686	373	280	101	5	11.60	NA	NA	NA	NA
14	Pd/Ta-electroless (NETL)	1	~1	623	106.2-106.9	94.3-94.9	127.1	0.66-0.71	1.92	NA	NA	NA	NA
15	Pd/Ta-electroless (NETL)	1	~1	923	106.2-2910.5	94.3-2585.7	125.0-127.1	0.04-0.77	0.12-0.58	0.793	0.0044	1.01	0.996
16	Pd/Ta-electroless (NETL)	1	~1	1173	106.2-1248.2	94.3-1108.9	125.7-127.1	0.14-0.18	0.38-0.39	0.911	5.95	0.46	0.896
17	Pd/Ta1-sputter (NETL)	1	~0.04	623	106.2	94.3	127.1	1.81	4.65	NA	NA	NA	NA
18	Pd/Ta2-sputter (NETL)1	1	~0.04	623	104.8	93.1	127.1	3.42	12.6	NA	NA	NA	NA
19	Pd/Ta3-sputter (NETL)	1	~0.04	1173	117.0-123.0	104.9-111.1	140.0-141.0	0.69-0.74	1.83-2.28	NA	NA	NA	NA
20	Pd/Ta4-sputter (NETL)	1	~0.04	923	122.3-2845	110.0-2560	143.8-2886	0-1.63	0.04-3.88	NA	NA	NA	NA
21	Pd/Ta4-sputter (NETL)	1	~0.04	1173	120.7-2859	108.6-2573	142.7-2887	0.58-13.2	0.22-2.76	NA	NA	NA	NA
22	Pd/Ta10-sputter (NETL)	1	~0.04	623	200.6	180.5	161.3	3.44	6.38	NA	NA	NA	NA
23	Pd/Ta6-sputter (NETL)	1	~1.2	923	136.9-2896.6	123.2-2606.9	138.9-2896.6	0.22-121.22	1.16	0.954	0.108	0.65	0.997
24	Pd/Ta7-sputter (NETL)	1	~1.2	1173	139.7-140.4	125.7-126.4	138.3-139.7	2.00-2.73	1.43-2.40	NA	NA	NA	NA
25	Pd/Ta8-sputter (NETL)	1	~1.2	773	158.6-940.9	142.7-846.8	151.6-865.4	3.11-36.24	6.33-8.55	0.995	649.0	0.44	0.995

2.6 Thermodynamics of Hydrogen in Metals

The thermodynamics of interaction of hydrogen with metal is usually described by presenting the pressure-composition-temperature (*P-C-T*) relationship. A schematic *P-C-T* curve for a metal -hydrogen system is shown in Fig. 2.6 [83].

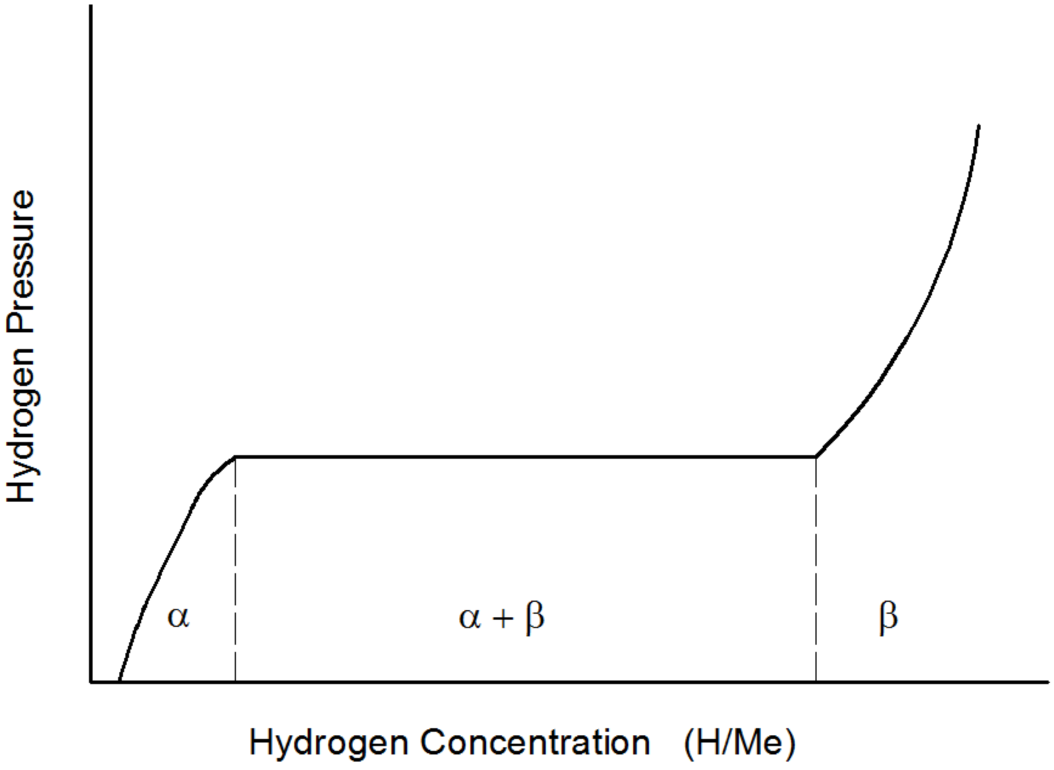

Fig. 2.6 **Schematic pressure - composition isotherm,** *When the terminal solubility of the α-phase is reached at the plateau pressure, the precipitation of the hydride phase β starts* [83].

In the *P-C-T* curve in Fig. 2.6, initially on increase of the hydrogen pressure the solubility of hydrogen in metal or alloy forming α-phase increases. Further increases in the hydrogen concentration in the lattice, results in precipitation of the hydride phase (β-phase). When hydrogen is consumed to form the hydride, the equilibrium pressure of hydrogen does not change. The hydride formation is indicated by the plateau of the plot. In the plateau region, the solid solution and the hydride phase coexist (α and β phases).

The length of the plateau determines how much amount of hydrogen can be stored and recovered by means of a small change in pressure. The last portion represents the hydride phase only, the hydrogen pressure increases steeply with concentration in this region, due to the change in stoichiometry of the hydride phase.

Thermodynamic parameters for the solubility of hydrogen in metals are described by applying Sievert's law as given in Eq. (2.11). The equilibrium between metal and hydrogen can be represented by the following equation:

$$M + (x/2)H_2 \leftrightarrow x[H]_M \tag{2.17}$$

Combining the Gibbs free energy expression,

$$\overline{\Delta G_H} = \overline{\Delta H_H} - T\overline{\Delta S_H} \tag{2.18}$$

And, the relation

$$\overline{\Delta G_H} = RT \ln p_{H_2} \tag{2.19}$$

The hydrogen pressure and enthalpy of hydrogen solution are related with each other as follows

$$\ln p_{H_2} = \overline{\Delta H_H} \big/ RT - \overline{\Delta S_H} \big/ R \tag{2.20}$$

This relation, the well known van't Hoff relation, where $\overline{\Delta H_H}$ and $\overline{\Delta S_H}$ are the relative change in enthalpy and entropy per mole of H_2 gas respectively, permit calculation of the relative change in enthalpy and the entropy of the solution of hydrogen, by information from the pressure composition isotherm at different temperatures as shown in Fig. 2.7 [83,150].

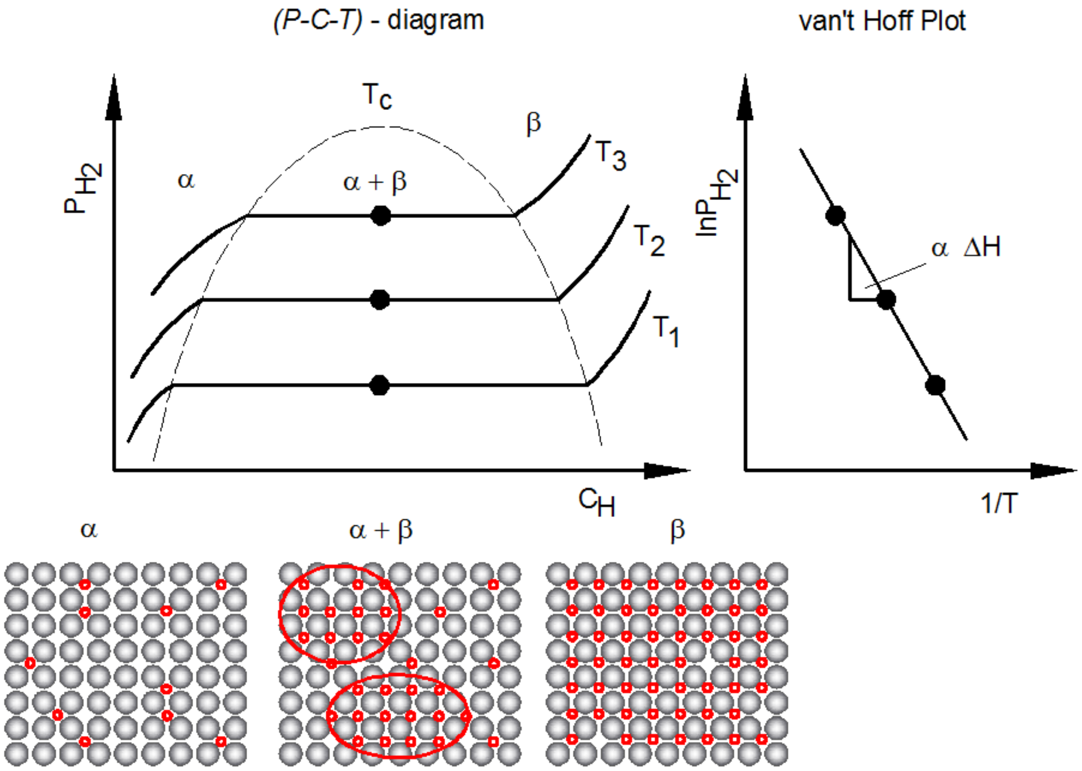

Fig. 2.7 **Schematic *P-C-T* diagram at different temperature *(T_1<T_2<T_3<T_c)*, and the van't Hoff plot.** *α-phase is the solid solution phase, the β-phase is the hydride phase and in the (α-β) two phase region both the metal-hydrogen solution and the hydride phase coexist* [83, 150].

The plateau pressure or equilibrium pressure of the *P-C-T* diagram depends on the working temperature. With increase in the temperature, the plateau pressure increases and the width of plateau region decreases. At a critical temperature (T_c), no plateau exists. The plot of logarithm of hydrogen pressure $(\ln p_{H_2})$ verses reciprocal of temperature *(1/ T)* (known as van't Hoff plot) is also shown in Fig. 2.7 for the single phase regions.

The enthalpy of the solution of hydrogen in metals can be calculated from the slope of the $\ln p_{H_2}$ vs *1/ T* plot; and the intercept of the curve gives the entropy of solution. The value of $\overline{\Delta H_H}$ can vary widely for different materials as it may vary from a large negative to a positive value whereas the entropy of hydrogen solution, $\overline{\Delta S_H}$ is approximately constant for all metal-hydrogen systems as it arises mainly from the entropy loss of gaseous hydrogen during hydrogen uptake by the metal [151].

Some of the typical enthalpy values for the solution of hydrogen in different metals have been listed in Table 2.4.

Table 2.4 Enthalpy of solution of hydrogen in elements of periodic system [151]

Element	Enthalpy of solution (kJ/mol H)	Element	Enthalpy of solution (kJ/mol H)
He	-	Ag	63
Li	-51	Cd	-94
Be	-2	In	-
B	-4	Sn	125
C	-	Sb	-
N	-	Te	-84
O	-	I	-
F	-	Xe	-
Ne	-	Cs	-56
Na	2	Ba	-88
Mg	21	La	-67
Al	60	Ce	-74
Si	180	Pr	-68
P	-	Nd	-50
S	-	Pm	-
Cl	-	Sm	-70
Ar	-	Eu	-
K	0	Gd	-69
Ca	-94	Tb	-78
Sc	-90	Dy	-79
Ti	-52	Ho	-
V	-30	Er	-
Cr	28	Tm	-
Mn	1	Yb	-
Fe	25	Lu	-79
Co	21	Hf	-38
Ni	12	Ta	-36
Cu	46	W	96
Zn	15	Re	-
Ga	-	Os	-
Ge	221	Ir	74
As	-	Pt	35
Se	35	Au	32
Br	-	Hg	-
Kr	-	Tl	-
Rb	-54	Pb	62
Sr	-61	Bi	-
Y	-79	Po	-
Zr	-58	At	-
Nb	-35	Rn	-
Mo	25	Fr	-
Tc	-12	Ra	-
Ru	54	Ac	-
Rh	27	Th	-40
Pd	-10	Pa	-
		U	7

The group V elements, vanadium, niobium and tantalum form the wide range of solid solution with hydrogen above critical temperature [79,108]. For Pd-H system, *P-C-T* data have been obtained both above and below the critical temperature but in case of V-H, Nb-H and Ta-H systems, obtaining the *P-C-T* data below critical temperature are difficult because of the slowness of achieving equilibrium [152]. However, large number of *P-C-T* data is available for these systems above the critical temperature. The objective in the present work is to review the *P-C-T* data for Ta-H system and evaluation of thermodynamics parameters from these *P-C-T* data for tantalum-hydrogen system and find out the effects of alloying elements on the solubility and thermodynamic properties for Ta-H system. Thermodynamic quantities for Ta-H system have been reported by many investigators separately using *P-C-T* curves [79-80,119,152-156]. Pressure-composition-isotherms for Ta-H system in the temperature range of (350 - 631) ^{o}C are shown in Fig. 2.8 [152]. All isotherms show monotonic increases of the equilibrium hydrogen pressure with composition, which indicate that in this region only single homogeneous phase exist for Ta-H system. It is observed that with increase in temperature and consequently decrease in hydrogen solubility, the isotherms progressively move toward linearity as required by the Sievert’s law.

With decrease in temperature, the isotherms become progressively more curved suggesting that a miscibility gap exists in the Ta-H system at still lower temperatures. The hydrogen desorption data is also shown in Fig. 2.8. There is no hysteresis between absorption and desorption curves which indicate that hydrogen-metal reactions are reversible in Ta-H system.

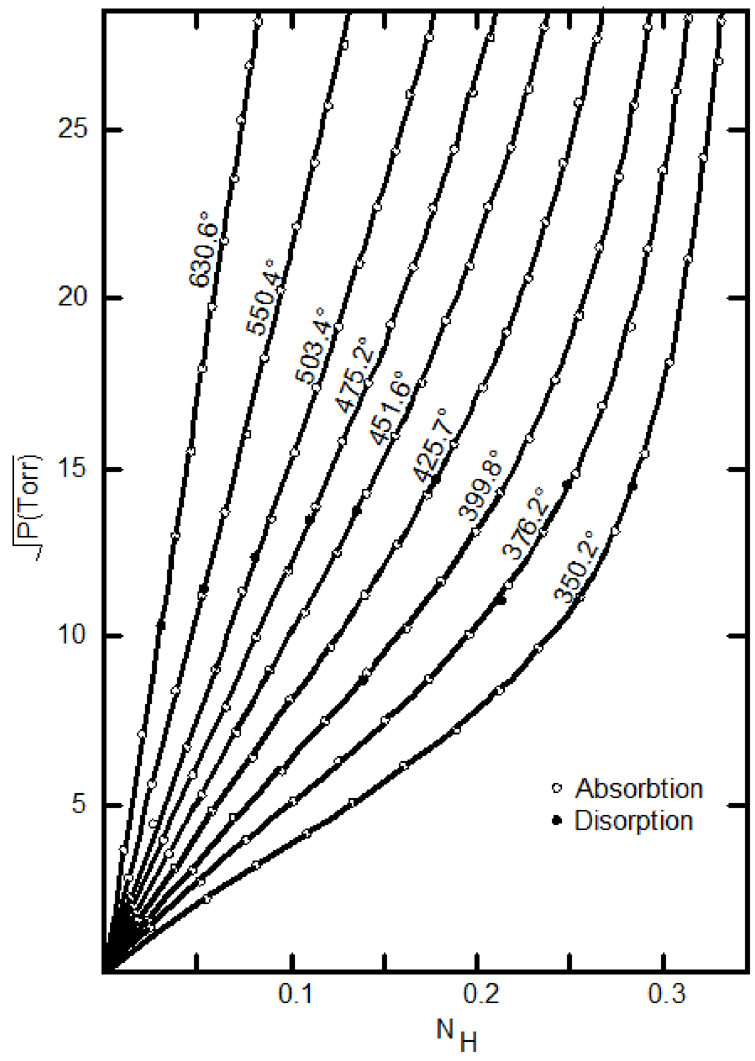

Fig. 2.8 **Pressure-composition-isotherms for the Ta-H system** [152]

Literature values for the thermodynamic data for Ta-H system are shown in Fig. 2.9; where, Veleckis and Edwards data [152] is represented by solid line, dashed line represents the data given by Kofstad, Wallace and Hyvonen, [153] while dashed line along with dots represents the Mallet and Koehl data [80].

It was found that the relative partial molar enthalpies, $\overline{\Delta H_H}$ and entropies, $\overline{\Delta S_H}$, of hydrogen are virtually constant with respect to temperature for a given concentration in the given temperature range [79-80,119,152-156]. The free energies in Fig. 2.9 **[**152**]** are calculated at 400 ^{o}C.

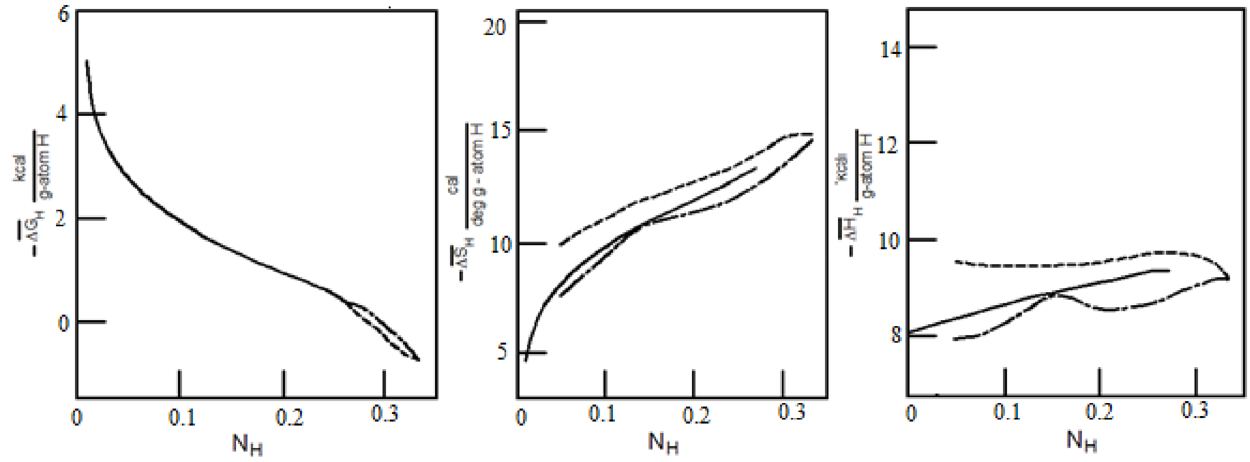

Fig. 2.9 **Thermodynamic data for Ta-H system [152] [1cal = 4.184 Joules]**

In the present thesis, the thermodynamic values for Ta-H system were calculated from the equilibrium *P-C-T* data in the temperature range of (673-873) K and compared with the literature values (chapter 4). The effect of alloying elements on the *P-C-T* data for Ta-H system and their thermodynamic parameters are also presented.

2.7 Mechanism and Kinetics of Hydrogen Entry into Metallic Systems

Hydrogen dissolves in metals in the form of atomic hydrogen [157]. The atom separates into protons and electrons by a simple ionization process. The hydrogen atom can lose its electron to the electronic bands of metallic materials, especially the transition metals. This is indicated by the observed linear decrease of magnetic susceptibility with increasing hydrogen concentration [158].

The kinetics of hydrogen absorption in tantalum calculated by the time dependent amount of hydrogen absorbed by weighted tantalum sample has been reported in the literature [159]. Hydrogen absorption isotherms of tantalum at various temperatures are shown in Fig. 2.10. The process of hydrogen absorption is very slow at temperature below 573 K while at temperature 573 K or higher, the processes occur at a reasonable rate. Hence, the time needed to achieve maximum hydrogen uptake is temperature dependent. Fig. 2.10 has indicates that the hydriding capacity decreases with increase in temperature.

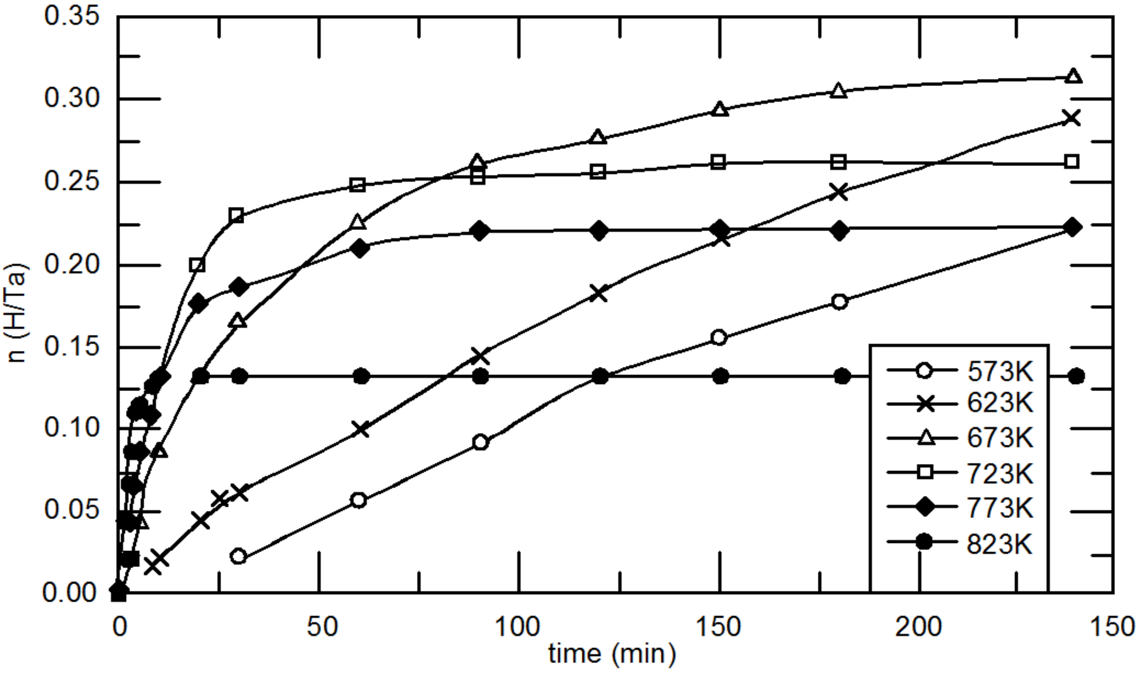

Fig. 2.10 **Hydrogen absorption isotherms of tantalum at various temperatures [159]**

The amount of hydrogen in tantalum is represented by the H/Ta mole ratio. The H/Ta mole ratio decreases with increasing temperature which indicates that the equilibrium of the hydriding reaction $Ta + x/2\ H_2 = TaH_x$ is shifted towards left. Therefore, the composition of the absorbed hydrogen is temperature dependent. Addition of a small amount of palladium (0.03 wt. %) significantly accelerates the kinetics of hydrogen absorption in tantalum. It is also reported that the hydriding rate at 673 K is about 30 times more for palladized Ta than for the pure Ta, although the capacity for hydrogen absorption has not been affected **[159]**.

The hydrogen absorption in tantalum has followed the first order kinetics as shown in Fig. 2.11. The first order kinetics equation is as follow:

$$\log k = \frac{2.303}{t} \log \frac{a}{a-x} \tag{2.21}$$

Where, *k* is the rate constant, *a* is the initial mole fraction of Ta, and *x* is the mole fraction of tantalum hydride formed in time *t*.

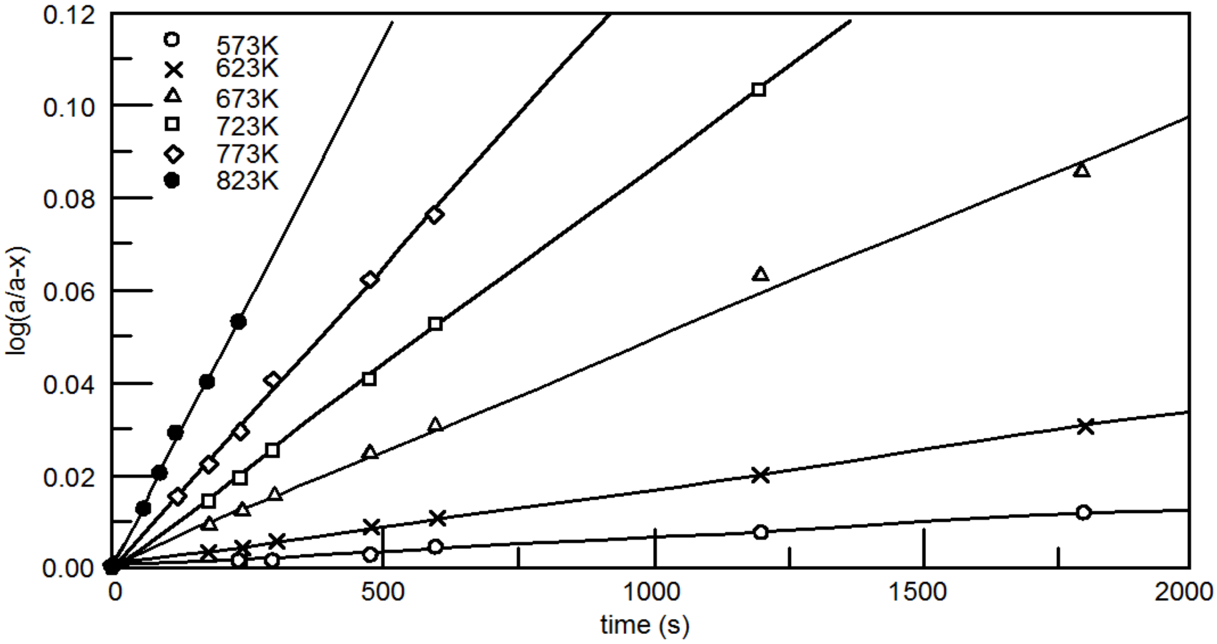

Fig. 2.11 ***log (a/(a-x))* vs. time plot for tantalum hydriding at different temperatures [159]**

The rate constants for hydrogen absorption in Ta were determined at each temperature from the slope of curves in Fig. 2.11. The activation energy of hydrogen absorption in tantalum calculated by using Arrhenius plot is found to be 56.2 kJ/mol **[159]**.

The rate of hydrogen absorption in tantalum is strongly hindered by the presence of oxygen at temperature below 700 K [160]. The hydrogen absorption rates, ν_H, of three pretreated tantalum specimens are shown in Fig. 2.12. A huge difference is observed between the hydrogen absorption rates in these samples at lower temperatures. However, around 750K all three specimens exhibit a similar absorption rate [160]. These observations from Fig. 2.12

has demonstrated that the previous treatment of the specimen become less important at reaction temperature higher than 750 K.

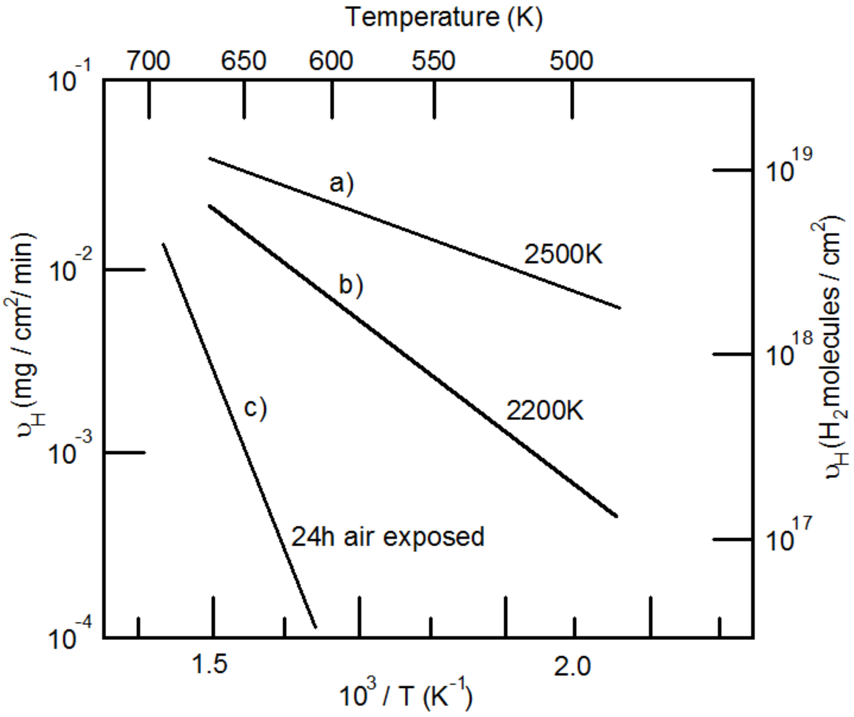

Fig. 2.12 Temperature dependence of the hydrogen absorption rate of three typically prepared tantalum specimens: *(a) degassed at 2500 K; (b) degassed at 2200 K; (c) degassed at 2500 K and exposed to air for 24 hours at room temperature* [160]

The kinetics for the hydrogen evolution from tantalum wire has also been reported in the literature [161]. To find out the rate of evolution of hydrogen from the tantalum wire maintained at constant temperature, the variations of square root of hydrogen pressure with time are shown in Fig. 2.13. The logarithms for the slopes of the curves in Fig. 2.13 have been plotted against *1/ T* as shown in Fig. 2.14. The value of the activation energy for the degassing process, as calculated from the slope of curve in Fig. 2.14 was found to be – (33.0 ± 1.5) kJ/mol.

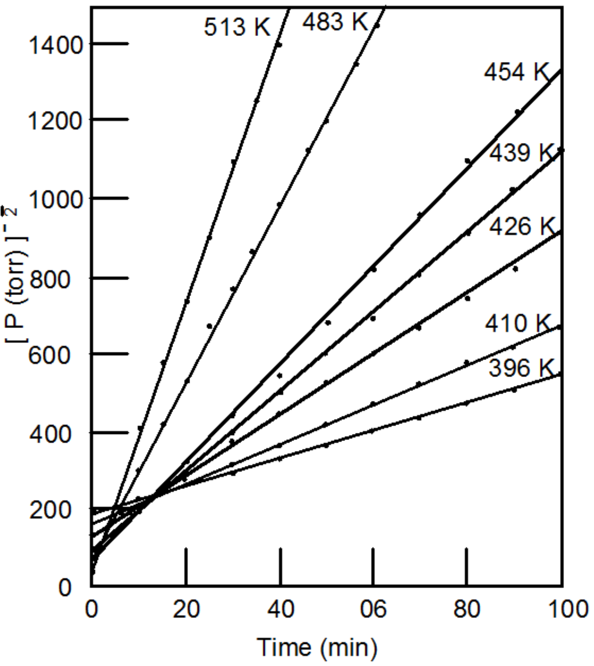

Fig. 2.13 **Typical variation of *1/√p* as a function of time for the rate of evolution of hydrogen from tantalum wire at different temperatures** [161]

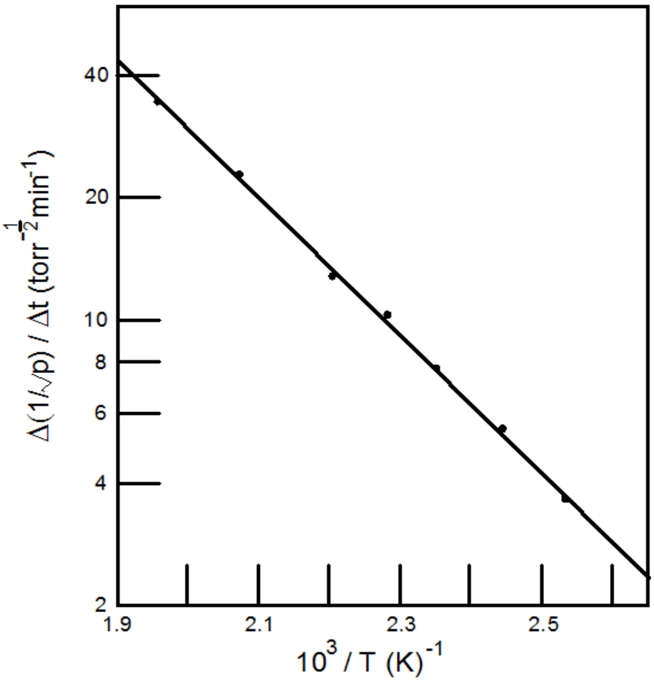

Fig. 2.14 **Logarithms of the slopes of the curves in Fig. 2.13 plotted as a function of reciprocal temperature** [161]

2.8 Summary

Tantalum is a potential candidate material for the hydrogen separation membrane due to its good hydrogen solubility and large hydrogen diffusivity. The permeability is a product of solubility and diffusivity. The hydrogen solubility in tantalum and its alloys is one of the parameters responsible to estimate the permeability. The hydrogen embrittlement associated with tantalum at low temperature is the main limitation of its use in membrane applications. Alloying with the elements which are having less hydrogen solubility or destabilize the hydrides can be a way to overcome this limitation. In the present work, the effect of nickel, chromium, iron and aluminium on the solubility of hydrogen in tantalum has been investigated. In addition, the effect of alloying element on the hydrogen absorption kinetics is also examined. Much information on the Ta-H interaction can be presented as and obtained from the *P*-*C*-*T* curves. This style is followed in the present work too, not only for pure tantalum but also its solid solution alloys with the elements mentioned.

Chapter 3

Experimental Techniques

3.1 Introduction

This chapter deals with the experimental methodologies used for the preparation of various tantalum-alloys, the design and construction of the Sievert's apparatus and the procedure for hydrogen charging and the physical and chemical characterization of materials at various stages.

3.2 Materials Preparation

3.2.1 Preparation of Alloys by Arc Melting Technique

Tantalum, nickel, chromium, iron and aluminium metal foils (Aldrich make, high pure > 99.9 %) were used for the synthesis of the alloys. Vacuum arc melting is an effective technique to prepare the alloys and intermetallic compounds of refractory metals [162]. In this, the elemental components of the desired alloy are melted together using electric arc as the source of heat on water cooled copper crucible [162] under a controlled atmosphere which is either vacuum or a high purity inert gas.

Arc Melting

The arc source is made up of a pair of metal electrodes spaced few millimeters apart. Initially a low current spark is generated to ignite the arc which results in the formation of ionic plasma (ions for electrical conduction) in the gap [163]. Once the arc is struck, thermal ionization maintains the current. Alternatively, the arc can be initiated by bringing two electrodes in contact with each other for a while so that heat is produced for ionization; after that these electrodes are separated up to the desired distance [163-165].

A fixed amount of heat expressed in KWH (minimum power of 4 KW) is required to melt the given amount of materials. To maintain the constant power, $P = VI$, low voltage (20-30 V) and high current (200-600 A) is maintained in furnace. High current is given to melt the samples completely as heat input is directly proportional to the power which is related through the relation $P(KW) = I^2R$. The magnitude of the current supplied is decided depending upon the requirement of the melting sample.

The steps involved in the arc melting procedure are as follow: sample and hearth was thoroughly cleaned with acetone, the charging system was evacuated to 10^{-5} Torr or less, flushed out the hearth chamber with inert gas (pure argon), a dummy charge (Ti or Zr sponge) is melted to remove the remaining gases as Ti and Zr are good absorber (getter) of residual gases, melting of the charge (required metallic samples), 6-7 times repeated melting to make the alloy homogeneous, cooling of the furnace to room temperature and release of vacuum to take out the melted stock.

The arc melting furnace used for melting the samples was connected with vacuum pumps as shown in Fig. 3.1.

Fig. 3.1 **Arc melting furnace connected with vacuum pumps**

To prepare the alloys, weighted quantities of thoroughly degreased and cleaned alloy components were stacked/blended together and charged in the furnace in a water cooled copper hearth. Several solid solution alloys of tantalum (Ta-Ni, Ta-Cr, Ta-Fe and-Ta-Al) were thus prepared. The weight of the alloy was typically 20 grams.

3.2.2 Analysis of the Samples

The compositional characterization of the alloys was carried out using Glow Discharge-Quadrupole Mass Spectrometry (GD-QMS). The homogeneity of the alloys was checked by measuring Vickers Hardness in different regions of the sample and also by line scan SEM-EDS analysis of the alloys. Phase characterization was performed using XRD technique.

3.2.3 *Samples Cutting and Preparation for Hydrogen Charging*

The arc melted alloys obtained in the button shape were cold rolled to 0.3 mm thickness using rolling machine. All the alloys were cut into the small specimens of dimensions of $0.3 \times 10 \times 15$ mm^3 using EDM (Electrical Discharge Machining) cutting machine. The wire EDM machining also known as Spark EDM is an electro thermal cutting process [166]. The sparks are created in a dielectric liquid, generally water or oil, between the workpiece and an electrode, which can be considered as the cutting tool. After machining, the samples were cleaned chemically using an acid solution ($HF:HNO_3:H_2SO_4::2:2:5$) and mechanically polished on emery papers followed by cleaning with acetone. These dried samples were then used for hydrogen charging.

3.3 Equipment Used for Hydrogen Charging

3.3.1 *Sievert's Apparatus*

A Sievert's apparatus was used for hydrogen charging of tantalum alloys using 5N (99.9995%) pure hydrogen gas. The set-up was developed in our laboratory and a photograph is shown in Fig. 3.2 with the block diagram of the apparatus appearing in Fig. 3.3.

The apparatus consists of a reaction chamber made of quartz and connected to the vacuum system through a stainless steel pipe. A manually moveable furnace whose temperature was controlled by the PID temperature controller (model: PRC-309) was used to heat the reaction chamber. The furnace can heat up to 1223 K and control temperature to within ± 1K in the uniform temperature zone which was 2.5 cm. The furnace temperature was measured by placing a K-type (Chromel (90% Ni and 10% Cr) – Alumel (95% Ni, 2% Mn, 2% Al and 1% Si)) thermocouple adjacent to the sample.

Fig.3.2 Sievert's apparatus

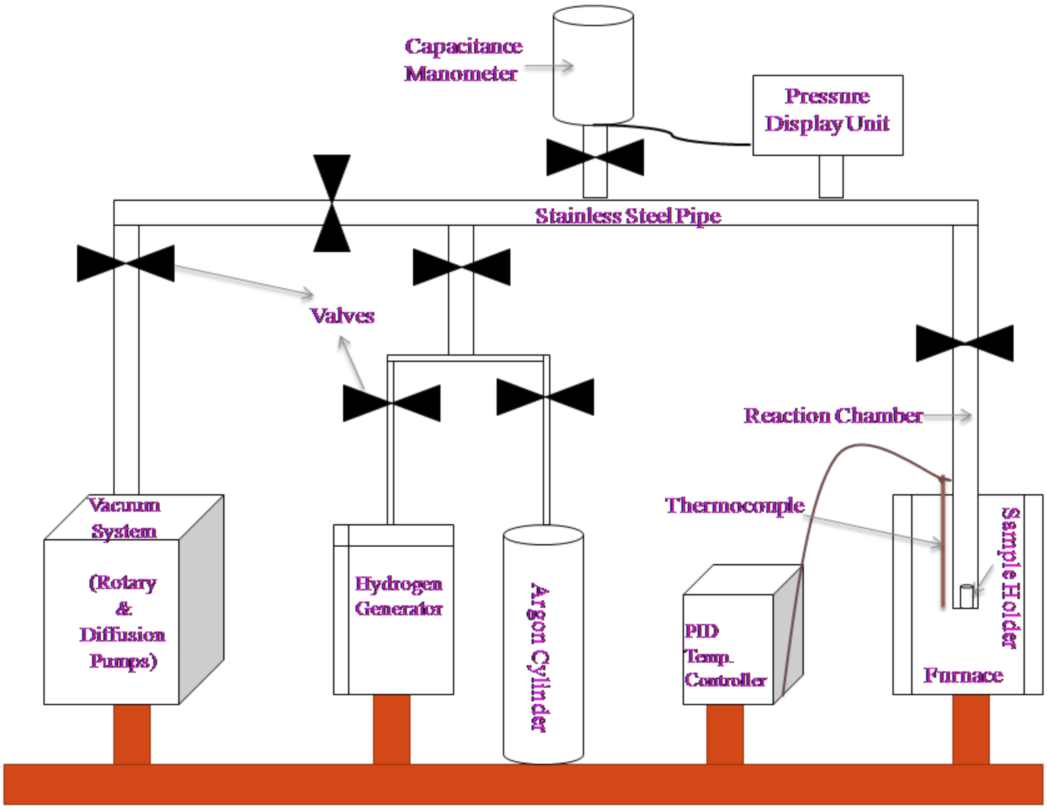

Fig. 3.3 **A block diagram of Sievert's apparatus**

A capacitance manometer (model: mks BARATRON Type 631 C) with display unit (model: mks PR4000B) were used to read the pressure changes. A schematic diagram (Fig. 3.4) and working principle of capacitance manometer are given below [167].

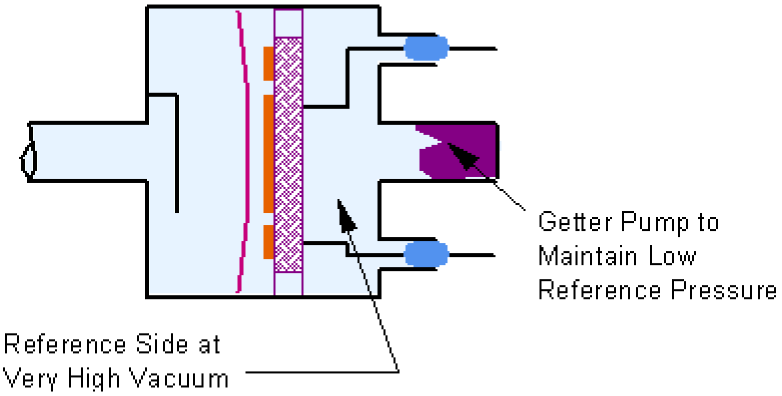

Fig. 3.4 **Schematic of capacitance manometer [167]**

Working principle of capacitance manometer

The sensor capsule contains the diaphragm and the metal-on-ceramic electrode structure. The reference side (backside) of the diaphragm is evacuated to a very high vacuum, much lower than the pressures that are to be measured. The high vacuum on the reference side is maintained over the life of the manometer by means of an internal chemical getter pump. The sensors are made of Inconel, all-welded construction for roughness and compatibility with process environments.

A capacitance manometer determines the pressure by measuring the change in capacitance between the metal diaphragm and an adjacent, fixed dual electrode. The radially tensioned diaphragm provides very low hysteresis, excellent repeatability, remarkably high resolution ($1x10^{-5}$ of Full Scale), fast response, and the ability to measure extremely low pressures. The full scale pressure range of this manometer is upto 1000 Torr [167].

If a high overpressure is applied to the manometer, the diaphragm will bottom out on the electrode substrate, preventing permanent damage to the sensor. Pressures of greater than the allowable limit can cause internal mechanical failure.

3.3.2 Hydrogen Generator

A commercially available hydrogen generator (model: CIC-PW-SPE500HC) was used as a source for 5N (99.9995%) pure hydrogen gas from which required amount of hydrogen can be released and then disconnected from the system.

Working principle

The CIC-PW-SPE500HC hydrogen generator working on electrolysis principle and generate hydrogen from pure water. The assembly consists of composite catalyst and ion membrane separation technology to completely separate H_2 and O_2 to provide high purity hydrogen containing less than 20 ppm of O_2 [168].

The decomposition of water takes place at anode as per the following equation:

$$2H_2O = 4H^+ + 2O^{2-} \tag{3.1}$$

The decomposed negative oxyanions release electrons to form oxygen which is then discharged from the anode chamber carrying moisture into the water tank for reuse. The O_2 gas bubbles out through the water and is discharged from the hole on the cap of the water tank.

The proton in form of aqua ion (H^+. xH_2O), goes through Solid Polymer Electrolyte (SPE) membrane under electric field force and forms hydrogen at cathode after picking up an electron as shown below:

$$2H^+ + 2e^- = H_2 \tag{3.2}$$

The hydrogen outflows from cathode chamber to gas water separator where 99% moisture is removed. It then passes through Dryers (Filters) upstream of the membrane separator to remove trace moisture level and provide ultra high pure (UHP) grade 1 gas at the desired flow rates. Purity analysis of Hydrogen can be done on Gas Chromatograph using high end detectors such as Micro TCD, DID and PDHID Detectors.

3.4 Procedure for Hydrogen Charging

The Sievert's apparatus was used for both hydrogen solubility as well as kinetic studies.

3.4.1 Procedure for P-C-T Equilibrium Hydrogen Measurement

The steps involved in equilibrium hydrogen charging process for the pressure-composition-temperature *(P-C-T)* data measurement are as follows:

1. The sample was weighted and placed into a quartz sample holder which was then kept inside the reaction chamber.
2. A vacuum, of the order of 10^{-6} Torr, was created inside the system using rotary and diffusion pumps. The leak tightness of the system was assured by checking the constant pressure reading with the capacitance manometer up to 24 hours.
3. The sample was heated at 1183 K for two hours under the high dynamic vacuum condition to activate the sample surface. The oxide layer on the metal surface that would have prevented access of hydrogen to the metal, gets inside the bulk of the metal and sample surface become active.
4. The system was filled with hydrogen and then cooled down to room temperature. The temperature was again raised to 1183 K and system was re-evacuated to 10^{-6} Torr to release the entire hydrogen from the sample. The process is repeated several times. This procedure is necessary to activate the sample by introducing micro cracks before hydrogen charging.
5. The sample was cooled up to the required temperature.
6. Hydrogen gas was introduced into the system from the hydrogen generator at the constant temperature and to a predetermined pressure level (initial pressure reading).

7. The sample started absorption of hydrogen at the preset temperature and drop in the system pressure was observed.
8. After some time, pressure inside the system became constant. When constant pressure was observed continuously for 24 hrs, it was considered that equilibrium has been achieved in the system (final pressure reading). Equilibrium values were confirmed by repeating the whole cycle.
9. At the end of the run, the furnace was switched off and removed away from the reaction chamber and the valve connecting the sample holder to the remaining system was closed.
10. Within one minute after switching off the furnace, the reaction chamber was rapidly cooled by immersing in an ice-water mixture so that hydrogen absorption during cooling could be minimized, and sample was taken out from the tube.
11. The amounts of hydrogen dissolved in the samples were determined by inert gas fusion technique, and the results were checked against the value obtained by pressure drop method as well as by gravimetric technique.

3.4.2 Procedure for Hydrogen Absorption Kinetics Study

To carry out the hydrogen absorption kinetics study, the procedure was almost same as used for the *P-C-T* equilibrium hydrogen measurement as discussed above. To measure the rate of hydrogen absorption in Ta and Ta-alloys, the change in hydrogen pressure with time was measured at constant temperature. The details for kinetics measurement are given in chapter 5.

3.5 Analytical Techniques

3.5.1 Glow Discharge-Quadrupole Mass Spectrometry (GD-QMS)

Glow Discharge-Quadrupole Mass Spectrometry (GD-QMS) is a method for the direct determination of trace elements qualitatively and quantitatively in the solid samples. A glow-discharge (GD) device is an atomization device that performs both sample introduction and sample atomization simultaneously [169].

In addition to atomizing samples, it also produces a cloud of positive ions from the analyte solid samples. This device consists of a simple two - electrodes closed system containing argon gas at low - pressure (0.1-10 torr). A schematic GDMS probe tip is shown in Fig. 3.5.

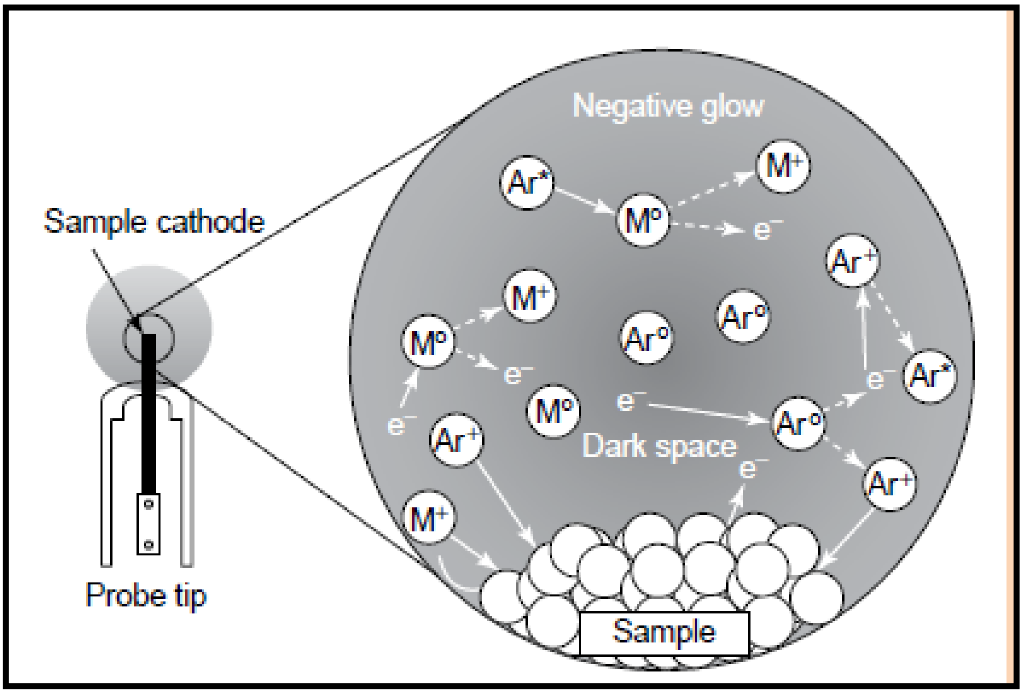

Fig. 3.5 Schematic GDMS Probe Tip. *Inset: atomization and ionization processes. Bombardment of the sample cathode by argon ions (Ar^+) formed in the negative glow results in the release of sample atoms, M^0, via sputtering. Any sputtered secondary ions redeposit on the sample surface owing to the electric field. M^0 escape into the negative glow region where collisions with electrons, e^-, and metastable argon atoms,*

Ar, result in their ionization. The ionized sample atoms,* M^+*, are then available for mass spectrometric monitoring* [**170**].

A DC voltage of 5-15 kV is applied between the electrodes that breakdown argon gas into positively charged argon ions and electrons. The electric field accelerates the argon ions to the cathode surface that contains the sample. Neutral sample atoms are then ejected into the region between two electrodes by a process called sputtering, where they are converted to positive ions by collision with electrons or positive argon ions. The rate of sputtering may be as high as 100 µg/min. Analyte ions are then drawn into the mass spectrometer by differential pumping. The ions are then filtered in to a quadrupole mass analyzer for detection and determination [169].

The most important application of the glow-discharge atomizer is for the direct analysis of the metals as well as for the multi-elemental analysis. The concentration below ppb level can be measured by this technique [163].

3.5.2 Inert Gas Fusion Technique

The inert gas fusion (IGF) technique is a quantitative analytical technique for determining the concentrations of nitrogen, oxygen, and hydrogen in a sample. Quantitative results for most metals and alloys can be obtained in the parts-per-million to parts-per-billion range for nitrogen, hydrogen, and oxygen [171-172].

The sample is accurately weighted and placed in a pure graphite crucible containing Ni or Sn fluxes in a fusion furnace with an inert gas atmosphere. The crucible is heated to 2000 - 2500°C, resulting in the sample fusing to a molten state [172]. The hydrogen and nitrogen gases evolved from the molten material and are carried away from the fusion chamber as H_2 and N_2. The oxygen released from the material forms CO or CO_2 and is carried away.

An inert carrier gas flushes the gases evolved from the sample out of the fusion chamber to the detector. The individual concentrations for the evolved gases are detected by infrared absorption (for CO and CO_2) and by thermal conductivity techniques (for N_2 and H_2) [171].

Two different types of analytical instruments are used, one for the analysis of hydrogen and other one for the analysis of nitrogen and oxygen.

Hydrogen Determinator

The amount of dissolved hydrogen is determined using a hydrogen determinator (CIC HTS). A flow chart for hydrogen analysis is shown in Fig. 3.6.

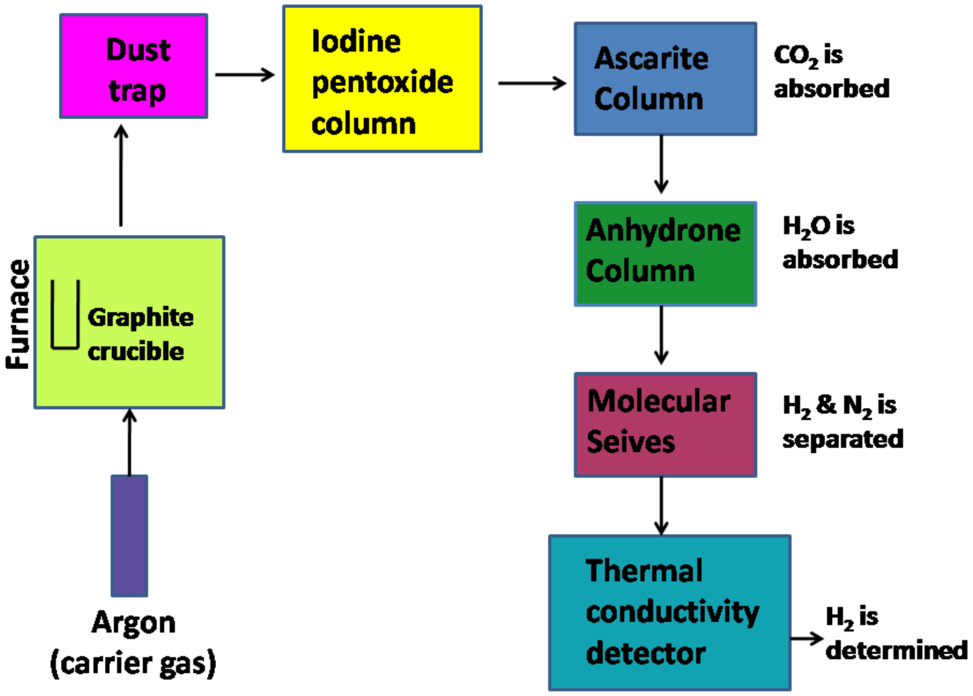

Fig. 3.6 A flow chart for hydrogen analysis

In this determinator, the sample (charge) is melted in a graphite crucible. H_2, O_2, N_2 and other gases are evolved out from the sample. The oxygen released from the sample combined with carbon to form CO, which is further oxidized to CO_2. These gaseous mixtures pass through ascarite column and anhydrone column where CO_2 and water vapors are adsorbed, respectively. Then remaining gaseous mixture is passed through molecular sieve through which H_2 diffused out rapidly and detected by thermal conductivity detector (TCD) [9]. Argon is used as a carrier gas.

Oxygen/Nitrogen Determinator

Oxygen and nitrogen in the metallic samples are analyzed using oxygen/nitrogen determinator (LECO TC 300). A flow chart for oxygen and nitrogen analysis is shown in Fig. 3.7.

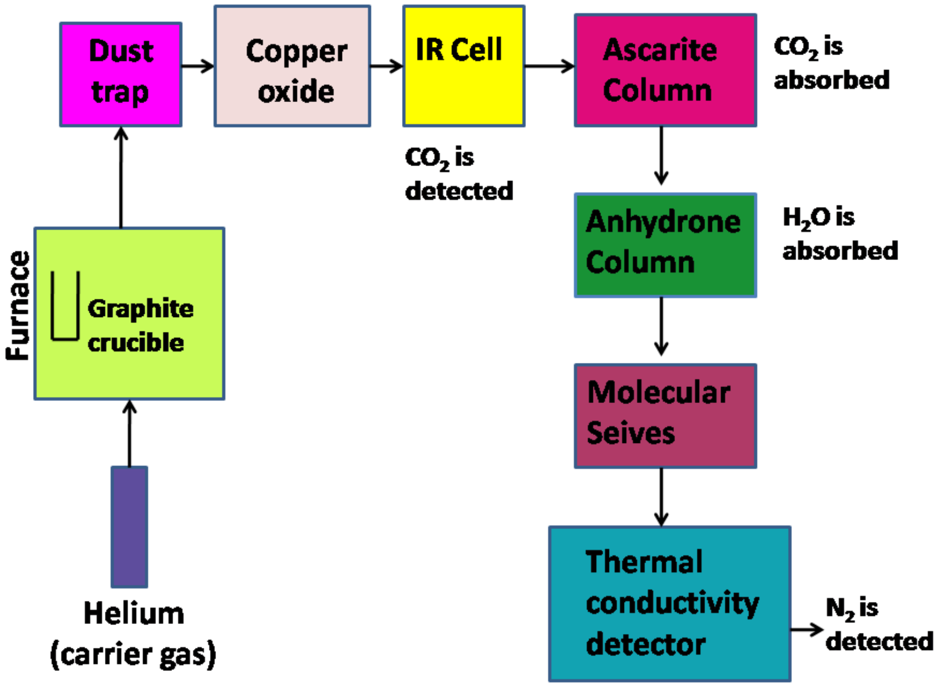

Fig. 3.7 A flow chart for oxygen and nitrogen analysis

In this determinator, the sample (charge) is melted in a graphite crucible. The oxygen released from the sample combined with carbon to form CO, which is further oxidized to CO_2. The amount of CO_2 is analyzed by using infrared cell. The determinators are consistently calibrated using oxygen standard samples. These gaseous mixtures passed through ascarite column and anhydrone column where CO_2 and water vapors are adsorbed. The remaining nitrogen is determined using thermal conductivity detector (TCD) [173]. Helium is used as a carrier gas in the TCD.

3.5.3 X-Ray Diffraction (XRD)

X-Ray diffraction (XRD) is the most commonly used technique for characterization of the crystalline materials, as well as for determination of their unit cell type, lattice parameters, phase and crystal structure [174].

The theory of diffraction is based on the Bragg's law, which is as follow:

$$n\lambda = 2d_{hkl} \sin\theta \qquad (3.3)$$

Where, n is a positive integer, d_{hkl} represents the inter planer spacing between the crystal planes that cause constructive interference, and λ is the wavelength of the incident X-ray beam.

In XRD, the sample is irradiated by a monochromatic X-ray beam, which are generated by a cathode ray tube, by heating a filament to produce electrons, accelerating the electrons toward a target, by applying a voltage, and bombarding the target material (Cu, Fe, Mo, Cr) with the electrons [163].

In the present thesis, the phase characterization of the samples was carried out by using X-ray diffraction (XRD) (model: Inel) with Cr-Kα radiation at 30 mA and 40 kV using a curved position-sensitive detector. In this way, diffraction data in complete 2θ range was recorded. The XRD unit was equipped with parabolic mirrors to enhance the intensity of x-ray beam. The samples were spinned during the XRD analysis around the vertical axis, so that diffraction effect due to orientation in r and θ directions could be eliminated. With this unit, a satisfactory XRD pattern could be obtained in 4-5 minutes.

3.5.4 Scanning Electron Microscopy (SEM)

SEM gives information about topography, morphology, composition and details of the arrangement of the atoms in a material.

In a typical SEM, a source or bunch of electrons are focused into a beam having a very fine spot size of ~5 nm, and having energy ranging from a few hundred eV to 50 KeV. The beam examines a very small area of an object [175].

Usually a tungsten filament source is used as an electron source. The electrons are accelerated to energy between 1 to 30 KeV. The beam size is reduced to a diameter of 2 - 10 nm using the magnetic condenser and objective lens systems before or at the surface of the specimen. Scanning is controlled by applying an electrical signal to the pairs of electromagnetic coil situated within the objective lens. Thus by rapid beam movement, the whole sample surface can be irradiated with the electron beam [163]

The magnification (M) in the SEM image is given by

$$M = W/w \qquad (3.4)$$

Where, W is the width of CRT display and w is the single line scan width across the sample. The achievable magnification is increased by decreasing w because W is constant.

When the electron beam impinges upon the surface of a crystal, a fraction or whole energy of the electron is transferred to the solid. The excited solid then emits secondary electrons, backscattered electrons, auger electrons, x-rays and some longer wavelength photons also. The energy of the striking electron beam is assumed to be 20 KeV, which can penetrate up to a depth of 1.5 µm or more [163]. Secondary electrons are most often detected by a scintillator-photomultiplier system, called the Everhart-Thornley detector. Semiconductor detectors (high collection efficiency but slow response time) are widely used for the backscattered electrons. The X-ray analysis is the energy dispersive analyzer in most SEMs, using a semiconductor detector, such as a lithium-drifted silicon, Si(Li) or lithium-drifted germanium, Ge(Li) detectors.

In the present thesis, the surface morphology of the samples has been analyzed, using AIS2100 SERON Tech. SEM from South Korea, equipped with energy dispersive X-ray (EDX) spectrometer (Model: INCA E350 from Oxford, UK).

3.5.5 Energy-Dispersive X-ray Spectroscopy (EDS/EDX)

EDS or EDX is an analytical technique used for the elemental analysis or chemical characterization of the surface of a sample. It is one of the variants of X-ray fluorescence spectroscopy [163]. In principle, all elements from atomic number (Z) in the range of Z = 4 (Be) to Z = 92 (U) can be detected by EDS, though not all instruments are equipped for light elements (Z < 10). The detection limit of EDS is usually about 1000 ppm (by weight) but can be reduced by using long counting times [176].

In this technique, the sample investigation is done on the basis of an interaction of electromagnetic radiation or charged particles with matter. The interaction results in the emission of characteristic X-rays which are used for the elemental analysis. The intensity and energy of the X-rays emitted from a specimen can be measured by an energy-dispersive spectrometer. Each element has a unique atomic structure and emits X-rays are the characteristic of the particular element. Hence, unique identification of the elements is possible. In the present study AIS-2100 CERON make EDS unit was used.

3.5.6 Vickers Hardness

The Vickers hardness test was developed in 1921 by Robert L. Smith and George E. Sandland at Vickers Ltd to measure the hardness of materials [177]. The Vickers test is often easier to use than other hardness tests since the required calculations are independent of the size of the indenter, and the indenter can be used for all materials irrespective of hardness. A Vickers hardness tester is shown in Fig. 3.8.

Hardness is defined as the resistance to indentation or material's ability to resist plastic deformation. It is therefore a characteristic of a material and not a fundamental physical property. The Vickers test can be used for all metals and has one of the widest scales among hardness tests. The unit of hardness given by the test is known as the Vickers Pyramid Number (HVN) or Diamond Pyramid Hardness (DPH).

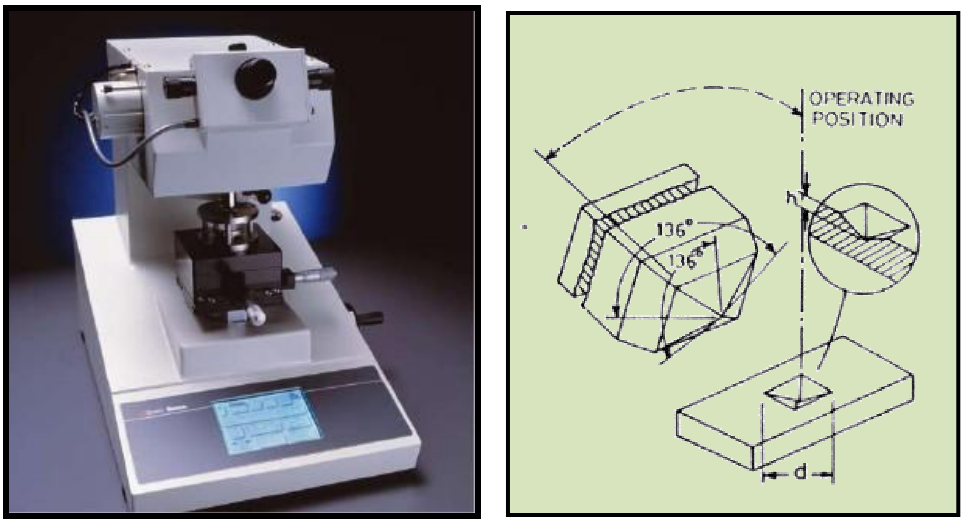

Fig.3.8 (a) A Vickers hardness tester [178] (b) Schematic diagram of Vickers hardness test [179]

It was essential that the indenter shape should be capable of producing geometrically similar impressions, irrespective of size; the impression should have well-defined points of measurement; and the indenter should have high resistance to self-deformation. A diamond in the form of a square-based pyramid satisfies these conditions. It was found that the hardness value obtained on a homogeneous piece of material remained constant, irrespective of load [177]. Accordingly, loads of various magnitudes are applied to a flat surface, depending on the hardness of the material to be measured. The hardness is determined by measuring the permanent depth of indentation. More simply, when using a fixed load (force) and a given indenter, the smaller the indentation, the harder the material and higher will be the tensile strength. If Vickers hardness, H_V is expressed in kg/mm^2, the tensile strength, σ_μ (in *MPa*) of the material can be approximated as:

$$\sigma_\mu \approx H_V \times c \approx H_V \times 3.33 \qquad (3.5)$$

Where, c is a constant determined by geometrical factors usually ranging between 2 and 4.

When carrying out the hardness tests, the minimum distance between two indentations and the distance from the indentation to the edge of the specimen must be taken into account to avoid interaction between the work-hardened regions and effects of the edge.

In the present thesis, Vickers hardness was performed (model: Duramin-2) with a 100 g load for a duration of 15 seconds. The minimum distance between two indentations was 3 times of the average length of the diagonal left by the indenter in millimetres (d).

3.6 Methods Used for the Solubility, Thermodynamics and Kinetics Studies

3.6.1 Hydrogen Solubility Calculation

3.6.1.1 Using Pressure Drop Method

Amount of hydrogen dissolved in metals and alloys is estimated by the extent of drop in hydrogen pressure in a system of known volume. Let ΔP torr is the difference between the initial and final pressure readings at room temperature; V cc is the total internal volume of the system and W grams is the weight of sample.

The molar volume of a gas at STP is equal to 22400 cc of H_2 gas which is equivalent to 2 g of H_2. Therefore, V cc H_2 gas at STP will be equivalent to ({2 / 22400} ×V) g or say, x g of H_2.

As hydrogen pressure of 760 torr has x g of H_2, therefore, ΔP torr will have ({x /760} × Δp) = y g of H_2

Thus, the amount of hydrogen absorbed (ppm) in the sample is given as below:

$$H_{ppm} = \frac{w_{H_2}(y)}{w_s(W)} \times 10^6 \qquad (3.6)$$

Where, w_{H2} or y is the weight of hydrogen absorbed in the sample and w_s or W is the weight of sample. Thus, knowing the weight of sample, internal volume of the system and the difference between the initial and final hydrogen pressure, the average concentration of hydrogen absorbed by the sample can be estimated.

3.6.1.2 Using Gas Law

The number of moles of hydrogen absorbed by the sample is given by:

$$n = \frac{\Delta pV}{RT} \tag{3.7}$$

Where, n is the number of moles of hydrogen absorbed by the sample, Δp is the pressure change in S.I. unit, V is volume of the system, R is universal gas constant, and T is Temperature in Kelvin

Thus weight of hydrogen absorbed by the sample will be given by:

Weight of hydrogen = 2n = 2 × $(\Delta pV / RT)$ grams

Hence, the weight ppm of hydrogen can be approximated as

$$H_{ppm} = \frac{2 \times \Delta pV/RT}{W} \times 10^6 \tag{3.8}$$

In this way, knowing the weight of sample *(W)*, volume of the system *(V)* and the difference between the initial and final hydrogen pressure (Δp), the average concentration of hydrogen picked up by the sample can be estimated [180].

3.6.1.3 Using Gravimetric Techniques

The amount of hydrogen absorbed by the samples can also be calculated by weight change using highly sensitive microbalance [181]. The mass sensitivity of the microbalance is ± $0.1 \mu g$. The weight *ppm* of hydrogen can be calculated as

$$H_{ppm} = \frac{(\Delta w)}{(W)} \times 10^6 \tag{3.9}$$

Where, Δw is the change in weight of sample in gram and W is weight of sample in gram.

For example, if 100 *ppm* of hydrogen is absorbed by 5 *g* of tantalum specimen, then weight change of the sample will be 0.0005 *g*, that can be measured by microbalance.

3.6.2 Estimation of Thermodynamic Parameters for the Solution of Hydrogen in Ta and Ta-alloys from P-C-T Data

The thermodynamic data for the solution of hydrogen in tantalum and its alloys can be used to process the design for Ta-based materials for various hydrogen atmosphere applications and can also be utilized in various modeling studies for hydrogen solubility and permeability. The determination of thermodynamic parameters: the relative change in enthalpy, entropy and Gibb's free energy of solution for hydrogen in tantalum metal and alloys can be carried out in the following ways:

3.6.2.1 Application of van't Hoff Equation

The enthalpy for the solid solution of hydrogen in metals / alloys can be determined using van't Hoff equation as follows [108]

$$\frac{d\ln K}{dT} = \frac{\Delta H}{RT^2} \qquad (3.10).$$

It was assumed that ΔH is constant in a temperature range from T_1 to T_2. On integrating above Eq. from K_1 to K_2 on L.H.S. and from T_1 to T_2 on R.H.S., we get

$$\int_{K_1}^{K_2} d\ln K = \frac{\Delta H}{R}\int_{T_1}^{T_2}\frac{dT}{T^2} \qquad (3.11)$$

$$\ln\left(\frac{K_2}{K_1}\right) = -\frac{\Delta H}{R}\left(\frac{1}{T_2}-\frac{1}{T_1}\right) \qquad (3.12)$$

Where, ΔH is enthalpy of solution, R is the gas constant, T is temperature and K is the equilibrium constant of the reaction.

From the definition of Gibbs free energy,

$$\Delta G = \Delta H - T\Delta S \tag{3.13}$$

and

$$\Delta G = -RT \ln K \tag{3.14}$$

It follows that

$$\ln K = -\frac{\Delta H}{RT} + \frac{\Delta S}{R} \tag{3.15}$$

Where, ΔS is the entropy of the solution. Therefore, from the plot of lnK vs $1/T$, the enthalpy and entropy for the solution of hydrogen in metals/alloys can be calculated from the slope and intercept, respectively.

Moreover, one can define van't Hoff equation in term of pressure as below:

$$\frac{d \ln p}{dT} = -\frac{\Delta H}{RT^2} \tag{3.16}$$

It was assumed that ΔH is constant in a temperature range from T_1 to T_2. Integrating on both sides, we have

$$\int_{p_1}^{p_2} d \ln p = -\frac{\Delta H}{R} \int_{T_1}^{T_2} \frac{dT}{T^2} \tag{3.17}$$

$$\ln\left(\frac{p_2}{p_1}\right) = -\frac{\Delta H}{R}\left(\frac{1}{T_1} - \frac{1}{T_2}\right) \tag{3.18}$$

Where, ΔH is enthalpy of solution, R is the gas constant, p_1 and p_2 are the gaseous pressure at temperature T_1 and T_2.

Thus, by knowing the values of p_1 and p_2 or K_1 and K_2 at temperature T_1 and T_2, the enthalpy for the solution of hydrogen in metals can be calculated.

3.6.2.2 Use of Sievert's Law

The relative change in enthalpy and entropy for the solution of hydrogen in tantalum metal and its alloys can be calculated by applying Sievert's law as follows [128]

$$c \alpha \sqrt{p} \tag{3.19}$$

or

$$c = K_s \sqrt{p} \tag{3.20}$$

Where,c is the concentration of hydrogen dissolved in metal in equilibrium with gaseous hydrogen at pressure p, and K_s is the Sievert's constant.

The Sievert's law constant (K_S) is related to change in enthalpy, $\overline{\Delta H_H}$ and change in entropy, $\overline{\Delta S_H}$ of the solution for hydrogen by the following relation,

$$K_s = {}^{c}\!\big/\!{}_{\sqrt{p}} = \exp\left(-\frac{\overline{\Delta H_H}}{RT}\right)\exp\left(\frac{\overline{\Delta S_H}}{R}\right) \tag{3.21}$$

or

$$\ln K_s = \ln\frac{c}{\sqrt{p}} = -\frac{\overline{\Delta H_H}}{RT} + \frac{\overline{\Delta S_H}}{R} \tag{3.22}$$

The slopes of lnK_S vs $1/T$ plots give the value of $\left(-\frac{\overline{\Delta H_H}}{R}\right)$, whereas intercepts give the value of $\left(\frac{\overline{\Delta S_H}}{R}\right)$, thus from the slope and intercepts of these plots, the values of relative change in enthalpy and entropy of hydrogen solutions can be calculated respectively.

The values for relative change in Gibb's free energy, $\overline{\Delta G_H}$ can also be calculated at different temperatures using the $\overline{\Delta H_H}$ and $\overline{\Delta S_H}$ values by the relation as follow:

$$\overline{\Delta G_H} = \overline{\Delta H_H} - T\overline{\Delta S_H} \tag{3.23}$$

Thus thermodynamic parameters can be calculated by applying these above equations for the solution of hydrogen in metals and alloys.

3.6.3 Kinetics Equation

3.6.3.1 The Rate Equation for the Kinetics of Solid-Gas Reaction

The mechanism of a reaction is usually determined by fitting the time dependent reacted fraction *α (t)* to various analytical rate expressions, through which intrinsic rate limiting steps are obtained. The rate expression is an equation expressing the reaction rate in term of the concentration of reactant as shown below:

$$Rate = k[conc]^n \tag{3.24}$$

Where, *k* is the rate constant and *n* is the order of the reaction. It is also called rate equation or rate law.

The intrinsic rate limiting step is the slowest step of the reaction in a process occurring in a series. Solid-gas reaction is usually controlled either by the diffusion process or a chemical reaction [182] and the reaction kinetics rate equation can be expressed as follows [183-185]

$$\frac{d\alpha}{dt} = kf(\alpha) \tag{3.25}$$

Where, α is the reacted fraction at time t, k is rate constant, $f(\alpha)$ is a function determining the mechanism of the reaction and $g(\alpha)$ is the integral form of $f(\alpha)$, i.e.

$$g(\alpha) = \int \frac{d\alpha}{f(\alpha)} = kt \tag{3.26}$$

$f(\alpha)$ and $g(\alpha)$ refers to the reaction mechanism functions including chemical reaction, diffusion, nucleation and nuclei growth.

Based on the experimental data of hydrogen absorption curve, the reacted fraction, α can be calculated as follows:

$$\alpha = \frac{p_0 - p_t}{p_0 - p_{eq}} \tag{3.27}$$

Where, p_0 is the initial pressure, p_t is the pressure at time t and p_{eq} is the final equilibrium pressure.

The function $g(\alpha)$ giving the best linearity with time is considered as the mechanism for hydrogen absorption reaction in tantalum-alloys. The rate function of hydrogen absorption and the kinetic parameters k are obtained from the linear regression fitting. The apparent activation energy for hydrogen absorption in these alloys is calculated using Arrhenius equation.

3.6.3.2 Arrhenius Equation

The rate constant is related with activation energy according to Arrhenius equation:

$$k = Ae^{-E_a/RT} \tag{3.28}$$

or

$$\ln k = \ln A - \frac{E_a}{RT} \tag{3.29}$$

Where, *A* is the frequency factor or pre-exponential factor or pre-exponential constant (total number of collisions per second), *R* is the molar gas constant (*J/mol K*), *T* is the process temperature (*K*) and E_a is the activation energy of the process (*kJ/mol*).

When rate constants at different temperatures are extracted from hydrogen absorption curves for tantalum-alloys, the E_a for hydrogen absorption can be obtained from the slope of *lnk* vs 1/*T* plots [183-185].

3.7 Summary

Various tantalum alloys like Ta-Ni, Ta-Cr, Ta-Fe and Ta-Al were successfully prepared using vacuum arc melting technique. The Sievert’s apparatus fabricated in our lab was used to conduct the experiments for the hydrogen solubility and kinetic studies. The details of other instruments and techniques used in the present thesis work have also been discussed. The methods used to calculate the equilibrium hydrogen solubility as well as thermodynamic parameters like relative change in enthalpy, entropy and Gibb’s free energy for the solution of hydrogen in metals has been elucidated. The techniques related to the kinetics for hydrogen absorption in tantalum metal and its alloys have been explained.

Chapter 4

Results & Discussion

4.1 Introduction

Apart from temperature and pressure, equilibrium hydrogen solubility in a metal substantially depends upon the presence of one or more of other elements either present as impurities or added deliberately as alloying elements. The present chapter deals with the equilibrium solid solubility of hydrogen in tantalum and effect of nickel, chromium, iron and aluminium as alloying elements on the solubility. Tantalum-nickel, tantalum-chromium, tantalum-iron and tantalum-aluminium alloys of varying compositions within solid solubility limit were prepared by vacuum arc melting technique using high purity constituents under high pure argon gas. The homogeneity of the alloys was checked by measuring Vickers-hardness at different points and further confirmed by the line scan SEM-EDS analysis. Chemical characterization of the alloys was carried out by GD-QMS. Phase analysis was performed by XRD technique. Isothermal as well as isobaric pressure-composition-temperature *(P-C-T)* equilibrium measurements were carried out in the temperature range of (673 – 873) K and in the hydrogen pressure range of (0.60 - 1.20) atmospheres. Three techniques: Inert gas fusion, pressure drop and gravimetric (mass change), were used to measure the hydrogen contents in the samples. Using the experimentally measured *P-C-T* data, the thermodynamic parameters: relative partial molar enthalpy, entropy and Gibb's free energy for solutions of hydrogen in tantalum and all its alloys were evaluated. The effects of alloying elements on these thermodynamics parameters were observed and correlated with the hydrogen solubility behavior.

4.2 Materials Characterization

The alloys prepared by vacuum arc melting were in button shape as shown in Fig. 4.1 (a) and (b). These alloys button were cold rolled to 0.3mm to 0.4mm thickness using rolling machine. All the alloys were sliced into pieces of the required dimensions using EDM cutting machine. After rolling and machining, the samples were cleaned with acetone. Typical sliced pieces of the alloys are shown in Fig. 4.1(c) and (d).

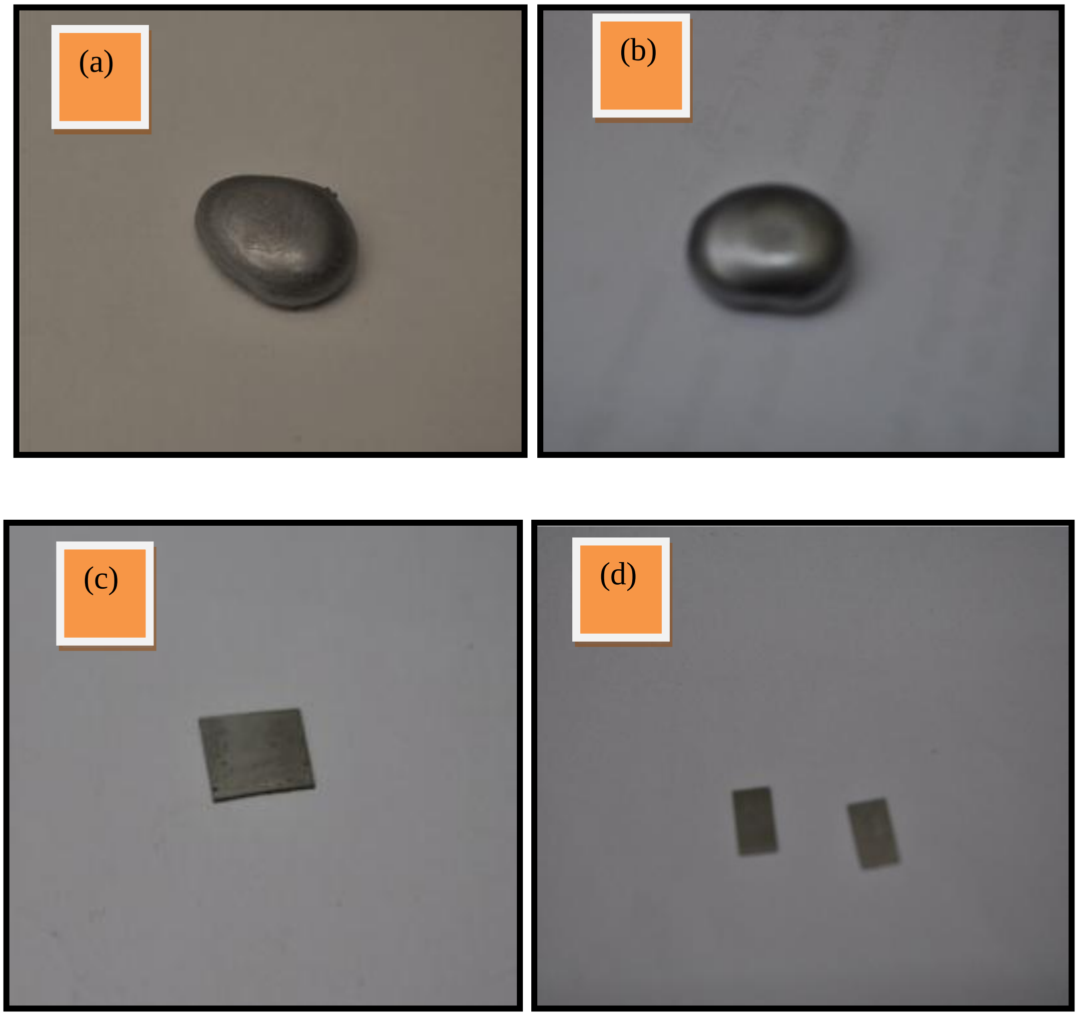

Fig. 4.1 (a) & (b) As prepared alloy buttons and (c) & (d) Pieces of alloys after EDM machining

The EDM cut pieces were of good surface finish, although, the sliced pieces were further polished using high grade diamond paste. These sliced pieces were further annealed at temperature of 1000 ^{o}C under 0.001Pa (~ 10^{-6} torr) dynamic vacuum for 2 hours to activate the sample surface (surface oxygen will move inside the bulk of sample) and to release the residual stress developed during slicing.

These annealed pieces were used for the Vickers hardness measurement to check the alloy homogeneity. The Vickers Hardness was measured at 10-13 different locations in each sample. Almost constant values within ± 3 - 5 % variations were observed, which indicates that alloys are homogeneous. Table 4.1 represents the Vickers Hardness values for tantalum and tantalum-alloys at room temperature.

Table 4.1 **Vickers hardness of Ta and Ta-alloys at room temperature** (uncertainty is ± 3 - 5 %)

Alloys (Atomic %)	Vickers Hardness (HVN)
Unalloyed Ta	230
Ta-1Al	240
Ta-1.6Al	253
Ta-2.4Al	270
Ta-3.2Al	285
Ta-1.6Fe	268
Ta-3.2Fe	303
Ta-1Cr	262
Ta-2Cr	288
Ta1.7Ni	334
Ta-4.9Ni	430

From the Vickers hardness values, the ultimate tensile strength *(UTS)* of the alloys can be determined according to the relationship given in Eq. (4.1) [177]:

$$UTS\ (MPa) = \sigma_u \approx 3.33 \times HV\ (Kg/mm^2) \qquad (4.1)$$

Where, σ_u is the ultimate tensile strength *(UTS)* in *MPa* and *HV* is the Vickers hardness number in Kg/mm^2.

From Table 4.1, it was observed that addition of these alloying elements enhances the Vickers hardness of the Ta-alloys, also reflecting the enhancement of the mechanical strength of the alloys according to equation (4.1).

The homogeneity of the alloys was further verified by using line scans scanning electron microscopy and energy dispersive spectroscopy (SEM-EDS) including X-ray dot mapping by characterizing the phase structure and the distribution of alloying elements. Results of different Ta-alloys are shown in Fig. 4.2 to Fig. 4.5.

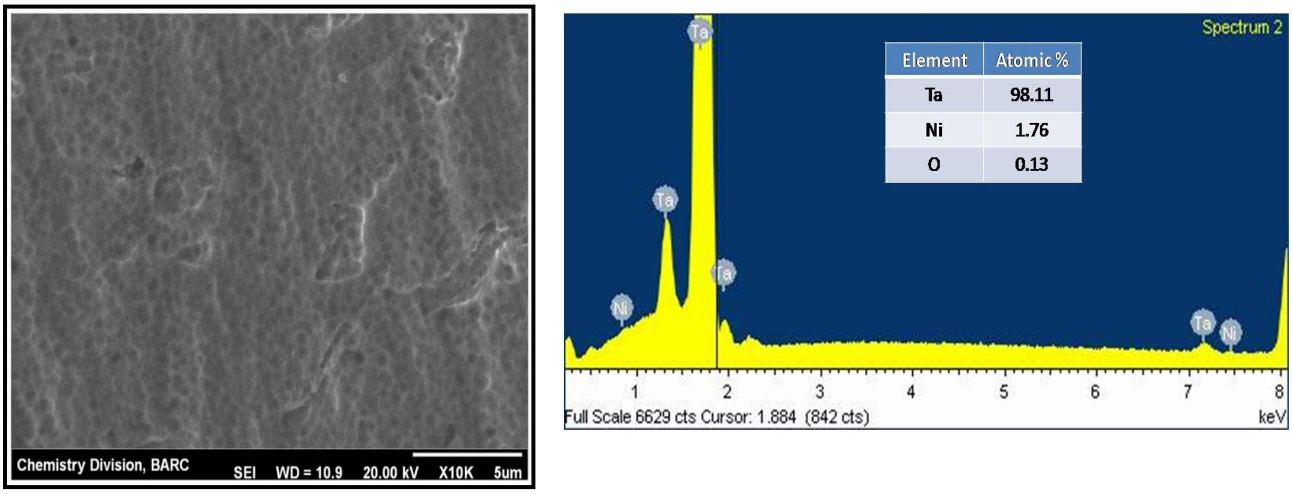

Element	Atomic %
Ta	98.11
Ni	1.76
O	0.13

Fig. 4.2 SEM micrograph and EDS analysis of the Ta – 1.7Ni alloy

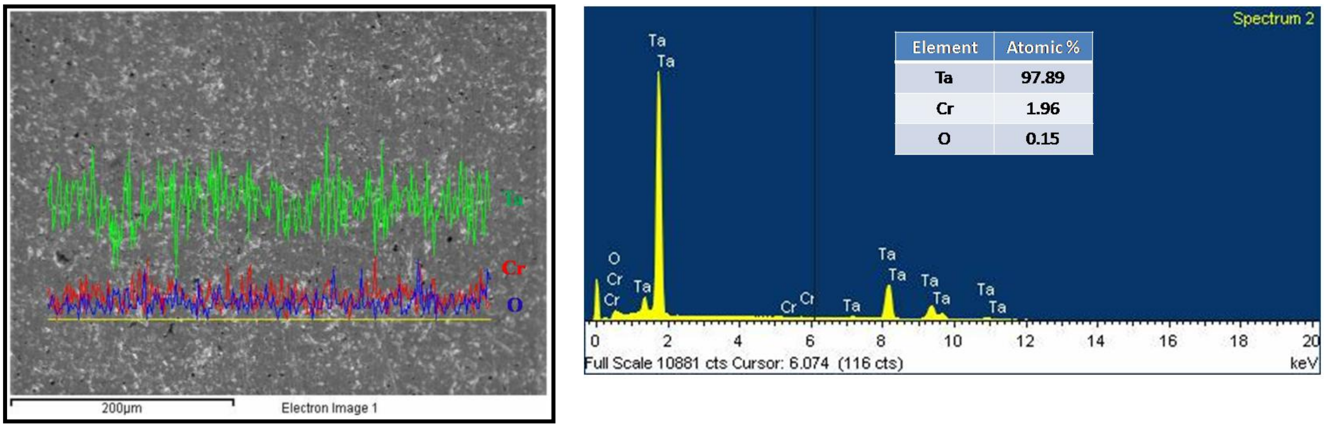

Element	Atomic %
Ta	97.89
Cr	1.96
O	0.15

Fig. 4.3 SEM micrograph and EDS analysis of the Ta – 2Cr alloy

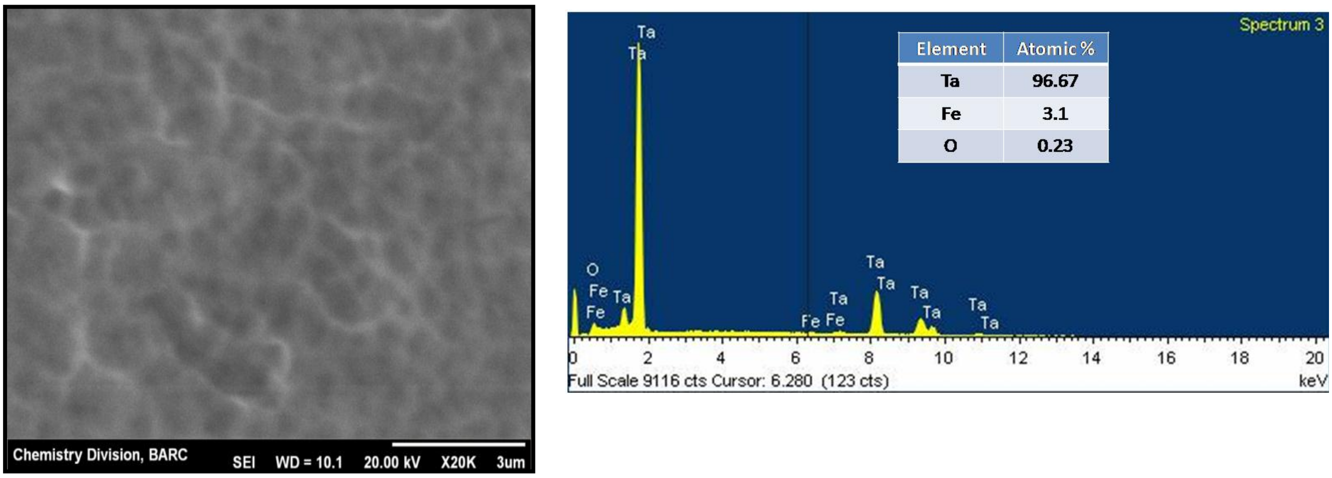

Element	Atomic %
Ta	96.67
Fe	3.1
O	0.23

Fig. 4.4 SEM micrograph and EDS analysis of the Ta – 3.2Fe alloy

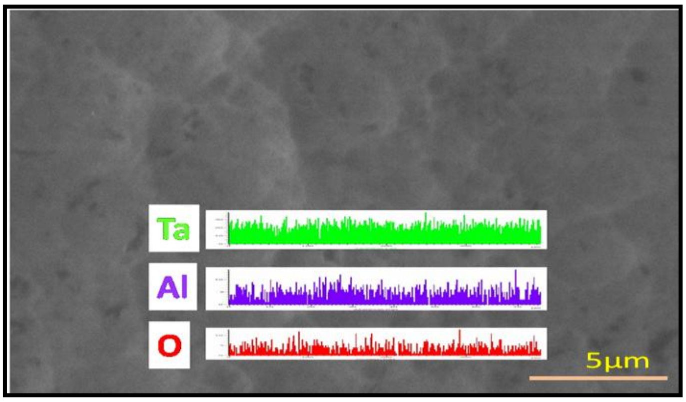

Fig. 4.5 SEM micrograph and EDS analysis of the Ta – 2.4Al alloy

From these figures, it is clear that all the alloying elements are uniformly distributed in the tantalum matrix. The uniform distribution of oxygen has also been observed. The presence of oxygen could be from the oxygen originally present in the Ta as Ta is prone to oxidation. Line scanning EDS indicates that no other metallic impurities are present other than alloying elements.

Chemical analysis was also carried out on the alloys. The elemental compositions of all the alloys were ascertained by the Glow Discharge - Quadrupole Mass Spectrometry (GD-QMS). The results are given in Table 4.2

Table 4.2 Chemical compositions (atom percent) of tantalum and its alloys

Alloys	**Ni**	**Cr**	**Fe**	**Al**	**O**	**N**	**C**
Ta	-	-	-	-	0.10	0.06	0.03
Ta-2 Ni	1.7	-	-	-	0.11	0.05	0.04
Ta-5 Ni	4.9	-	-	-	0.13	0.06	0.02
Ta-1 Cr	-	1	-	-	0.10	0.06	0.04
Ta-2 Cr	-	2	-	-	0.15	0.07	0.03
Ta-1.5 Fe	-	-	1.6	-	0.22	0.02	0.03
Ta-3.0 Fe	-	-	3.2	-	0.23	0.06	0.02
Ta-1Al	-	-	-	1.0	0.15	0.06	0.02
Ta-1.5 Al	-	-	-	1.6	0.18	0.03	0.03
Ta-2.5 Al	-	-	-	2.4	0.17	0.01	0.04
Ta-3.5 Al	-	-	-	3.2	0.18	0.02	0.02

All these compositions lie within the solid solubility region as seen from the Ta-Ni, Ta-Cr, Ta-Fe and Ta-Al phase diagrams as shown in Fig. 4.6 to Fig. 4.9, [186-189] respectively and further verified by their XRD analysis. From Ta-Ni phase diagram [186], solid solubility is observed upto 2 atom % Ni in Ta but Semboshi [141] has found that dissolution of nickel upto 5 at % in tantalum remains within the solid solubility limit. In case of Ta-Cr system, the solubility of Cr in Ta is more than 3 atom % [187]. Ta-Fe phase diagram [188] has indicated that around 2 atom % Fe in Ta is present as solid solution at 800 °C whereas the maximum solid solubility limit of aluminium in tantalum is 4 at % at 1400 °C [189].

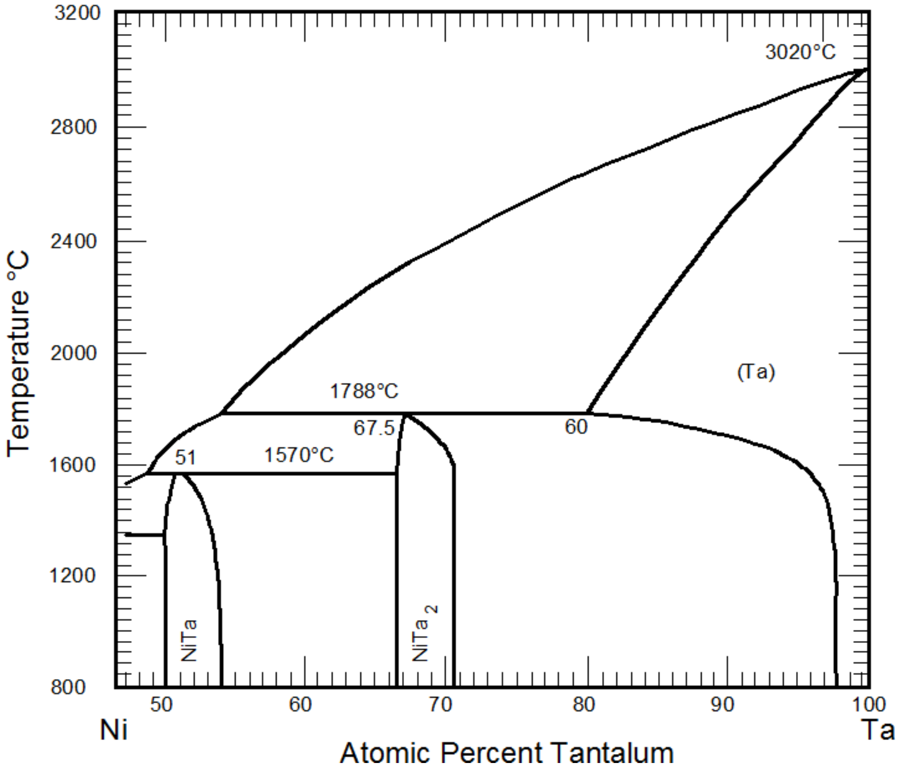

Fig. 4.6 Ta-Ni phase diagram [186]

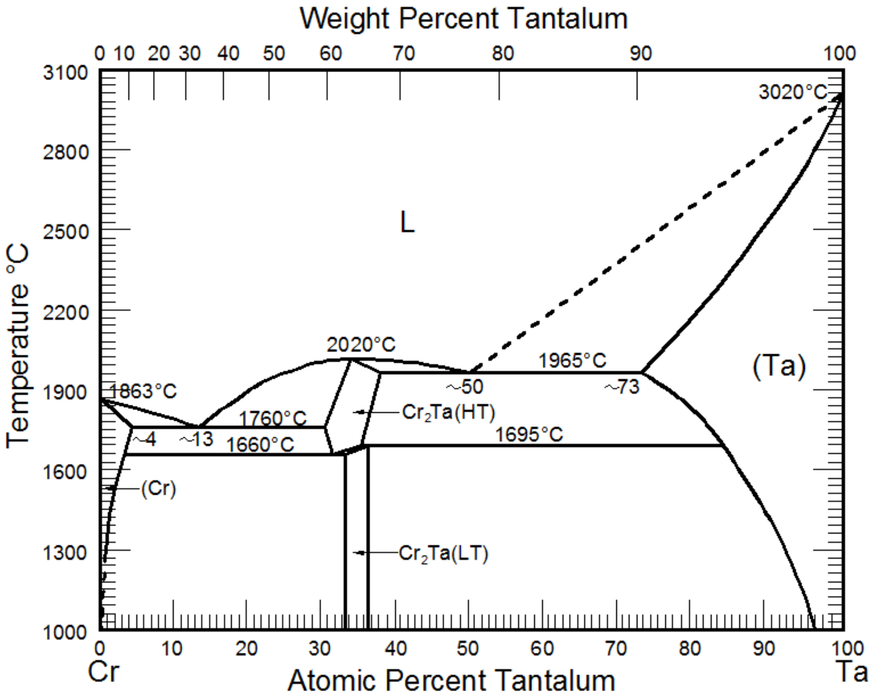

Fig. 4.7 Ta-Cr phase diagram [187]

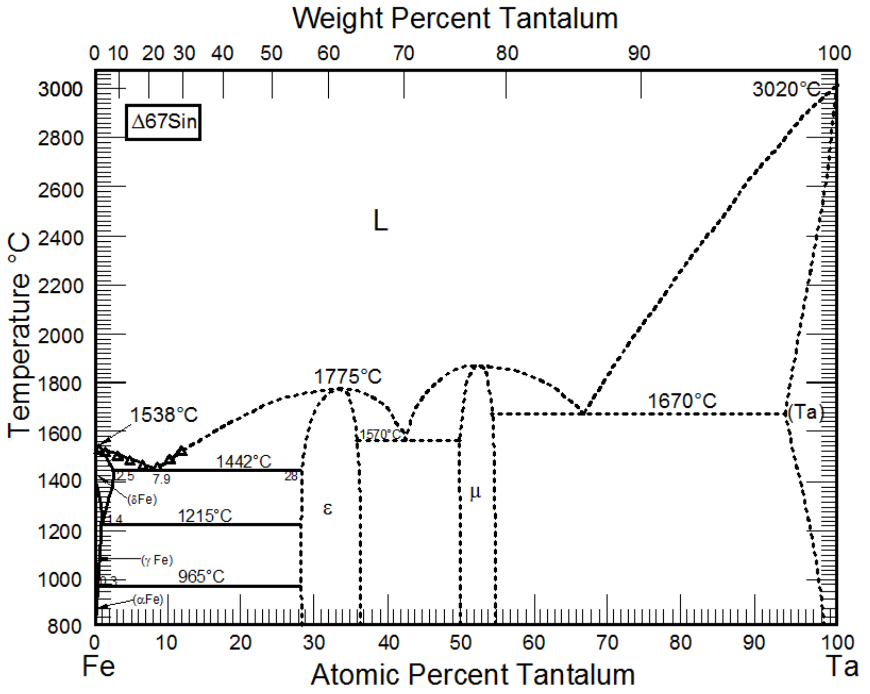

Fig. 4.8 Ta-Fe phase diagram [188]

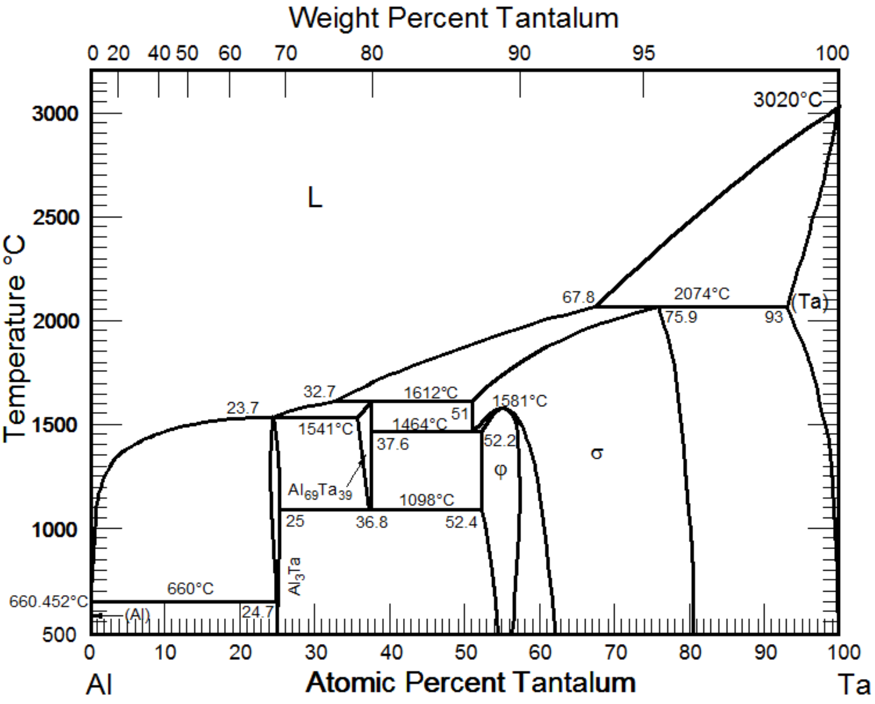

Fig. 4.9 Ta-Al phase diagram [189]

Furthermore, phase recognition of the alloys was confirmed by XRD. The XRD pattern of all the alloys (Ta-Ni, Ta-Cr, Ta-Fe and Ta-Al) along with the XRD of unalloyed tantalum is presented in Fig. 4.10 to Fig. 4.13. The peaks of major phase of all XRD patterns are indexed in plot (a). Plot (b) of each XRD pattern shows the shifting of (211) peak, the data points corresponding to (211) peak are smoothened for clarity.

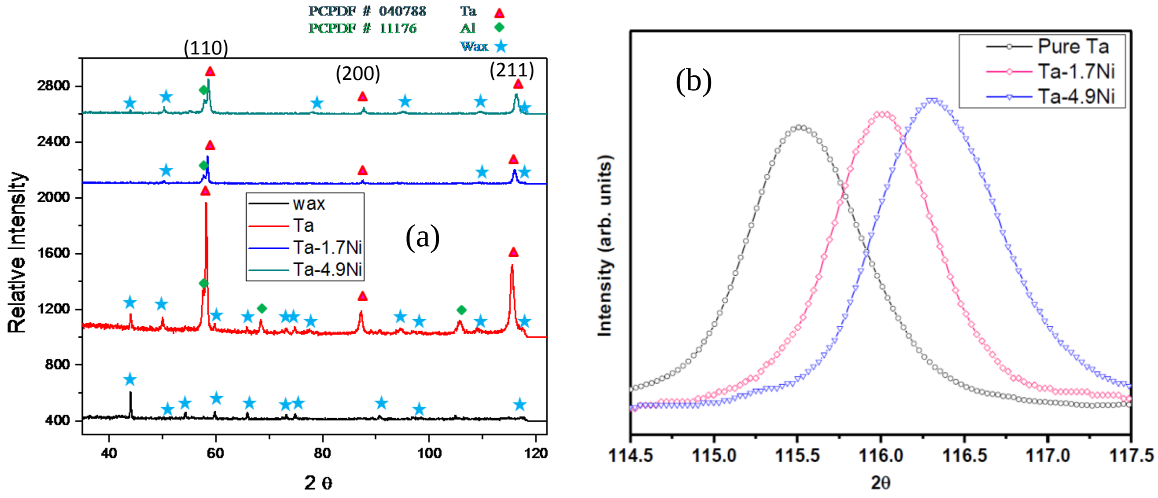

Fig. 4.10 (a) XRD pattern of Ta and Ta-Ni alloys (b) Shifting of (211) peak position with Ni content

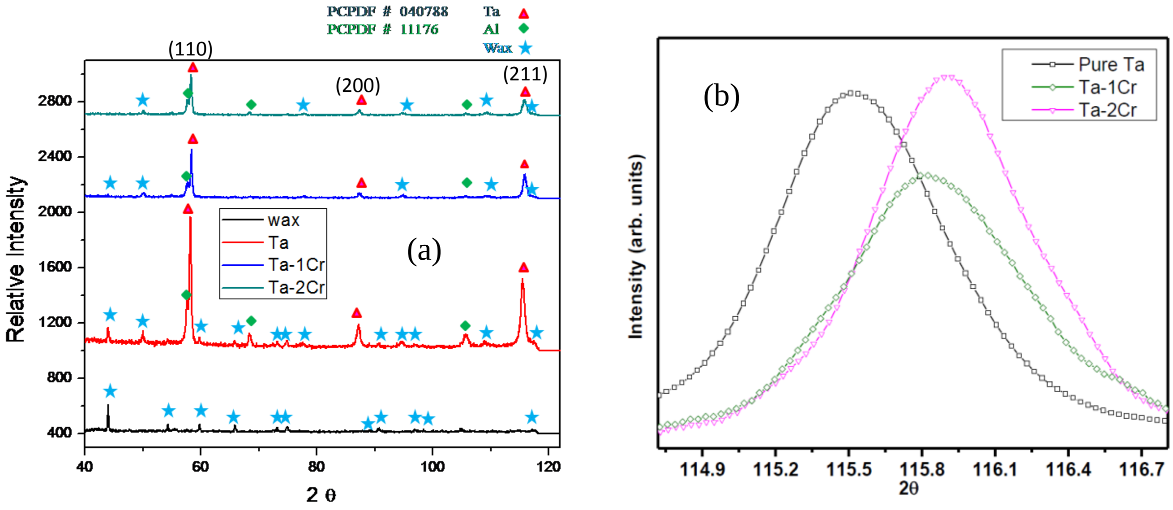

Fig. 4.11 (a) XRD pattern of Ta and Ta-Cr alloys (b) Shifting of (211) peak position with Cr content

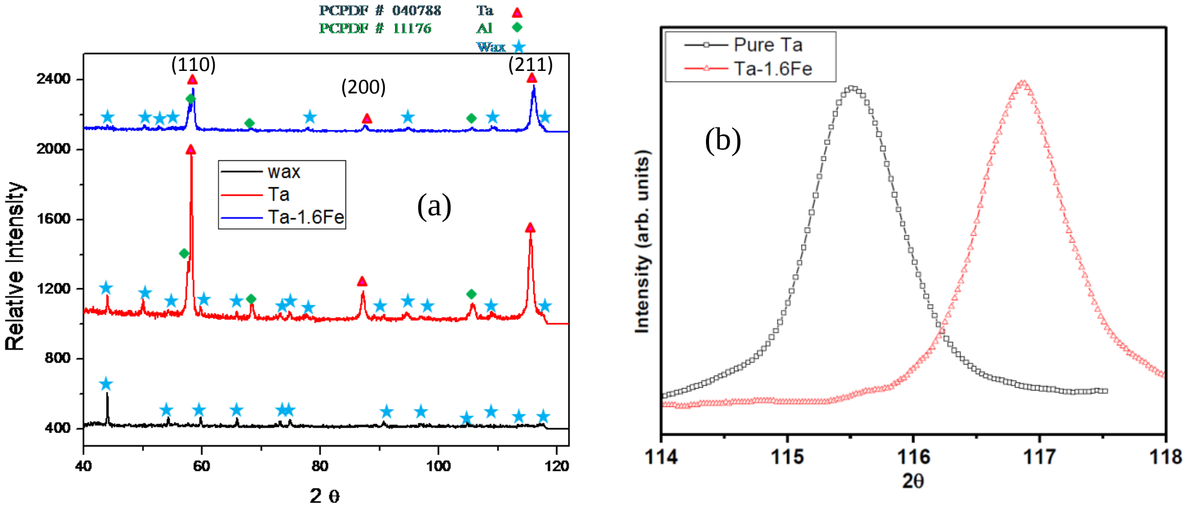

Fig. 4.12 (a) XRD pattern of Ta and Ta-Fe alloy (b) Shifting of (211) peak position with Fe content

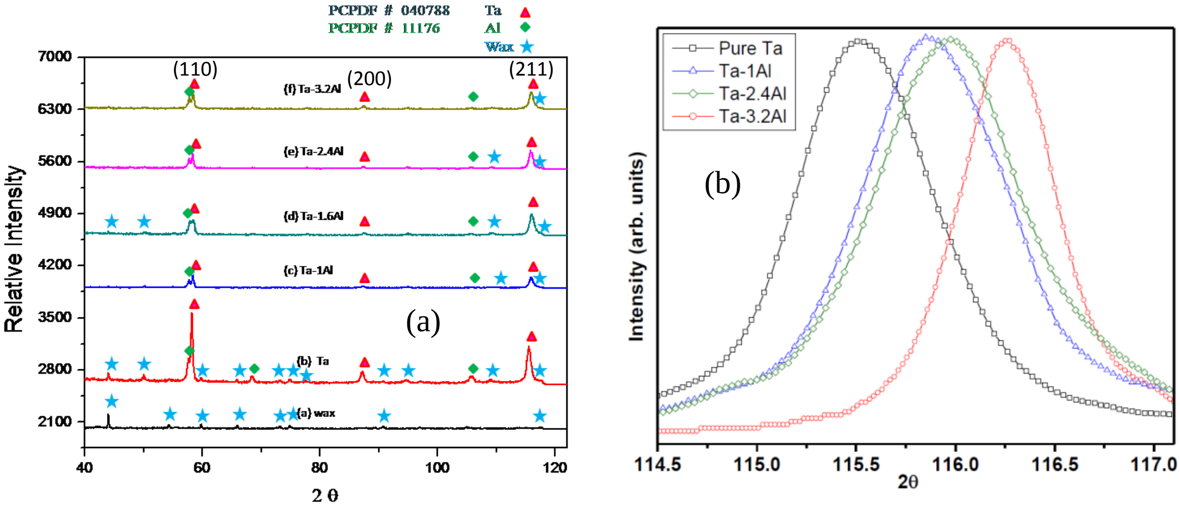

Fig. 4.13 (a) XRD pattern of Ta and Ta-Al alloys (b) Shifting of (211) peak position with Al content

XRD analysis has also indicated that all the alloys are single phase bcc solid solution. Addition of the alloying elements to tantalum shifted the pure Ta peaks toward the higher 2θ values which are shown clearly for (211) peak in part b of these figures. Moreover, higher shifting is observed with increasing content of these alloying elements which indicates that lattice parameter of Ta matrix decreases more with increase in the addition of the these alloying elements. Some peaks from the wax substance (used to mount the sample in the sample holder) and from the sample holder (made up of Al) are also observed in XRD pattern.

4.3 Hydrogen Solubility in Tantalum

4.3.1 Change in Lattice Parameter of Tantalum due to Dissolved Hydrogen

Several methods of hydrogen charging/loading have been reported in the literature [149, 190-191], but in the present investigation, Sievert’s apparatus (section 3.3 of chapter 3) was used to conduct the experiments for hydrogen charging. Hydrogen charging was carried out at constant temperature 633 K and constant hydrogen pressure 0.13 atmospheres (100 torr or 13332 Pa). The amount of hydrogen uptake in tantalum was controlled by the hydrogen charging duration and the hydrogen concentration was maintained below the solubility limit which is about 1200 ppm at room temperature and 1 atmosphere pressure and increases with increase in temperature (3200 ppm at 633 K) as shown in Ta-H phase diagram [79]. Table 4.3 represents the concentration of dissolved hydrogen in tantalum with respect to time duration of hydrogen charging. In the present analysis, the maximum amount of dissolved hydrogen in the unalloyed tantalum is 470 ppm as shown in Table 4.3. Hence, in all the samples, the dissolved hydrogen is within solid solubility limit. This was further verified by XRD analysis.

Table 4.3 **Variation in dissolved hydrogen concentration in tantalum as a function of charging time**

Sr. No.	Time (sec)	H in Ta (ppm)
1	0	0
2	180	203
3	210	271
4	240	331
5	270	470

XRD patterns of various tantalum specimens after hydrogen charging are shown in Fig. 4.14. It is clearly indicated that all the samples are bcc solid solution and there is no hydride phase.

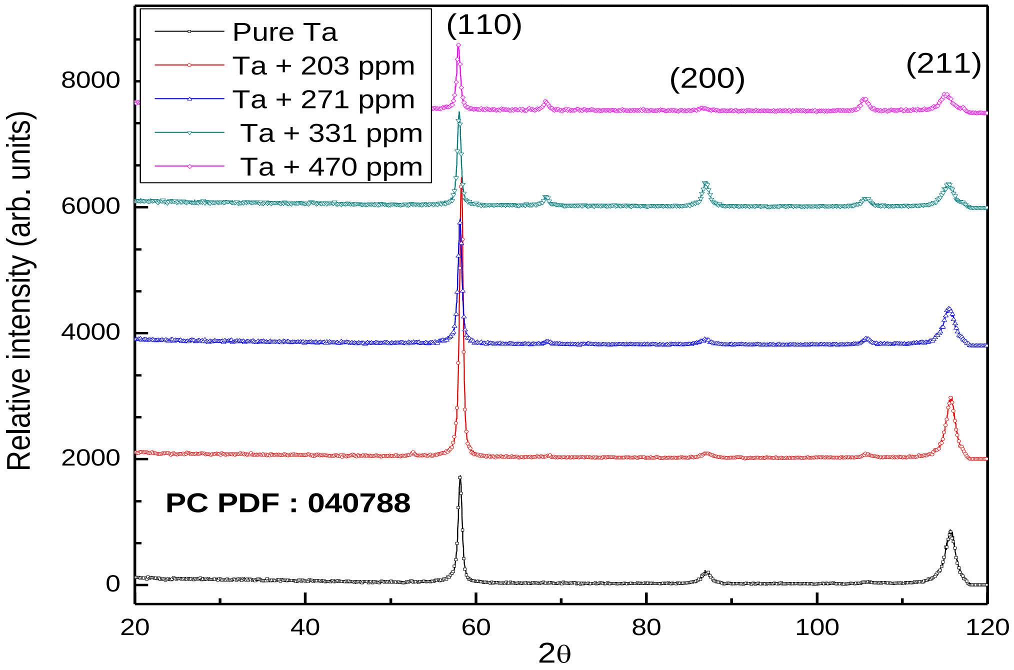

Fig. 4.14 **XRD pattern of pure and hydrogen charged Ta specimens**

It was observed from Fig. 4.14, that XRD peaks have been shifted toward lower 2θ value which results in expansion of lattice of pure tantalum. Peak shifting was more with increasing hydrogen concentration.

On the basis of XRD analysis data, the distance between the two planes *(d)* was calculated using Bragg relations, $n\lambda = 2d_{hkl}\sin\theta$. Three high intense peaks for three different θ values were used for the calculation. Using these d_{hkl} values, the lattices parameter '*a*' was calculated by using the relation

$$d_{hkl} = \frac{a}{\sqrt{h^2+k^2+l^2}} \qquad (4.2)$$

The mean value of lattice parameter (*a*) was determined. The values for lattice parameter '*a*' obtained for different hydrogen concentrations are given in the Table 4.4. It is observed that the lattice parameter of tantalum increases linearly with increase of hydrogen concentration as shown in Fig. 4.15.

Table 4.4 Change in the lattice parameters of tantalum as a function of dissolved hydrogen concentration

Sr. No.	H in Ta (ppm)	Lattice parameter *(a)* (Å)
1	0	3.3097
2	203	3.3207
3	271	3.3237
4	331	3.3288
5	470	3.3332

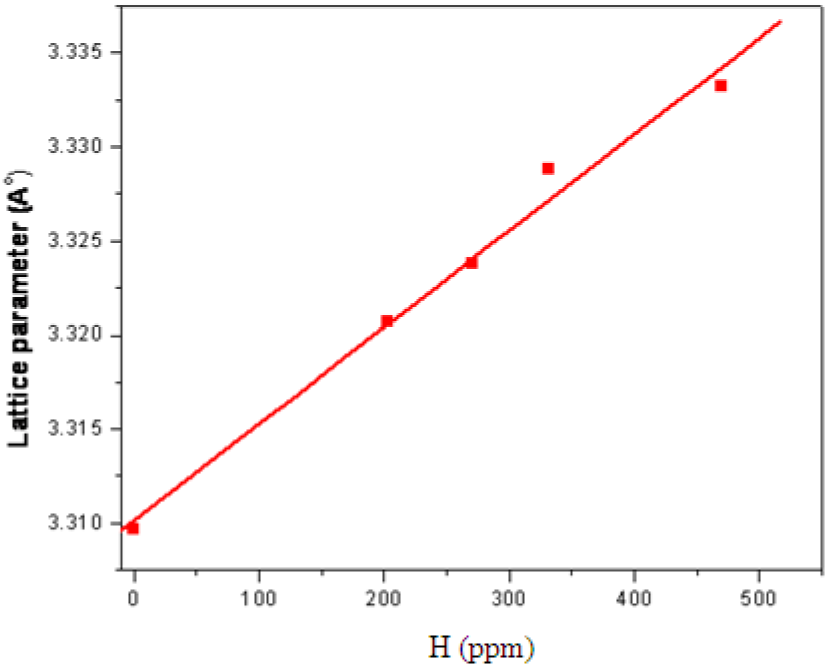

Fig. 4.15 **Lattice parameter of tantalum as a function of the dissolved hydrogen concentration**

The results obtained here followed the Vegard's law [50] which states that in solid solution alloys, lattice parameter is linearly varying with the alloying concentration [192].

The variations in relative change in lattice parameter (change in lattice parameter of Ta-H alloys with respect to pure tantalum) of tantalum-hydrogen alloys with respect to hydrogen concentration were also seen and a linear change was observed as shown in Fig. 4.16.

.

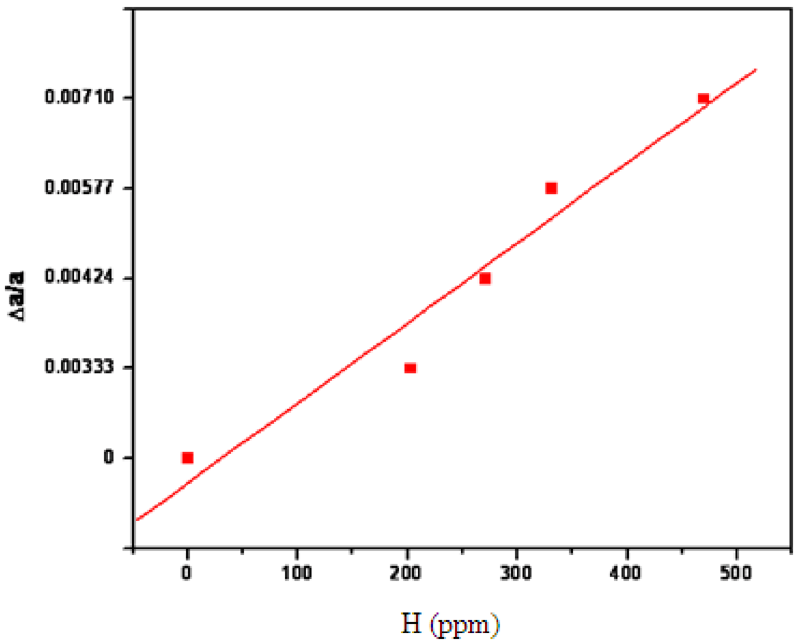

Fig. 4.16 **The relative change in lattice parameter of Ta-H alloys as a function of hydrogen concentration**

4.3.1.1 Ta-H System - Increase in the Lattice Parameter

The expansion of lattice parameter on the dissolution of hydrogen in metals has been explained by various theories and aspects. The neutron diffraction study shows that hydrogen goes into interstitial sites in the metal lattice [193]. This causes an increase in volume of nearest-neighbor shell of atoms because the hydrogen atoms force the nearest-neighbor metal atoms to move away from each other. The free surface of metal specimen expands out to produce a larger volume increase than the volume increase of inner shell of nearest-neighbor atoms. This is a physical phenomenon for the increase of lattice parameter of the metal upon hydrogen absorption [193]. At equilibrium, uniformly distributed dissolved hydrogen in a metal causes zero hydrostatic stress in the lattice, although each hydrogen atom is individually under a hydrostatic stress. Dissolved hydrogen does not show any tendency to form clusters or transform in hydrogen gas molecules.

The above observation could be explained on the basis of density functional theory (DFT) [136,194-196]. According to this theory, irrespective of other functions, an electron density plays an important role to determine the lattice parameter. Hydrogen goes in the refractory metal behave like metal. They occupy interstitial positions in the form of hydrogen ions. The electron goes in the Fermi energy level of the metal matrix. A Schematic diagram is shown in the Fig. 4.17.

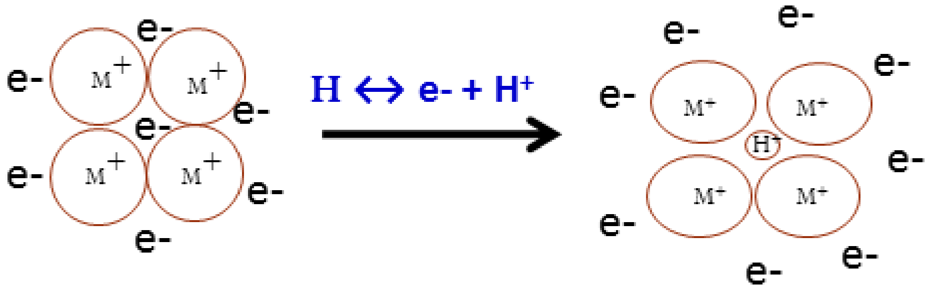

Fig. 4.17 Schematic representation of H in metals

As the electronic density in the Fermi energy level increases, they feel a repulsive force. On the other hand hydrogen ions force the neighbor metal atoms apart from each other as much as possible due to electrostatic repulsive force leads to increase in the lattice parameters.

4.3.2 The Equilibrium P-C-T Data for Ta-H System

The equilibrium hydrogen solubility in tantalum at one atmosphere hydrogen pressure and in the temperature range 673 K – 873 K was determined. Each experiment was carried out 2-3 times. The values obtained were within ± 1% variation. The average equilibrium solubility (*P-C-T*) data thus obtained in the present study were marked on the dotted line of the Ta-H phase diagrams shown in Fig 4.18.

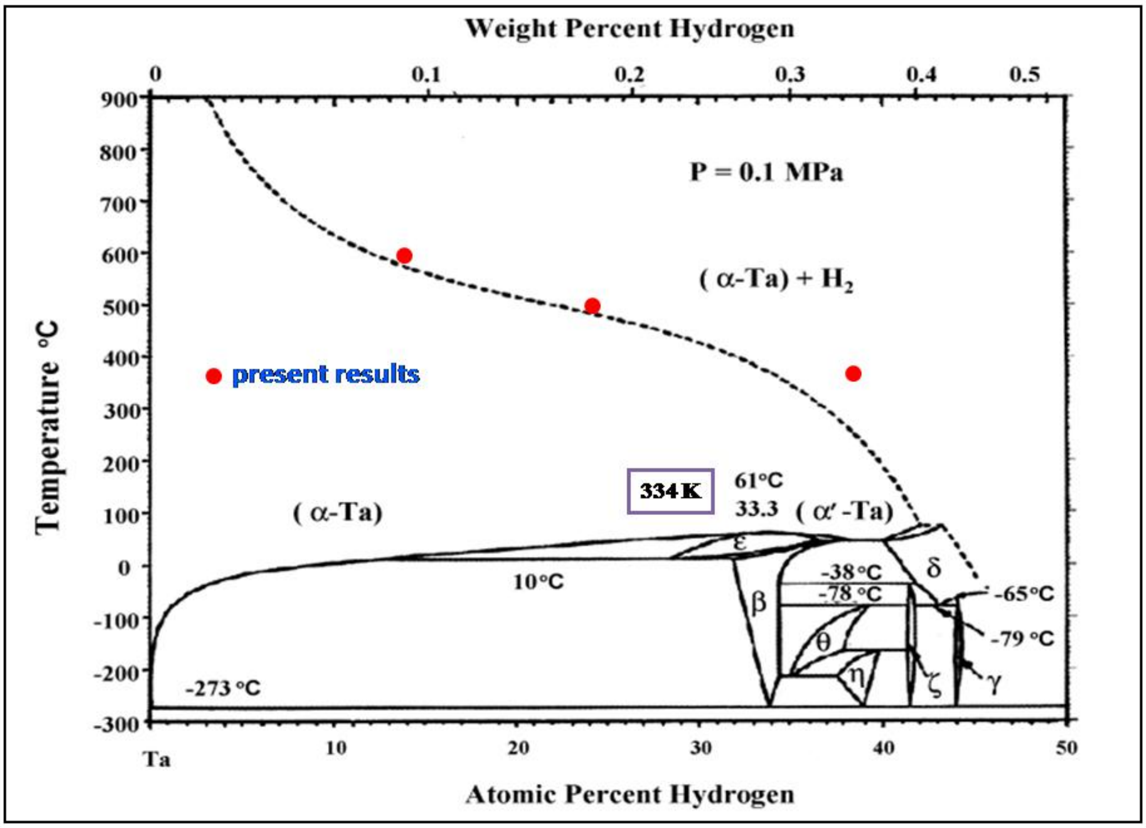

Fig. 4.18 **Experimental data for the solubility of hydrogen in tantalum is shown on Ta-H phase diagram**

The equilibrium hydrogen solubility data obtained in the present study are agree with the information given by Ta-H phase diagram confirming the experimental methods used presently.

4.4 Solid Solubility of Hydrogen in Ta–X Alloys (X = Ni, Cr, Fe, and Al)

As mentioned in the introduction, the presence and quantity of the alloying elements could change the hydrogen interaction solubility in tantalum. The effects of four alloying elements namely nickel, chromium, iron and aluminum on the equilibrium hydrogen solubility in tantalum was investigated in the hydrogen pressure range of (0.6 -

1.2) atmospheres and temperature range of (673 – 873) K. The pressure and temperature range were selected on the basis of the actual device working condition proposed in literature. The equilibrium solubility of hydrogen in these alloys was studied in a Seivert's apparatus. The details of hydrogen charging procedure have been explained in chapter 3.

The equilibrium solubility data obtained from the experiments conducted presently for all the alloys studied are listed in Table 4.5. The hydrogen solubility data for unalloyed tantalum is also given in the same table for making comparison with alloys. The table indicates that the solubility of hydrogen in unalloyed Ta is larger than in all the Ta-alloys at all temperatures and pressures studied in the present thesis and solubility decreases with increase of temperature whereas increases with increase of hydrogen pressure.

Table 4.5 **The amount of hydrogen in wt %, dissolved in tantalum and its – alloys at three temperatures 673, 773 and 873 K and different hydrogen pressures**

	673 K						**773 K**				**873 K**			
Pressure (atm)	**P1 0.64**	**P2 0.74**	**P3 0.80**	**P4 0.88**	**P5 1.0**	**P6 1.13**	**P1 0.64**	**P2 0.72**	**P3 0.80**	**P4 0.88**	**P1 0.66**	**P2 0.73**	**P3 0.80**	**P4 0.88**
H in Ta (wt %)	0.294	0.315	0.329	0.347	0.364	0.387	0.130	0.136	0.145	0.152	0.069	0.073	0.076	0.080
H in Ta-1.7 Ni (wt %)	0.283	0.305	0.317	0.333	0.353	0.377	0.127	0.133	0.142	0.149	0.067	0.070	0.074	0.077
H in Ta-4.9 Ni (wt %)	0.252	0.272	0.282	0.297	0.315	0.336	0.118	0.125	0.133	0.140	0.064	0.067	0.071	0.074
H in Ta-1 Cr (wt %)	0.256	0.276	0.286	0.302	0.319	0.341	0.110	0.115	0.123	0.129	0.063	0.066	0.069	0.073
H in Ta-2 Cr (wt %)	0.229	0.247	0.256	0.270	0.285	0.305	0.095	0.10	0.107	0.112	0.059	0.062	0.065	0.068
H in Ta-1.6 Fe (wt %)	0.274	0.296	0.307	0.323	0.342	0.366	0.121	0.128	0.136	0.142	0.065	0.068	0.071	0.075
H in Ta-3.2 Fe (wt %)	0.252	0.272	0.282	0.297	0.315	0.336	0.112	0.118	0.126	0.132	0.061	0.064	0.067	0.070
H in Ta-1 Al (wt %)	0.265	0.285	0.297	0.312	0.33	0.353	0.113	0.119	0.127	0.133	0.065	0.068	0.071	0.075
H in Ta-1.6 Al (wt %)	0.238	0.257	0.267	0.281	0.298	0.318	0.106	0.111	0.119	0.124	0.061	0.064	0.067	0.070
H inTa-2.4 Al (wt %)	0.205	0.22	0.229	0.241	0.255	0.273	0.095	0.1	0.107	0.112	0.058	0.061	0.064	0.067
H in Ta-3.2 Al (wt %)	0.178	0.192	0.199	0.21	0.222	0.237	0.088	0.092	0.098	0.103	0.056	0.059	0.061	0.064

It was found that the equilibrium hydrogen solubility in Ta-alloys was varying with the composition of alloying elements at constant temperature and pressure. The variation in dissolved hydrogen concentrations in different tantalum-alloys with respect to concentration of alloying element is shown in Fig. 4.19 to Fig. 4.22 at three different temperatures (673-873K) and one atmosphere hydrogen pressure.

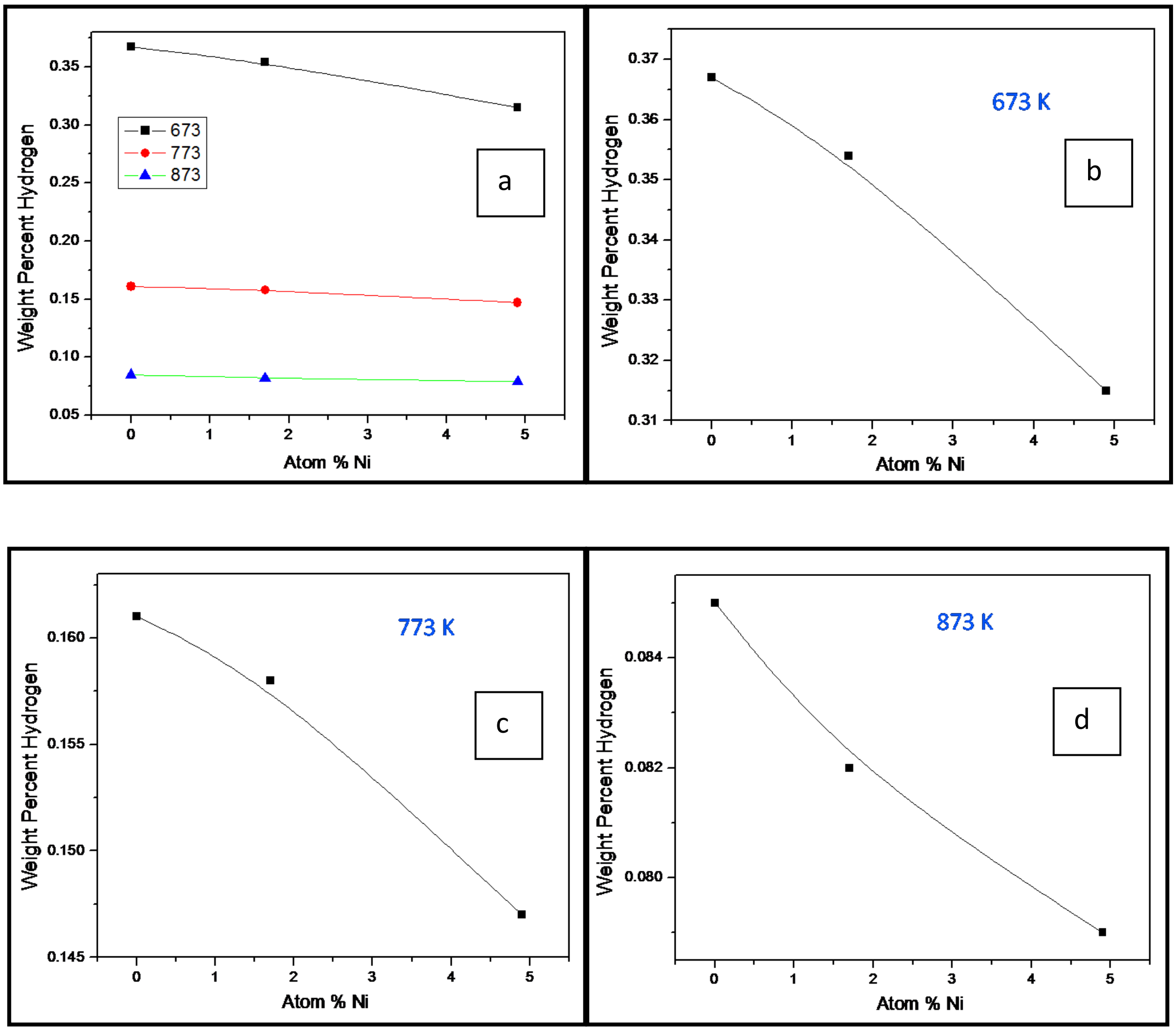

Fig. 4.19 **Amount of hydrogen dissolved in tantalum with respect to nickel concentration in tantalum**

The part (a) in each Figs. (4.19 – 4.22) is representing the variation in hydrogen solubility in tantalum with respect to the composition of alloying elements at three different temperatures. But to clearly see the effect of alloying composition, the effects are shown separately at each temperature for each and every alloying element in part (b-d) in Figs. (4.19 - 4.22).

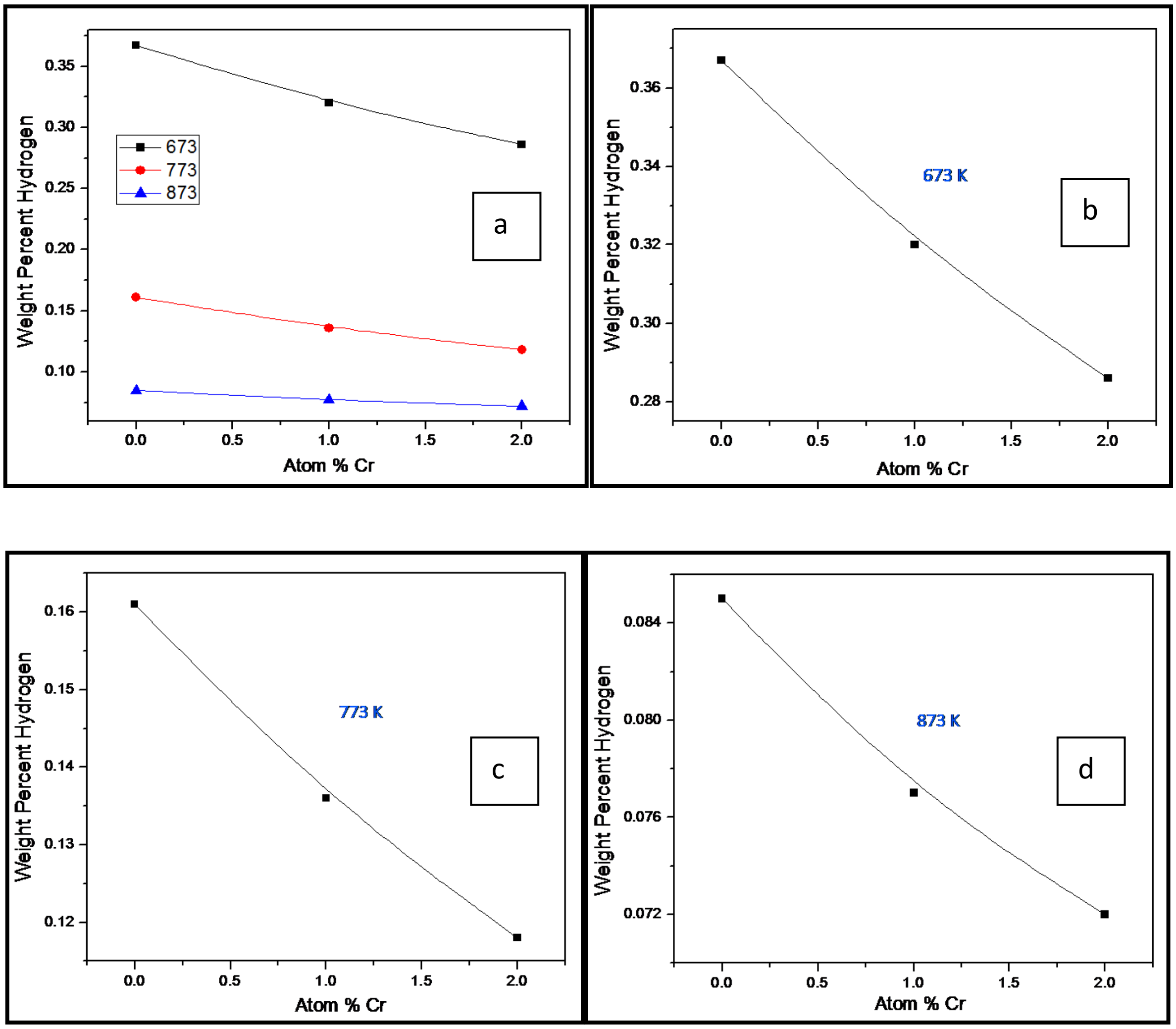

Fig. 4.20 **Amount of hydrogen dissolved in tantalum with respect to chromium concentration in tantalum**

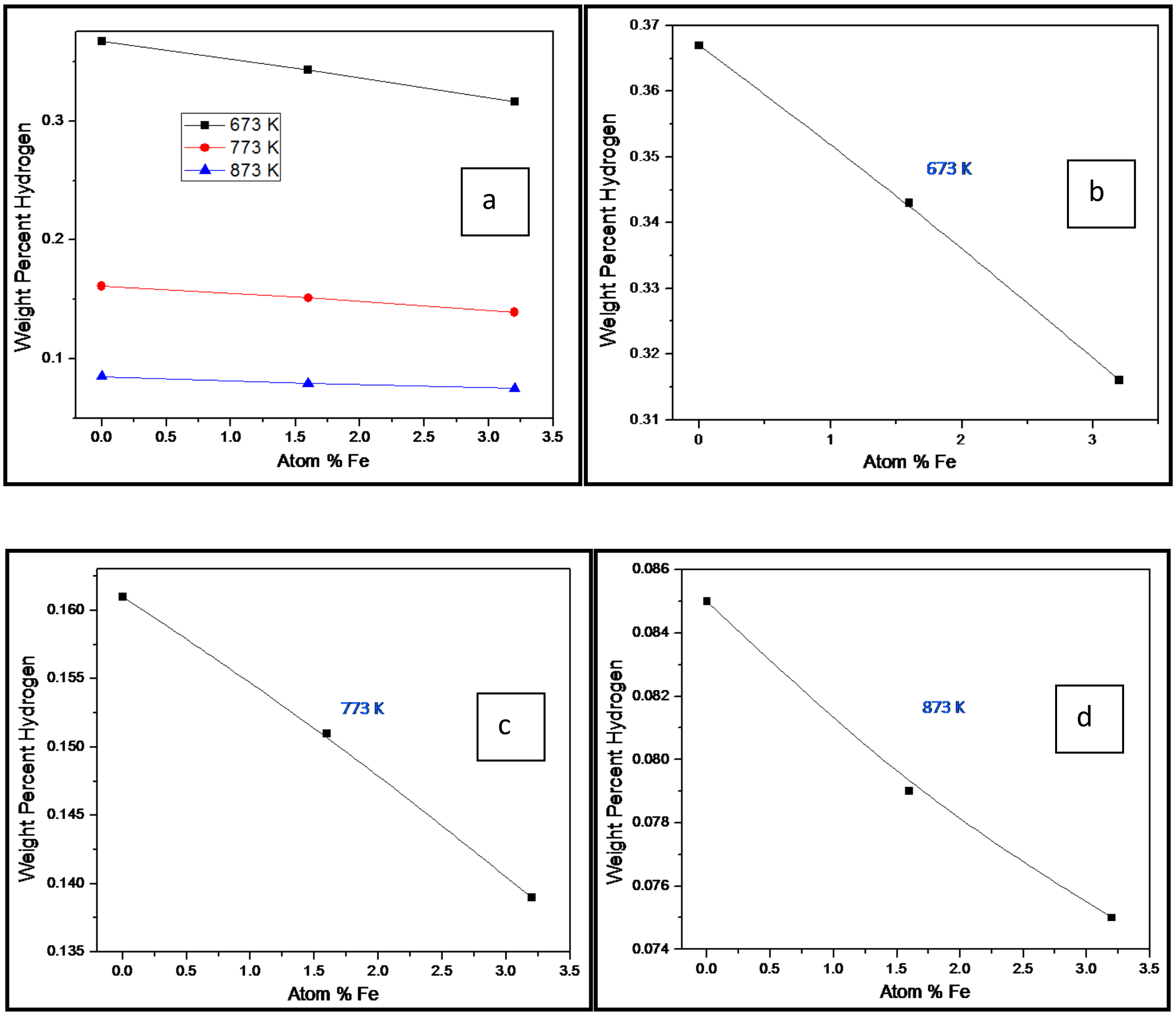

Fig. 4.21 Amount of hydrogen dissolved in tantalum with respect to iron concentration in tantalum

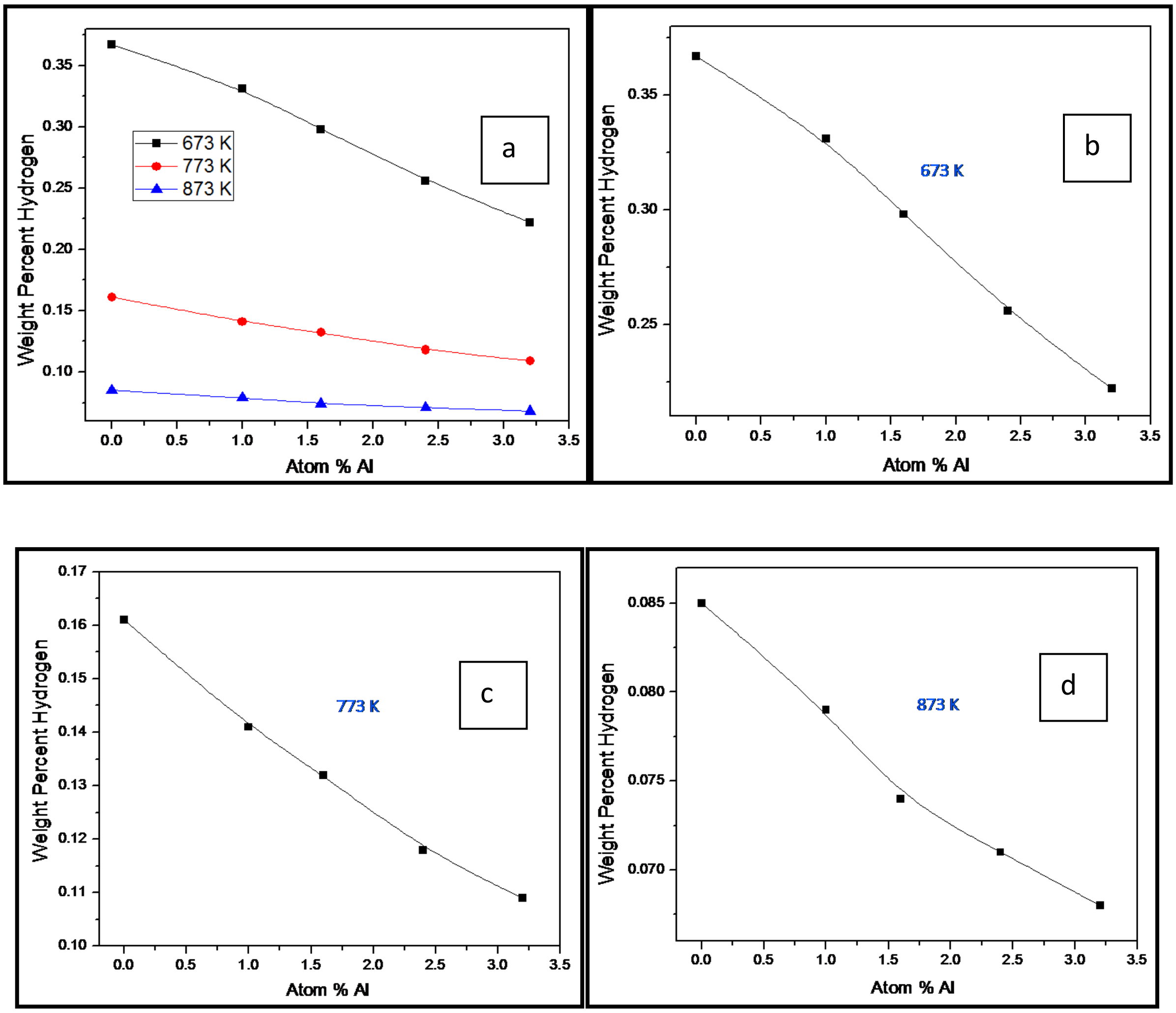

Fig. 4.22 **Amount of hydrogen dissolved in tantalum with respect to aluminium concentration in tantalum**

The amount of hydrogen dissolved in various tantalum alloys with respect to the concentration of alloying elements is shown in Fig. 4.23 at three different temperatures (673 K, 773 K and 873 K).

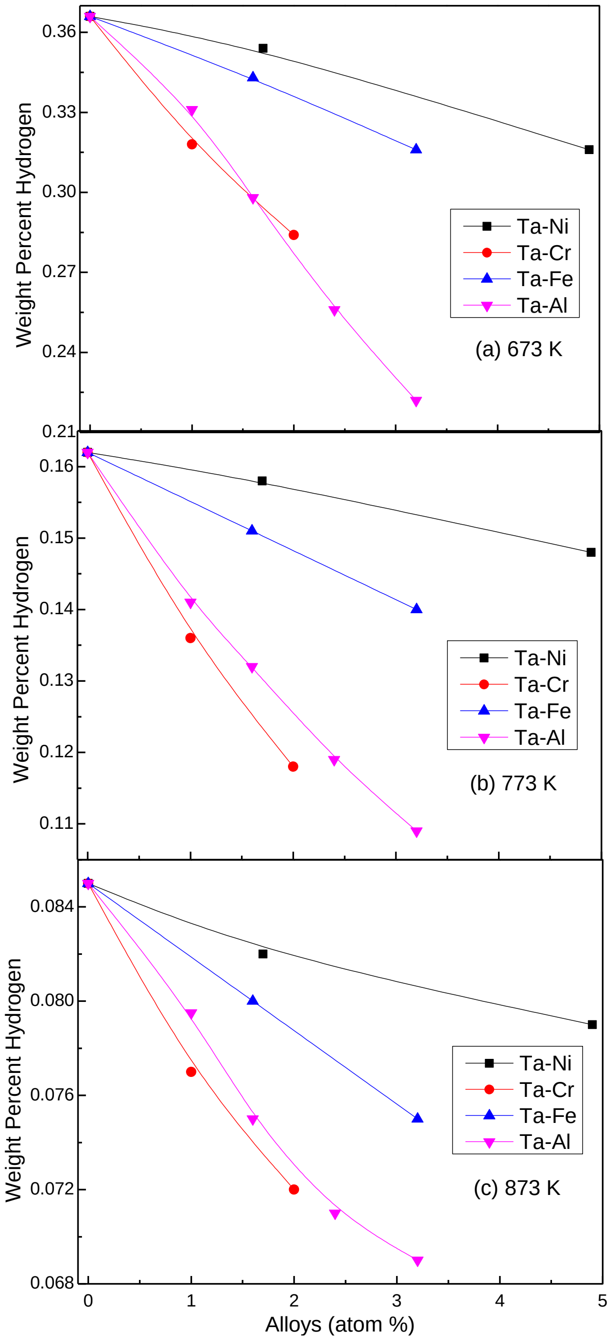

Fig. 4.23 **Variation in amount of dissolved hydrogen with respect to the concentration of alloying elements in different tantalum alloys at (a) 673 K (b) 773 K and (c) 873 K.**

It is clearly observed from Fig. (4.19 - 4.23) that the equilibrium solubility of hydrogen in tantalum decreases with the addition of these alloying elements [Ni, Cr, Fe and Al] and more decrease is observed with their increasing compositions. The variation in hydrogen solubility was less at higher temperature as compared to low temperature. The alloys-hydrogen solid solution approaches toward ideal behaviour with increase of temperature and, hence, the effect of alloying elements on hydrogen solubility is substantially less at higher temperatures as shown in Figs. (4.19 - 4.23).

The isobaric *P-C-T* curves for pure Ta and its different alloys (mentioned above) are shown in Fig. 4.24 to Fig. 4.27. These curves are representing the weight percent hydrogen with respect to temperature at four different constant pressures.

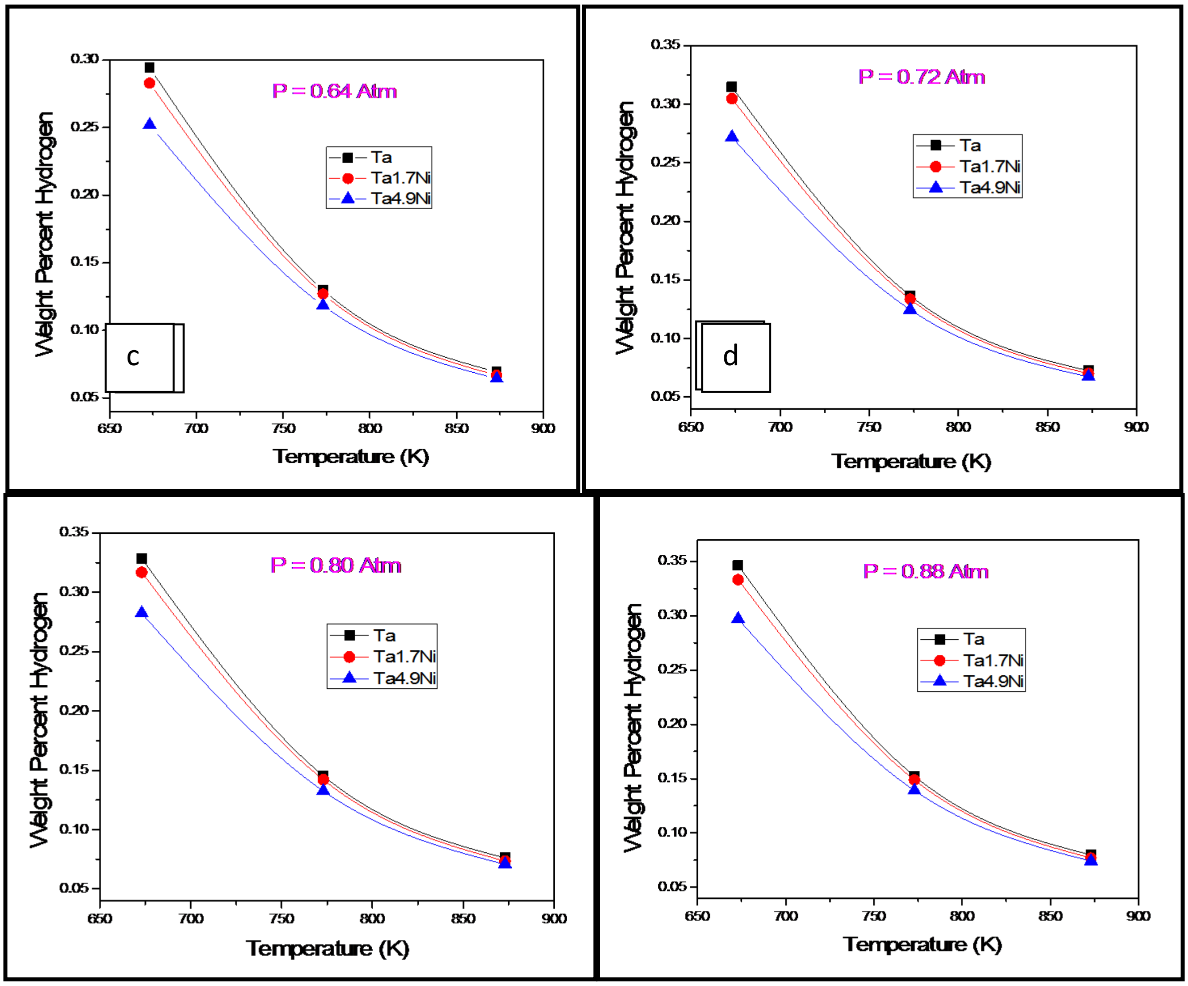

Fig. 4.24 **Isobaric *P-C-T* equilibrium curves for the solubility of hydrogen in Ta and Ta-Ni alloys at (a) 0.64 Atm, (b) 0.72 Atm, (c) 0.8 Atm and (d) 0.88 Atm**

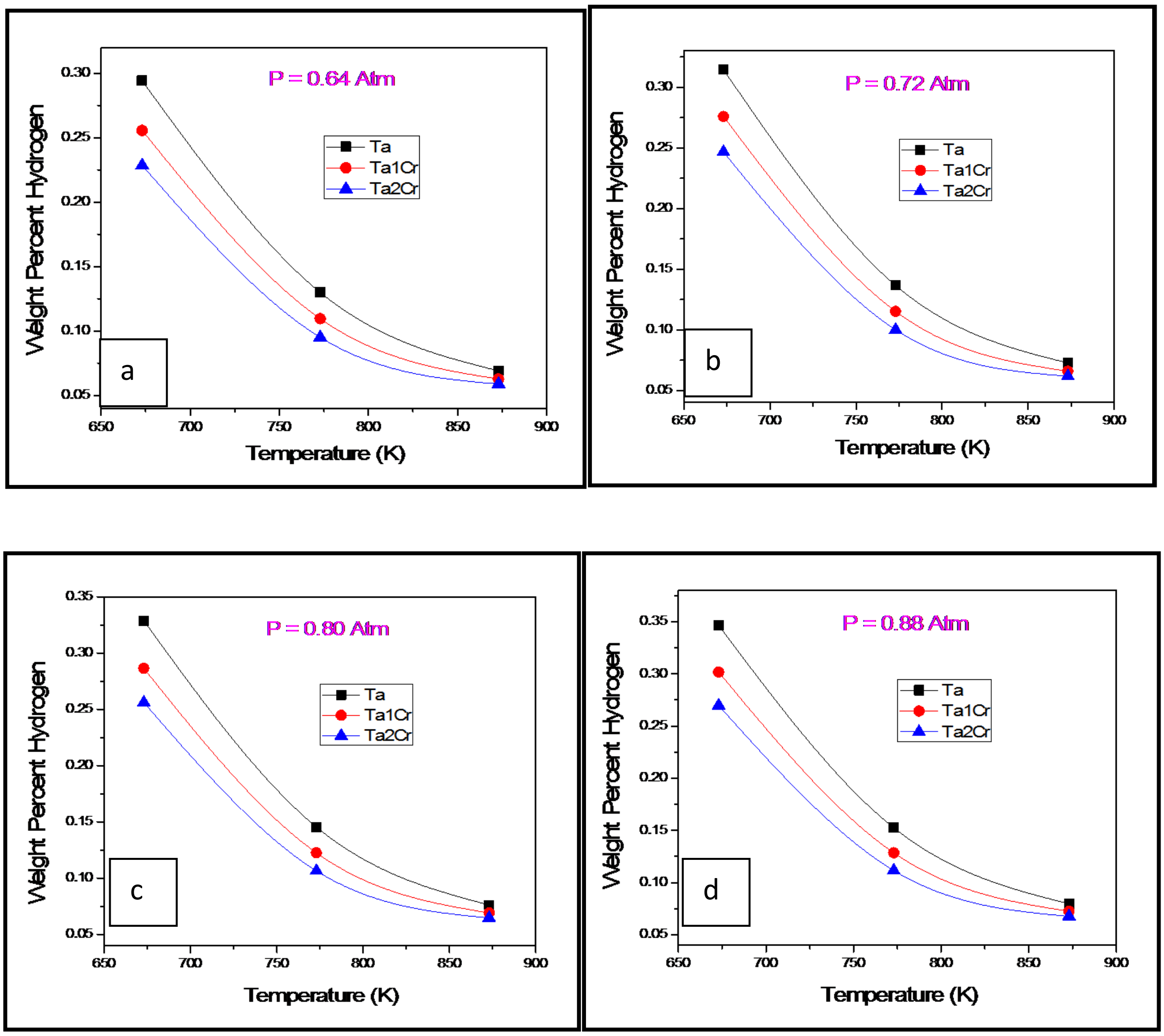

Fig. 4.25 Isobaric P-C-T equilibrium curves for the solubility of hydrogen in Ta and Ta-Cr alloys at (a) 0.64 Atm, (b) 0.72 Atm, (c) 0.8 Atm and (d) 0.88 Atm

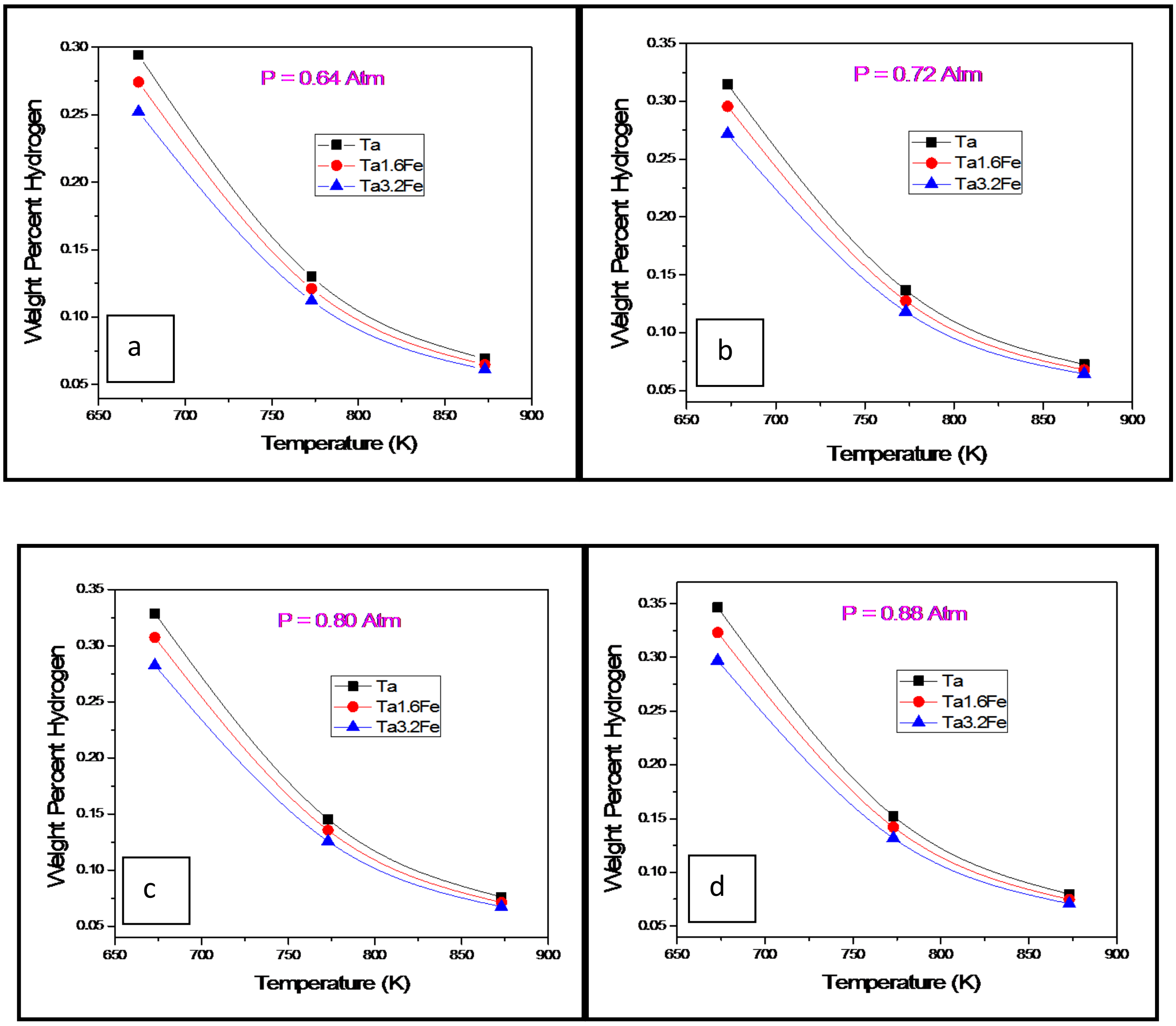

Fig. 4.26 Isobaric *P-C-T* equilibrium curves for the solubility of hydrogen in Ta and Ta-Fe alloys at (a) 0.64 Atm, (b) 0.72 Atm, (c) 0.8 Atm and (d) 0.88 Atm

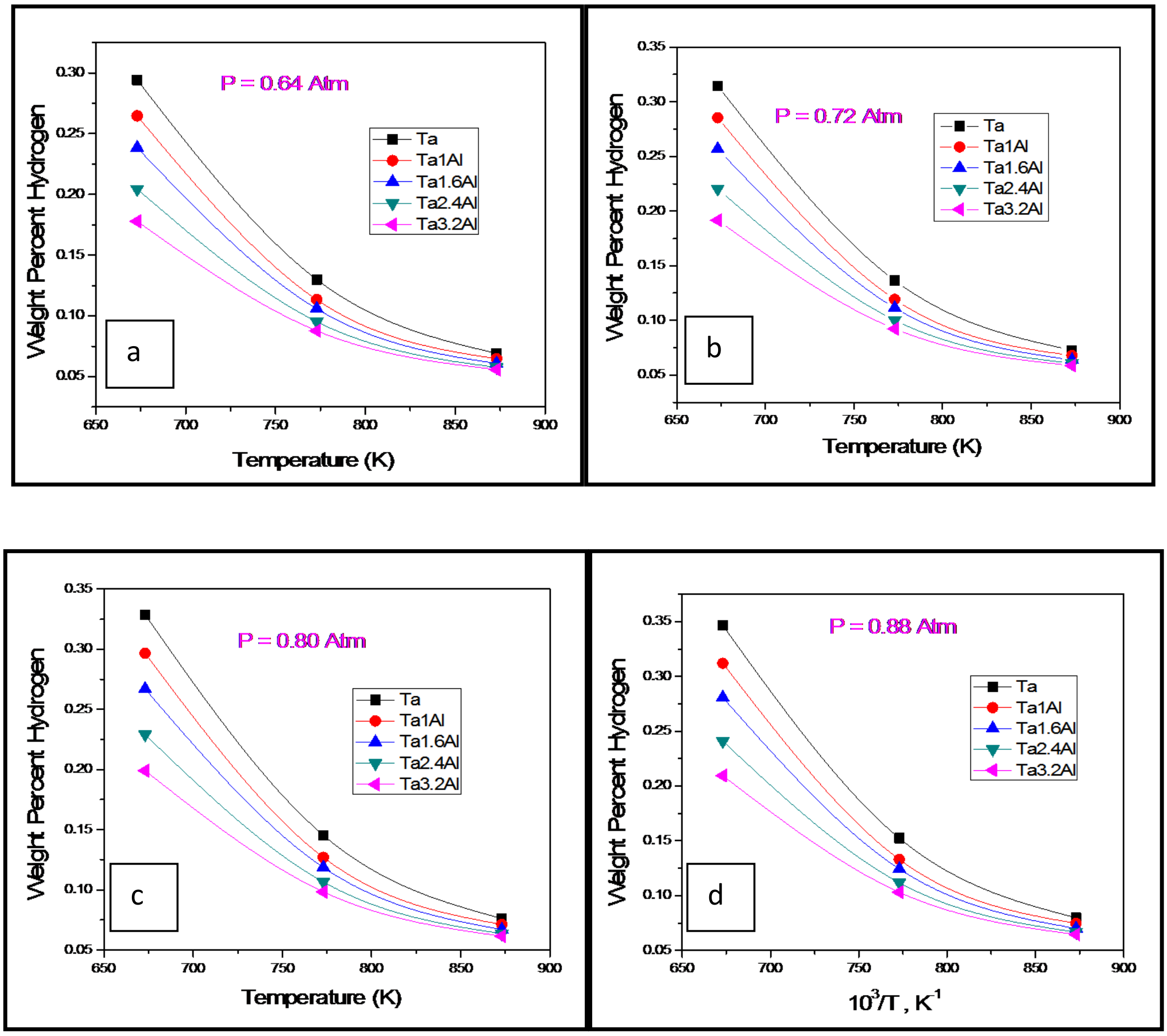

Fig. 4.27 **Isobaric *P-C-T* equilibrium curves for the solubility of hydrogen in Ta and Ta-Al alloys at (a) 0.64 Atm, (b) 0.72 Atm, (c) 0.8 Atm and (d) 0.88 Atm**

Fig. 4.24 to Fig. 4.27 has clearly indicated that the equilibrium solubility of hydrogen in tantalum decreases with increase in temperature at a constant pressure. The decrease in hydrogen solubility is also seen with increasing content of alloying elements.

Similarly isothermal *P-C-T* curves for the solubility of hydrogen in Ta and its alloys are shown in Fig. 4.28 to Fig. 4.31. These curves are representing the variations in dissolved hydrogen concentration (weight percent) with respect to square root of the hydrogen pressure at three different constant temperatures.

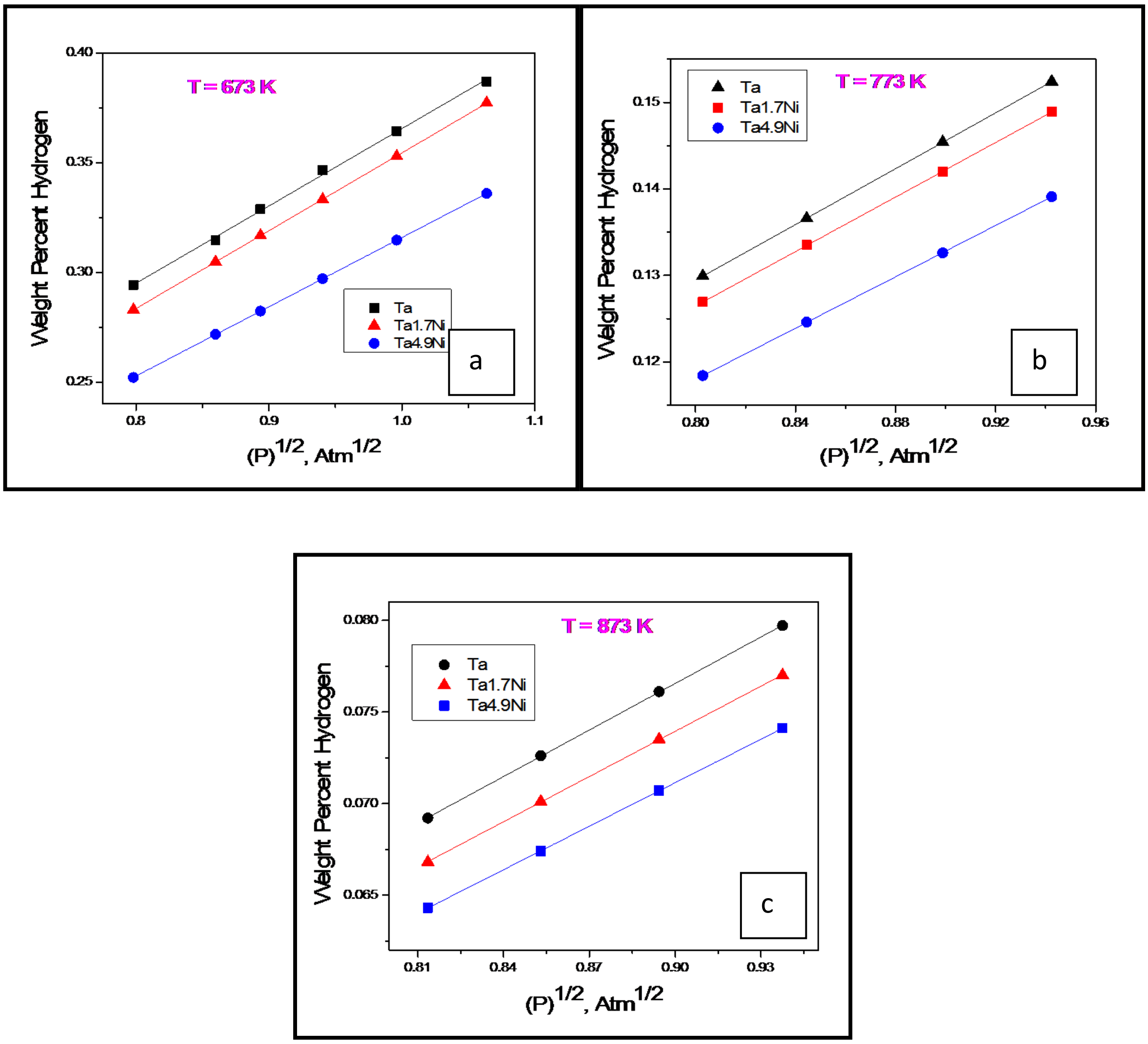

Fig. 4.28 Isothermal *P-C-T* equilibrium curves for the solubility of hydrogen in Ta and Ta-Ni alloys at (a) 673 K, (b) 773 K and (c) 873 K

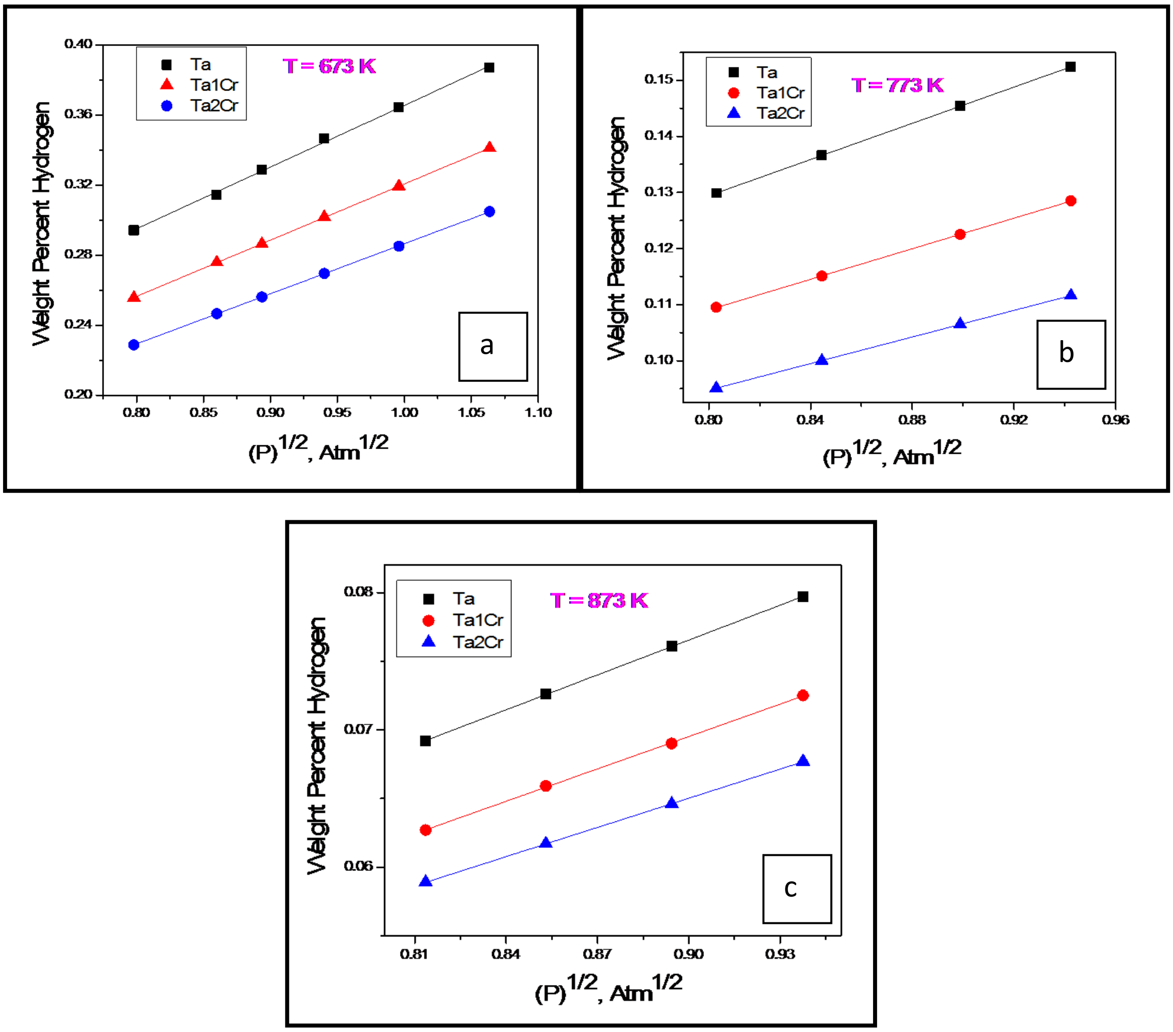

Fig. 4.29 **Isothermal *P-C-T* equilibrium curves for the solubility of hydrogen in Ta and Ta-Cr alloys at (a) 673 K, (b) 773 K and (c) 873 K**

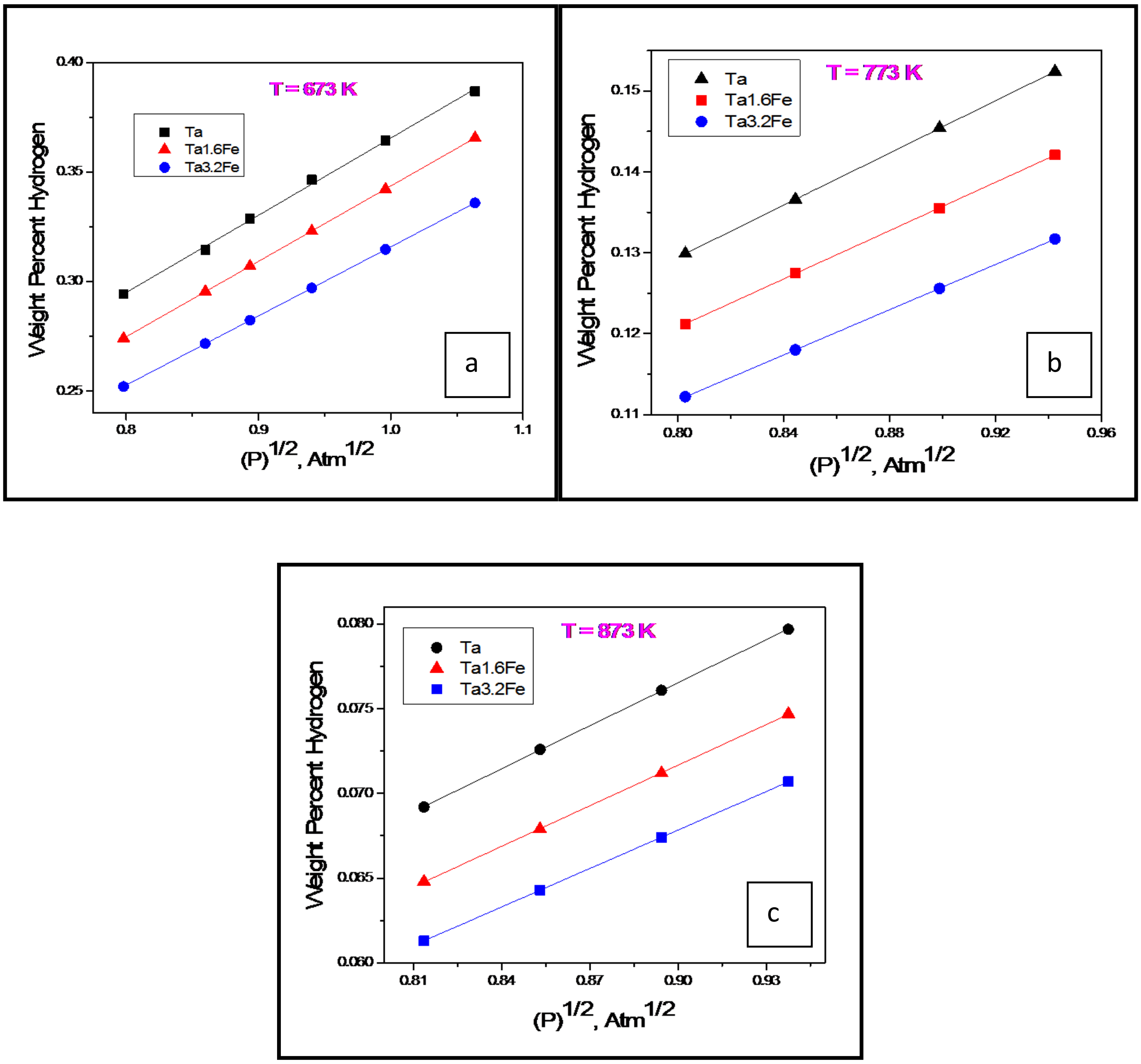

Fig. 4.30 Isothermal ***P-C-T*** **equilibrium curves for the solubility of hydrogen in Ta and Ta-Fe alloys at (a) 673 K, (b) 773 K and (c) 873 K**

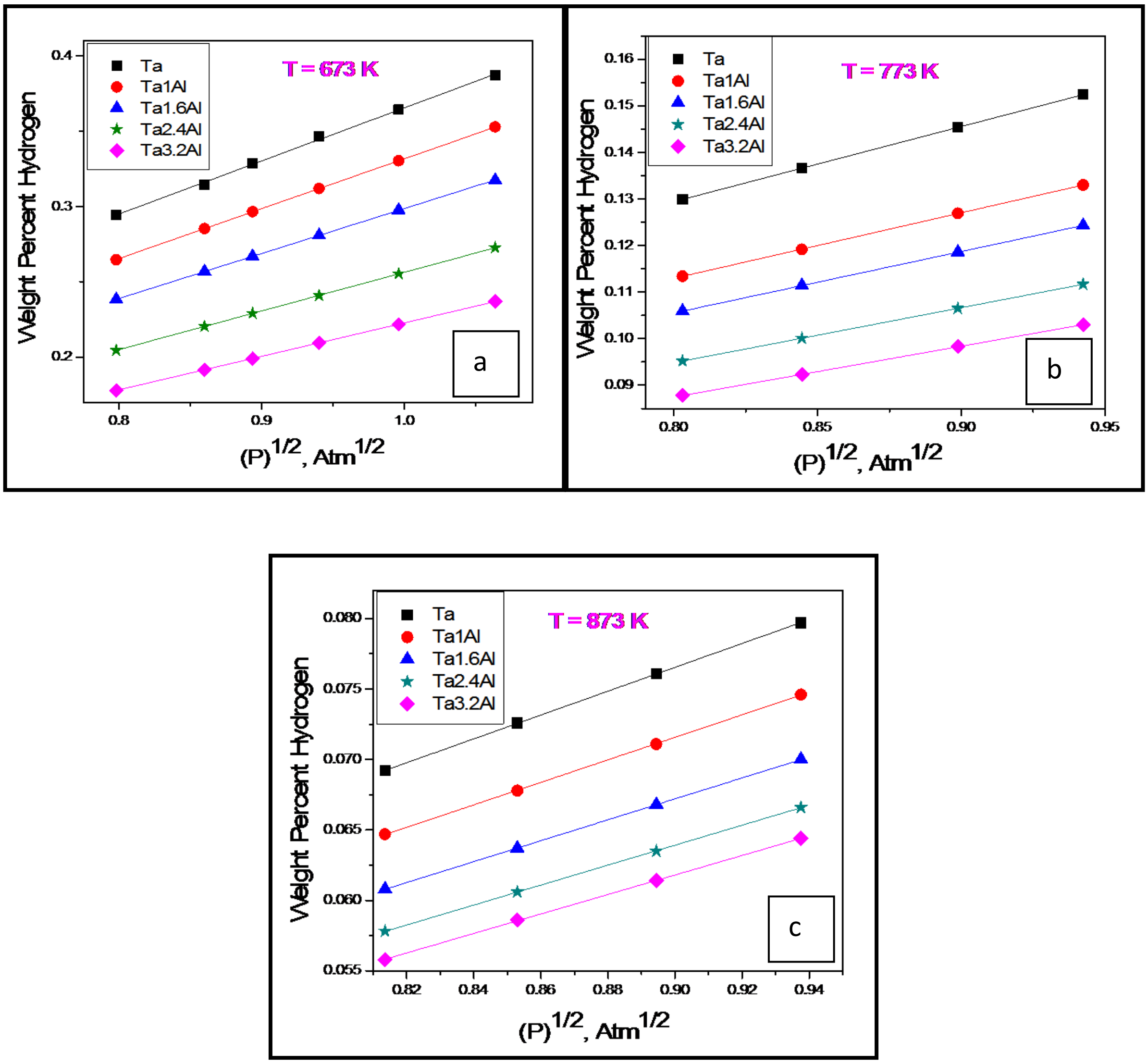

Fig. 4.31 **Isothermal *P-C-T* equilibrium curves for the solubility of hydrogen in Ta and Ta-Al alloys at (a) 673 K, (b) 773 K and (c) 873 K**

These isothermal curves, in Fig. 4.28 to Fig. 4.31, have shown that the equilibrium solubility of hydrogen is linearly increasing with square root of hydrogen pressure and following the Sievert's law. The similar behaviors of alloying elements were noticed as in case of isobaric curves i.e. hydrogen solubility was decreasing with increasing concentration of alloying elements.

Furthermore, the effect of all alloying elements have also shown together in isothermal as well as in isobaric *P-C-T* curves in Fig. 4.32 and Fig. 4.33, respectively, to indicate their relative behavior.

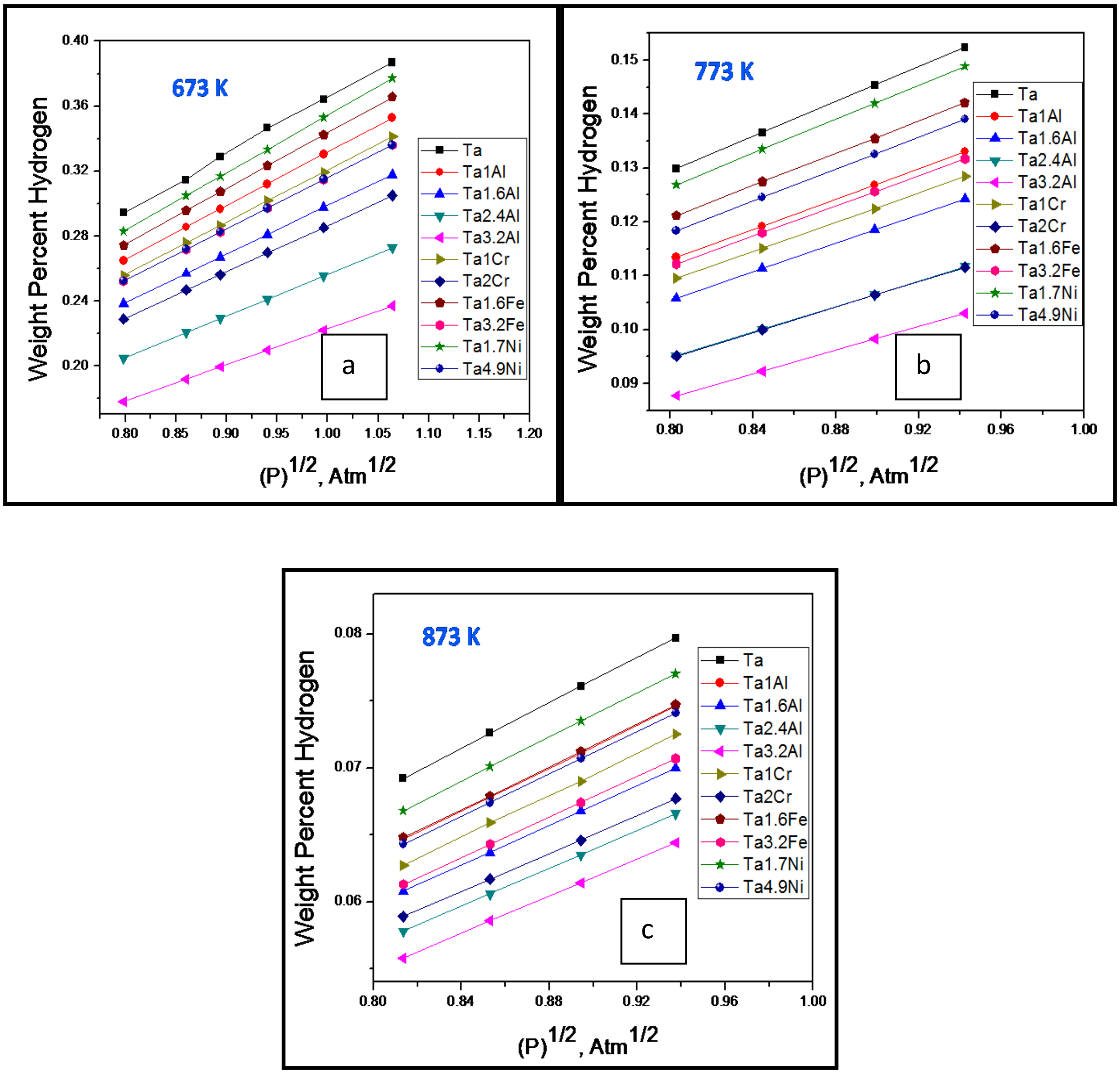

Fig. 4.32 **Isothermal *P-C-T* equilibrium curves showing the comparison behavior of alloying elements on the solubility of hydrogen in tantalum at (a) 673 K, (b) 773 K and (c) 873 K**

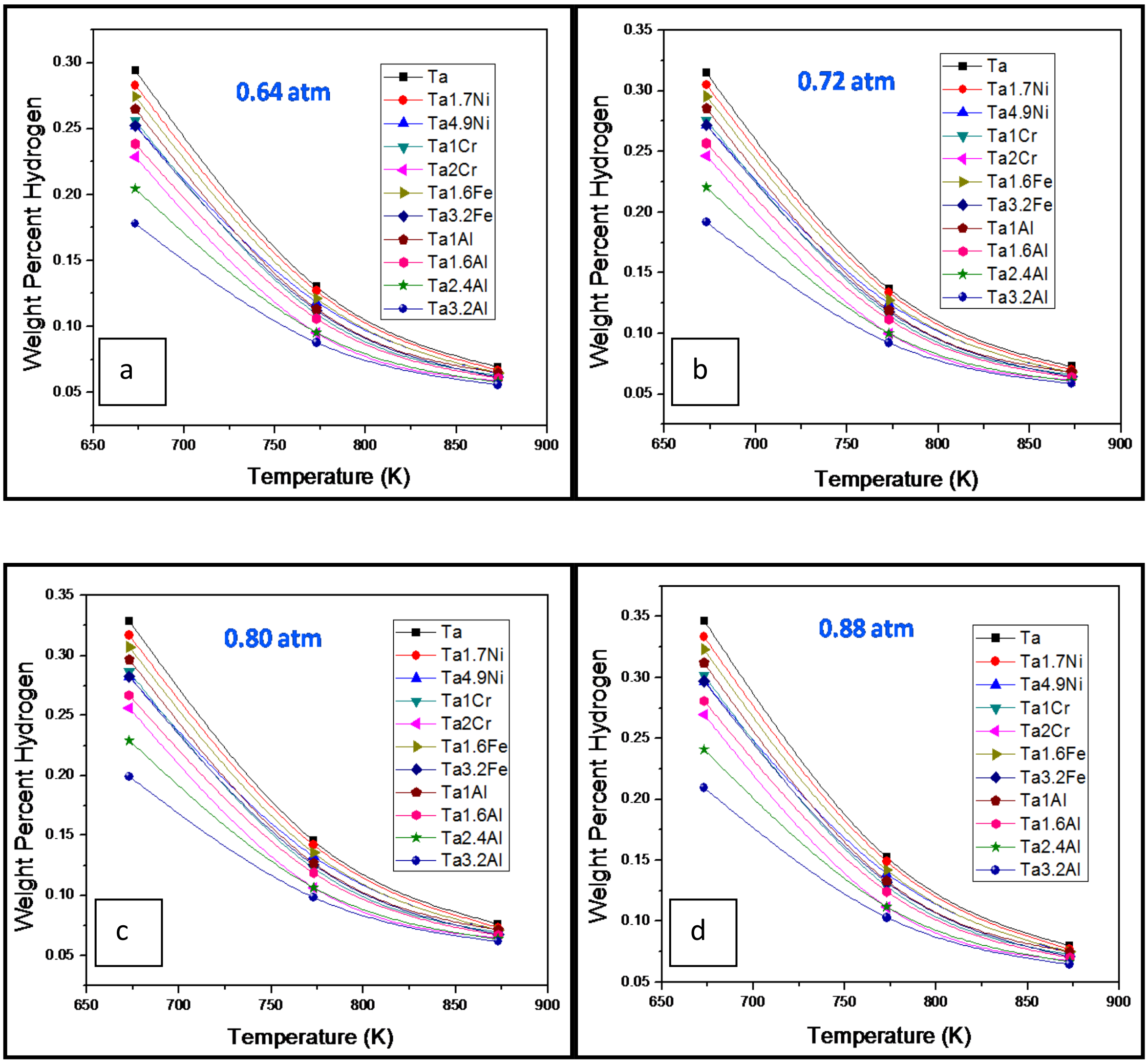

Fig. 4.33 **Isobaric *P-C-T* equilibrium curves showing the comparison behavior of alloying elements on the solubility of hydrogen in tantalum at (a) 0.64 Atm, (b) 0.72 Atm, (c) 0.8 Atm and (d) 0.88 Atm**

From Fig. 4.32 and Fig. 4.33, it was observed that the hydrogen solubility in all the alloys was less than the hydrogen solubility in pure tantalum metal. Moreover, among the four alloying elements (Ni, Cr, Fe and Al), the addition of Cr as alloying element has the largest effect on the hydrogen solubility in tantalum if the same composition of all alloying elements was considered (Fig. 4.23) and the order followed for the decreasing effect on hydrogen solubility in tantalum was (Cr > Al > Fe > Ni). Chromium decreases the hydrogen solubility to the greatest extent and nickel to the smallest extent.

4.4.1 Thermodynamics Parameters for the Ta-X-H System (X = Ni, Cr, Fe and Al)

The equilibrium *P-C-T* data have been used to obtain thermodynamic parameters for the solution of hydrogen in Group V transition metals [79,139]. Thermodynamic quantities for Ta-H system have been calculated by various researchers using experimentally determined *P-C-T* curves. It was found that the relative partial molar enthalpies, $\overline{\Delta H_H}$ and entropies, $\overline{\Delta S_H}$, of hydrogen are virtually constant with respect to temperature for a given concentration in certain temperature ranges [79-80,152-156,197]. The present section describes the thermodynamic parameters calculated for the solution of hydrogen in tantalum and its alloys from the equilibrium *P-C-T* data.

The change in relative partial molar enthalpy, $\overline{\Delta H_H}$ and entropy, $\overline{\Delta S_H}$ for solution of hydrogen in tantalum metal and its alloys were calculated using the relation:

$$K_s = {c}/{\sqrt{p}} = \exp\left(-\frac{\overline{\Delta H_H}}{RT}\right)\exp\left(\frac{\overline{\Delta S_H}}{R}\right) \qquad (4.3)$$

Logarithmic form of the above equation could be expressed as

$$\log K_s = \log\frac{c}{\sqrt{p}} = -\frac{\overline{\Delta H_H}}{2.303RT} + \frac{\overline{\Delta S_H}}{2.303R} \qquad (4.4)$$

Where, K_s is the Sievert's constant, R is the gas constant and T is the temperature.

The values for the Sievert's constant, K_s were determined by applying Sievert's law, which states that the concentration, c of dissolved hydrogen is directly proportional to the square root of hydrogen pressure, p and is given by the relation as follow:

$c \alpha \sqrt{p}$ or $c = K_s \sqrt{p}$

or

$$K_s = c / \sqrt{p} \qquad (4.5)$$

Where, c is the concentration of hydrogen dissolved in metal (in wt %) in equilibrium with gaseous hydrogen at pressure p, and K_s is the Sievert's constant. The square root dependence follows from the fact that hydrogen dissolves in atomic form in the host matrix [128,198-199].

Thus, K_s values were calculated according to Eq. (4.5) for the solution of hydrogen in tantalum and tantalum-alloys from the data in Table 4.5, at three different temperatures and at one atmosphere hydrogen pressure. Table 4.6 lists the Sievert's constant, K_s for hydrogen in tantalum and its alloys.

Table 4.6 Sievert's constant, K_s for hydrogen in Ta and its alloys

Sample (atom %)	**K_{s}, 10^{-2}**		
	673 K	**773 K**	**873 K**
Ta	36.8	16.1	8.5
Ta-1.7Ni	35.4	15.8	8.2
Ta-4.9Ni	31.5	14.7	7.9
Ta-1Cr	32.0	13.6	7.7
Ta-2Cr	28.6	11.8	7.2
Ta-1.6Fe	34.3	15.0	7.9
Ta-3.2Fe	31.5	13.9	7.5
Ta-1Al	33.1	14.1	7.9
Ta-1.6Al	29.8	13.1	7.4
Ta-2.4Al	25.6	11.8	7.1
Ta-3.2Al	22.2	10.9	6.8

The variations in K_s values with temperature are represented in Fig. 4.34. Thermodynamic parameters for the solution of hydrogen were calculated from the graphs. The slope of $\log K_S$ vs $1/T$ plots gives the value of $\left(-\overline{\Delta H_H}/2.303R\right)$, whereas intercept give the value of $\left(\overline{\Delta S_H}/2.303R\right)$.

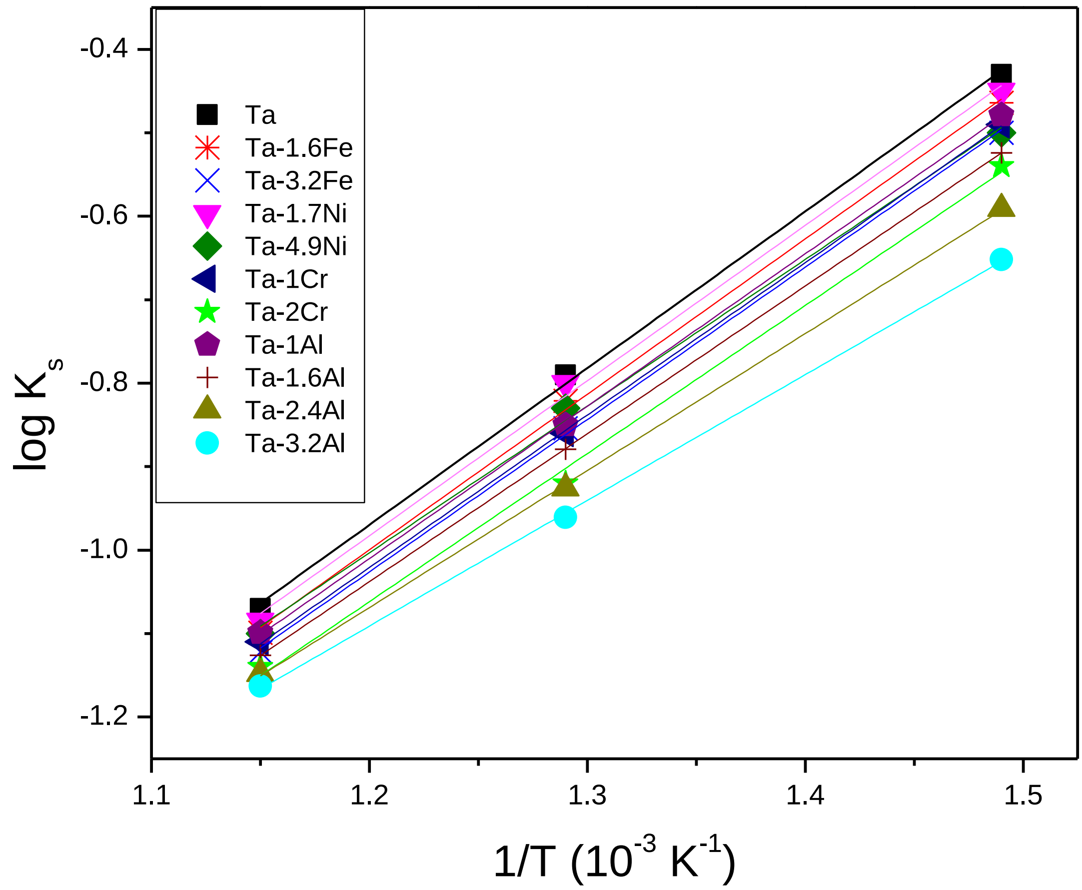

Fig. 4.34 **Variations in K_s values with temperature for Ta-H and Ta-M-H systems (M = alloying elements)**

The values for the relative partial molar enthalpy and entropy for the solution of hydrogen in the tantalum metal and its alloys were calculated using the slope and intercept of Fig. 4.34, respectively and are listed in Table 4.7. The enthalpy and entropy values for Ta-H system calculated in the present work were compared with the literature values. It was found that the experimental values in the present results are comparable with the existing literature values for Ta-H system. A small variation in these values may be due to different methods of sample preparation applied by different researchers.

Table 4.7 **The values for the relative partial molar enthalpy and entropy for the solution of hydrogen in the tantalum metal and its alloys [1 cal = 4.184 J]**

Sample (atom %)	$\overline{\Delta H_H}$ **(cal/g atom H)**	$\overline{\Delta S_H}$ **(cal/K/g atom H)**	**Temperature range (K)**
Ta	- 8600 ± 20	- 14.7 ± 0.02	673-873
Ta-1.7Ni	- 8520 ± 128	- 14.7 ± 0.1	673-873
Ta-4.9Ni	- 8050 ± 132	- 14.2 ± 0.1	673-873
Ta-1Cr	- 8350 ± 80	- 14.7 ± 0.09	673-873
Ta-2Cr	- 8110 ± 400	- 14.6 ± 0.5	673-873
Ta-1.6Fe	- 8500 ± 20	- 14.7 ± 0.03	673-873
Ta-3.2Fe	- 8360 ± 40	- 14.7 ± 0.05	673-873
Ta-1Al	- 8350 ± 96	- 14.6 ± 0.09	673-873
Ta-1.6Al	- 8100 ± 13	- 14.5 ± 0.01	673-873
Ta-2.4Al	- 7500 ± 109	- 13.9 ± 0.1	673-873
Ta-3.2Al	- 6890 ± 128	- 13.3 ± 0.1	673-873
Ta*	- 7700 ± 100	-	703-717 **[113,156,197]**
Ta*	- 9400 ± 100	- 13.3 ± 0.2	195 -513 [**154**]
Ta*	- 8850 ± 350	- 12.6 ± 2	573-773 [**80**]

Table 4.7 has indicated that the addition of alloying elements in tantalum reduces the magnitude of relative change in enthalpy with negative sign for the solution of hydrogen in

Ta-alloys whereas no considerable variations have been observed for the relative change in entropy values. However, the relative partial molar enthalpies, $\overline{\Delta H_H}$ and entropies, $\overline{\Delta S_H}$ for the solution of hydrogen in tantalum and its alloys are the function of the concentration of alloying elements but independent of temperature in a range of (673 – 873) K and hydrogen concentration in a range of (0.38 – 0.05) wt %.

The relative partial molar enthalpy, $\overline{\Delta H_H}$ and the relative partial molar entropy, $\overline{\Delta S_H}$ are related with the relative partial molar Gibb's free energy, $\overline{\Delta G_H}$ by the following relation:

$$\overline{\Delta G_H} = \overline{\Delta H_H} - T\overline{\Delta S_H} \tag{4.6}$$

Thus, using the $\overline{\Delta H_H}$ and $\overline{\Delta S_H}$ values from Table 4.7, the relative partial molar Gibb's free energy were also calculated at different temperatures and listed in Table 4.8. The asterisk * in Table 4.7 and 4.8 represents the values from the literature.

Table 4.8 Relative partial molar Gibb's free energy for the solution of hydrogen in the tantalum metal and its alloys [1 cal = 4.184 J]

Temperature (K)	$\overline{\Delta G_H}$ **(cal/g atom H)**										
	Ta (H)	Ta-1.7Ni (H)	Ta-4.9Ni (H)	Ta-1Cr (H)	Ta-2Cr (H)	Ta-1.6Fe (H)	Ta-3.2Fe (H)	Ta-1Al (H)	Ta-1.6Al (H)	Ta-2.4Al (H)	Ta-3.2Al (H)
673	1290	1370	1510	1540	1710	1360	1530	1480	1660	1850	2060
773	2760	2840	2930	3010	3170	2830	3000	2940	3100	3240	3390
873	4230	4310	4350	4480	4630	4300	4470	4400	4550	4630	4720
917* [**139**]	4390										
973* [**139**]	5100										
1023* [**139**]	5760										

4.4.2 Discussion on Hydrogen Solubility in Ta-X Alloys (X = Ni, Cr, Fe and Al)

The hydrogen solubility in all the Ta-X (X = Ni, Cr, Fe & Al) alloys was less than the pure tantalum at all the temperature and pressure range investigated. Furthermore, at given temperature and pressure, hydrogen solubility in Ta-alloys decreases with increasing alloy compositions. The change in hydrogen solubility in tantalum on the addition of alloying elements could be explained on the basis of chemical as well as physical considerations. Valence (*e /a* ratio) and interstitial size could be the governing factors. Although, the efforts made to correlate the effect of alloying elements on the solubility of hydrogen in metals with the average elastic and electronic interaction have met only with a limited success [108]. In the present section, possible factors responsible for the change in hydrogen solubility in tantalum on the addition of alloying elements are discussed.

4.4.2.1 Thermodynamics Consideration

Generally, the alloying effect can be examined by investigating the entropy of solution, $\overline{\Delta S_H}$ at the infinite dilution. In Pd-based alloys, $\overline{\Delta S_H}$ decrease with solute concentration for all the solute species [108]. This suggests that the number of available interstitial sites, r, is decreases with increasing solute concentration, more probable due to repulsive interaction between H and solute atoms. Similar observations have been made in Ti, V and Nb alloys. Only exception is Ti in V metal, in which $\overline{\Delta S_H}$ increases with increasing Ti content [108]. In the present work, $\overline{\Delta S_H}$ values are almost constant with solute (alloying elements) concentration. This is because of no change in crystal structure of tantalum on the addition of the above mentioned alloying elements; the number of interstitial sites per unit cell remains unchanged upon alloying with nickel, chromium, iron and aluminum with solid solubility limit. Accordingly, the addition of these alloying elements will not give rise to any change in the $\overline{\Delta S_H}$. It is therefore appeared that the explanations based on configurational entropy, thermodynamic function changes are not applicable to the present results. In order to understand the alloying effect on the solubility of hydrogen in tantalum, a further knowledge about the strength of solute-hydrogen interaction at a large number of sites around each solute atom is required.

4.4.2.2 Electronic Contribution

Hume Rothery has recognized the effect of variation in electron concentration on the thermodynamic properties and subsequently on the solubility of one element in another element [200]. For instance, the solubility limit of various elements in copper corresponds to different atomic percentages but to approximately the same concentration of valence electrons. According to Wagner [199], the same concept can be used to explain the alloying behavior of hydrogen in metals.

Hydrogen gas dissolves in the metal in the form of protons and electrons according to the equation given below:

$$\frac{1}{2}H_2(gas) = \left[H^+\right] + \left[e^-\right] \qquad (4.7)$$

And, at equilibrium condition,

$$\frac{1}{2}G_{H_2}^{(gas)} = \overline{G_{H^+}} + \overline{G_{e^-}} \qquad (4.8)$$

Where, $G_{H_2}^{(gas)}$ is the molar free energy of hydrogen gas at a given pressure, $\overline{G_{H^+}}$ and $\overline{G_{e^-}}$ are the partial molar free energies of protons and electrons, respectively, in the metal. If the gas phase is ideal and the concentration of proton in the metallic phase is small, above Eq. can be rewritten as [199],

$$\frac{1}{2}G^0_{H_2} + \frac{1}{2}RT\ln P_{H_2} = \overline{G^*_{H^+}} + RT\ln c + \overline{G_{e^-}} \qquad (4.9)$$

Where, $G^0_{H_2}$ is the molar free energy of hydrogen gas at 1 atmosphere pressure, c is the concentration of hydrogen in metal and $\overline{G^*_{H^+}}$ is the partial molar free energy of protons extrapolated to unit concentration. Solving above Eq. for c, we have

$$c = \sqrt{p_{H_2}}\exp\left[\frac{\frac{1}{2}G^0_{H_2} - \overline{G^*_{H^+}} - \overline{G_{e^-}}}{RT}\right] \qquad (4.10)$$

Hence, for given hydrogen pressure, if partial molar free energy of electrons is increased by the addition of alloying elements, the solubility of hydrogen will decrease.

A correlation between the solubility of hydrogen vs. average electron to atom (*e/a*) ratio is observed for several systems which indicate the electronic interaction is eventually related to the Fermi energy level (the highest occupied energy level); play more important role in determining the effect of alloying elements on the solubility of hydrogen in metals [108]. If an alloying element donate its electron to valence band of the host metal, the number of electrons in Fermi level increases and consequently *e /a* ratio increases which results in increase of electronic contribution to the total free energy of electron $\overline{G_{e^-}}$ in the system and hence, according to Eq. (4.10), the solubility of hydrogen decreases. For examples, the addition of Mo to niobium reduces the hydrogen solubility in Nb-Mo alloys [146]. Similarly, the solubility of hydrogen in V-Mo and V-Al alloys decreases with increasing concentration of molybdenum and aluminium in vanadium [50]. Mo and Al contribute more electrons to the Fermi energy level of the host matrix niobium and vanadium and hence the observed solubility could be explained on the basis of the increase in *e /a* ratio. Another example is increase of hydrogen solubility in $LaNi_5$, intermetallic compound, with increasing Ni content.

Nickel addition decreases the electron to atom ratio in $LaNi_5$, intermetalic compound and consequently, the Fermi energy level of the system decrease, which results in enhancing the hydrogen solubility and storage capacity of compound [201]. The hydrogen solubility in lead lithium eutectic alloy ($Pb_{83}Li_{17}$), decreases with addition of excess Pb [202]. This decrease in hydrogen solubility is attributed to increases in electron to atom ratio contributed by lead. In such cases, the electronic interaction is more important factor in determining solubility than the volume effect.

In the present study, the electronegativity on Pauling scale of tantalum metal is smaller than all of these alloying elements (Ni, Cr, Fe and Al) as shown in Table 4.9. The variation in H-solubility with respect to change in electron to atom *(e/a)* ratio is represented in Table 4.10.

Table 4.9 **Electronegativity of the elements (Pauling scale)**

Element	Crystal Structure	Electronegativity
Ta	BCC	1.5
Al	FCC	1.61
Cr	BCC	1.66
Fe	BCC	1.83
Ni	FCC	1.91

Table 4.10 Variation in H-solubility with respect to change in (*e /a)* ratio

Element	*e /a* Ratio	H-Solubility (wt %)
Ta	5	0.367
Ta-1Cr	4.96	0.32
Ta-2Cr	4.92	0.286
Ta-1.7Ni	4.949	0.354
Ta-4.9Ni	4.853	0.315
Ta-1.6Fe	4.952	0.343
Ta-3.2Fe	4.904	0.316
Ta-1Al	4.98	0.331
Ta-1.6Al	4.968	0.298
Ta-2.4Al	4.952	0.256
Ta-3.2Al	4.936	0.222

Here valences taken for Ta, Cr, Ni, Fe and Al are +5, +1, +2, +2 and +3 respectively.

From Table 4.10, it is clear that both electron to atom (*e/a*) ratio as well as solubility of hydrogen in tantalum decrease with increase in the concentration of these alloying elements. Therefore, in the present study, electron factor does not seem to be more important similar to as in case of Pd [108] whereas no systematic variations exist between the solubility of hydrogen and $\overline{\Delta H_H}$ vs. (*e /a*) ratio while a correlation is found between $\overline{\Delta H_H}$ and the lattice parameter.

4.4.2.3 Atomic Size Consideration

The atomic size of alloying elements may be a reason for change in hydrogen solubility. Tantalum forms substitutional alloys with nickel, chromium, iron and aluminum.

According to Pauling scale, the atomic radii of tantalum, nickel, chromium, iron and aluminum are 146, 124, 128, 126 and 143 pm, respectively. The lattice parameter of tantalum decreases with the addition of these atoms. Therefore, the lattice size and interstitial sites size decrease and hence solubility decreases [203-204]. The decrease of hydrogen solubility in Ta-alloys could be explained due to increase in lattice strain energy as proposed by Brodowsky [205]. The change in strain energy of dissolved hydrogen due to the presence of different size interstitial sites around a substitutional atom may be responsible for change in hydrogen solubility [144]. The variation in hydrogen-solubility in different tantalum alloys with respect to change in lattice parameter is shown in Table 4.11.

Table 4.11 Variation in hydrogen-solubility in different tantalum alloys with respect to change in lattice parameter.

Element	**2θ value of (211) plane**	**Lattice constant (before H-charging)**	**H-Solubility (wt % ± 1 %)**
Ta	115.519(6)	3.315(9)	0.367
Ta-1Cr	115.821(3)	3.310(4)	0.32
Ta-2Cr	115.902(1)	3.308(9)	0.286
Ta-1.7Ni	116.013(4)	3.306(9)	0.354
Ta-4.9Ni	116.314(1)	3.301(5)	0.315
Ta-1.6Fe	116.081(2)	3.305(7)	0.343
Ta-3.2Fe	116.223(1)	3.301(7)	0.316
Ta-1Al	115.865(7)	3.309(6)	0.331
Ta-1.6Al	115.918(3)	3.308(6)	0.298
Ta-2.4Al	115.971(2)	3.307(7)	0.256
Ta-3.2Al	116.017(5)	3.306(8)	0.222

Table 4.11, indicates a correlation between the solubility of hydrogen vs. lattice parameter. For better estimation of lattice constant value higher 2θ peak position (211) is used. Values in the parenthesis correspond to the standard deviation in the last decimal place. It is seen that both the lattice parameter as well as the solubility of hydrogen in tantalum decrease on the addition of the alloying elements. The lattice effect (volume effect) appears to be more important than the average electronic effect in determining the change in hydrogen solubility in tantalum on the addition of these alloying elements. In addition, the lattice effect appears to be dependent also on the element causing lattice contraction. The possibility of additional factors influencing the solubility apparently exists.

4.4.2.4 Chemical Behavior of Alloying Elements

Furthermore, the solubility results could be explained on the basis of chemical behavior of the alloying elements like nickel, chromium, iron and aluminum with hydrogen. The solubility of hydrogen in solid nickel, chromium, iron and aluminum is very less. Table 4.12 represents the hydrogen solubility in these metals at one atmosphere hydrogen pressure and in the temperature range of 673-873 K (400 – 600 ^{o}C).

Table 4.12 Amount of hydrogen dissolved in pure Ta, Ni, Cr, Fe and Al at three different temperatures at one atmosphere hydrogen pressure [* indicates data measured presently]

Temperature	**Hydrogen (Wt %)**					
(K)	**Ta***	**Ta** [**79**]	**Ni** [**100**]	**Fe** [**100,128**]	**Cr** [**100**]	**Al** [**206**]
673	.3657	.2640	2.5×10^{-4}	3.4×10^{-5}	2×10^{-5}	3.7×10^{-7}
773	.1617	.1520	3.45×10^{-4}	6.5×10^{-5}	2.5×10^{-5}	1.1×10^{-6}
873	.085	.085	4.75×10^{-4}	1×10^{-4}	3.5×10^{-5}	2.4×10^{-6}

The hydrogen solubility in the alloying elements increases with increase in temperature and with the melting of these alloying elements (melting point for Ni, Cr, Fe and Al are 1452, 1860, 1538 and 660 °C, respectively) but always remains small and follows the Sievert's law. The solubility of hydrogen in different phase regions is shown in the phase diagrams from Fig. 4.35 to Fig. 4.38 [207-210].

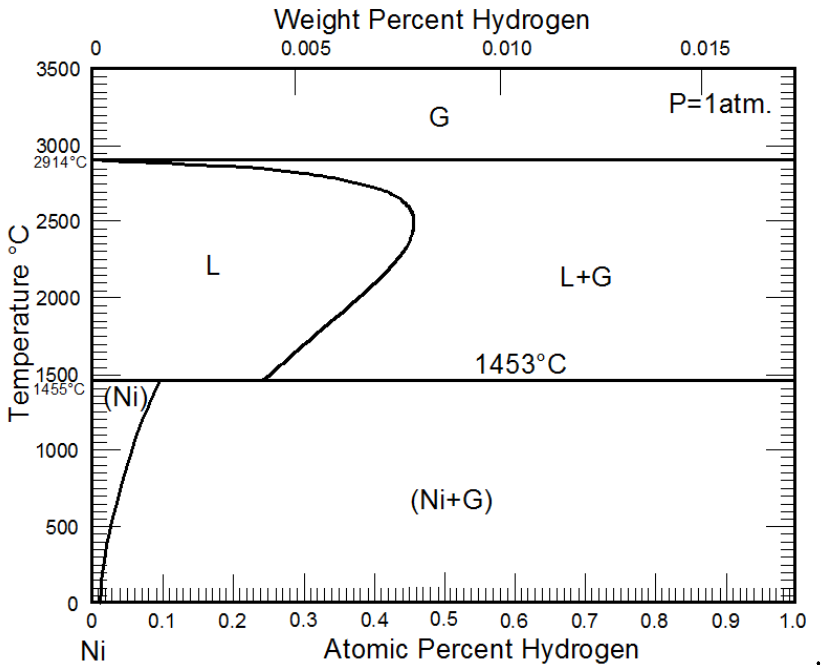

Fig. 4.35 **Ni-H phase diagram [207]**

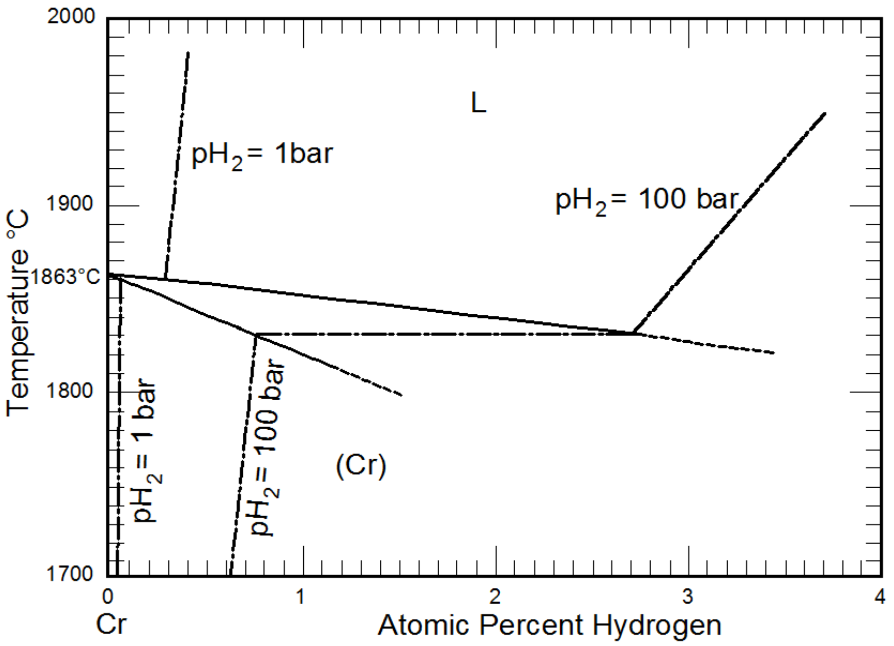

Fig. 4.36 **Cr-H phase diagram [208]**

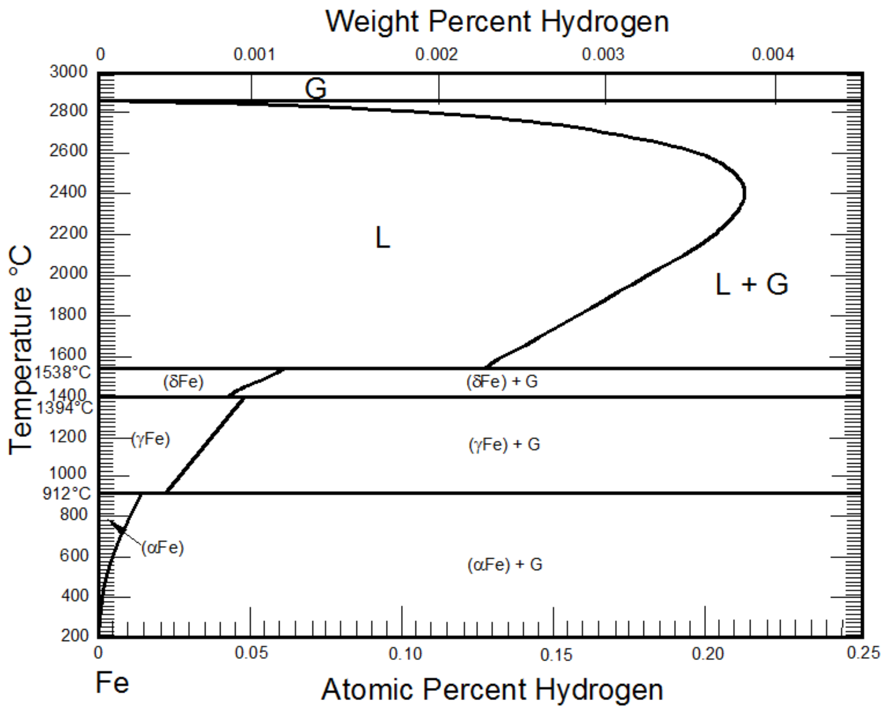

Fig. 4.37 **Fe-H phase diagram [209]**

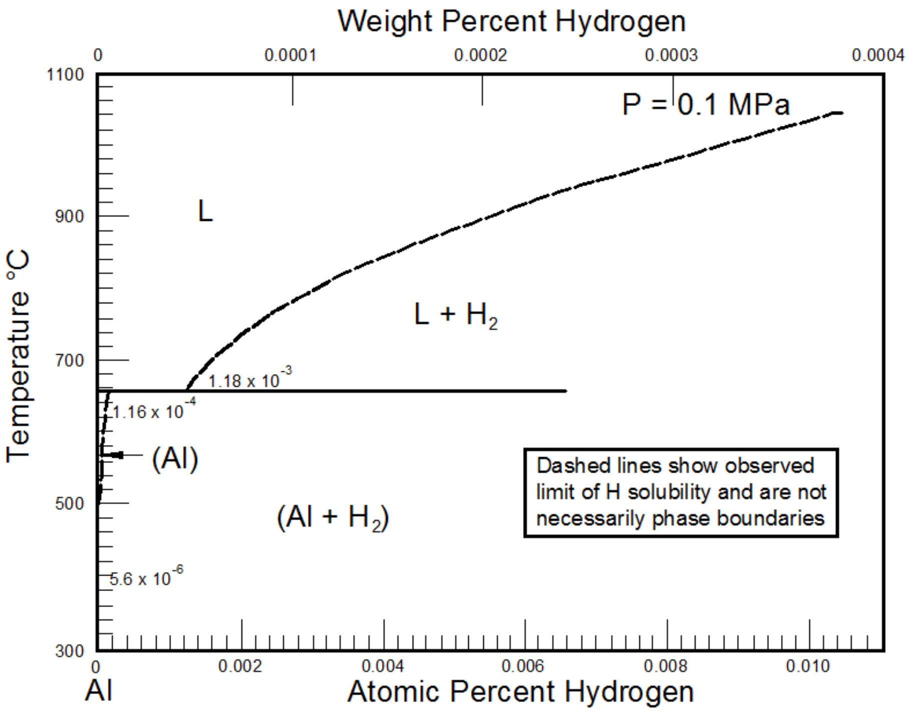

Fig. 4.38 Al-H phase diagram [210]

These entire phase diagrams (see Fig. 4.35 to Fig. 4.38) contain a eutectic type reaction near the melting point of these elements and a lowering of melting point due to dissolved hydrogen has been observed. The temperature dependent hydrogen solubility equations at one atmosphere hydrogen pressure have been reported in these elements [208,210-212] as listed in Table 4.13. These equations have been generated by least square fits of more than 100 measurements to give the polynomials. Sievert's law is obeyed at higher pressure also.

Table 4.13 Temperature dependent hydrogen solubility equations in metal-hydrogen systems at one atmosphere hydrogen pressure

System	Equation	Applicable range		Reference
		Temperature (K)	Composition	
Nickel-Hydrogen	$(X_H)_{Ni} = a'\sqrt{p}\exp - \frac{B'}{RT}$	623-703	Non-stoichiometric nickel hydride	[211]
Chromium-Hydrogen			CrH and CrH_2	[208]
For liquid state	$\log(at\%H)_{Cr} = 1.970 - \frac{5330}{T}(K)$	> melting point		
For solid state	$\log(at\%H)_{Cr} = 0.130 - \frac{2620}{T}(K)$	1000 to 1700		
For solid state	$\log(at\%H)_{Cr} = -1.430 - \frac{1065}{T}(K)$	700 to 1000		
Iron-Hydrogen			The dissolved hydrogen is within solid solubility limit up to the pressure of around 100 atm	[212]
For δFe	$(X_H)_{Fe} = 6.8905\times10^{-4} - (1.8690\times10^{-6})T + (1.2118\times10^{-9})T^2$	1667 to 1811		
For γFe	$(X_H)_{Fe} = -1.8691\times10^{-4} + (2.2203\times10^{-7})T - (2.0059\times10^{-10})T^2$	1185 to 1667		
For αFe	$(X_H)_{Fe} = 7.1030\times10^{-5} - (3.2214\times10^{-7})T + (4.7522\times10^{-10})T^2$	673 to 1185		
For αFe	$(\log X_H)_{Fe} = -7.8845 + (1.2264\times10^{-2})T - (1.2469\times10^{-5})T^2$	273 to 673		
For liquid Fe	$(X_H)_{Fe} = -9.0510\times10^{-3} + (1.1492\times10^{-5})T - (3.1065\times10^{-9})T^2$	1811 to 2023		
Aluminium-Hydrogen			The dissolved hydrogen is within solid solubility limit	[210]
For solid state	$(X_H)_{Al} = 2.164\times10^{-6} - (1.105\times10^{-8})T + (1.444\times10^{-11})T^2$	T < 933 K		
For liquid phase	$(X_H)_{Al} = 1.570\times10^{-4} - (5.064\times10^{-7})T + (4.340\times10^{-10})T^2$	T > 933 K		

In Table 4.13, a' = 0.18 ± 0.007, p is pressure in *MPa*, B' = 12.5 ± 0.3 *kJ/mol*, T is temperature in K and X_H is the hydrogen concentration as the atomic ratio, H/M.

The atomic percent of dissolved hydrogen is calculated as

$$at\% = \frac{atomicratio}{1 + atomicratio} \times 100 \qquad (4.11)$$

The solubility of hydrogen in these alloying elements is very less as seen from phase diagram or from Table 4.12. It was found that the solubility of the hydrogen in tantalum decreases with increasing content of the alloying elements like nickel, chromium, iron and aluminum. It could be in some way related to lesser solubility of hydrogen in these elements.

Zhang et.al [50] proposed that in case of vanadium-aluminium system, Al atoms in the V–lattice will repel hydrogen and block their incorporation in the lattice in their local neighborhood on the account of chemical inertness towards each other. This hypothesis appears to be working in the case of Ta-alloys also. Another explanation on hydrogen solubility in alloys is based on the formation of adherent oxide layer on the specimen surface, which can acts as a strong activation barrier for the hydrogen absorption into the metal matrix and consequently reduction in hydrogen solubility [50,213]. In the present investigation hydrogen charging apparatus was flushed with argon gas followed by evacuation. Evacuated apparatus was filled with argon and then specimen was placed inside the apparatus under the coverage of argon gas. Whole apparatus was again evacuated and then hydrogen gas was filled. The specimen was exposed to high temperature only in the argon atmosphere. These conditions don't favor the formation of oxide film on the specimen surface, but still some extent of oxygen is found in the alloys. This oxygen content in the alloys will affect the kinetics of hydrogen absorption but not equilibrium hydrogen solubility. Therefore, it is appeared that the decrease in hydrogen solubility on the addition of alloying element is a genuine phenomenon reflects the inherent characteristics of Ta-alloys brought about by the presence of solute atoms (Ni, Cr, Fe and Al).

4.5 Summary

The lattice parameter of tantalum-hydrogen solid solution alloys increases linearly with increase of hydrogen concentration. The equilibrium solubility of hydrogen in unalloyed Ta and Ta-alloys decreases with increase of temperature whereas increases linearly with the square root of hydrogen pressure. The hydrogen solubility in all the Ta-alloys was less than the hydrogen solubility in unalloyed tantalum and more decrease is observed with the increasing compositions of alloying elements. Moreover, among the four alloying elements (Ni, Cr, Fe and Al), the addition of Cr as alloying element has the largest effect on the hydrogen solubility in tantalum if the same composition of all alloying elements is considered and the order followed for the decreasing effect on hydrogen solubility in tantalum is (Cr > Al > Fe > Ni). Chromium decreases the hydrogen solubility to the greatest extent and nickel to the smallest extent. The variation in hydrogen solubility was less at higher temperature as compared to low temperature. The alloys-hydrogen solid solution approaches toward ideal behavior with increase of temperature and, hence, the effect of alloying elements on hydrogen solubility is substantially less at higher temperatures.

The decrease in hydrogen solubility is attributed to increase in lattice strain energy. The decrease in lattice parameter of tantalum on the addition of alloying elements decreases the size of interstitial sites and consequently lattice strain energy increases and hence, hydrogen solubility decreases. The lattice effect (volume effect) appears to be more important than the average electronic effect in determining the change in hydrogen solubility in tantalum on the addition of these alloying elements. In addition, the lattice effect appears to be dependent also on the element causing lattice contraction. The decrease in hydrogen solubility on the addition of alloying element is a genuine phenomenon reflects the inherent characteristics of Ta-alloys brought about by the presence of solute atoms (Ni, Cr, Fe and Al).

The addition of alloying elements in tantalum reduces the magnitude of relative change in enthalpy with negative sign for the solution of hydrogen in Ta-alloys whereas no considerable variations have been observed for the relative change in entropy values. The relative partial molar enthalpies, $\overline{\Delta H_H}$ and entropies, $\overline{\Delta S_H}$ for the solution of hydrogen in tantalum and its alloys are the function of the concentration of alloying elements but independent of temperature in a range of (673 – 873) K and hydrogen concentration in a range of (0.38 – 0.05) wt %.

Chapter 5

Hydrogen Absorption Kinetics of Ta-Al Alloys

5.1 Introduction

The present chapter is concerned with the experimental studies on the isothermal hydrogen absorption kinetics of tantalum-aluminium alloys as a function of aluminium composition in the temperature range of (673-973) K. Tantalum-aluminium alloys with different compositions were subjected to isothermal hydrogen uptake as discussed in chapter 3. The absorption of hydrogen in Ta and Ta-Al alloys was recorded with respect to time and the fraction of absorbed hydrogen, α, was calculated from the experimental data. The function $g(\alpha)$, integral form of $f(\alpha)$, (a function determining the mechanism of reaction) giving the best linearity with time was indicative of the mechanism of hydrogen absorption. The rate function of hydrogen absorption and the kinetic parameters were obtained from the linear regression fitting of $g(\alpha)$ versus time plots. The activation energy for hydrogen absorption in these alloys was also calculated using Arrhenius equation.

5.2 Theory of Gas-Solid Reaction Kinetics

Two alternative methods have been used in kinetic investigations for the reactions of gases with solids: (a) isothermal and (b) non-isothermal [214-215]. Both the techniques have been widely and variously used for the determination of kinetics of reactions.

The rate determining step in any heterogeneous gas-solid reaction can be either diffusion or a chemical reaction [182]. The characteristic features of the reacted fraction, α versus time, t curves for the reaction of solids are explained according to Fig. 5.1 as shown below, a generalized reduced time plot in which time values have been scaled to $t_{0.5} = 1.00$ when $\alpha = 0.5$.

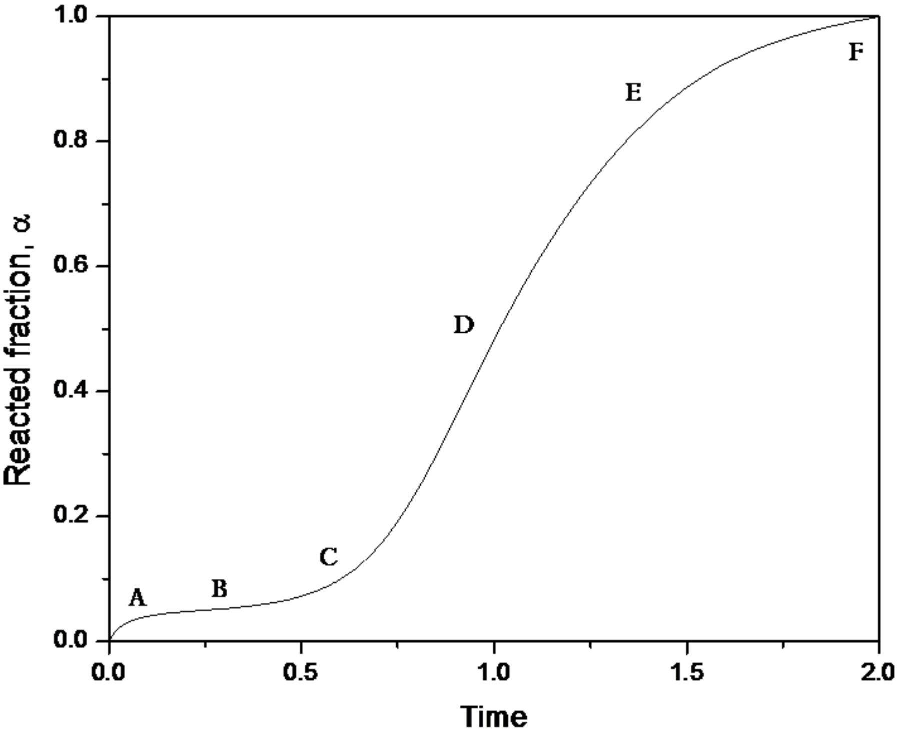

Fig. 5.1 **Generalized α – time plot, summarizing kinetic behavior observed for isothermal decompositions of solids**. *A, initial reaction; B, induction period; C, acceleratory period; D, point of inflection at maximum rate; E, decelerator period; and F, completion of reaction*.[182]

There are wide variations in the relative significance of the various stages (marked by the alphabets A to E in the Fig. 5.1) [182]. *A* is an initial reaction, *B* is the induction period, *C* is the acceleratory period of growth of nuclei, perhaps accompanied by further nucleation, and which extends to the maximum rate of reaction at *D*, *E* is the decelerator or decay period and *F* is the completion of reaction. Depending upon nature of chemical and physical processes, some stages may be negligible or absent in specific cases. Variations in their relative importance results in the appearance of a wide variety of different types of kinetic behavior in which the maximum reaction rate, *D*, is achieved at different values of α. In the quantitative investigation of the shapes of α-*time* curves, it is usually assumed that the isothermal rate of reaction per unit area of interface is constant, so that progressive changes in the rate provide a measure of the time-dependent variations in the effective areas of the reactant – product contact.

Generally, the increases in reaction rate with temperature found to be obeying the Arrhenius equation, from which the apparent values of the Arrhenius factor / frequency factor, A, and the activation energy, E_a are calculated. The possibility that the kinetics changes with temperature must also be considered.

There are some effects which result in exit from strict agreement to any proposed model [182].

a) There may be a period of initial relatively slow growth of nuclei.
b) The rate of interface extension across a surface may be different from the rate of bulk penetration.
c) Reactivity of surfaces and rates of interface advance may vary with crystallographic direction.
d) Subsidiary interfaces may develop from the reactant/ product contact resulting in a zone, rather than a surface, of reaction.
e) The volume of the product will generally be different from that of the reactant from which it was derived, and thus the effective interface may not extend across the whole surface of the nucleus.
f) In reversible reactions, a volatile product may be adsorbed on the surface of the residual phase and diffusive escape from the reaction interface hindered.
g) Diffusion control may become significant in reversible reactions.

h) The sizes and distribution of sizes of reactant particles may influence kinetics characteristics of rate processes.

While, in principle, these effects can be accounted into any quantitative kinetic analysis, in practice the integration is made more complicated or the rate expressions become difficult. The kinetic expressions for chain-type reactions, for diffusion-limited reactions, influence of particle size distribution on kinetic characteristics and rate equations commonly used in kinetic analysis of isothermal reactions of solids have also been derived and documented in the literature [182] and shown in Table 5.1. In Table 5.1, k represents the rate coefficient i.e. different in each expression and times are assumed to have been corrected for any induction period, t_0, c is the concentration.

Table 5.1 Rate equations which have found application in kinetic studies of solid phase reaction [182]

Mechanism	**Rate equation = *kt***
1 Acceleratory rate equations	
Power law	$\alpha^{1/n}$
Exponential law	$\ln\alpha$
2 Sigmoid rate equations	
(Avrami-Erofe'ev Eq.)	$[-\ln(1-\alpha)]^r$ (here r = ½, 1/3, 1/4)
(Prout-Tompkins Eq.)	$\ln[\alpha/1-\alpha]$
3 Deceleratory rate equations	
3.1 Based on diffusion mechanisms	
(One-dimensional diffusion)	α^2
(Two-dimensional diffusion)	$\alpha+(1-\alpha)\ln(1-\alpha)$
(Three-dimensional diffusion)	$[1-(1-\alpha)^{1/3}]^2$
(Ginstling-Brounshtein Eq.)	$1-2\alpha/3-(1-\alpha)^{2/3}$
3.2 Based on geometric models	
(Contracting area)	$1-(1-\alpha)^{1/2}$
(Contracting volume)	$1-(1-\alpha)^{1/3}$
3.3 Based on order with respect to α^c	
(First order)	$[-\ln(1-\alpha)]$
(Second order)	$(1-\alpha)^{-1}$
(Third order)	$(1-\alpha)^{-2}$

The mechanism functions of kinetics are represented in details in Table 5.2 [185].

Table 5.2 Mechanism function of the kinetics [185]

Mechanism	***f(α)***	***g(α)***	***r***
Nucleation and growth	$(1/r)(1-\alpha)[-\ln(1-\alpha)]^{1-r}$	$[-\ln(1-\alpha)]^{r}$	¼, 1/3, 2/5, ½, 2/3, ¾, 1, 3/2, 2,3,4
Power law	$(1/r)\alpha^{1-r}$	α^{r}	¼, 1/3, ½, 1, 3/2, 2
Exponential	$(1/r)\alpha$	$\ln\alpha^{r}$	1,2
Branching nucleation	$(\alpha)(1-\alpha)$	$\ln[\alpha/1-\alpha]$	
Phase boundary reaction	$(1-\alpha)^{r}/(1-r)$	$1-(1-\alpha)^{1-r}$	½, 2/3
Chemical reaction	$(1/r)(1-\alpha)^{r}$	$1-(1-\alpha)^{r}$	½, 2, 3, 4, ¼, 1/3
Chemical reaction	$(1/2)(1-\alpha)^{3}$	$(1-\alpha)^{-2}$	
Chemical reaction	$(1-\alpha)^{2}$	$(1-\alpha)^{-1}-1$	
Chemical reaction	$2(1-\alpha)^{3/2}$	$(1-\alpha)^{-1/2}$	
Chemical reaction	$(1/2)(1-\alpha)^{-2/3}$	$(1-\alpha)^{-1}$	
One-dimensional diffusion	$(1/2)\alpha^{-1}$	α^{2}	
Two-dimensional diffusion	$[-\ln(1-\alpha)]^{-1}$	$\alpha+(1-\alpha)\ln(1-\alpha)$	
Two-dimensional diffusion	$(1-\alpha)^{1/2}\left[1-(1-\alpha)^{1/2}\right]^{-1}$	$\left[1-(1-\alpha)^{1/2}\right]^{2}$	
Two-dimensional diffusion	$4(1-\alpha)^{1/2}\left[1-(1-\alpha)^{1/2}\right]^{1/2}$	$\left[1-(1-\alpha)^{1/2}\right]^{1/2}$	
Three-dimensional diffusion	$(3/2)(1-\alpha)^{2/3}\left[1-(1-\alpha)^{1/3}\right]^{-1}$	$\left[1-(1-\alpha)^{1/3}\right]^{2}$	
Three-dimensional diffusion	$6(1-\alpha)^{2/3}\left[1-(1-\alpha)^{1/3}\right]^{1/2}$	$\left[1-(1-\alpha)^{1/3}\right]^{1/2}$	
Three-dimensional diffusion	$(3/2)\left[(1-\alpha)^{-1/3}-1\right]^{-1}$	$1-2\alpha/3-(1-\alpha)^{2/3}$	
Three-dimensional diffusion	$(3/2)(1+\alpha)^{2/3}\left[(1+\alpha)^{1/3}-1\right]^{-1}$	$\left[(1+\alpha)^{1/3}-1\right]^{2}$	
Three-dimensional diffusion	$(3/2)(1-\alpha)^{4/3}\left[(1-\alpha)^{-1/3}-1\right]^{-1}$	$\left[(1-\alpha)^{-1/3}-1\right]^{2}$	
Three-dimensional diffusion		$(1+\alpha)^{2/3}+(1-\alpha)^{2/3}$	

5.3 Reaction Models for Hydrogen Absorption

The particles which come in contact with hydrogen gas during hydrogen absorption process are assumed to be spheres with constant diameter. A schematic diagram for the mechanism of hydrogen absorption is shown in Fig. 5.2 which indicates the steps occurring during hydrogen absorption process [216-217]. In this process, the hydrogen solid solution (α phase) is formed first with a concentration gradient from the surface to the centre and saturation of α phase takes place first at the metal/gas interface resulting in the formation of hydride phase (β phase). The hydride phase then grows from metal/gas interface towards the centre as shown in Fig. 5.2. It is also observed that lattice expansion associated with hydride phase requires less energy at the solid/gas interface than in the bulk of solid. The reaction mechanism for the absorption of hydrogen in any alloy/material is made up of a set of five intermediates partial processes for the overall reaction as shown in Fig. 5.2.

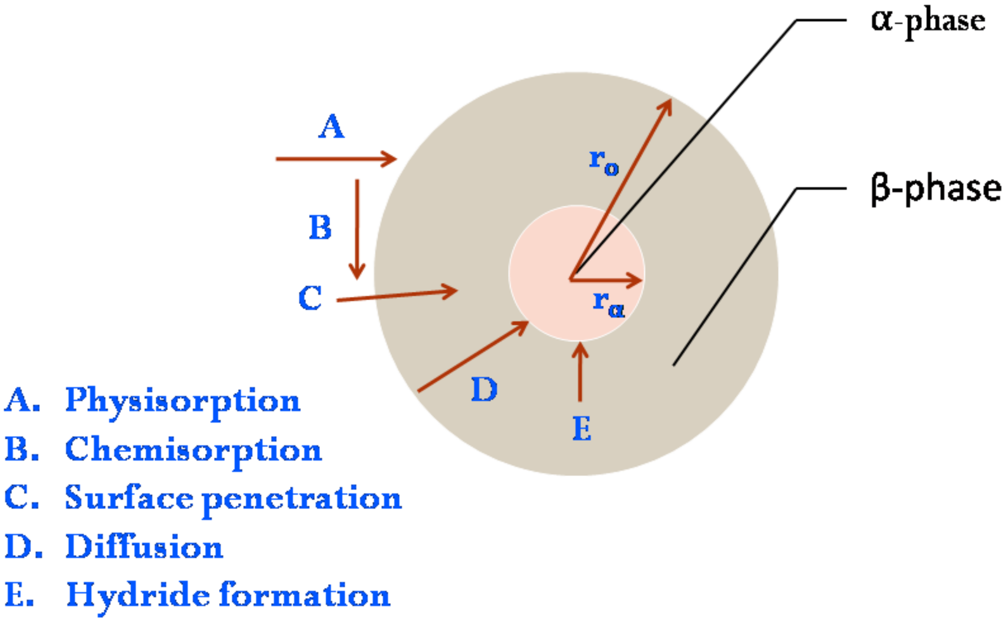

Fig. 5.2 Schematic representation of hydrogen absorption mechanism [216]

A Physisorption

The Physisorption of hydrogen molecules on the metals/alloys surface is given by [216-217]

$$H_2(gas) + \phi(ph) = H_2(ph) \tag{5.1}$$

Where ϕ denotes the number of empty physisorption sites on the surface of metals/alloys. Generally no activation energy is required for the physisorption of gas molecules on the surface and the impingement rate of the hydrogen molecules on the surface is very large at higher gas pressure. The gas phase is certainly in equilibrium with the physisorbed state and the process physisorption is not a rate determining step. The concentrations of physisorbed hydrogen (θ_{ph}) can then be expressed by the equilibrium relation

$$\frac{\theta_{ph}}{(1-\theta_{ph})p} = K_1(T) \tag{5.2}$$

or

$$K_1(T) = K_1^0 \exp\left(\Delta H_{ph}^0 / RT\right) \tag{5.3}$$

Where, $K_1(T)$ is the equilibrium constant and ΔH_{ph}^0 is the enthalpy for physisorption of hydrogen. Since, at room temperature, the amount of physisorbed hydrogen molecules is small, therefore, the θ_{ph} is directly proportional to hydrogen pressure p that is given by following relation,

$$\theta_{ph} = K_1(T)p \tag{5.4}$$

B Chemisorption

In chemisorption process, the dissociation of hydrogen gas molecules occurs. The chemisorption of hydrogen atoms on the surface of metal/alloys is given by the reaction [216-217],

$$H_2(ph) + 2\phi(ch) \rightarrow 2H(ch) + \phi(ph) \tag{5.5}$$

The reaction rate per unit area for chemisorption is thus given by

$$r = k_{2f}\theta_{ph} - k_{2b}\theta_{ch}^2 \tag{5.6}$$

Where, θ_{ch} is the concentration of chemisorbed hydrogen and k_{2f} and k_{2b} are the reaction constants in the forward and backward directions, respectively which are calculated by the following equations

$$k_{2f} = k_{2f}^0 \exp\left({-E_{2f}} \big/ {RT} \right) \tag{5.7}$$

$$k_{2b} = k_{2b}^0 \exp\left({-E_{2b}} \big/ {RT} \right) \tag{5.8}$$

Here, E_{2f} and E_{2b} are the corresponding activation energies for the forward and backward directions, respectively.

It is assumed that a large number of chemisorption and physisorption sites are available for the forward and backward reactions and factor $(1-\theta)$ becomes equal to 1. If chemisorption is not the rate determining step, then chemisorbed hydrogen atoms are in equilibrium with the gas phase according to the following relation,

$$H_2 + 2\phi(ch) = 2H(ch) \tag{5.9}$$

And the concentration is given by

$$\frac{\theta_{ch}^2}{(1-\theta_{ch})^2 p} = K_2(T) \tag{5.10}$$

or for small coverages,

$$\theta_{ch} = \sqrt{K_2}\sqrt{p} \tag{5.11}$$

Here, K_2 is the equilibrium constant.

C Surface Penetration

The movement of chemisorbed hydrogen from the surface to the first subsurface layer in the metals/alloys can be considered as a single diffusion pump. The activation energy required in this process is different from the diffusion in the bulk of matrix. Here, it is assumed that the diffusion of hydrogen take place by a vacancy mechanism of hydrogen in the metal lattice. The assumption of an interstitial mechanism would lead to the similar results. The surface penetration process is given by [216-217]

$$H(ch) + \phi_\beta(r_0) \rightarrow \phi(ch) \tag{5.12}$$

Where, $\phi_\beta(r_0)$ denotes a vacancy in the sublattice just below the surface. The reaction rate per unit area is thus given by

$$r' = k_{3f}\theta_{ch}c_{\phi\beta}(r_0) - k_{3b}(1-\theta_{ch}) \tag{5.13}$$

Where, $c_{\phi\beta}(r_0)$ is the hydrogen concentration in the vacancies in subsurface layer just below the surface and k_{3f} and k_{3b} are the reaction constants in the forward and backward directions, respectively.

D Diffusion

The next step in the mechanism of hydrogen absorption is the diffusion of hydrogen atoms from the subsurface to the bulk. The diffusion current density, *j* for a system with radial symmetry is given by [216-217]

$$j = -bc\frac{\partial u}{\partial r} \qquad (5.14)$$

Where, *b* is the mobility, *c* is the concentration and *μ* the chemical potential of the diffusing species.

E Hydride Formation

The final step in the hydrogen absorption mechanism is the formation of hydride phase. For the vacancy mechanism considered here, the reaction is given by

$$Me(r_\alpha) \rightarrow \phi_\beta(r_\alpha) + MeH \qquad (5.15)$$

For this reaction, the rate of forward reaction per unit area is constant and decreases with the surface area of metal core and is given by

$$r'' = 4\pi r_\alpha^2 \left[k_{5f} - k_{5b} c_{\phi\beta}(r_\alpha)\right] \qquad (5.16)$$

Here, $\phi_\beta(r_\alpha)$ denotes a vacancy in α phase, $c_{\phi\beta}(r_\alpha)$ is the hydrogen concentration in the vacancies in *α* phase and k_{5f} and k_{5b} are the reaction constants in the forward and backward directions, respectively.

Graphs of governing equations for the different rate determining steps in the hydrogen absorption process are shown in Fig. 5.3. A replication of experiments in a Sievert's apparatus is selected. The change in pressure in Sievert's apparatus during hydrogen absorption is plotted as a function of process time. The reaction constants selected for different model types give similar initial reaction rates except for the diffusion model [216].

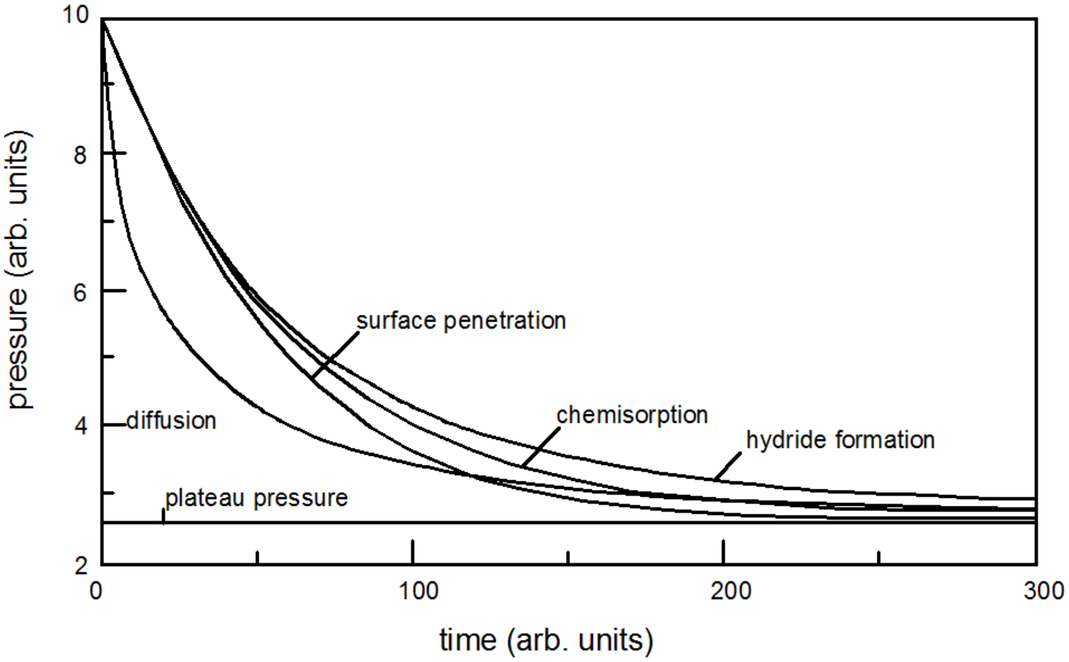

Fig. 5.3 **Results of model calculations for the absorption of hydrogen [216].** *Simulation of a volumetric measurement in a plot of pressure change versus reaction time for different rate determining reaction steps.*

Limitations of the Models

The models are derived by assuming particles of spherical shape with uniform radius. However, the models associated with chemisorptions and surface penetration as rate controlling steps are not sensitive to the size or shape effects. Only the total surface areas of the samples are important for both models. The processes in which the diffusion and hydride formation are the rate controlling steps, the shape and size enter the equations. The existence of two phase region is another restricting assumption which neglects the initial process of hydrogen solution in α phase. The validity of equations also ends after the completion of hydride phase (β phase). The limitation to only one rate determining step throughout the entire absorption process must be kept in mind when surface models are applied [216].

5.4 Kinetic Equations

The kinetics of hydrogen absorption is affected by temperature, pressure and surface properties of the materials [183]. The reaction mechanism for the absorption of hydrogen in the metals and alloys involves the several steps as follows [216,218-220]: gas-phase mass transport of hydrogen on the alloy surface, physisorption of hydrogen gas molecules, dissociation of hydrogen molecules into atomic form and chemisorptions on the surface, surface penetration of hydrogen atoms, hydrogen atoms diffusion through the bulk of metal and hydride formation as outlined in section 5.3. The slowest among these steps is the rate determining step. Generally the method used to study the kinetics is to fit the time dependent reacted fraction (α) to various analytical rate expressions, through which reaction mechanism and intrinsic rate limiting steps are determined. The rate equation for the kinetics of solid-gas reaction is expressed as follows [183-184]:

$$\frac{d\alpha}{dt} = kf(\alpha) \tag{5.17}$$

Where, α is the reacted fraction at time t, k is rate constant, $f(\alpha)$ is a function determining the mechanism of the reaction and $g(\alpha)$ is the integral form of $f(\alpha)$, i.e. given by

$$g(\alpha) = \int \frac{d\alpha}{f(\alpha)} = kt \tag{5.18}$$

$f(\alpha)$ and $g(\alpha)$ refers to the 42 reaction mechanism functions including nucleation and nuclei growth, phase-boundary controlled reactions, chemical reactions and diffusion. Their relation with reaction mechanisms are shown in Table 5.1 and Table 5.2. Based on the experimental data of hydrogen absorption curve in Ta and Ta-Al alloys, the reacted fraction, α can be calculated as follow:

$$\alpha = \frac{p_0 - p_t}{p_0 - p_{eq}} \tag{5.19}$$

Where, p_0 is the initial pressure, p_t is the pressure at time t and p_{eq} is the final equilibrium pressure.

The function $f(\alpha)$ or $g(\alpha)$ giving the best linearity with time is considered as the mechanism for hydrogen absorption in Ta and Ta-Al alloys. The rate function of hydrogen absorption and the kinetic parameters k are obtained from the linear regression fitting. The activation energy for hydrogen absorption in Ta and its alloys is calculated using Arrhenius equation.

5.5 Hydrogen Absorption Curves

In the present study, the hydrogen charging in Ta and Ta-Al alloys was carried out in a Sievert's apparatus having constant volume, in the temperature range of (673-973) K and at one atmosphere hydrogen pressure. The hydrogen gas was filled inside the system at a constant temperature. Since, the time taken during hydrogen filling process was quite short, and hence, the influence of hydrogen absorption during filling process could be neglected. The hydrogen absorption in the alloys was monitored with pressure drop inside the system with respect to time. The isothermal hydrogen absorption kinetic curves for Ta, Ta-1Al, Ta-1.6Aland Ta-2.4Al alloys at different temperatures are shown in Fig. 5.4. In the studied temperature range (673 – 973 K), the equilibrium in system was observed within 6 hours of processing time.

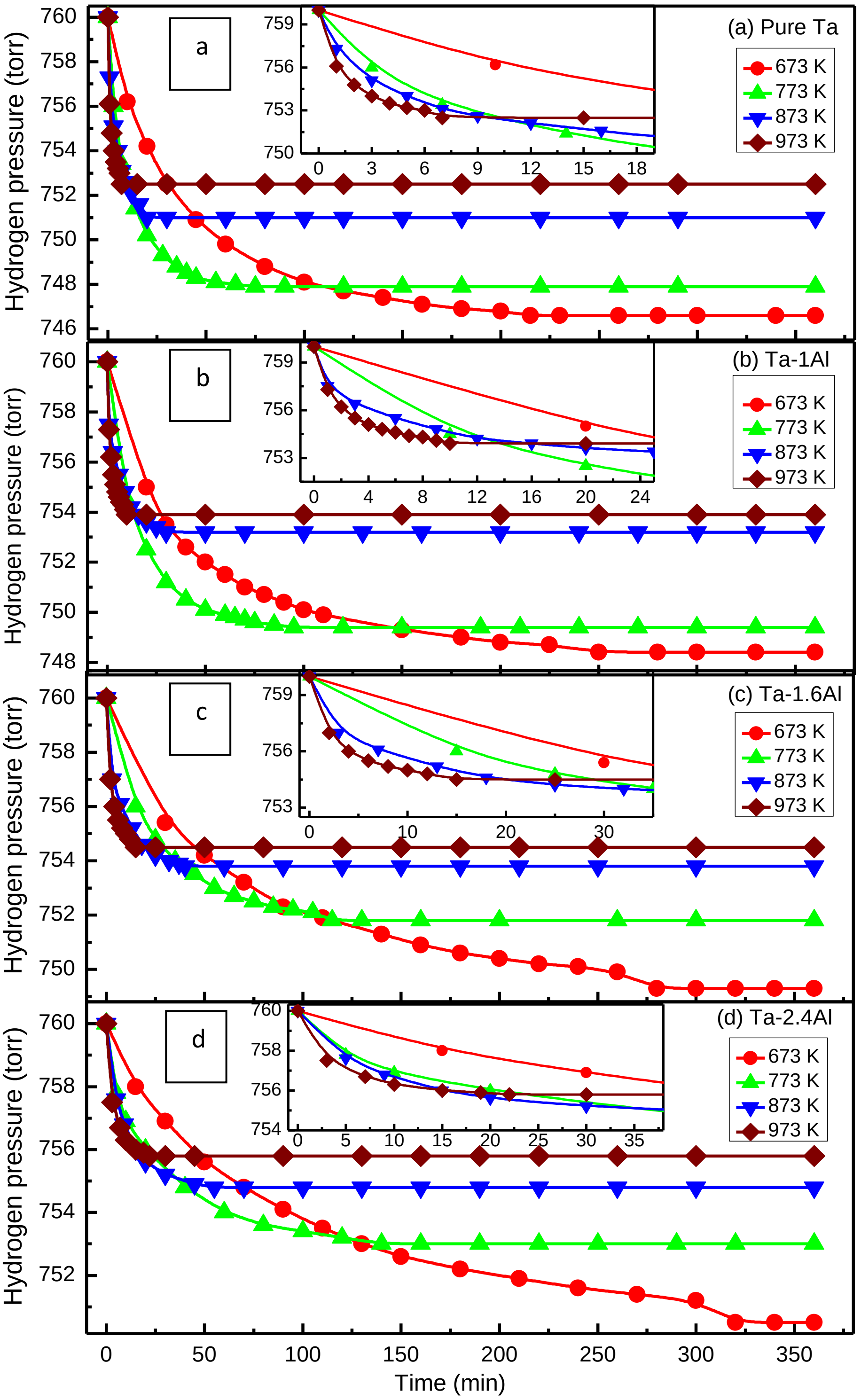

Fig. 5.4 **Isothermal hydrogen absorption kinetics curves for (a) pure Ta, (b) Ta-1Al, (c) Ta-1.6 Al and (d) Ta-2.4 Al alloys at different temperatures. In Inset:** *the zoomed views are shown to clearly represent the drop in hydrogen pressure with respect to time at different temperatures.*

Fig. 5.4 has clearly indicated that the time required to achieve equilibrium is decreases with increasing temperature whereas the equilibrium hydrogen pressure increases with increasing temperature. Moreover, the solubility of hydrogen in Ta-Al alloys decreases with temperature as well as with increase in Al composition. In case of unalloyed Ta, at temperature 673 K, the equilibrium in the system was achieved in 215 minutes and hydrogen pressure drop from 760 torr to 746.6 torr whereas at temperature 973 K, equilibrium achieved in 7 minutes and hydrogen pressure drop from 760 torr to 752.5 torr while in case of Ta-2.4Al alloy, at temperature 673 K, the equilibrium in the system was achieved in 320 minutes and hydrogen pressure drop from 760 torr to 750.5 torr whereas at temperature 973 K, equilibrium achieved in 22 minutes and hydrogen pressure drop from 760 torr to 755.8 torr. This data indicates that the hydrogen absorption kinetics in Ta-Al alloys becomes faster with increase in temperature but slower with increase in Al composition.

The reacted fraction *(α)*, calculated from time dependent hydrogen absorption curves is plotted as a function of time at different temperatures for Ta and Ta-Al alloys and shown in Fig. 5.5 which has also clearly displayed that the time required to reach equilibrium decreases with increasing temperature or the reacted fraction α, approaches to 1 very rapidly at higher temperature as compared to lower temperature.

The zoomed views are shown in insets in Fig. 5.4 and Fig. 5.5 to clearly represent the drop in hydrogen pressure and reacted fraction α, with respect to time, respectively at different temperatures.

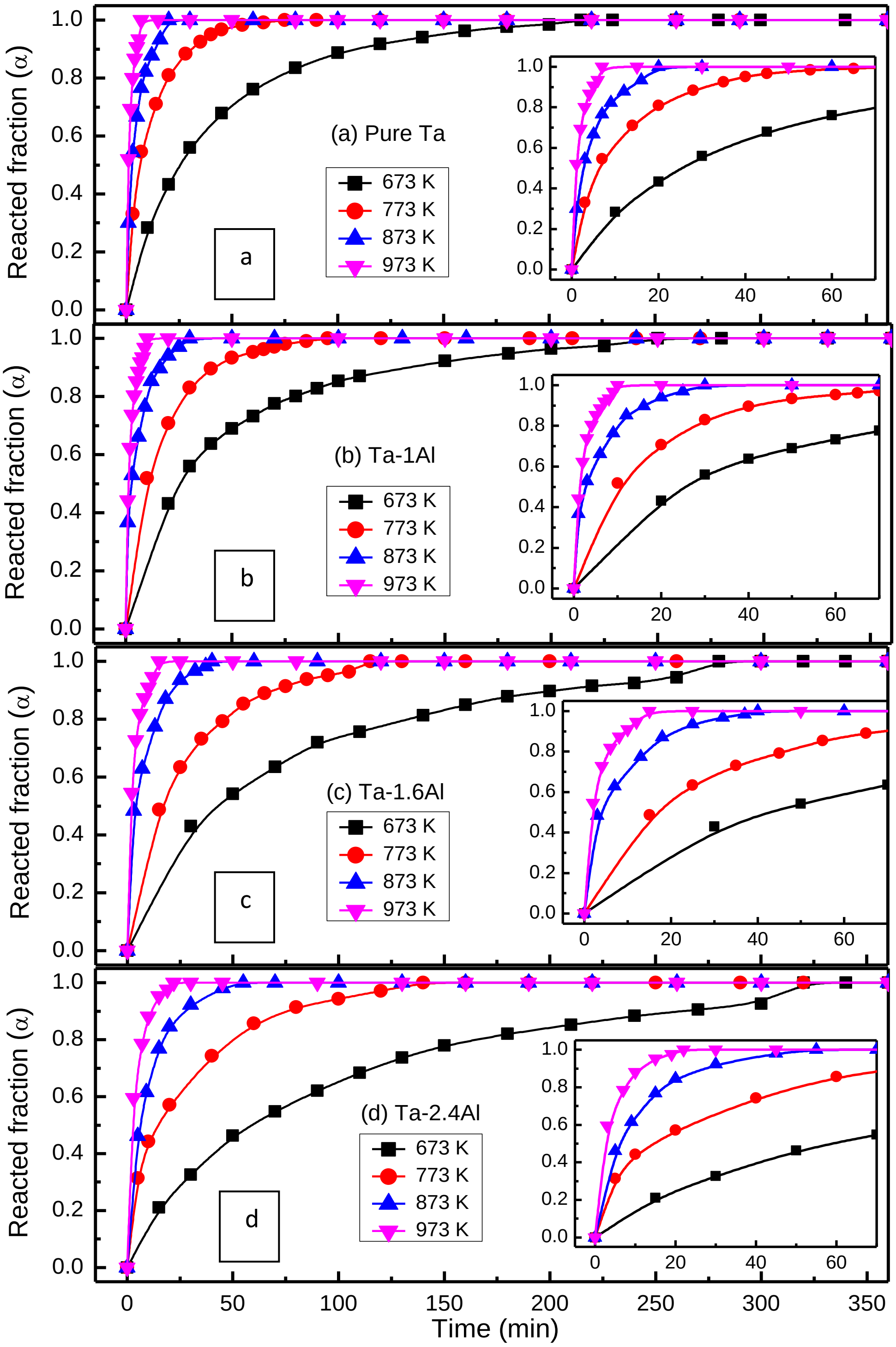

Fig. 5.5 Reacted fraction *(α)* vs Time (min) curves for hydrogen absorption at different temperatures in (a) pure Ta, (b) Ta-1Al, (c) Ta-1.6 Al and (d) Ta-2.4 Al alloys. In Inset: *The zoomed views have shown clearly* that reacted fraction *α,* approaches to 1 very rapidly at higher temperature as compared to lower temperature.

5.6 Reaction Mechanism

Generally, the reaction mechanism can be analyzed by evaluating the observed hydrogen absorption kinetic curves with the rate equations derived from different processes such as nucleation and growth process, auto-catalytic reactions, phase-boundary-controlled reactions, diffusion and so on. Some rate equations proposed in the literature have been used to treat the experimental data with varying degree of success [185,221-223]. The experimental results obtained for the kinetics of hydrogen absorption in Ta and Ta-Al alloys were fitted one by one according to various rate equations as shown in Table 5.2. The fitting equation with largest correlation coefficient *r* and smallest standard deviation *SD* were considered to be indicating kinetic reaction mechanisms to describe the hydrogen absorption process. The best fitting mechanism functions for the hydrogen absorption process in Ta and Ta-Al alloys at different temperatures are shown in Fig. 5.6.

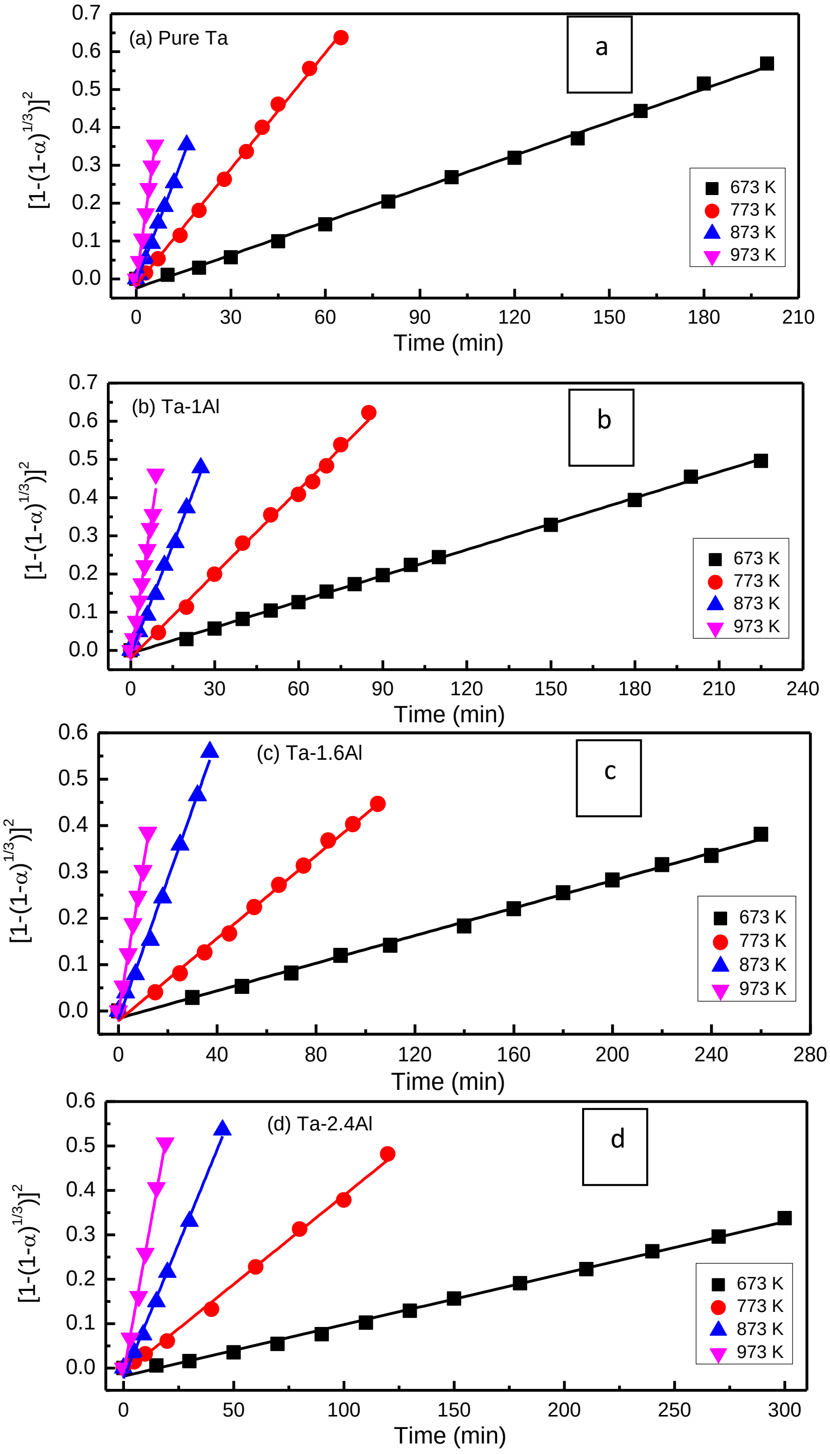

Fig.5.6 The best fitting mechanism functions for hydrogen absorption at different temperatures in (a) pure Ta, (b) Ta-1Al, (c) Ta-1.6 Al and (d) Ta-2.4 Al alloys. Solid lines represent linear fitting.

The experimental data show that the mechanism of three-dimensional diffusion, dominates the hydrogen absorption processes at all the temperatures which is clearly indicated in Fig 5.6. The kinetic parameters, mechanism equations and the apparent activation energy calculated for hydrogen absorption in Ta and Ta-Al alloys are listed in Table 5.3. The rate of three-dimensional diffusion was the slowest step in each setting temperature, thus it was reasonable to summarize that the three-dimensional diffusion process was the rate – limiting step of the hydrogen absorption process.

Table 5.3 **Kinetic parameters, equations and activation energies for hydrogen absorption reaction in Ta and Ta-Al alloys**

Samples	**Stages**	**Temperature (K)**			
		673	**773**	**873**	**973**
Ta	Best fitting equation	$[1-(1-\alpha)^{1/3}]^2$			
	Rate-limiting step (Mechanism)	Three-dimensional diffusion			
	Rate constant (min^{-1})	0.0029	0.0102	0.0223	0.0606
	Correl. Coeff.	0.9969	0.9974	0.9975	0.9978
	Activation energy (kJ/mol)	**53.7**			
Ta-1Al	Best fitting equation	$[1-(1-\alpha)^{1/3}]^2$			
	Rate-limiting step (Mechanism)	Three-dimensional diffusion			
	Rate constant (min^{-1})	0.0022	0.0073	0.019	0.049
	Correl. Coeff.	0.9988	0.9957	0.9952	0.99
	Activation energy (kJ/mol)	**55.3**			
Ta-1.6Al	Best fitting equation	$[1-(1-\alpha)^{1/3}]^2$			
	Rate-limiting step (Mechanism)	Three-dimensional diffusion			
	Rate constant (min^{-1})	0.0015	0.0044	0.0151	0.0317
	Correl. Coeff.	0.9963	0.9955	0.9938	0.9974
	Activation energy (kJ/mol)	**56.6**			
Ta-2.4Al	Best fitting equation	$[1-(1-\alpha)^{1/3}]^2$			
	Rate-limiting step (Mechanism)	Three-dimensional diffusion			
	Rate constant (min^{-1})	0.0011	0.004	0.0121	0.0273
	Correl. Coeff.	0.9952	0.9963	0.994	0.9964
	Activation energy (kJ/mol)	**57.7**			

5.7 Activation Energy

Assuming that the reaction mechanisms were same at different experimental temperatures, the function $g(\alpha)$ giving the best linearity with time was considered as representing the mechanism for hydrogen absorption in Ta and Ta-Al alloys. The rate function of hydrogen absorption and the kinetic parameters k were obtained from the linear regression fitting of $g(\alpha)$ vs time plots. The activation energy, E_a for hydrogen absorption in these alloys was calculated using Arrhenius equation

$$k = Ae^{-E_a/RT} \tag{5.20}$$

or

$$\ln k = \ln A - \frac{E_a}{RT} \tag{5.21}$$

Where, A is the pre-exponential factor, R is the molar gas constant *(J/mol K)*, T is the process temperature *(K)* and E_a is the activation energy of the process *(kJ/mol)*.

The rate constants at different temperatures were extracted from hydrogen absorption curves (from the slope of $g(\alpha)$ vs *time* plots) for Ta and Ta-Al alloys and the activation energy, E_a for hydrogen absorption was calculated from the slope of *lnk* versus *1/ T* plots.

Since the hydrogen absorption process in Ta and Ta-Al alloys was controlled by the same reaction mechanism (three-dimensional diffusion) in the temperature range of (673 – 973) K, the Arrhenius plot was derived as shown in Fig. 5.7. The fitting correlation coefficient is greater than 99 %, indicating that the method is feasible.

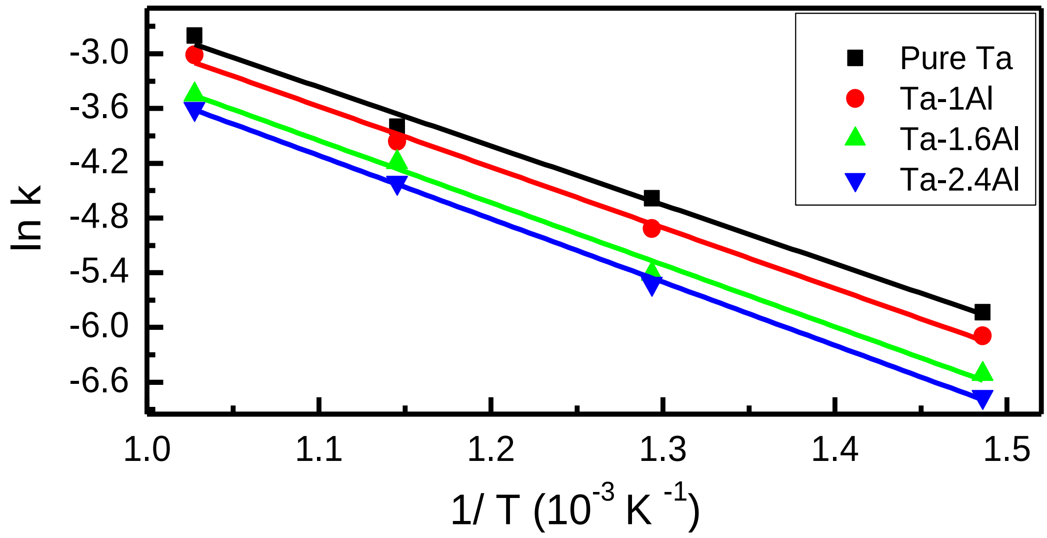

Fig. 5.7 **Arrhenius plots, *lnk* vs 1/*T* (10^{-3} K^{-1}) for the hydrogen absorption kinetics in Ta and Ta-Al alloys**

The activation energy obtained for the absorption of hydrogen in Ta and Ta-Al alloys was in the range of 53.7 *kJ/mol* to 57.7 *kJ/mol* as listed in Table 5.3. It was observed that the activation energy for the absorption of hydrogen by tantalum increases linearly with increase in the aluminium content in the alloys as shown in Fig. 5.8.

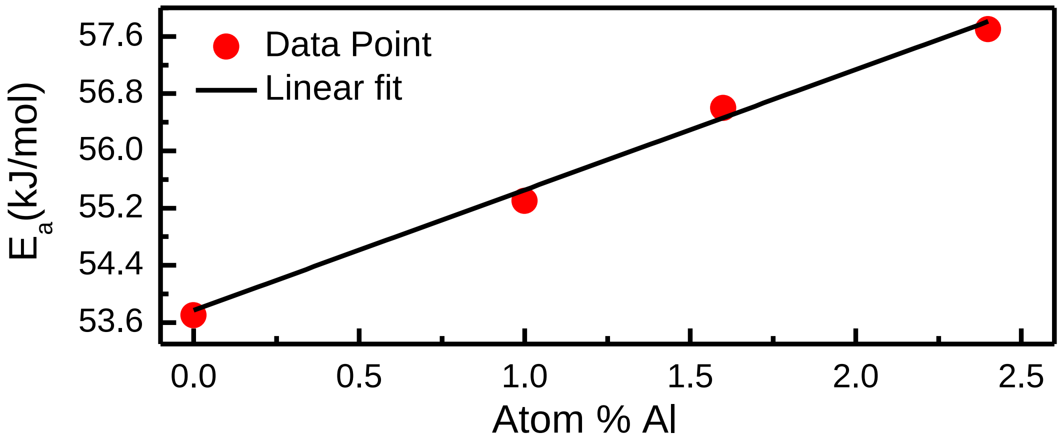

Fig. 5.8 **Variation in activation energy for hydrogen absorption in Ta-Al alloys as a function of aluminium composition.**

The increase in activation energy with aluminium content could be explained by various theories. A very less solubility of hydrogen in aluminium or inert behavior of aluminium towards the hydrogen [206,210] prevents the absorption of hydrogen in various hydrogen absorbing alloys when it is present in the matrix within solid solubility limit or in a two phase region [50,195,213,224]. The aluminium present in the host matrix forms the adherent layer of alumina (Al_2O_3) on the surface of matrix which results in the creation of a strong activation barrier for the absorption of hydrogen [50]. In the present study, the experiments were carried out under the control of high pure argon gas and even oxide layer has been removed from the sample surface by polishing the samples before and after arc melting. Eventhough, some oxygen content was found in the alloys during analysis (given in section 4.2), that could be responsible for the formation of adherent alumina layer on the surface of matrix and hence, consequently results in the enhancement of activation energy for the absorption of hydrogen in Ta-Al alloys.

Another explanation is based on the chemical inertness of aluminium towards other metal-hydrogen systems [46,225]. The Al atoms in the host matrix will repel hydrogen and block their incorporation in the lattices in their local neighborhood [50,224]. The increase in aluminium content results in increase of the repulsive forces for the absorption of hydrogen in the matrix and hence, activation energy increase. This explanation seems to be logical. The explanation given by Brodowsky [205] appears to be valid here that is based on increase in lattice strain energy. The lattice parameter of tantalum decreases with the addition of aluminium atoms. Therefore, the lattice size and interstitial sites size decrease and hence hydrogen solubility decreases due to increase in lattice strain energy [205]. The change in strain energy of dissolved hydrogen due to presence of different size interstitial sites around a substitutional atom may be responsible for change in hydrogen solubility as well as increase in activation energy for hydrogen absorption [144]. The absorption of hydrogen is also influenced by the electronic structure of the host matrix [194]. Density-functional theory (DFT) [194] has revealed that the activation energy of hydrogen absorption is extremely subjective to the electronic structure and Fermi energy level of host matrix. According to this theory, the increase in Fermi energy level due to the addition of alloying element enhances the activation barrier for hydrogen absorption and consequently decreases the hydrogen absorption kinetics. However, in the present study, the electronegativity of Al (1.61) is higher than Ta (1.5) and the electron to atom ratio *(e /a)* of Ta (5) decreases on the addition of Al in Ta. Therefore, the electronic effect does not seem to be more dominant in controlling the overall kinetics of hydrogen absorption in Ta-Al alloys.

5.8 Summary

The equilibrium hydrogen pressure increases with increasing temperature whereas the time required to achieve equilibrium is decreases with increasing temperature. Moreover, the solubility of hydrogen in Ta-Al alloys decreases with temperature as well as with increase in Al composition. The hydrogen absorption kinetics in Ta-Al alloys becomes faster with increase in temperature or the rate constant for the hydrogen absorption process in tantalum and tantalum-aluminium alloys increases with temperature. In the temperature range of 673 - 973 K, the three-dimensional diffusion process is the rate – limiting step of the hydrogen absorption process in these alloys. The hydrogen absorption kinetics in Ta-Al alloys becomes slower with increase in Al composition. The activation energy obtained for the absorption of hydrogen in Ta-Al alloys is in the range of 53.7 kJ/mol to 57.7 kJ/mol and it increases linearly with increase in the aluminium content.

Chapter 6

Conclusions and Suggestions for further R&D Work

6.1 Conclusions

- ☐ Vacuum arc melting is a suitable technique for the preparation of homogeneous alloys of tantalum with nickel, chromium, iron and aluminium.

- ☐ The solubility of hydrogen in tantalum and its alloys is obeying the Sievert's law in the considered temperature range (673 K-873 K) and it is decreasing on the addition of nickel, chromium, iron and aluminium as alloying elements.

- ☐ The decrease in hydrogen solubility is attributed to increase in lattice strain energy. The decrease in lattice parameter of tantalum on the addition of alloying elements decreases the size of interstitial sites and consequently lattice strain energy increases and hence, hydrogen solubility decreases.

- ☐ The solubility of hydrogen in tantalum and its alloys increases with increase of hydrogen pressure but the solubility decreases with increase in temperature. This is also reflected by exothermic solution of hydrogen in all these samples.

- ☐ The relative change in enthalpy for the solution of hydrogen in tantalum decreases in magnitude with negative sign with increase in concentration of these alloying elements whereas entropies values are nearly constant.

- The $\overline{\Delta H_H}$ and $\overline{\Delta S_H}$ values are constant in the considered temperature range (673 – 873) K and virtually independent of dissolved hydrogen concentration (0.367 - 0.068) wt%.
- From kinetics point of view, the rate constant for the absorption of hydrogen as well as equilibrium hydrogen pressure increase with increasing temperature.
- In the temperature range of (673 – 973) K, the three-dimensional diffusion process is the rate – limiting step of the hydrogen absorption process in tantalum and tantalum-aluminium alloys.
- The rate constant for the absorption of hydrogen decreases with increase in the aluminium content in the alloys and correspondingly the activation energy for the absorption of hydrogen increases.
- The calculated apparent activation energy for the hydrogen absorption in Ta-z Al alloys [z = 0 – 2.4 at % Al] is in the range of 53.7 kJ/mol to 57.7 kJ/mol.

6.2 Suggestions for Further R&D Work

Tantalum is considered as a potential candidate material for hydrogen separation membrane functioning in a flowing gas at high temperature and high pressure for the separation of hydrogen from a mixture of gases. In the present thesis, the investigation is carried out on the solubility of hydrogen in various tantalum alloys with nickel, chromium, iron and aluminium at different compositions. The ultimate objective is to see if alloying in any way helps tailor the properties of tantalum for use as a hydrogen permeation membrane. It is clear that the equilibrium hydrogen solubility in tantalum can be modified by the use of Fe, Ni, Cr and Al in small quantities to form dilute solid solution alloys with tantalum. To evaluate the use of tantalum alloys for membranes for hydrogen permeation, further investigations especially on the mechanical properties of these alloys vis-à-vis unalloyed tantalum in the temperature range 300-700^o C (573-973 K), will be helpful. This could be eventually followed up with the characterization of the alloys for the metallurgical properties before using them for testing in devices for permeation separation of hydrogen from gas mixtures at high temperatures.

References

[1] H. Michael, Handbook of Hydrogen Storage. WILEY-VCH Verlag Gmbh & Co. KGaA, Weinheim, 2010.

[2] E. K. Stefanakos, D. Y. Goswami, S. S. Srinivasan and J. T. Wolan, Hydrogen Energy, In: Myer Kutz, editor. Environmentally conscious alternative energy production. John Wiley & Sons, Inc.; 2007. p. 165.

[3] Ozzie Zehner, Green Illusions. Lincoln and London: University of Nebraska Press. 2012.

[4] http://www.benefits-of-recycling.com/alternativeformsofenergy/

[5] John R. Fanchi, Energy: Technology and Directions for the Future. Elsevier Academic Press, USA, 2004.

[6] http://www.altenergy.org/renewables/solar.html

[7] http://www.solarpanelinfo.com/solar-panels/how-solar-panels-work.php

[8] http://www.unc.edu/~jannap/solarpanels_files/Page391.htm

[9] http://www.altenergy.org/renewables/wind.html

[10] http://en.wikipedia.org/wiki/Windmill

[11] http://www.mpoweruk.com/hydro_power.htm

[12] http://www.benefits-of-recycling.com/alternativeenergywater/

[13] http://environment.nationalgeographic.co.in/environment/global-warming/hydropower-profile/

[14] http://www.benefits-of-recycling.com/whatisgeothermalenergy/

[15] http://www.renewableenergyworld.com/rea/tech/geothermal-energy/geoheatpumps

[16] http://www.altenergy.org/renewables/biomass.html

[17] J. Alper, Science, 299, 2003; 1686.

[18] R. D. Cortright, R. R. Davda, J. A. Dumesic, Nature 418, 2002; 964.

[19] I. P. Jain, P. Jain, A. Jain, J Alloys and Comp. 503, 2010; 303.

[20] M. D. Dolan, J Membrane Sci. 362, 2010; 12.

[21] G. Q. Lu, J. C. Diniz da Costa, M. Duke, S. Giessler, R. Socolow, R. H. Williams, T. Kreutz, J Colloid and Interface Sci. 314, 2007; 589.

[22] S. Miura, A. Fujisawa, M. Ishida, Int J Hydrogen Energy 37 (3) 2012; 2794.

[23] K. H. Kim, J. H. Shim, B. J. Lee, Int. J. Hydrogen Energy 37, 2012; 7836.

[24] T. S. Moss, N. M. Peachey, R. C. Snow, R. C. Dye, Int. J. Hydrogen Energy 23, 1998; 99.

[25] S.N. Paglieri, N.K. Pal, M.D. Dolan, S. Kim, W. Chien, J. Lamb, D. Chandra, K.M. Hubbard, D.P. Moore, J. Membrane Sci., 378, 2011; 42.

[26] N. M. Peachey, R. C. Snow, R. C. Dye, J. Membrane Science, 111, 1996; 123.

[27] B. Sakintuna, F. L. Darkrim, M. Hirscher, Int. J. Hydrogen Energy 32, 2007; 1121.

[28] http://www.window.state.tx.us/specialrpt/energy/renewable/h2.php#exhibit22-1

[29] C. Pellerin, Use of hydrogen grows to fuel vehicles, produce electricity, http://www.america.gov/st/energyenglish/2008/march/20080304175603lcnirellep0.471676.html

[30] M. P. Ramage, et al., The Hydrogen Economy: Opportunities, Costs, Barriers and R&D Needs, The National Academy Press, Washington, DC, 2004.

[31] T. M. Adams, J. Mickalonis, Materials Letters 61, 2007; 817.

[32] B. Ernst, S. Haag, M. Burgard, J. Membrane Sci. 288, 2007; 208.

[33] K.S. Rothenberger, B.H. Howard, R.P. Killmeyer, A.V. Cugini, R.M. Enick, F. Bustamante, M.V. Ciacoo, B.D. Morreale, R.E. Buxbaum, J. Membrane Sci. 218, 2003; 19.

[34] S.-Y. Jeon, D.-K. Lim, M.-B. Choi, E.D. Wachsman, S.-J. Song, Separation and Purification Technology 79, 2011; 337.

[35] Review of DOE's Vision 21 Research and Development Program -- Phase 1, Committee to Review DOE’s Vision 21 R&D Program - Phase I, The National Academies Press. Washington, D.C. http://www.nap.edu/catalog/10596.html ISBN: 0-309-50425-2, (2003).

[36] D. Hart, P. Freud, and A. Smith, Hydrogen Today and Tomorrow, International Energy Agency Greenhouse Gas Programme (IEA GHG), 1999.

[37] K. Hashi, K. Ishikawa, T. Matsuda, K. Aoki, J. alloys and Comp. 404-406, 2005; 273.

[38] N. W. Ockwig and T. M. Nenoff, Chemical Reviews 107, 2007; 4078.

[39] S. C. A. Kluiters, Status review on membrane systems for hydrogen separation,

Energy Center of The Netherlands, 2004.

[40] S. Adhikari and S. Fernando, Ind. Eng. Chem. Res. 45, 2006; 875.

[41] R. Baker, Membrane Technology and Applications, John Wiley and Sons, New Jersey, 2004.

[42] Y. Zhang, R. Maeda, M. Komaki, C. Nishimura, J Membrane Sci 269, 2006; 60.

[43] S. M. Kim, D. Chandra, N. K. Pal, M. D. Dolan,W. M. Chien, A. Talekar, J. Lamb, S.N. Paglieri, T. B. Flanagan, Int. J. Hydrogen Energy 37, 2012; 3904.

[44] H. S. C. Deville and L. Troost, C. R. Hebd Seanc. Acad. Sci. 57, 1863; 965.

[45] T. Graham, Phil. Trans. Roy. Soc. Lond. 156, 1866; 399.

[46] G. Alefeld and J. Volkl, eds., Hydrogen in Metals I, Topics in Applied Physics, Vol. 28, Springer-Verlag, Berlin, Heidelberg, New York, 1978.

[47] http://scholar.lib.vt.edu/theses/available/etd-12042002-124439/unrestricted/chapter4.pdf

[48] Y. Fukai, H. Sugimoto, Adv. Phys. 34 (2) 1985; 263.

[49] C. Nishimura, M. Komaki, M. Amano, Trans. Mater. Res. Soc. Jpn. 18 B, 1994; 1273.

[50] Y. Zhang, T. Ozaki, M. Komaki, C. Nishimura, Scripta Mater. 47, 2002; 601.

[51] T. Ozaki, Y. Zhang, M. Komaki, C. Nishimura, Int. J. Hydrogen Energy 28, 2002; 297.

[52] C. Nishimura, M. Komaki, S. Hwang, M. Amano, J. Alloys Compd. 330-332, 2002; 902.

[53] T. Ozaki, Y. Zhang, M. Komaki, C. Nishimura, Int. J. Hydrogen Energy 28, 2003; 1229.

[54] C. Nishimura, T. Ozaki, M. Komaki, Y. Zhang, J. Alloys Compd. 356-357, 2003; 295.

[55] C.A. Hampel (Ed.), Rare Metals Handbook, 2nd Edn., Reinhold, New York, 1961.

[56] W.C. Butterman, Mineral Processing and Extractive Metallurgy Review, 3, 1988; 69.

[57] C.K. Gupta, N. Krishnamurthy, Extractive Metallurgy of Rare Earths, CRC Press, Boca Raton, 2004.

[58] F.H. Spedding, A.H. Daane, The Rare Earths, Wiley, New York, 1961.

[59] M. Semchyshen and J.J. Harwood, Refractory Metals and Alloys. Interscience Publishers, New York. London. 1960.

[60] S.M. Cardonne, P. Kumar, C.A. Michaluk and H.D. Schwartz, Tantalum and its alloys, Int. J. of Refractory Metals and hard Materials 13, 1995; 187.

[61] R. E. Drogkamp, M. Schussler, J. B. Lambert and D.T. Taylor, in: M. Grayson and D. Eckroth (Eds.), Kirk-Othmer Encyclopedia of Chemical Technology, 3rd edn., vol. 22, John Wiley, New York, 1983.

[62] Colakis Marianthe, Masello, Mary Joan, "Tantalum". ISBN 9780865165731. 2007.

[63] O.P. Kolchin, The Great Soviet Encyclopedia, 3rd edition, 1970-1979.

[64] Tugoplavkie materialy v mashinostroenii: Spravochnik, Moscow, 1967.

[65] C. K. Gupta, A. K. Suri, Extractive Metallurgy of Niobium, CRC Press Inc. 1994, p. 49.

[66] Francesco Brossa, Giovanni Piatti and Michel bardy, Journal of Nuclear Materials 103 & 104, 1981; 261.

[67] Thermal Energy Equipment: Furnaces and Refractories, Energy Efficiency Guide for Industry in Asia, UNEP 2006.

[68] R.W. Buckman, Jr., Refractory Metals Technology**,** JOM, March 2000.

[69] P. M. Morse, et al. Organometallics 27 (5) 2008; 984.

[70] A. F. Holleman, E. Wiberg, N. Wiberg, Lehrbuch der Anorganischen Chemie, 102nd ed., de Gruyter. ISBN 978-3-11-017770-1, 2007.

[71] Donald J. Soisson, J. J. McLafferty, James A. Pierret, Ind. Eng. Chem. 53 (11) 1961; 861.

[72] Agulyansky Anatoly, The Chemistry of Tantalum and Niobium Fluoride Compounds. Elsevier. ISBN 9780444516046. 2004.

[73] S. Tsukimoto, M. Moriyama, Murakami Masanori, Thin Solid Films 460 (1-2): 1961; 222.

[74] Braun, Hilarion "Substance for front surface mirror" U.S. Patent 5,923,464, Issued on July 13, 1999.

[75] John D. Prymak, Tantalum Capacitors in Power Supply Applications, PCIM and Intertec International, Inc., Japan. 1998.

[76] Metals Handbook, Vol. 2, American Society for Metals, Metals Park, Ohio,

1990.

[77] H.Plenk Jr, S. Schider, in: M. B. Bever (Ed.), Encyclopedia of Materials Science and Engineering, Pergamon, Oxford, 1986; p. 4849.

[78] I. Machlin, R. T. Begley, E.D. Weisert, Refractory Metal Alloys, Proceedings of a Symposium on Metallurgy and Technology of Refractory Metals held in Washington, D. C., Plenum Press, New York, 1968.

[79] A. San-Martin and F.D. Manchester, Journal of Phase Equilibria, 12 (3) 1991; 332.

[80] M.W. Mallett and B.G. Koehl, J. Electrochem. Soc., 109, 1962; 611.

[81] G. Alefeld and J. Volkl, eds., Hydrogen in Metals II, Topics in Applied Physics, Vol. 29, Springer-Verlag, Berlin, 1978.

[82] H. Pfeiffer and H. Peisl, Physics Letters, 60 (4) 1977; 363.

[83] Martin Dornheim, Thermodynamics of Metal Hydrides: Tailoring Reaction Enthalpies of Hydrogen Storage Materials, Thermodynamics - Interaction Studies - Solids, Liquids and Gases, Ed. By Juan Carlos Moreno Pirajajn, ISBN: 978-953-307-563-1, InTech, DOI: 10.5772/21662, 2011.

[84] http://i2cner.kyushu-u.ac.jp/~h.shao/geometrical.html

[85] Y. Ohsumi, Hydrogen storage alloys-physical properties and applications, 1993, P. 65.

[86] E. Akiba and H. Iba, Intermetallics, 6, 1998; 461.

[87] H. Shao, K. Asano, H. Enoki and E. Akiba, Scripta Materialia, 60, 2009; 818.

[88] H. Shao, K. Asano, H. Enoki and E. Akiba, International Journal of Hydrogen Energy, 34, 2009; 2312.

[89] J. D. Fast, Interaction of metals and Gases, vol.2, Kinetics and Mechanism, Macmilllan Press Ltd., London and Basingstoke, Philips, 1971.

[90] L. Schlapbach, Hydrogen in Intermetallic Compounds II, Topics in Applied Physics Volume 67, Springer-Verlag Berlin Heidelberg New York 1992.

[91] J. E. Lennard-Jones, Transactions of the Faraday Society 28, 1932; 0333.

[92] http://www.hydropole.ch/index.php?go=hydrogen_storage

[93] W. M. Mueller, J. P. Blackledge, and G. Libowitz, G., Metal Hydrides, Academic Press, Inc., New York, 1968.

[94] D. O. Hayward and B. M. Trapnell, Chemisorption, Butterworth and Co. Ltd.,

London, 1964.

[95] N. Boes, H. Zuchner, Phys. Status Solidi A 17, 1973; K111.

[96] R. E. Buxbaum and A. B. Kinney, Ind. Eng. Chem. Res. 35, 1996; 530.

[97] D. J. Edlund and J. Mccarthy, J. Membr. Sci. 107, 1995; 147.

[98] R. E. Buxbaum and T. L. Marker, J. Membr. Sci. 85, 1993; 29.

[99] K.S. Rothenberger, B.H. Howard, A.V. Cugini, R.M. Enick, F. Bustamante, M.V. Ciacoo, B.D. Morreale, R.E. Buxbaum, Am. Chem. Soc., Fuel Chem. Div. Preprints, 47 (2) 2002; 814.

[100] D. P. Smith, Hydrogen in Metals, Chicago University Press, Illinois, U.S.A. 1948.

[101] M. R. Shanabarger, Surf. Sci. 52, 1975; 689.

[102] Tomoyasu Tanaka, Keita Mamadou, Azofeifa Daniel E. Theory of hydrogen absorption in metal hydrides, Physical Review B, Vol. 24 (4) 1981; 1771.

[103] H. H. Johnson, Metall. Trans. A 19, 1988; 2371.

[104] L. I. Sokol' Skaya, Gases in Light Metals, Pergamon Press, Oxford. London. New York. Paris 1961.

[105] Keith J. Laidler, Chemical Kinetics, 3rd edition, Pearson Education (Singapore) Pte. Ltd., Delhi. India. 2004.

[106] M.W. Roberts, J.M. Thomas and R. Burch, The Adsorption and Absorption of Hydrogen by Metals by R. Burch, Chemical Physics of Solid and Their Surface, The Chemical Society, vol.8, 1980.

[107] L.M. Melnick, L.L. Lewis, B.D. Holt, Determination of Gaseous Elements in Metals, A Wiley-Interscience Publication, 1974.

[108] Y. Fukai, The Metal-Hydrogen System, 2nd edition, Springer-Verlag Berlin Heidelberg NY 2005.

[109] F. A. Lewis, The Palladium/Hydrogen System, Academic Press Inc., New York, 1967.

[110] H. Wipf, ed., Hydrogen in Metals III, Topics in Applied Physics, Vol. 73, Springer, Berlin, 1997.

[111] M. Fullenwider, Hydrogen Entry and Action in Metals, Pergamon Press, Inc., New York, 1983.

[112] M. Sastri, B. Viswanathan, and S. Murthy, Metal Hydrides: Fundamentals and

Applications, Springer-Verlag, New York, 1998.

[113] T. Schober, Solid State Phenomena 49-50, 1996; 357.

[114] W. E. Wallace, Magnetic properties of metal hydrides and hydrogenated intermettalic compounds, in Hydrogen in Metals 1, Topics in Applied Physics, eds. G. Alefeld and J. Völkl, Springer-Verlag, Berlin, Heiderberg, New York Vol. 28, chap. 7, 1978; p. 169.

[115] A. Sieverts and A. Gotta, Zeitschrift Fur Anorganische Und Allgemeine Chemie 172, 1928; 1.

[116] A. Sieverts and A. Gotta, Zeitschrift Fur Anorganische Und Allgemeine Chemie 187, 1930; 155.

[117] F. Ducastelle, R. Caudron, P. Costa, J. Phys. Chem. Solids 31, 1970; 1247.

[118] T. Schober and A. Carl, Scripta Metal. 11, 1977; 397.

[119] J. C. Langeberg and R. B. Mclellan, Acta Metal. 21, 1973; 897.

[120] K. Papathanassopoulos, T. Scober and H. Wenzl, Solid State Communications, 52 (6) 1984; 575.

[121] L. Miranda, P. Vargas, H. Ceron, M. Lagos, Physics Letters A 131 (7,8) 1988; 445.

[122] S. M. Hosseini, Z. Metallkd., 67, 1976; 123.

[123] M. Hansen, Constitution of Binary Alloys, 2nd ed., Mcgraw-Hill, New York, 1958.

[124] R. Bakish, J. electrochem. Soc., 105, 1958; 574.

[125] G. Hagg, Z. Phys. Chem. B 11, 1931; 433.

[126] F. H. Horn and W. T. Ziegler, J. Am. Chem. Soc., 69, 1947; 2762.

[127] M. Taxak, S. Kumar, N. Krishnamurthy, A. K. Suri, G. P. Tiwari, Int. J. Processing and Application of Ceramics 6 (2) 2012; 73.

[128] J. D. Fast, Interaction of metals and Gases, vol.1, Thermodynamics and Phase Relations. Macmilllan Press Ltd., London and Basingstoke, Philips, 1965.

[129] O. Kubaschewski, A. Cibula, D.C. Moore, Gases and Metals, London Iliffe Books Ltd., New York American Elsevier Publishing Company, Inc., 1970.

[130] Y. Ebisuzaki and M. O’Keeffe, Prog. Solid State Chem. 4, 1967; 187.

[131] H. Mehrer, Diffusion in Solids, Springer, New York, 2007.

[132] J. Voelkl and H. Wipf, Hyperfine Interactions 8, 1981; 631.

[133] S. Uemiya, Sep. & Pur. Methods 28, 1999; 51.

[134] S. A. Steward, Review of hydrogen isotope permeability through metals, Lawrence Livermore National Laboratory Report UCRL – 53441, 1983.

[135] S. Hara, N. Hatakeyama, N. Itoh, H.M. Kimura, A. Inoue, Journal of Membrane Science 211, 2003; 149.

[136] R. Grena, M. Celino, P. Tarquini, Int. J. Hydrogen Energy 36, 2011; 13858.

[137] K. Hashi, K. Ishikawa, T. Matsuda, K. Aoki, J. Alloys Compd. 368, 2004; 215.

[138] W. Luo, K. Ishikawa, K. Aoki, J. Alloys and Compounds 407, 2006; 115.

[139] H.F. Franzen, A.S. Khan and D.T. Peterson, J. Less-Common Metals 55, 1977; 143.

[140] M. D. Dolan, G. Song, D. Liang, M.E. Kellam, D. Chandra, J.H. Lamb, J. Membrane Science, 373, 2011; 14.

[141] S. Semboshi, N. Masahashi, S. Hanada, J alloys Comp 359, 2003; 236.

[142] M. Amano, M. Komaki and C. Nishimura, J. Less Comm. Metals, 172-174, 1991; 727.

[143] T. Eguchi, S. Morozumi, Nippon Kinzoku Gakkaishi N K 38, 1974; 1025.

[144] T. Matsumoto, Y. Sasaki, M. Hihara, J. Phys. Chem. Solids, 36, 1975; 215.

[145] R. Burch , N. B. Francis, J Less-Common Metals 49, 1976; 371.

[146] A. Inoue, M. Katsura and T. Sano, J Less-Common Metals 55, 1977; 9.

[147] J. F. Lynch, J. J. Reilly and F. Millot, J. Phys. Chem. Solids 39, 1978; 883.

[148] E. Fleury, J. Y. Suh, D. Kim, C. H. Jeong, J. H. Park, Current Applied Physics 12, 2012; 1131.

[149] H. Nakajima, M. Yoshioka, M. Koiwa, Acta Metal. 35 (11) 1987; 2731.

[150] http://www.intechopen.com/books/thermodynamics-interaction-studies-solids-liquids-and-gases/thermodynamics-of-metal-hydrides-tailoring-reaction-enthalpies-of-hydrogen-storage-materials

[151] R. Griessen, Science and Technology of Hydrogen in Metals, III Chapter: Thermodynamics of Hydrogen in Metals, 2009.

[152] E. Veleckis and R.K. Edwards, J. Phys. Chem. 73(3) 1969; 683.

[153] P. Kofstad, W.E. Wallace, and L. J. Hyvonen, J. Am. Chem. Soc. 81(19) 1959; 5015.

[154] J.A. Pryde and I.S.T. Tsong, Trans. Faraday Soc. 67, 1971; 297.

[155] Philippe Lecocq and Charles Wert, Thin solid Films 25, 1975; 77.

[156] O. J. Kleppa, P. Dantzer, and M. E. Melnichak, J. Chem. Phys. 61 (10) 1974; 4048.

[157] R. A. Oriani, Proc. conf. fundamentals aspects of stress corrosion cracking, Ohio State University, 1967, ed. Staehle R W, Forty A J, Van- Rooyen D, Houston: Natl. Assoc. Corros. Eng. 1969; p. 32.

[158] R. N. Iyer, H. W. Pickering, Annu. Rev. Mater. Sci. 20, 1990; 299.

[159] B. R. Simonovic, S.V. Mentus, R. Dimitrijevic, J. Serb. Chem. Soc. 68 (8-9) 2003; 657.

[160] E. Fromm, H. Uchida, J. Less Comm. Metals, 66, 1979; 77.

[161] J. A. Pryde and I. S. T. Tsong, Trans. Faraday Soc.**,** 65, 1969; 2766.

[162] R. Schlatter, Overview of vacuum and specialized melting techniques, Latrobe Steel Co., Latrobe, 1975.

[163] D.A. Skoog, F.J. Holler, S.R. Crouch, Principles of Instrumental Analysis, 6th Edition, Thomson Brooks/Cole, 2007.

[164] http://en.wikipedia.org/wiki/Vacuum_Arc_Remelting

[165] http://www.indiamart.com/vacuum-techniques-limited/products.html

[166] http://infoscience.epfl.ch/record/84931/files/EPFL_TH3542.pdf

[167] http://www.mksinst.com/docs/UR/barainfo2b.aspx

[168] www.chromatographyinst.com

[169] W. Clay Davis, Jacob L. Venzie, Bert Willis, R. Lane Coffee Jr.,Dev P. Arya and R. Kenneth Marcus, Rapid Communications in Mass Spectrometry, 17, 2003; 1749.

[170] F. L. King, J. Teng and R. E. Steiner, J. Mass Spectrometry, 30, 1995; 1061.

[171] http://mee-inc.com/chemical-analysis.html

[172] Y. Jobin, Technical note 25. www. Jyhoriba.com and http://www.eag.com/mc/instrumental-gas-analysis.html

[173] www.elementalanalyser.com

[174] B.D. Cullity, Elements of X-ray diffraction, 2nd Edition, Addison-Wesley Publishing Company, Inc, USA. 1978.

[175] D. McMullan, Scanning electron microscopy 1928–1965, Scanning 17 (3): 175, doi:10.1002/sca.4950170309, 2006.

[176] http://micron.ucr.edu/public/manuals/EDS-intro.pdf

[177] http://en.wikipedia.org/wiki/Vickers_hardness_test

[178] http://www.azonano.com/equipment-details.aspx?EquipID=66

[179] http://www.oocities.org/venkatej/mech/sm/sm.htm

[180] BARC report by Dr. R.N. Singh “BARC/2003/E/034”

[181] http://en.wikipedia.org/wiki/Gravimetric_analysis

[182] C.H. Bamford and C.F.H. Tipper, Chemical Kinetics, Vol. 22, Reactions in the Solid State, Elsevier Scientific Publishing Company, Amsterdam-Oxford-Newyork, 1980, Chap.3.

[183] Q. Guo, H. Hou, X. Ren, J. alloys and Comp. 486, 2009; 754.

[184] Q. Lin, N. Chen, W. Ye, R.M. Liu, J. Univ. Sci. Technol. Beijing, 4, 1997; 34.

[185] Q. Li, K.C. Chou, Q. Lin, L.J. Jiang, F. Zhan, Hydrogen absorption and desorption kinetics of Ag-Mg-Ni alloys, Int. J. Hydrogen Energy, 29, 2004; 843.

[186] P. Nash, D.R.F. West, Met Sci. 17, 1983; 99.

[187] M. Venkatraman and J.P. Neumann, Bull. Alloy Phase Diagrams 8 (2) 1987; 112.

[188] L. J. Swartzendruber and E. Paul, Bull. Alloy Phase Diagram, 7(3) 1986; 254.

[189] U.R. Kattner, Binary alloy Phase Diagram, 2nd ed., T.B. Massalski, H. Okamoto, P.R. Subramanian and L. Kacprzak, ed., ASM International, Materials Park, OH, 1990; 218.

[190] B. Bandyopadhyay, A. Ghoshray, N. Chatterjee, Bull. Mater. Sci. 9 (4) 1987; 305.

[191] R. Checchetto, G. Trettel, A. Mioptello, Meas. Sci. Technol. 15, 2004; 127.

[192] J. Cermak, Czechoslovak Journal of Physics B, 23 (12) 1973; 1355.

[193] R.A. Oriani, “A brief survey of useful information about hydrogen in metals”, International Symposium on Cold Fusion and Advanced Energy Sources, Eds. by Hal Fox, Fusion Information Center, Inc. Belarusian State University, Minsk, Belarus, 1994.

[194] X. Ke, J.G. Kramer, O.M. Lovvik, J. Phys. Condens. Matter, 16, 2004; 6267.

[195] S. Kumar, M. Taxak, N. Krishnamurthy, A. K Suri and G.P. Tiwari, Int. J. Refractory and Hard Materials, 31, 2012; 76.

[196] S. Kumar, M. Taxak, N. Krishnamurthy, Int. J. Hydrogen Energy, 37(4) 2012;

3283.

[197] P.G. Dantzer and O.J. Kleppa, J. Solid State Chem. 24, 1978; 1.

[198] D.T. Peterson and S. O. Nelson, Metallurgical Transactions A, 16A, (1985) 367.

[199] C. Wagner, Thermodynamics of alloys, Addison–Wesley Press, 1952.

[200] W. Hume-Rothery, Structure of metals and alloys. The Institute of Metals London; 1988.

[201] D. Lu, W. Li, S. Hu, F. Xiao, R. Tang, Int. J. Hydrogen Energy 31(6) 2006; 678.

[202] S. Kumar, M. Taxak, N. Krishnamurthy, A. K. Suri. Interaction of hydrogen with Pb83Li17eutectic alloy. 2nd international symposium on advance nuclear materials ANM Mumbai, India; 2011. p. 205.

[203] M. Taxak, S. Kumar, B. Kalekar, N. Krishnamurthy, Int. J. Hydrogen Energy, 38, 2013; 7561.

[204] M. Taxak, S. Kumar, N. Krishnamurthy, J. Chem. Thermodyn. 67, 2013; 48.

[205] H. Brodowsky, Ber. Bunsenges. Phys. Chem. 76, 1972; 740.

[206] C. Qiu, G. B. Olson, S. M. Opalka and D. L. Anton, J. Phase Equilibria and Diffusion, 25 (6) 2004; 520.

[207] H. Okamoto, J. Phase Equilibria, 22 (5) 2001; 600.

[208] M. Venkatraman and J.P. Neumann, J. Phase Equilibria, 12 (6) 1991; 672.

[209] H. Okamoto, J. Phase Equilibria and Diffusion, 25 (1) 2004; 101.

[210] A. San-Martin and F.D. Manchester, J. Phase Equilibria, 13 (1) 1992; 17.

[211] M. L. Wayman and G. C. Weatherly: Bull. Alloy Phase Diagrams, 10 (5) 1989; 569.

[212] A. San-Martin and F.D. Manchester, Bull. Alloy Phase Diagrams, 11 (2) 1990; 173.

[213] S. Kumar, M. Taxak, N. Krishnamurthy, J. Therm. Anal. Calorim. 112 (1) 2013; 5.

[214] P.W.M. Jacobs and F.C. Tompkins, in W.E. Garner (Ed.), Chemistry of Solid State, Butterworth, London, 1955, Chap.7.

[215] J. Sestak, V. Satava and W.W. Wendlandt, Thermochim. Acta, 7, 1973; 333.

[216] M. Martin, C. Gommel, C. Borkhart, E. Fromm, J. alloys and Comp., 238, 1996; 193.

[217] P.S. Rudman, J. Less Common Met, 89, 1983; 93.

[218] K.C. Chou, Q. Li, Q. Lin, L.J. Jiang, K.D. Xu, Int. J. Hydrogen Energy, 30, 2005; 301.

[219] Q. Li, K.D. Xu, K.C. Chou, X.G. Lu, Q. Lin, J. Univ. Sci. Technol. Beijing, 13, 2006; 359.

[220] G. Mazzolai, Int. J. Hydrogen Energy, 36, 2011; 4507.

[221] G. Liang, J. Huot, S. Boily, J. alloys Comp. 305, 2000; 239.

[222] W. Zhang, J. Cimato, A.J. Goudy, J. alloys Comp. 201, 1993; 176.

[223] M. N. Mungole, R. Balasubramanima, Int. J. Hydrogen Energy, 23 (5) 1998; 349.

[224] S. Kumar, N. Krishnamurthy, Int. J. Hydrogen Energy, 37 (18) 2012; 13429.

[225] J. L. Waisman, G. Sine, L. B. Robinson, Metall. Trans. 4 (1) 1973; 291.